MAGNETIC DIFFERENTIATION AND QUANTIFICATION OF AIRBORNE PARTICULATE MATTER FROM VEHICULAR BRAKE SYSTEMS

Tomasz Gonet

September 2021

A thesis submitted for the degree
of Doctor of Philosophy in Environmental Science
at Lancaster Environment Centre, Lancaster University, United Kingdom

Lancaster
Environment Centre

Lancaster
University

ACKNOWLEDGEMENTS

Firstly, I would like to thank my supervisor, Professor Barbara Maher, who with her patience and perseverance has guided me through a slalom of seemingly insurmountable obstacles, both scientific and diplomatic in nature. Your unparalleled enthusiasm has changed the way I look at science. Thank you, Barbara!

Secondly, thanks to Vassil Karloukovski, one of the kindest people I know. I will always be grateful for your invaluable advice and help with even my most insane ideas.

Completion of my PhD would not have been possible without my collaborators from Ostrava, Jana Kukutschová and Miroslav Vaculík, who have shared their knowledge and extensive experience with me and also provided access to their fantastic laboratory and equipment.

I also thank Ilona Nyirő-Kósa and Mihaly Pósfai for key advice and in-depth discussions regarding our joint paper.

My PhD project was funded by Jaguar Land Rover and I am grateful for their financial support. I would also like to thank Andrew Stephenson, Ian Hadley, and Phil Ferdani for showing me the industrial side of our research.

Chciałbym również podziękować Jakubowi, który, czasem przy Hiroskach, a czasem bez, zawsze mnie wspierał i wysłuchiwał moich narzekań często do późnej nocy, a zwykle nawet do wczesnego rana. Dziękuję!

ABSTRACT

Exposure to particulate air pollution poses a threat to pulmonary, cardiovascular and neurological health, being associated significantly with increased morbidity and premature mortality worldwide. Ultrafine, metal-rich particles (UFPs; < 0.1 μm) are especially hazardous to humans as they can reach major organs in the human body, including the heart and brain, and are highly bioreactive, leading to increased oxidative stress and inflammatory response in the human tissues. Fe-bearing (and especially Fe^{2+}-bearing) UFPs might be especially important. They are reportedly associated with neurodegeneration and Alzheimer's disease (AD). Moreover, they are usually co-associated with other toxic metals and organic species. It is thus both timely and important to identify and quantify the sources of Fe-rich UFPs in the urban environment.

Here, the current knowledge regarding the sources of vehicle-derived Fe-bearing UFPs, their composition, particle size distribution and potential hazard to human health is first reviewed (Paper I). This chapter focuses on the data reported for the following sources of Fe-bearing UFPs: brake-wear emissions, engine-exhaust emissions (both diesel and petrol), tyre and road surface wear, resuspension of roadside dust, underground, train and tram emissions, and aircraft and shipping emissions. Brake-wear emissions were identified as one of the major sources of Fe-bearing UFPs in urban environments.

While magnetite ($Fe_3O_4 = FeO \cdot Fe_3O_4$) is known to be one of the most common Fe^{2+}-bearing minerals in urban particulate matter (PM), its sources have not so far been precisely quantified. Here, a set of roadside dust samples (from roadside and urban background sites in Birmingham and Lancaster, U.K.), engine-exhaust emissions (both petrol and diesel), and dynamometer-generated brake-wear PM emissions were collected, to quantify the contributions made by specific traffic-related sources to the total airborne magnetite at the roadside (Paper II).

The concentration of magnetic grains, as measured by magnetic remanence (SIRM), is notably higher (i.e. ~100 – 10,000 times higher) for brake-wear emissions, compared to other types of PM pollutants in most urban environments. A detailed AF demagnetisation of SIRM and magnetic component analysis allowed the separation of the magnetite signal from other contributing magnetic components, and the subsequent quantification of magnetite in the roadside dust and engine-exhaust PM samples.

The mass concentration of magnetite in petrol-engine exhaust emissions is ~0.06 – 0.12 wt.%; in diesel-engine exhaust emissions ~0.08 – 0.18 wt.%; in background dust ~0.05 – 0.20 wt.%; and in roadside dust ~0.18 – 0.95 wt.%. In contrast, magnetite constitutes as much as ~20.2 wt.% of brake-derived PM_{10} (PM with aerodynamic diameter < 10 µm). Based on these calculations and reported source apportionment of PM_{10} at the roadside, I show that vehicle brake-wear is by far the most dominant source of airborne magnetite at the roadside of two U.K. cities (Lancaster and Birmingham), contributing ~77% and ~85% of total airborne magnetite at the Lancaster and Birmingham roadside sites, respectively. In comparison, petrol-engine exhaust emissions account for ~2 – 4%, diesel-engine exhaust emissions ~7 – 12%, and background dust ~6 – 10%.

Paper III examines morphological, structural, chemical and magnetic properties of size-resolved brake-wear PM emissions. A set of dynamometer-generated brake-wear particulate emissions was collected, in a wide size range, from 16 nm up to 10 µm (in 14 size fractions). Using magnetic component analysis, low- and high-temperature magnetic measurements, and electron microscopy, the mass concentration of metallic Fe (α-Fe) was estimated to be ~1.6 wt.% in brake-derived PM_{10}. Magnetite content reached levels of ~20 wt.% for particles > 0.600 µm and decreased to 2 – 15 wt.% for particles < 0.380 µm. Most brake-derived airborne particles are smaller than 200 nm (> 99% of particle number concentration). Moreover, even larger fractions (e.g. ~2.5 µm) are dominated by agglomerated UFPs ~10 – 50 nm in size, as demonstrated by electron microscopy.

Overall, my thesis demonstrates that vehicle brake systems are one of the major sources of Fe-bearing UFPs in urban environments. Such UFPs (especially Fe^{2+}-bearing magnetite, often co-associated with other potentially toxic metals and organic species) might pose a particular threat to neuronal and cardiovascular health. The observed abundance of magnetite in the ultrafine size fraction of brake-wear PM (estimated to be ~7.6 wt.% of PM < 200 nm) might be especially hazardous to the human brain, where ultrafine magnetite particles have been reported to have a causal link with neurodegeneration and Alzheimer's disease (through generation of excess oxidative stress). Prospectively, given the potential risk to human health, the high concentrations of magnetite, specifically, in brake-wear PM might need to be reduced in order to mitigate such risk, especially for vulnerable population groups.

TABLE OF CONTENTS

LIST OF FIGURES

Appendix A:

Appendix B:

LIST OF TABLES

Appendix A:

Appendix B:

LIST OF PAPERS

This thesis is based upon the research summarised in the four following papers, published in international, peer-review journals.

I. **Gonet, T.**; Maher, B. A. Airborne, vehicle-derived Fe-bearing nanoparticles in the urban environment – A review. *Environmental Science and Technology* **2019**, 53, 9970-9991.

II. **Gonet, T.**; Maher, B. A.; Kukutschová, J. Source apportionment of magnetite particles in roadside airborne particulate matter. *Science of the Total Environment* **2021**, 752, 141828.

III. **Gonet, T.**; Maher, B. A.; Nyirő-Kósa, I.; Pósfai, M.; Vaculík, M.; Kukutschová, J. Size-resolved, quantitative evaluation of the magnetic mineralogy of airborne brake-wear particulate emissions. *Environmental Pollution* **2021**, 288, 117808.

IV. [Appendix B] Maher, B. A.; **Gonet, T.** Prolific shedding of magnetite nanoparticles from banknote surfaces. *Science of the Total Environment* **2021**, 768, 144490.

LIST OF ABBREVIATIONS

AD – Alzheimer's disease
CPs – coarse particles, i.e. with aerodynamic diameter of 2.5 µm – 10 µm
EC – elemental carbon
EDS – energy dispersive X-ray spectrometry
EM – electron microscopy
FFT – fast Fourier transform
HAADF – high angle annular dark-field mode of transmission electron microscopy (TEM)
HRTEM – high-resolution transmission electron microscopy (TEM)
EF – emission factor
FPs – fine particles, i.e. with aerodynamic diameter of 0.1 µm – 2.5 µm
IRM – isothermal remanence magnetisation, or magnetic remanence
$\kappa_{fd\%}$ - frequency dependence of magnetic susceptibility
LM – low-metallic brake pad
MDF_{IRM} – median destructive field of IRM
MRI – magnetic resonance imaging
NAO – non-asbestos organic brake pad
NPs – nanoparticles, i.e. with aerodynamic diameter < 0.1 µm; also called ultrafine particles (UFPs)
PAHs – polycyclic aromatic hydrocarbons
PCA – principal component analysis
PM – particulate matter
PM_{10} – particulate matter with aerodynamic diameter < 10 µm
$PM_{2.5}$ –particulate matter with aerodynamic diameter < 2.5 µm
$PM_{0.2}$ – particulate matter with aerodynamic diameter < 0.2 µm
PMF – positive matrix factorization
PNC – particle number concentration
PSD – particle size distribution
ROS – reactive oxygen species
SAED – selected-area electron diffraction
SD – single domain
SEM – scanning electron microscopy
SM – semi-metallic brake pad
SP – superparamagnetic
STEM – scanning transmission electron microscopy
T_M – temperature of the Morin transition in haematite
T_V – temperature of the Verwey transition in magnetite
TEM – transmission electron microscopy
UDP – urban driving programme
UFPs – ultrafine particles, i.e. with aerodynamic diameter < 0.1 µm; also called nanoparticles (NPs)
XRD – X-ray diffraction

Aims and Thesis Structure

Aims and objectives

The aim of the thesis is to identify and characterise airborne particulate emissions originating from car brake systems. The research papers arising from the study examine the particle size distribution, structure, morphology, chemical and magnetic properties of brake-wear emissions, with a special focus on ultrafine (< 0.1 μm in size) particles of magnetite (highly magnetic, mixed Fe^{2+}/Fe^{3+} oxide), reportedly causally linked with neurodegenerative diseases.

Thesis Structure

Chapter one reviews the sources of vehicle-derived Fe-bearing ultrafine particles, their composition, particle size distribution and potential hazard to human health. It identifies vehicular brake systems as one of the major sources of Fe-bearing ultrafine particles in urban environments. Chapter two discusses current knowledge regarding brake-wear emissions, including friction materials, experiments and studies, chemical composition, particle size distribution, tracers and health hazard of PM emitted by car brake systems. Chapter three describes the methodology applied in the three research papers presented in chapters four, five and Appendix B. Chapter six discusses the main findings of the research papers. Finally, chapter seven presents conclusions and prospects for future work.

Chapter One (Paper I): Airborne, vehicle-derived Fe-bearing nanoparticles in the urban environment – A review

1.1. Abstract

Airborne particulate matter (PM) poses a serious threat to human health. Exposure to nano-sized (< 0.1 μm), vehicle-derived particulates may be hazardous due to their bioreactivity, their ability to penetrate every organ, including the brain, and their abundance in the urban atmosphere. Fe-bearing nanoparticles (NPs; < 0.1 μm) in urban environments may be especially important because of their pathogenicity and possible association with neurodegenerative diseases, such as Alzheimer's and Parkinson's diseases. This review examines current knowledge regarding the sources of vehicle-derived Fe-bearing nanoparticles, their chemical and mineralogical compositions, grain size distribution, and potential hazard to human health. We focus on data reported for the following sources of Fe-bearing nanoparticles: exhaust emissions (both diesel and gasoline), brake-wear, tire and road surface wear, resuspension of roadside dust, underground, train and tram emissions, and aircraft and shipping emissions. We identify limitations and gaps in existing knowledge as well as future challenges and perspectives for studies of airborne Fe-bearing nanoparticles.

Published:

Gonet, T.; Maher, B. A. Airborne, vehicle-derived Fe-bearing nanoparticles in the urban environment – A review. *Environmental Science and Technology* **2019**, 53, 9970-9991.

1.2. Introduction

Exposure to airborne particulate matter (PM) is known to pose a serious threat to human health, linked with damage not only to respiratory and cardiovascular health, but also to neurodevelopment and cognitive function. Metal-bearing, nano-sized (< 0.1 µm) particles may be especially hazardous to human health (Ferin *et al*., 1992; Seaton *et al*., 1995; Gilmour *et al*., 1996, 1997; Stone *et al*., 1998; Donaldson *et al*., 2002; Brook *et al*., 2010) because of their abundance in the urban atmosphere (Ntziachristos *et al*., 2007; Hays *et al*., 2011; Sanderson *et al*., 2014, 2016; Maher *et al*., 2016; Yang *et al*., 2016), bioreactivity (Ferin *et al*., 1991; Donaldson *et al*., 2001; Nel *et al*., 2006; Maher *et al*., 2016), and their ability to reach all major organs of the human body by inhalation (Oberdörster *et al*., 1992, 1994, 1995, 2005; Elder *et al*., 2006; Maher *et al*., 2016) and by circulation in the bloodstream (Miller *et al*., 2017).

As evident from Figure 1, metal-bearing (e.g. Au-, Ba-, Cd-, Fe-, Mn-, Ti-bearing) particles may be translocated from the lungs to sites of vascular inflammation (Miller *et al*., 2017), the central nervous system (Tjälve *et al*., 1996; Oberdörster *et al*., 2004; Geiser & Kreyling, 2010), liver (Oberdörster *et al*., 2002; Miller *et al*., 2017) and amniotic fluid (Barošová *et al*., 2015). Particles < 200 nm can access the brain directly, bypassing the blood-brain barrier, via transport through the neuronal axons of the olfactory and/or trigeminal nerves (Oberdörster *et al*., 2004; Maher *et al*., 2016). Exposure to particulate air pollution may thus cause damage to neurodevelopment and cognitive functions (Calderón-Garcidueñas *et al*., 2002, 2004, 2008a; Block & Calderón-Garcidueñas, 2009; Guxens & Sunyer, 2012; Jung *et al*., 2015; Maher *et al*., 2016). Large population-scale epidemiological studies show that living close to heavy traffic is associated with a higher incidence of dementia (Jung *et al.*, 2015; Wu *et al*., 2015; Oudin *et al*., 2016; Chen *et al*., 2017a). Other epidemiological studies in the USA and Mexico indicate that young and old subjects living in areas with high airborne PM concentrations have cognitive deficits (Suglia *et al*., 2007; Calderón-Garcidueñas *et al.*, 2008b, 2012; Ailshire & Crimmins, 2014). In an MRI analysis of elderly women (age from 71 to 89 years; the Women's Health Initiative Memory Study cohort), white matter loss was increased by 1% per 3 $\mu g/m^3$ of $PM_{2.5}$ (Chen *et al*., 2015). Post-mortem brain samples from clinically healthy subjects (and dogs) exposed to lifetime high pollution, while living in Mexico City (Calderón-Garcidueñas *et al*., 2002, 2008a; Maher *et al*., 2016) or Manchester, U.K. (Maher *et al*., 2016) display: (i) typical hallmarks of Alzheimer's disease (AD) pathogenesis (e.g. tau-P, β-amyloid deposition), (ii) inflammation, oxidative stress and DNA signaling damage (Calderón-Garcidueñas *et al*., 2008a); and (iii) the abundant presence of metal-bearing NPs, including mixed Fe^{2+}/Fe^{3+} (magnetite) NPs, as determined by electron microscopy (EM) and magnetic analyses (Maher *et al.*, 2016). Mouse models for urban nanoparticulate air pollution show consistent induction of inflammatory responses in major brain regions (Cheng *et al.*, 2016) (see also Appendix A: Table A5).

Due to their large surface area and potentially high reactivity with biomolecules and tissues, metal-bearing nanoparticles may generate adverse health impacts related to oxidative stress, inflammation (Morrow *et al.*, 1988; Ferin *et al.*, 1991; Oberdörster *et al.*, 1994, 1995; Donaldson *et al.*, 1998; Brown *et al.*, 2000; Kreyling *et al.*, 2004) and generation of reactive oxygen species (ROS) (Gilmour *et al.*, 1996; Li *et al.*, 1996; Shuster-Meiseles *et al.*, 2016; Zhang *et al.*, 2019). Exposure to bioreactive airborne NPs can occur at every life stage; in the womb (Pinkerton *et al.*, 2006; Barošová *et al.*, 2015), as developing infants and children (Calderón-Garcidueñas *et al.*, 2008b, 2013, 2016; Mohai *et al.*, 2011; Sunyer *et al.*, 2015, 2017), and through adulthood to terminal decline. Both the young and the elderly are particularly vulnerable to air pollution (Bateson *et al.*, 2007; Burtscher *et al.*, 2012; Pieters *et al.*, 2015; Cacciottolo *et al.*, 2017; Li *et al.*, 2017). Pre-birth exposures to both PM_{10} and $PM_{2.5}$ are associated with low birth weight (e.g. Wang *et al.*, 1997; Lee *et al.*, 2003; Bell *et al.*, 2007; Li *et al.*, 2017). Childhood exposures to traffic-derived PM (elemental carbon – EC, nitrogen dioxide – NO_2 and PM < 700 nm) impair lung growth (Gauderman *et al.*, 2007) and cognitive development (Sunyer *et al.*, 2015; 2017). These early life exposures to airborne PM can thus set in train a sequence of health problems which progressively develop through later life. Children spend more time outdoors, are more physically active, and they have an increased breathing rate and immature immune system, all of which result in a higher dosage in the respiratory tract of children compared to adults, especially in the case of NPs (Ginsberg *et al.*, 2005). Compared to children living with clean air, those in polluted areas (e.g. Mexico City) display health problems, including systemic inflammation, and even Alzheimer's and Parkinson's hallmarks (Calderón-Garcidueñas *et al.*, 2008a; 2008b; 2012; 2013).

Exposure specifically to Fe-bearing airborne NPs may be especially hazardous to human health. Fe is an essential biometal, as a component of diverse metalloproteins, from cytochromes to haemoglobin, and playing key roles in neuronal function, ranging from nerve impulse transduction to neurotransmitter synthesis and mitochondrial energy production. Fe is mobilized and stored via changes in valence, controlled by sophisticated regulatory homeostasis processes. Such processes are vital, since labile Fe^{2+}, i.e. in the unbound, redox-active state, can be toxic to living cells. In humans, non-haem Fe is stored in a redox-inactive, oxidized (Fe^{3+}) form as ~8 nm spherical cores of ferrihydrite ($5Fe_2O_3 \cdot 9H_2O$) within the ~12 nm-diameter Fe-storage protein, ferritin. However, if redox-active, ferrous Fe^{2+} remains unbound and freely available, it can catalyze the formation of reactive oxygen species (ROS), including the damaging hydroxyl radical, through the Fenton reaction (Smith *et al.*, 1997).

Problems with transportation and storage of Fe have been linked with a variety of diseases, including Alzheimer's, Parkinson's, Huntington's, multiple sclerosis, amyotrophic lateral sclerosis and Hallervorden-Spatz disease (Swaiman, 1991; Beard *et al.*, 1993; Smith *et al.*, 1997; Rouault, 2001; Dobson, 2004; Zecca *et al.*, 2004; Castellani *et al.*, 2007). Some of the excess Fe found in the neurodegenerative brain occurs in the form of magnetite, a strongly magnetic, mixed Fe^{2+}/Fe^{3+} oxide (see Section 1.13. Specific toxicity of iron-bearing nanoparticles for more details).

Given the potential risks to human health posed by airborne Fe-bearing NPs, it is timely to examine information regarding their sources, abundance and composition, in order to identify major routes of exposure, and potential pathways to removing or reducing their particle number concentrations.

1.3. Iron-bearing nanoparticles in the environment

Fe-bearing NPs occur both abundantly and widely in the urban atmosphere (Ntziachristos *et al.*, 2007; Hays *et al.*, 2011; Sanderson *et al.*, 2014; 2016; Maher *et al.*, 2016; Yang *et al.*, 2016). Fe, in oxide, hydroxide and metallic forms, is a major contributor not only to the aerosol mass in urban environments but also, because of its abundant occurrence within primary, emitted NPs, to the particle number concentrations in urban air.

Fe has been found in high concentrations (11,000 – 94,000 ppm) in the sub-micrometer fraction of roadside PM (Yang *et al.*, 2016). Fe-bearing NPs are frequently associated both with transition and heavy metals, including Cr, Ni, Cu, Zn, Pb and Mn (Chen *et al.*, 2006; Maher *et al.*, 2016; Yang *et al.*, 2016). Most of the Fe-bearing particles emitted from vehicles are ferromagnetic (*sensu lato*) Fe oxides, comprising mixtures of strongly magnetic magnetite (Fe_3O_4), its oxidized counterpart, maghemite (γ-Fe_2O_3), and hematite (α-Fe_2O_3), with some metallic Fe (α-Fe) also reported (Muxworthy *et al.*, 2002; Halsall *et al.*, 2008; Maher *et al.*, 2008; Mitchell & Maher, 2009; Hansard *et al.*, 2011; Sanderson *et al.*, 2016). The magnetic ordering shown by these airborne Fe-oxide particles enables their measurement and quantification using a range of concentration- and particle size-dependent magnetic analyses (see Section 1.12. Magnetic measurements of vehicle-derived, Fe-bearing nanoparticles).

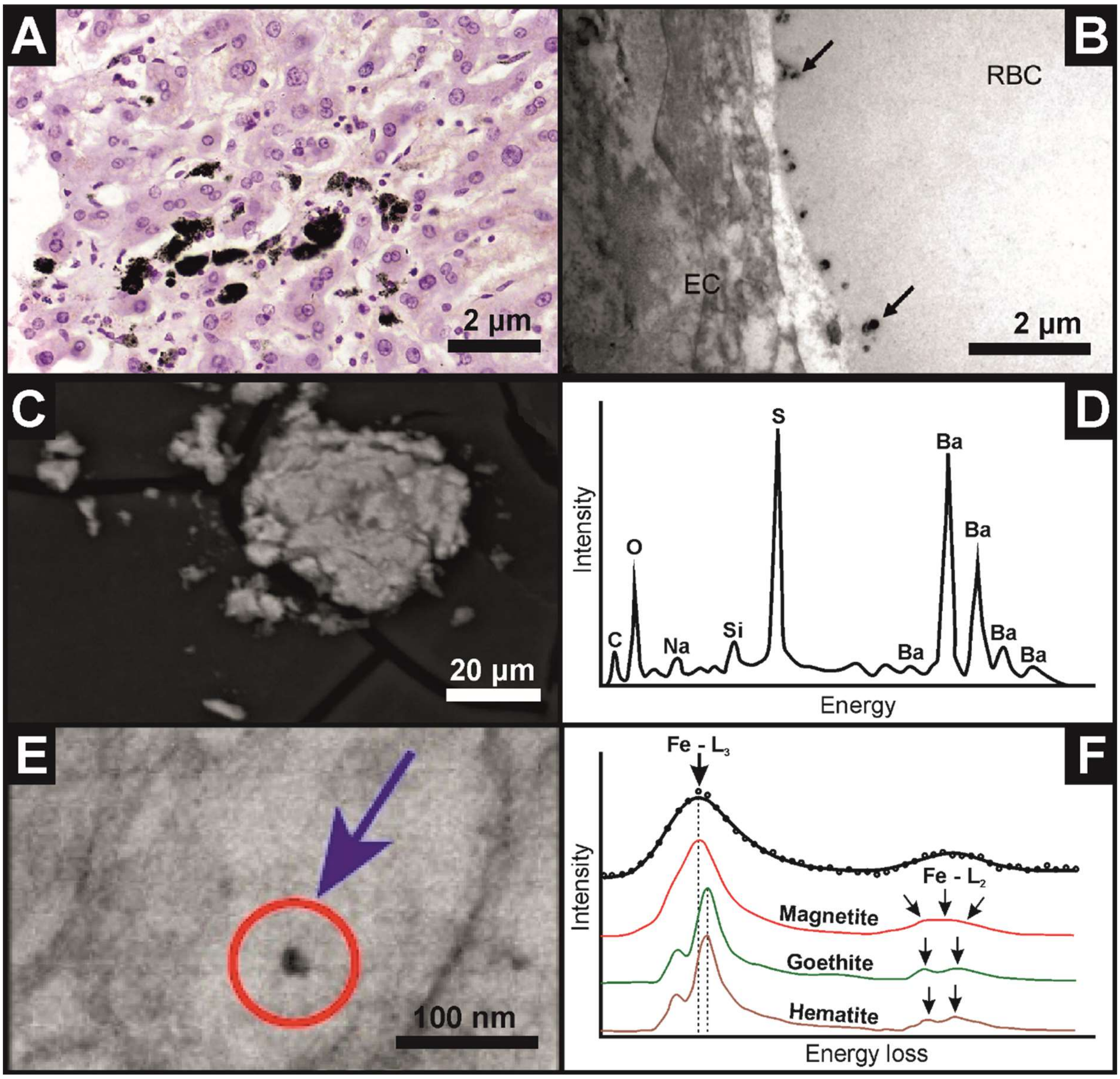

Figure 1. Metal-bearing particles found in the human body: (A) PM in the liver of a 32 year-old male (adapted from Calderón-Garcidueñas *et al.* (2008a)); (B) PM spherules in a lung capillary, RBC = red blood cell; EC = endothelial cell (adapted from Calderón-Garcidueñas *et al.* (2008a)); (C) SEM image of Ba-bearing particles in the amniotic fluid with (D) the corresponding EDS spectrum (adapted from Barošová *et al.* (2015); (E) TEM image of magnetite NPs in frontal cortex brain tissue with (F) corresponding EELS spectra (in black) for the rounded particle shown in E and for standard Fe oxide species (adapted from Maher *et al.* (2016)).

Magnetic particles in indoor and outdoor airborne PM can originate from a range of domestic (e.g. wood/coal burning, cigarette smoking, printer emissions), workplace, transport and industry sources (see also Appendix A: Section A3) (Buseck & Adachi, 2008; Maher *et al*., 2008; Maher, 2009; Mitchell & Maher, 2009; Morawska *et al*., 2009; Zhang *et al*., 2012; Kumar *et al*., 2013; Zajzon *et al*., 2013; Jeleńska *et al*., 2017). Such particles can occur over a great range of sizes, from several nm up to several hundred μm. Moreover, NPs < 100 nm can agglomerate with each other and/or surround bigger particles. However, until recently, most magnetic studies have focused on PM fractions ≥ 1 μm.

Vehicles are a major source of Fe-bearing NPs in the environment (Shi *et al*., 1999; Cass *et al*., 2000; Harrison *et al*., 2000; Popovicheva *et al*., 2009; Hansard *et al*., 2011; 2012; Mazaheri *et al*., 2011; Zajzon *et al*., 2013; Moreno *et al*., 2015; Peikertova *et al*., 2016; Sanderson *et al*., 2016; Yang *et al*., 2016; Kukutschová & Filip, 2018). Figure 2 shows Fe-bearing NPs in street dust, variously composed of magnetite, hematite, goethite and ferrihydrite (Yang *et al*., 2016). Vehicle-derived, Fe-bearing NPs originate from: exhaust emissions, both diesel (Abdul-Razzaq & Gautam, 2001; Lee *et al*., 2006) and gasoline (Zajzon *et al*., 2013); brake-wear (Kukutschová & Filip, 2018); tire wear (Gustafsson *et al*., 2008); resuspension of roadside dust (Ntziachristos *et al*., 2007); underground, rail and tram systems (Moreno *et al*., 2015); aircraft (Demirdjian *et al*., 2006); and shipping emissions (Popovicheva *et al*., 2009).

1.4. Exhaust emissions

Exhaust emissions constitute a substantial source of Fe-bearing NPs in urban environments (Harris & Maricq, 2001; Lombaert *et al*., 2004; Ntziachristos *et al*., 2007; Kam *et al*., 2012; Keuken *et al*., 2012). Although about 90 wt.% of tailpipe emissions is carbonaceous material, exhaust emissions contain up to 10 wt.% of trace metals (Brook *et al*., 2007; Robert *et al*., 2007; Fulper *et al*., 2010; Peltier *et al*., 2011; Pant & Harrison, 2013), n-alkanes and polycyclic aromatic hydrocarbons (PAHs) (e.g. Rogge *et al*., 1993; Lough *et al*., 2005; Alam *et al*., 2016). Diesel engines also generate soot nanospheres, of between ~10 and 60 nm (Su *et al*., 2004; Liati *et al*., 2012), which are often associated with Mg, Fe, Cu, Ca and Zn (Lombaert *et al*., 2004). Trace metals emitted by engines include Fe, Zn, Cr, Mo, Ti, Mg, Ni, Pb, Ca, Cu, Ba, Sb, Co, Cd, V, Pt and Pd (e.g. Wang *et al*., 2003; Sharma *et al*., 2005; Maricq, 2007; Liati *et al*., 2012; Prichard *et al*., 2012).

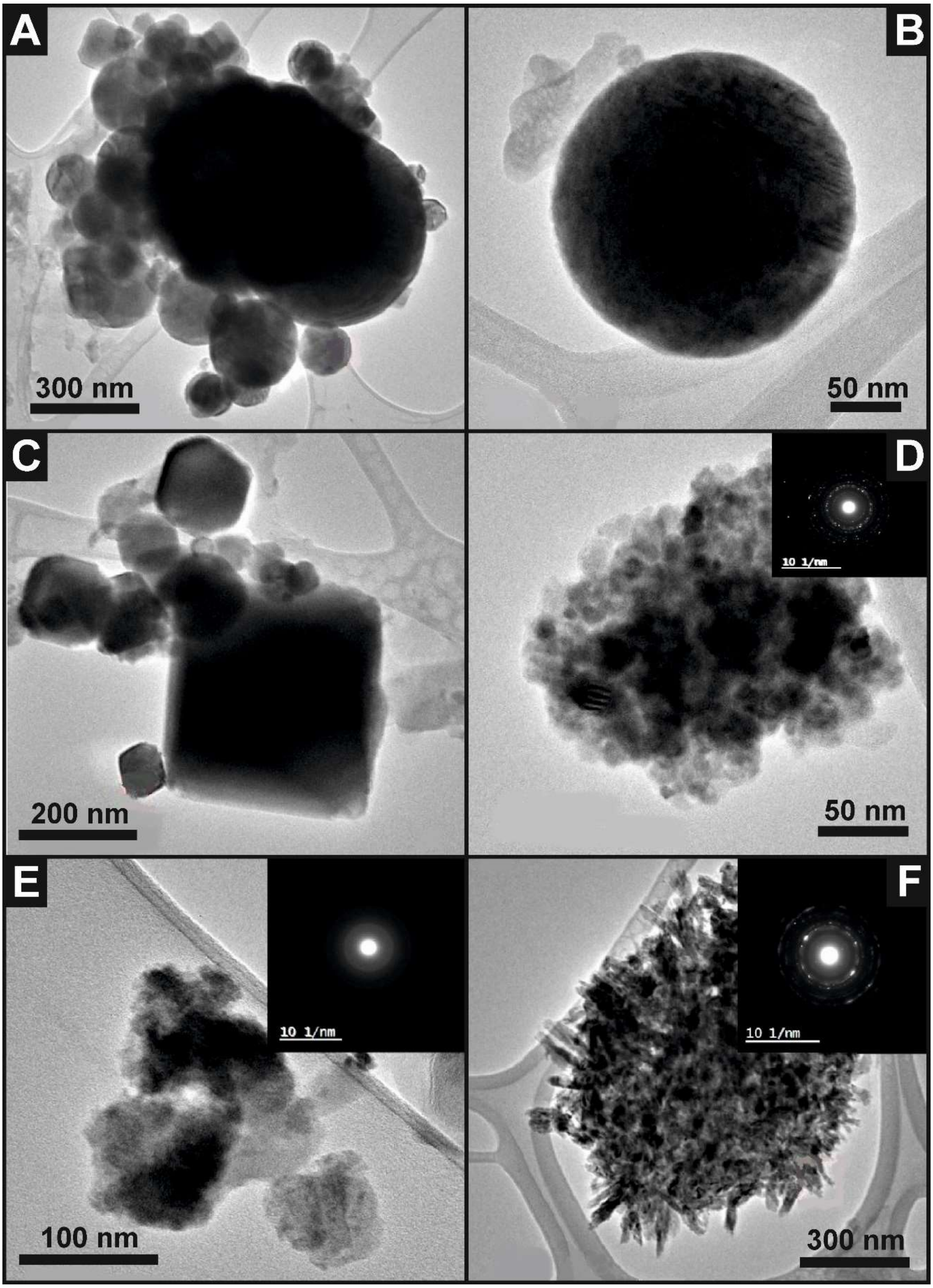

Figure 2. Fe-bearing NPs found in street dust: (A) aggregate of spherical magnetite particles, (B) Fe-rich fly ash, (C) magnetite particle with an octahedral shape, (D) hematite, (E) ferrihydrite, (F) goethite (adapted from Yang *et al.* (2006)).

Particle size distributions (PSD) can be measured in terms of mass and number. Number-normalized PSDs are more sensitive to the presence of nanoparticles (< 100 nm), which contribute most to the particle number concentrations while contributing very little to the PM mass. Number-normalized PSDs of exhaust emissions are typically bimodal, with peaks at ~20 – 40 nm and ~50 – 90 nm (Kumar *et al.*, 2008; Ondráček *et al.*, 2011) or unimodal, with a peak at ~10 – 70 nm (Bagley *et al.*, 1996; Harris & Maricq, 2001; El Haddad *et al.*, 2009; Karjalainen *et al.*, 2014) (Figure 3). Number-normalized PSDs often depend on nucleation processes and atmospheric conditions (e.g. Imhof *et al.*, 2006; Reche *et al.*, 2011). NP numbers are also heavily influenced by the proximity of traffic (or other emission sources), especially in the case of particles of diameter < 30 nm (Zhu *et al.*, 2002; Rose *et al.*, 2006; Puustinen *et al.*, 2007; Cyrys *et al.*, 2008; Beddows *et al.*, 2009; Keuken *et al.*, 2012); a point of vital importance from the epidemiological point of view as the key exposure zone for traffic is reported to be within 500 meters (Gauderman *et al.*, 2007; HEI, 2010), and more specifically, within 50 meters (Ranft *et al.*, 2009) of major roadways.

Ntziachristos *et al.* (2007) studied traffic-derived PM in Los Angeles, USA and reported that Fe was a predominant metal in the < 0.18 μm fraction, accounting for 10 – 25% of $PM_{0.18}$ mass. Magnetite particles in car (diesel) exhaust emissions were first observed by Abdul-Razzaq & Gautam (2001). Later studies (Lee *et al.*, 2006; Liati *et al.*, 2013; 2015; 2018) found Fe oxide NPs in diesel emissions, and superparamagnetic (SP) NPs of magnetite and hematite (Zajzon *et al.*, 2013) in gasoline emissions (cf. Figure 2A, B, D). Fe-bearing NPs often occur as rounded or even spherical particles – 'nanospheres' – of magnetite and/or hematite, depending on combustion/heating conditions (Figure 2A, B, D) (Abdul-Razzaq & Gautam, 2001; Zajzon *et al.*, 2013; Yang *et al.*, 2016). Miller *et al.* (2007) identified 4 groups of NPs containing Fe: homogeneously nucleated primary NPs of Fe; carbon agglomerates decorated with primary Fe NPs; agglomerates of Fe primary particles; and combined Fe/carbon agglomerates (Figure 4). Fe-bearing particles emitted from tailpipes often comprise a mixture of all these particle types.

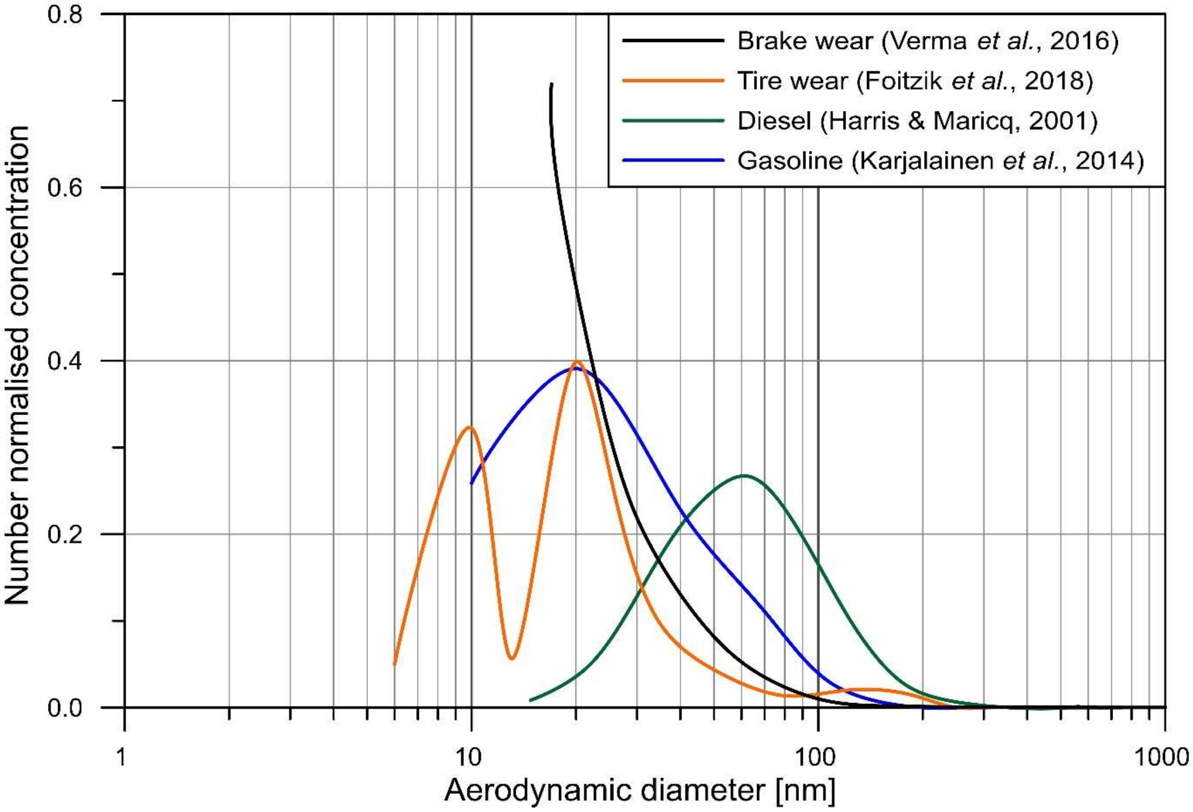

Figure 3. Examples of particle-size distributions for non-exhaust (brake and tire wear debris) and exhaust (diesel and gasoline) emissions. Brake-wear was collected using a pin-on-disc machine (sliding speed of 13 m/s, contact pressure of 1.39 MPa, for 3 h) (Verma *et al.*, 2016). Tire wear was collected using a tire test bench (inner diameter of 3.8 m, speed of 0, 30, 50 and 70 km/h) (Foitzik *et al.*, 2018). Diesel emissions were collected using an AC electric dynamometer and the U.S. UDDS (urban dynamometer drive schedule) test cycle (Harris & Maricq, 2001). Gasoline emissions were collected using a test vehicle (acceleration from 30 to 90 km/h; hot start) (Karjalainen *et al.*, 2014).

Fe-bearing NPs in exhaust emissions might originate from several sources. Magnetite was found in exhaust emissions when fuel additives (e.g. ferrocene) had been used (e.g. Braun *et al.*, 2006). Magnetic NPs may form due to Fe impurities in fuel which can convert to Fe oxides, such as magnetite and/or hematite, depending on combustion conditions (Abdul-Razzaq & Gautam, 2001; Maher *et al.*, 2008; Zajzon *et al.*, 2013; Yang *et al.*, 2016). Ferromagnetic NPs might also originate from aging of steel in the engine (Filippelli *et al.*, 2005) and/or melting of engine fragments in the combustion chamber and subsequent crystallization during cooling (Liati *et al.*, 2015). In modern engines, however, various coatings (mainly Al, Cr, Mo, Ti, Zr alloy) reportedly reduce the wear rate by up to 94% (Mehran *et al.*, 2018).

Studies on animals showed that exposure to exhaust emissions might be associated with developmental impairment in various ways, including changes in growth, sexual development, hormone levels, weight of the reproductive and accessory organs, expression of immune-related genes and susceptibility to allergies (e.g. Sugamata *et al.*, 2006; Ema *et al.*, 2013; Li *et al.*, 2013). The exposure to diesel and biodiesel emissions might also lead to cardiovascular alterations as well as pulmonary and systemic inflammation in mice (Brito *et al.*, 2010). Gasoline-derived PM has also been associated with health problems, e.g. impairment of epithelial defence mechanisms (Künzi *et al.*, 2015). Moreover, a study by Cheung *et al.* (2010), evaluating the oxidative potential of gasoline, diesel and biodiesel emissions, showed that soluble Fe is strongly associated ($R = 0.99$) with particulate ROS activity (see Appendix A: Table A5 for more details).

1.5. Brake-wear emissions

Brake-wear debris comprises primarily carbonaceous and metal-bearing components (Garg *et al.*, 2000). In contrast to tailpipe emissions, Fe often dominates, constituting > 50 wt.% of all brake-wear emissions (Sanders *et al.*, 2003; Adachi & Tainosho, 2004; Kukutschová *et al.*, 2011; Österle *et al.*, 2014). Besides Fe, brake dust emissions can also contain a wide range of elements, including Cu, C, Ba, Sb, Si, Al, Mo, S, Sn, Cd, Cr, Pb, Zr, Ti and Zn (Mosleh *et al.*, 2004; Thorpe & Harrison, 2008; Kukutschová *et al.*, 2010; 2011; Peikertová *et al.*, 2013; Verma *et al.*, 2016; Kukutschová & Filip, 2018).

Appendix A: Table A6 shows total dust emissions during a pin-on-disc test of a commercial, low-metallic brake pad (Verma *et al.*, 2016). The NP fraction (< 100 nm) constitutes > 90% of total particle number. Similarly, Garg *et al.* (2000) reported that most particles were < 30 nm (cf. Figure 3).

Although Fe-rich particles have been widely reported in brake-wear studies (Sanders *et al.*, 2003; Kukutschová *et al.*, 2010; 2011; Hagino *et al.*, 2016; Sanderson *et al.*, 2016; Verma *et al.*, 2016), little attention has yet been paid to identification of their properties (phase/mineralogical composition, concentrations of particular phases, size distribution) or potential health impact. Figure 5 shows an agglomerate of NPs ~20 – 100 nm in size, derived from brake-wear collected during a dynamometer test of a widely-available brake pad. These brake-wear NPs contain mostly magnetite and elemental Fe (Kukutschová *et al*., 2010). Other authors have reported other Fe oxides, mainly hematite, wüstite (FeO) and maghemite in the NP fraction (Peikertová *et al*., 2013; Sanderson *et al*., 2016; Verma *et al*., 2016).

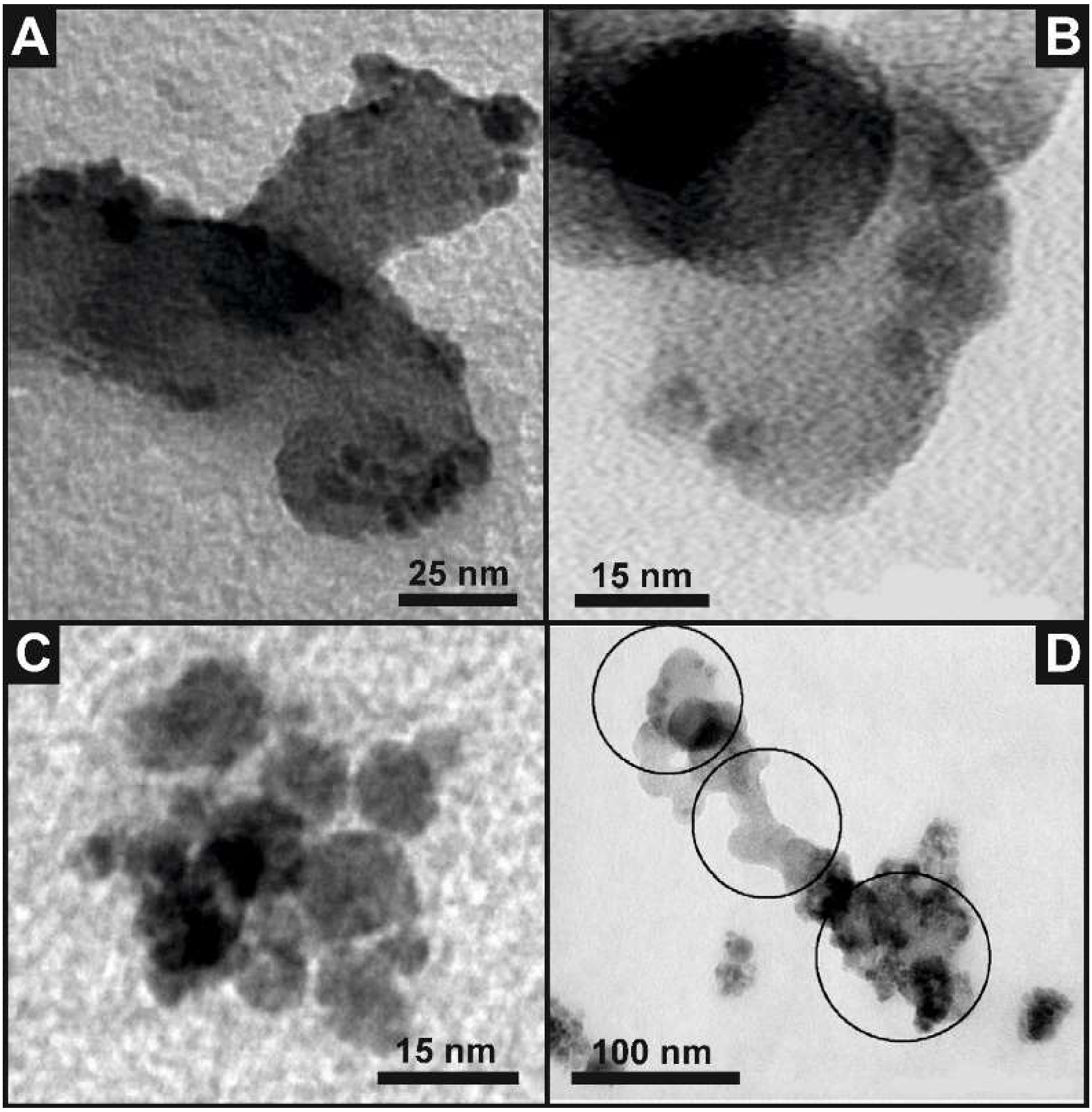

Figure 4. Examples of Fe-bearing NPs in diesel emissions: (A) and (B) carbon agglomerates decorated with primary Fe NPs, (C) nucleated primary particles of Fe and (D) combined carbon/iron agglomerates (adapted from Miller *et al.* (2007)).

Brake-wear debris results from friction between a brake pad, of diverse chemical compositions, and the cast iron brake disc. Both members of this friction couple can be a source of Fe-bearing NPs. Moreover, nano- and sub-micrometer-sized Fe powder, as magnetite, is often added (in concentrations up to 50 wt.%) to brake pads (Jang, 2013), as a solid lubricant. At brake pad temperatures below ~200ºC, abrasive processes dominate, and wear particles > 1 µm are mostly generated. But at higher temperatures (> ~190ºC), the concentration of nano-sized grains (< 100 nm) increases due to evaporation, condensation and aggregation processes (Garg *et al*., 2000; Kukutschová *et al*., 2010; 2011; Verma *et al*., 2016). As a result, high numbers (~10^{11} particles/stop/brake) of Fe-rich NPs are emitted (Garg *et al*., 2000; Kukutschová *et al*., 2010; 2011; Verma *et al*., 2016; Nosko & Olofsson, 2017a; Perricone *et al*., 2017; Kukutschová & Filip, 2018). The NP emission rate increases by 4 – 6 orders of magnitude at a critical temperature, usually ~160ºC to 190ºC (Nosko *et al*., 2015; 2017; Alemani *et al*., 2016; Perricone *et al*., 2018).

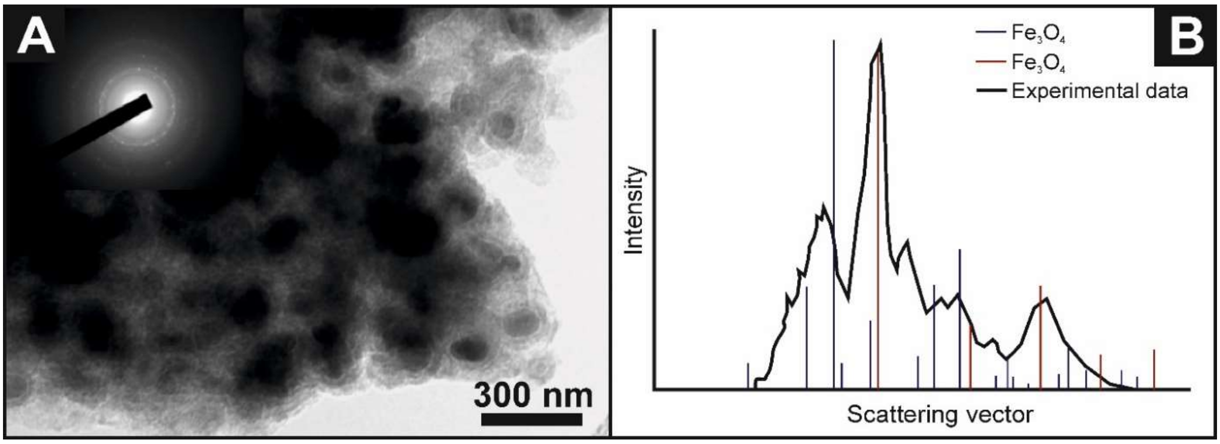

Figure 5. (A) TEM image of NP wear particles collected during a dynamometer test and (B) electron diffraction (EDX) intensity profile (adapted from Kukutschová *et al.* (2010)).

In vitro and *in vivo* studies (see Appendix A: Table A5) show that brake-wear emissions can induce oxidative stress and chromosomal damage, invoke pro-inflammatory response and cause increased ROS production (Gasser *et al*., 2009; Kukutschová *et al*., 2009; Zhao *et al*., 2015; Kazimirova *et al*., 2016; Malachova *et al*., 2016; Barosova *et al*., 2018; Puisney *et al*., 2018; Rajhelová *et al*., 2019). The effects were more severe for the emissions originating from non-asbestos organic brake pads, compared to low-metallic ones (Puisney *et al.*, 2018; Gerlofs-Nijland *et al.*, 2019).

Since NPs constitute the great majority of brake-wear particle numbers, and Fe is the dominant component of those NPs, brake-wear dust thus comprises a major source of airborne Fe-bearing NPs (see also Section 1.12. Magnetic measurements of vehicle-derived, iron-bearing nanoparticles).

1.6. Tire and road surface wear emissions

Other types of traffic-related NPs, from tire and road surface wear, contain lower concentrations of Fe-bearing NPs, but still display high genotoxicity and potential hazard to human health (Gualtieri *et al.*, 2005; Lindbom *et al.*, 2006; 2007; Wik & Dave, 2009).

Tire wear debris typically comprises ~47% rubber, 21.5% carbon black and as much as 16.5% metals (Milani *et al.*, 2004). Dominant components of tire wear include n-alkanes, n-alkanoic acids, PAHs, benzothiazoles (Rogge *et al.*, 1993; Reddy & Quinn, 1997; Camatini *et al.*, 2001; Kumata *et al.*, 2002; Adachi & Tainosho, 2004; Allen *et al.*, 2006; Hjortenkrans *et al.*, 2007; Thorpe & Harrison, 2008; Wik & Dave, 2009; Ondráček *et al.*, 2011) and elements such as Al, Si, Zn, Fe, S, K, Ca, Ti and Mg (Figure 6) (Lindbom *et al.*, 2006; Gustafsson *et al.*, 2008; Thorpe & Harrison, 2008). Notably, studies showed that Fe occurs in all size fractions < 10 μm of tire wear emissions, with concentrations up to 37 wt.% in the fractions < 460 nm (Figure 6) (Gustafsson *et al.*, 2008).

The PM (mass and number) emitted from tire/road surface wear depends on several factors; i.e. speed, slip angle, load and longitudinal force (Dahl *et al.*, 2006; Gustafsson *et al.*, 2008; Foitzik *et al.*, 2018). Tire/road surface wear particles > 10 μm constitute ~60 – 70%, PM_{10} ~30% and $PM_{2.5}$ ~4.5% of total tire emission mass (Kupiainen *et al.*, 2005). However, tire wear accounts for a negligible portion (< 5%) of road dust mass, contributing mainly to the NP (< 100 nm) fraction (Dahl *et al.*, 2006; Foitzik *et al.*, 2018) (cf. Figure 3 and Figure 7), whereas road surface wear is responsible for emission of the larger grains (Kupiainen *et al.*, 2005; Gustafsson *et al.*, 2008). Foitzik *et al.* (2018) found that the PSD of tire NP emissions is bimodal (with peaks at ~10 nm and ~25 nm) or unimodal (peak at ~10 – 15 nm) (cf. Figure 3). Other authors report number PSDs with slightly larger grains (main peak ~25 – 45 nm)

(Dahl *et al.*, 2006; Gustafsson *et al.*, 2008; Dall'Osto *et al.*, 2014). Some authors, however, dispute NP generation during real-world conditions (Mathissen *et al.*, 2011).

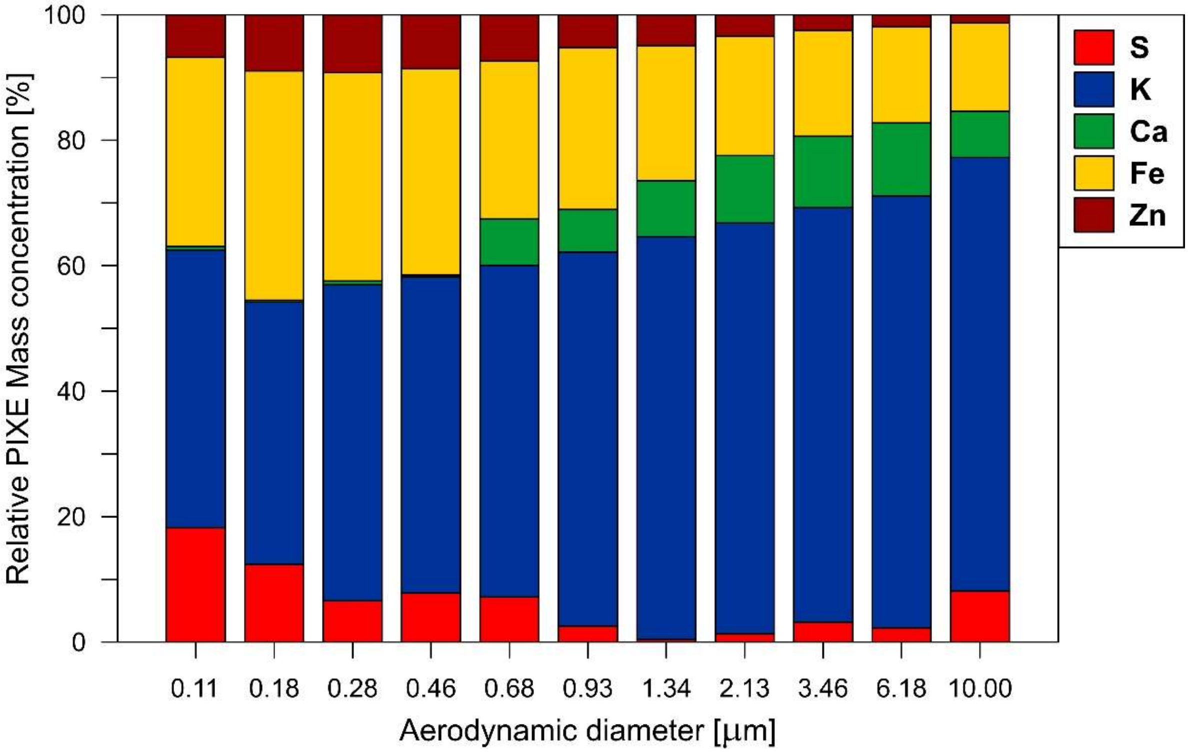

Figure 6. Relative mass concentration of Zn, Fe, Ca, K and S in tire wear, excluding dominating mineral elements Al and Si (adapted from Gustafsson *et al.* (2008)).

The interaction between tires, road surface and traction sanding (sand introduced on the road surface to improve vehicle traction) results in emission of substantial particle numbers, especially in, for example, Nordic countries and Japan where studded tires are used regularly during winter (Hosiokangas *et al.*, 1999). NPs from tires might derive from the evaporation of semi-volatile softening oils at temperatures > 100°C (Dahl *et al.*, 2006), or inclusions of zinc oxides and sulfates (Dahl *et al.*, 2006; Lindbom *et al.*, 2006; Gustasson *et al.*, 2008). Moreover, steel (and other metals) is often added (up to 25 wt.%) as reinforcement material (Evans & Evans, 2006) so is likely to be an additional source of tire-derived Fe-bearing NPs.

Toxicological studies (see Appendix A: Table A5) suggest that tire/road surface wear poses a threat to human health via damage to epithelial cells and ROS formation (Gualtieri *et al.*, 2005; Lindbom *et al.*, 2006; 2007; Wik & Dave, 2009).

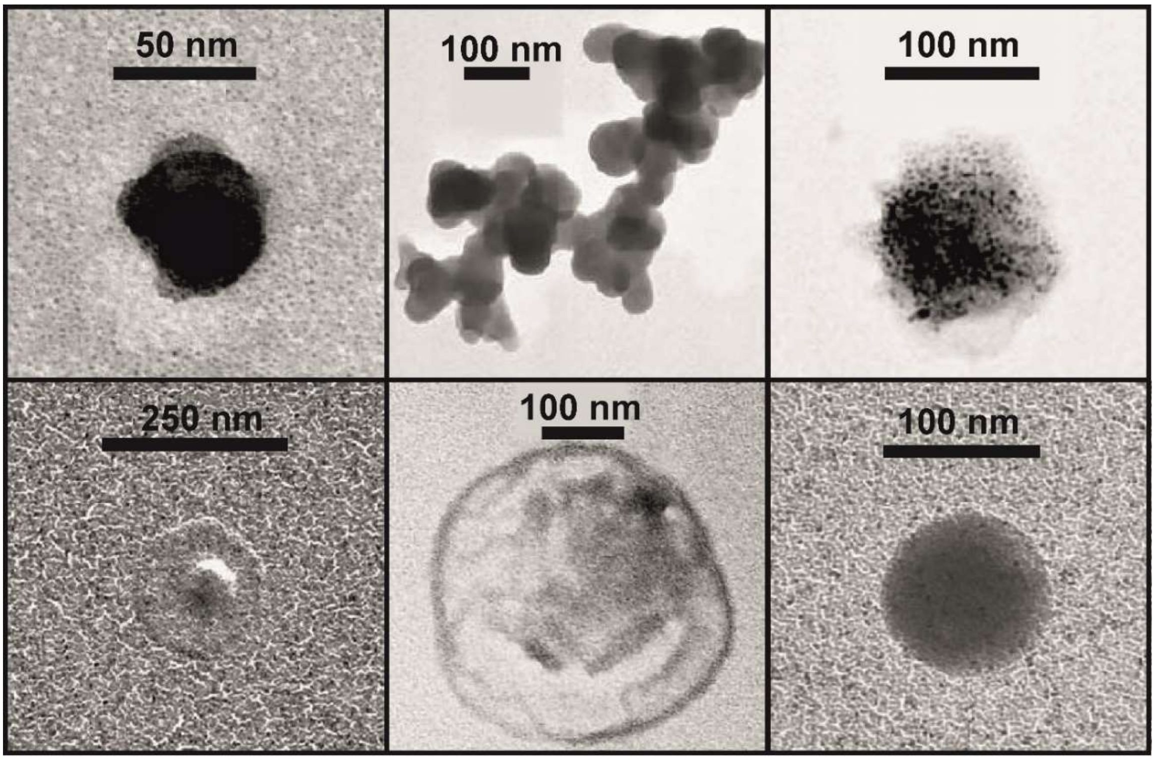

Figure 7. TEM images of tire wear NP generated by a road simulator (adapted from Dahl *et al.* (2006)). No compositional data were provided by the authors.

1.7. Resuspension of the roadside dust

Resuspension of road dust is one of the major sources (27 – 38 wt.%) of airborne PM in urban environments (e.g. Bukowiecki *et al*., 2009a; Martuzevicius *et al*., 2011; Chen *et al*., 2012; Lawrence *et al*., 2013; Pant & Harrison, 2013). PM fractions > 1 µm are predominant in resuspended dust (Kupiainen *et al*., 2005; Chen *et al*., 2006; Tanner *et al*., 2008; Duong & Lee, 2011; Pant & Harrison, 2013), with sub-micrometer particles constituting ~10 – 15 wt.% (Kupiainen *et al*., 2005).

High Fe concentrations (11,000 – 94,000 ppm) have been observed in the sub-micrometer fraction of roadside PM (Yang *et al*., 2013) in several different forms: magnetite, hematite, metallic Fe, ferrihydrite and goethite (Figure 2) (Xie *et al*., 1999; 2001; Goddu *et al*., 2004; Bućko *et al*., 2011; 2013; Wawer *et al*., 2015; Yang *et al*., 2010; 2016; Dytłow & Górka-Kostrubiec *et al*., 2019).

Roadside dust can be a complex mixture of natural, soil-derived particles, and of traffic- (both exhaust and non-exhaust) and industry-derived emissions. Hence, exposure to resuspended dust may also be hazardous to human health.

1.8. Underground, train and tram emissions

Underground transport systems are used daily by approximately 4 million people in London (Transport for London Website), 4.5 million in New York (The New York City Subway System Website) and 7 million in Tokyo (Tokyo's Metro Advertising Media Website). Although commuting typically constitutes only ~10% of the day (e.g. Klepeis *et al.*, 2001; Saksena *et al.*, 2008), subway commuters are exposed to high levels of pollutants (Knibbs *et al.*, 2011), especially Fe-bearing NPs (Moreno *et al.*, 2015; 2017b). Daily average $PM_{2.5}$ levels in subway environments reach 480 µg/m^3 and particle number concentrations (PNCs) up to 31,000 particles/cm^3 (Aarnio *et al.*, 2005; Seaton *et al.*, 2005; Abbasi *et al.*, 2013; Moreno *et al.*, 2015), greatly (up to 30 times) exceeding nearby above-ground PM levels, e.g. in Helsinki (Aarnio *et al.*, 2005), Rome (Ripanucci *et al.*, 2006), Seoul (Kim *et al.*, 2008), Buenos Aires (Murruni *et al.*, 2009), Paris (Raut *et al.*, 2009) or Mexico City (Mugica-Álvarez *et al.*, 2012).

Fe is a dominant element in subway, train and tram emissions, in coarse (10 – 2.5 µm), fine (< 2.5 µm) and NP (< 100 nm) fractions (Bukowiecki *et al.*, 2007; Gehrig *et al.*, 2007; Murruni *et al.*, 2009; Salma *et al.*, 2009; Kam *et al.*, 2011; Zhang *et al.*, 2011; Abbasi *et al.*, 2012; Gustafsson *et al.*, 2012; Jung *et al.*, 2012; Midander *et al.*, 2012; Mugica-Álvarez *et al.*, 2012; Abbasi *et al.*, 2013; Loxham *et al.*, 2013; Moreno *et al.*, 2015), constituting usually ~65 wt.% of PM_{10} and $PM_{2.5}$ (e.g. Seaton *et al.*, 2005; Abbasi *et al.*, 2012; Jung *et al.*, 2012), sometimes reaching levels as high as 86 wt.% of PM_{10} (Gustafsson *et al.*, 2012), 88 wt.% of $PM_{2.5\text{-}1.0}$ (Moreno *et al.*, 2017b) and 95% of PNC (Moreno *et al.*, 2017b). Fe is usually accompanied by other metals, including Cu, Ba, Zn, Si, Al, Ca, Ni, Ti, Sb, V, Co, Cr, Mn (Abbasi *et al.*, 2012; 2013; Moreno *et al.*, 2015; Namgung *et al.*, 2016; 2017).

The PSD of subway emissions is dominated by NPs < 100 nm (Salma *et al.*, 2009; Gustafsson *et al.*, 2012; Midander *et al.*, 2012; Lee *et al.*, 2018b). Airborne PM at subway stations contains a mixture of magnetite, maghemite, and hematite, with some additional evidence of the presence of metallic Fe, wüstite and Fe oxyhydroxides (goethite and/or lepidocrocite) (Karlsson *et al.*, 2005; Kang *et al.*, 2008; Salma *et* al., 2009; Zhang *et al.*, 2011; Midander *et al.*, 2012; Mugica-Álvarez *et al.*, 2012; Querol *et al.*, 2012; Eom *et al.*, 2013;

Moreno *et al.*, 2015). Fe-bearing NPs of 5 – 50 nm usually occur in the form of spherical, agglomerated grains of metallic Fe with oxidized rims of magnetite and/or hematite (Figure 8A) (Salma *et al.*, 2009; Zhang *et al.*, 2011; Midander *et al.*, 2012; Querol *et al.*, 2012; Moreno *et al.*, 2015). Some studies identify hematite as the dominant Fe phase in subway airborne NPs (Salma *et al.*, 2009; Querol *et al.*, 2012); others find magnetite in the highest concentrations (Karlsson *et al.*, 2005; Zhang *et al.*, 2011). It is evident that the composition of particulate air pollution is variable with location, and hence, that impacts on human health may also differ by location. The Fe oxidation level is important in terms of health hazard (see Section 1.13. Specific toxicity of iron-bearing nanoparticles); thus more data are needed to quantify the magnetite/hematite contributions to total subway PM and if necessary, to identify and introduce mitigation measures limiting subway PM emissions (Tokarek & Bernis, 2006; Moreno & de Miguel, 2018).

Subway-derived Fe-bearing NPs may form from braking (Moreno *et al.*, 2015; 2017b; Namgung *et al.*, 2016; 2017), wheel/rail track interactions (Querol *et al.*, 2012; Lee *et al.*, 2018a; 2018b) or sparking between a third-rail and collectors (Salma *et al.*, 2009). The presence of co-existing metallic Fe (often with oxidized rims), magnetite, maghemite and hematite suggests that particular Fe oxides reflect increasing stages of oxidation (Moreno *et al.*, 2015).

Fe-rich subway particles have been found to be toxic (see Appendix A: Table A5), causing mitochondrial depolarization, inflammatory responses and generation of ROS (Karlsson *et al.*, 2005; 2006; 2008; Nieuwenhuijsen *et al.*, 2007; Loxham *et al.*, 2013; 2015; Janssen *et al.*, 2014; Moreno *et al.*, 2017a), especially in the case of fractions < 2.5 μm and < 0.18 μm (Loxham *et al.*, 2015). Karlsson *et al.* (2005) found that subway particles are 8 times more genotoxic than roadside PM collected nearby a very busy street. The high genotoxicity of subway-derived PM probably results from synergistic effects of Fe-, Cu- and Zn-bearing, subway-derived pollution, possibly in the fraction < 0.1 μm (Karlsson *et al.*, 2008; Loxham *et al.*, 2015).

Trams and trains generate similar Fe-bearing NPs (e.g. Muxworthy *et al.*, 2002; Bukowiecki *et al.*, 2007; Gehrig *et al.*, 2007; Kardel *et al.*, 2012), which may be particularly hazardous at subway stations and/or tunnels due to confined spaces, poor ventilation and high congestion. Hence, commuters using underground systems are exposed to high levels of metal-rich, potentially hazardous airborne particulates (Knibbs *et al.*, 2011).

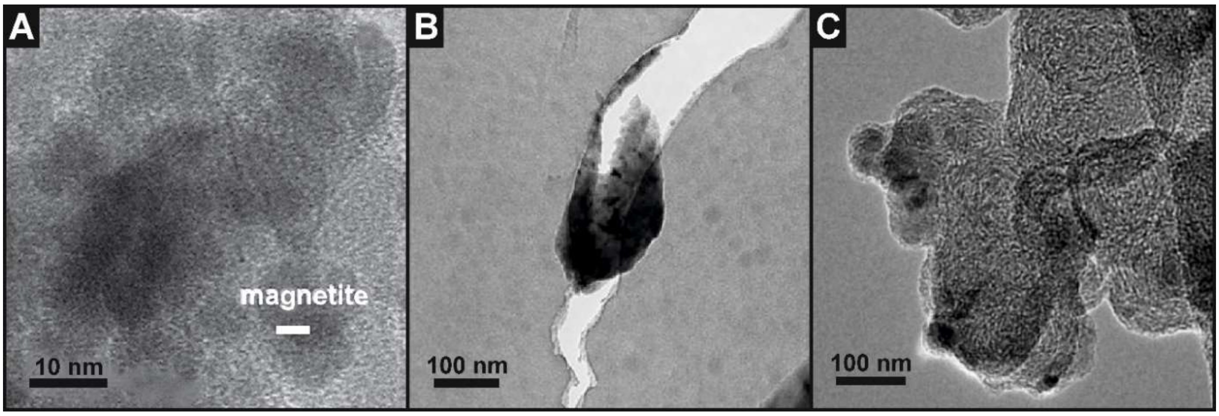

Figure 8. TEM images of (A) magnetite NPs found in subway PM (adapted from Moreno *et al.* (2015)) and (B) aircraft-derived NPs containing mainly Fe, Cr and Ni (adapted from Mazaheri *et al.* (2013)), (C) ship-derived soot particles with V-, Fe- and Ni-bearing speckles of 5-10 nm (adapted from Streibel *et al.* (2017)).

1.9. Aircraft emissions

Masiol & Harrison (2014) have reviewed aircraft emissions and other airport-related contributions to ambient air pollution. Airports, and their associated road traffic, are a source of Fe-bearing NPs.

Nanoparticulate aircraft emissions are dominated by soot particles, accompanied by smaller amounts (4 – 6 wt.%) of Fe (Popovicheva *et al*., 2004; Demirdjian *et al*., 2006; Lelièvre *et al*., 2006; Amato *et al*., 2010; Fine *et al*., 2010; Mazaheri *et al*., 2013) and other metals, including Cr, Ni, Ca and K (Lelièvre *et al*., 2006; Mazaheri *et al*., 2013).

Number-normalized PSDs of aircraft emissions are dominated by NPs (< 100 nm), with a main peak at ∼10 – 20 nm (Petzold *et al*., 1999; Biswas *et al*., 2005; Westerdahl *et al*., 2008; Hu *et al*., 2009; Mazaheri *et al*., 2013; Masiol *et al*., 2016; 2017).

From TEM and EDX, aircraft-derived Fe-bearing NPs occur in the form of magnetite and/or maghemite (Figure 8B) (Demirdjian *et al*., 2006). The presence of Fe in soot agglomerates might arise from chemical/mechanical corrosion of the liquid fuel atomizer (Demirdjian *et al*., 2006). Fe-bearing NPs in aircraft emissions might also originate from impurities in the kerosene fuel (Popovicheva *et al*., 2004).

Aircraft emissions are reported to have deleterious health impacts both globally and locally (Unal *et al*., 2005; Barrett *et al*., 2010). Aircraft-generated NPs, at Santa Monica

Airport, Southern California, USA, occurred at concentrations 11, 10, 5 and 2.5 times the background value for sites at distances from the airport of 80 m, 100 m, 380 m and 660 m, respectively (Hu *et al.*, 2009). Enhanced, aircraft-derived levels of NPs (up to 20 x background concentrations) persisted up to 900 m from a take-off area (Biswas *et al.*, 2005; Westerdahl *et al.*, 2008; Hu *et al.*, 2009), thus likely exerting an adverse influence on adjacent neighborhoods (see Appendix A: Table A5). Furthermore, there have recently been several lawsuits related to 'aerotoxic syndrome', linked to occupational exposure to polluted cabin air and associated with severe headaches, mental confusion, sight problems, insomnia, digestive and respiratory problems, and even death (Ramsden, 2016). The impacts of aircraft emissions on human health are poorly understood, but some evidence indicates that occupational exposure of airport personnel and aircraft crew has detrimental effects (Cavallo *et al.*, 2006; Schindler *et al.*, 2013; Masiol & Harrison, 2014; Harrison *et al.*, 2015; Ramsden, 2016; He *et al.*, 2018).

1.10. Shipping emissions

Shipping emissions, derived from combustion of so-called 'bunker fuel', affect air quality both locally (Saxe & Larsen, 2004; Healy *et al.*, 2010; Pandolfi *et al.*, 2011; Zhang *et al.*, 2014; 2017) and globally (Corbett & Koehler, 2003; Endresen *et al.*, 2003; Eyring *et al.*, 2010).

Most studies to date have focused on NO_x, SO_2, CO and CO_2 as they constitute the majority of ship-derived emissions (Isakson *et al.*, 2001; Endresen *et al.*, 2003; Saxe & Larsen, 2004; Chen *et al.*, 2005; González *et al.*, 2011; 2013; Juwono *et al.*, 2013). Fe-bearing particles occur in the $PM_{2.5}$ fraction in concentrations up to 10 $\mu g/m^3$ (Agrawal *et al.*, 2008; Healy *et al.*, 2009; Moldanová *et al.*, 2009; 2013; Popovicheva *et al.*, 2009; 2012; Zhang *et al.*, 2014; Oeder *et al.*, 2015; Streibel *et al.*, 2017; Corbin *et al.*, 2018), usually accompanied by other metals, including V, Ni, Zn, Ca, Na, P (Moldanová *et al.*, 2009; 2013; Popovicheva *et al.*, 2009; 2012; Oeder *et al.*, 2015). Using cluster analysis of elemental composition and electron microscopy observations, Popovicheva *et al.* (2012) distinguished 5 groups of particles in shipping emissions. The Fe-rich group, constituting ~3 – 4% of all PM mass, comprised ~50% Fe, with smaller portions of Si, S and Ca.

Shipping-derived Fe-bearing particles occur usually in the fraction < 100 nm, in the form of ~5 – 10 nm inclusions in soot particles (Figure 8C) (Streibel *et al.*, 2017; Corbin *et al.*, 2018). The NPs have been observed in the forms of Fe_2O_3, Fe_2S, Ni_2Fe, Ni_3Fe, $Ni_3Fe_2O_3$ and $NiFe_2O_4$ (Popovicheva *et al.*, 2009; 2012).

Those inclusions are formed as a result of the decomposition or oxidation of Fe-bearing minerals in heavy fuel oil, and/or corrosion of the engine (Popovicheva *et al.*, 2012).

Exposure to shipping-derived particles (see Appendix A: Table A5) results in acute cytotoxic effects in cell cultures *in vitro* (Oeder *et al.*, 2015; Sapcariu *et al.*, 2016) and oxidative stress (Mousavi *et al.*, 2019). Shipping emissions are related to ~60,000 cardiopulmonary and lung cancer deaths annually (Corbett *et al.*, 2007). In busy ports, the health impacts of shipping-derived Fe-bearing NPs are additive to the NP loadings from associated road/freight traffic.

1.11. Source apportionment of roadside-derived PM

Estimation of the contributions made by specific sources to total airborne PM or PNC is often difficult, and variable between different studies (Figure 9) (Ketzel *et al.*, 2007; Bukowiecki *et al.*, 2009a; Harrison *et al.*, 2011; 2012; Lawrence *et al.*, 2013; Vu *et al.*, 2015; Squizzato *et al.*, 2016; Crilley *et al.*, 2017). For a street canyon in Zurich, and using elemental data and positive matrix factorization (PMF) to distinguish between sources, Bukowiecki *et al.* (2009a) found that brake-wear, exhaust emissions and resuspension contributed 21%, 41% and 38% of total traffic-derived PM_{10} mass, respectively (Figure 9B). Lawrence *et al.* (2013) studied PM in a tunnel in Hatfield, UK, relying on principal component analysis (PCA) and multiple linear regression analysis, and reported that resuspension was responsible for 27% of PM_{10} mass, diesel emissions for 21%, gasoline emissions for 12%, brake-wear for 11%, road surface wear for 11%, with 18% of PM_{10} mass not attributed to any source. Harrison *et al.* (2012) studied roadside PM at a busy London street, assessing the contribution of non-exhaust emission sources using specific elemental tracers, i.e. Ba for brake emissions and Zn for tire emissions. They found that the mass of brake-wear (0.9 – 11.5 μm) was higher than that of resuspended dust (55.3 ± 7.0 % versus 38.1 ± 9.7 % of non-exhaust emissions). In this study, 10.7 ± 2.3 % of non-exhaust PM (0.9 – 11.5 μm) was attributed to tire wear (Figure 9A).

Some source apportionment studies have considered particle number and volume of PM_{10} (e.g. Harrison *et al.*, 2011; Vu *et al.*, 2015). The authors found that exhaust emissions accounted for 22.4% of total volume and 65.4% of total number, brake dust – 13.7% of total volume and 1.7% of total number, and resuspension – 4.4% of total volume and 4.8% of total number. Tire wear emissions were not identified in this study (Harrison *et al*., 2011).

Discrepancies between these estimates probably reflect the differing methodologies, instruments and characteristics of the sampling sites. There is presently no unambiguous tracer of resuspended dust, which makes estimation of the resuspension contribution challenging (Pant & Harrison, 2013). Pant & Harrison (2013) provide a detailed description of methodologies for the assessment of source apportionment of urban PM.

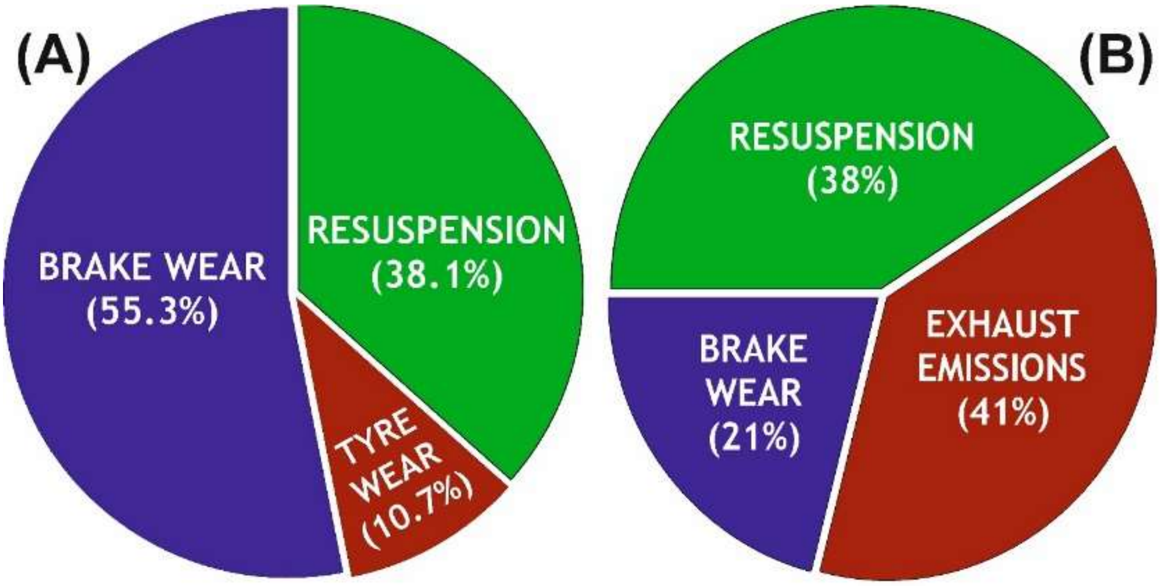

Figure 9. Source apportionment of (A) non-exhaust PM emissions (adapted from Harrison *et al.* (2012)) and (B) total traffic-derived PM (adapted from Bukowiecki *et al.* (2009a)).

Around the world, there are numerous emission standards limiting exhaust emissions, e.g. European Emission Standard (EURO) in European Union (EU), Tier motor vehicle emission and fuel standards in USA, WLTC-based (Worldwide Harmonized Light Vehicles Test Cycle) regulation in Japan, or Bharat Stage regulation in India (DieselNet. Engine & Emission Technology Website). In response to increasing regulation, the automotive industry has sought, with varying measures and outcomes, to reduce exhaust emissions. Non-tailpipe emissions are currently unregulated; yet constitute a similar proportion of total mass traffic-derived PM as exhaust emissions (Figure 9B) (Harrison *et al*., 2001; Querol *et al*., 2004; Bukowiecki *et al*., 2009a). Resuspension may become a more substantial source of roadside

PM, as electrification (both electric engines and regenerative braking systems) of the vehicle fleet will decrease both exhaust and brake-wear emissions (Timmers & Achten, 2016). Further research is needed to quantify the resuspension contribution to roadside PM.

1.12. Magnetic measurements of vehicle-derived, Fe-bearing nanoparticles

The majority of the Fe-bearing particles emitted by vehicles occur as ferromagnetic (*sensu lato*) – i.e. magnetically ordered minerals, especially as magnetite (Fe_3O_4), maghemite (γ-Fe_2O_3), hematite (α-Fe_2O_3) and metallic α-Fe (Muxworthy *et al*., 2002; 2003; Halsall *et al*., 2008; Maher *et al*., 2008; Mitchell & Maher, 2009; Hansard *et al*., 2011; 2012; Sanderson *et al*., 2016; Jeleńska *et al*., 2017). Thus, magnetic analyses, based on concentration- and magnetic grain size-dependent parameters, enable characterization and quantification of vehicle-derived PM (e.g. Matzka & Maher, 1999; Muxworthy *et al*., 2002; 2003; Spassov *et al*., 2004; Mitchell & Maher, 2009).

Magnetic methods have enabled mapping of heavy metal contaminations in soils (e.g. Hoffmann *et al*., 1999; Hanesch & Scholger, 2002; Magiera *et al*., 2006), as well as PM concentrations in the urban atmosphere (e.g. Hanesch *et al*., 2003, Moreno *et al*., 2003; Davila *et al*., 2006; Hansard *et al*., 2011; 2012; Kardel *et al*., 2012). Hofman *et al*. (2017) review data from biomagnetic monitoring studies of air pollution (see also Appendix A: Table A8).

Significant correlation has frequently been found between PM_{10}, NO_X, heavy metal content and concentration-dependent magnetic properties (e.g. magnetic susceptibility, saturation isothermal remanent magnetization) of PM (Figure 10) (Matzka & Maher, 1999; Muxworthy *et al*., 2003; Spassov *et al*., 2004; Maher *et al*., 2008; Mitchell & Maher, 2009; Hansard *et al*., 2011; Jordanova *et al*., 2012; Kardel *et al*., 2012). The magnetite content of roadside PM_{10} appears greater than PM_{10} from a power generation emissions stack (Figure 10C) (Hansard *et al*., 2011). An early study identified strong correlation ($n = 55$; $R^2 = 0.79$) between magnetic susceptibility of airborne PM and mutagenicity (Morris *et al*., 1995). Moreover, other composition- and magnetic grain size-dependent magnetic parameters (e.g. hysteresis properties, first-order reversal curves) have often been helpful in the distinction between different sources of vehicle-derived pollutants (e.g. Sagnotti *et al*., 2006; 2009; Sagnotti & Winkler, 2012). For example, Sagnotti *et al.* (2006) and Sagnotti & Winkler (2012) showed that exhaust emissions have distinctive magnetic hysteresis properties compared to brake-wear emissions.

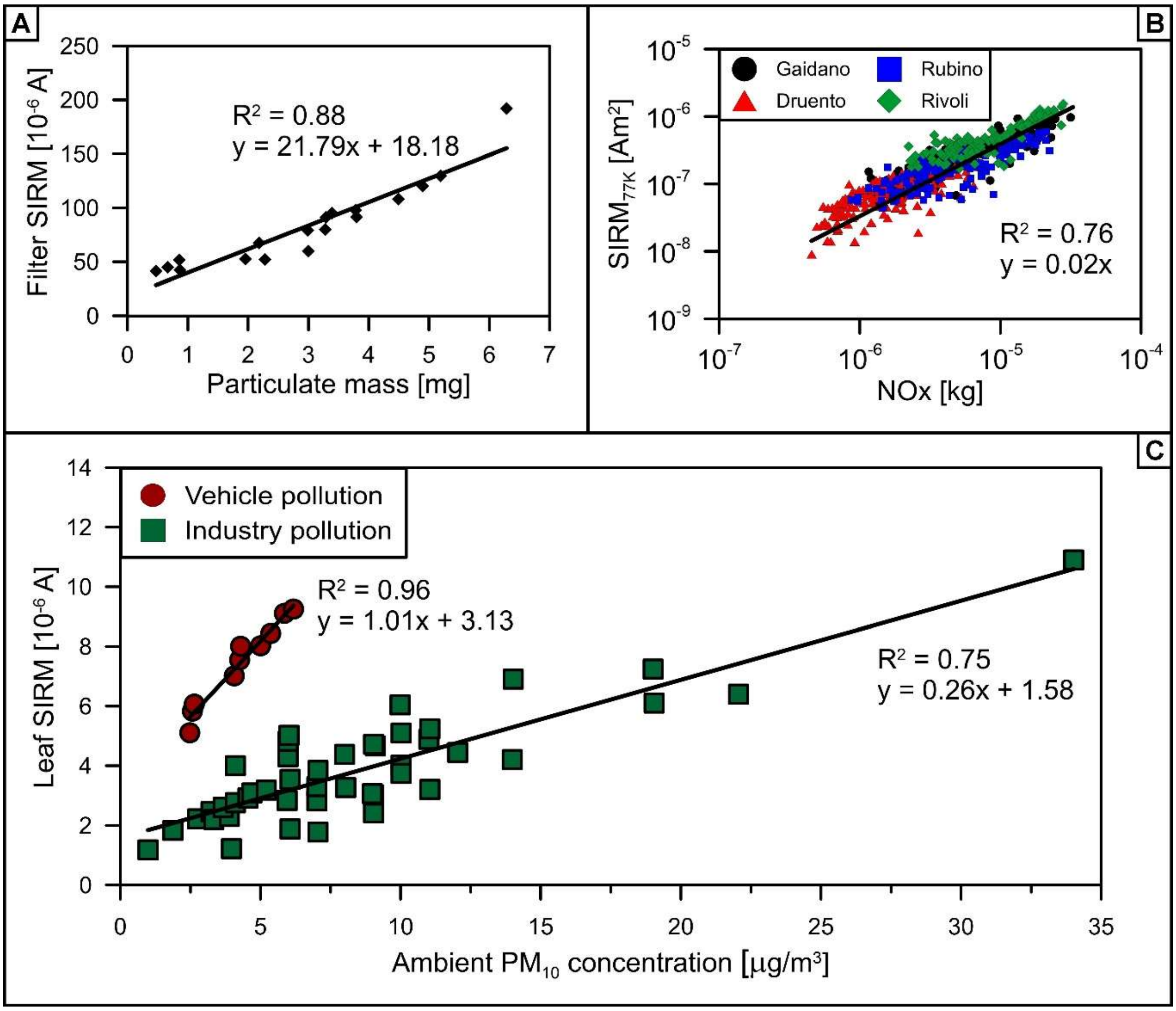

Figure 10. Correlation between: (A) air filter SIRM and roadside PM_{10} mass in Lancaster, U.K. (adapted from Mitchell & Maher (2009)); (B) air filter SIRM at 77K ($SIRM_{77K}$) and concentration of total nitrogen oxides (NO_X) at the roadside, in Turin, Italy (adapted from Saragnese *et al.* (2011)); (C) leaf SIRM and ambient PM_{10} concentrations, derived from vehicle pollution and industrial stack point source pollution (adapted from Mitchell *et al.* (2010) and Hansard *et al.* (2011)).

Magnetic NPs < 30 nm in size display distinctive magnetic behavior; they are 'superparamagnetic' (SP), unable to hold a magnetic remanence at room temperature, due to thermal agitation of their magnetic moments. Several magnetic studies have reported on the ultrafine, SP fraction of airborne roadside pollution (Muxworthy *et al*., 2002; 2003; Sagnotti *et al*., 2006; 2009; Sagnotti & Winkler, 2012; Saragnese *et al*., 2011; Szönyi *et al*., 2007; 2008). In Munich, Germany, SP ferrites contributed ~22% to the total saturation isothermal remanent magnetization (SIRM) of roadside PM and the SP fraction was dominated by 10 – 16 nm grains of maghemite and 5 – 8 nm grains of α-Fe (Muxworthy *et al.*, 2002). Higher SP contributions to the SIRM of roadside PM, even up to 88%, have since been reported (Sagnotti *et al.*, 2006; Saragnese *et al.*, 2011), possibly reflecting different measurement temperatures. Muxworthy *et al.* (Muxworthy *et al.*, 2002) measured SIRM at 77 K, Sagnotti *et al.* (2006) at 4 K and Saragnese *et al.* (2011) at 15 K. Due to thermal agitation, grains of magnetite < 16 nm, maghemite < 22 nm and hematite < 11 nm are unable to retain magnetic remanence at 77K (Dunlop, 1973; Özdemir *et al.*, 1993; Bødker & Mørup, 2000; Pankhurst *et al.*, 2008) and therefore are magnetically 'invisible' at this temperature. It should be noted that the SP fraction might occur not only as discrete magnetic grains < 30 nm in size but also as oxidized rims around larger particles (Özdemir *et al.*, 1993).

Magnetic PM, containing redox-active Fe, might not only be harmful to human health on its own; it is also usually associated with other toxic components, including Ba, Br, Cr, Cu, Mn, Mo, Ni, Pb, Zn (Spassov *et al.*, 2004; Chen *et al.*, 2006; Kim *et al.*, 2007; Maher *et al.*, 2016; Yang *et al.*, 2016) and PAHs (Lehndorff & Schwark, 2004; Jordanova *et al.*, 2012).

Critically, although Fe-bearing fine (< 2.5 μm) and nano-sized (< 0.1 μm) particles are present in almost all types of traffic-derived emissions (see previous sections), the magnetic signatures of specific particle sources appear to be distinctive (Figure 11; see also Appendix A: Table A8). For example, the ferrimagnetic content of brake-wear PM greatly exceeds that of many other PM sources (Figure 11). Furthermore, the SP fraction of brake-wear emissions contributes ~35% of SIRM, compared to 20% SP contribution in gasoline tailpipe emissions (Sagnotti *et al.*, 2009; Sagnotti & Winkler, 2012). Component analysis of magnetic coercivity distributions of roadside PM_{10} in Switzerland enabled identification of two magnetic components/PM sources: the first (C1), resuspended dust (a mixture of natural and anthropogenic street dust); the second (C2), traffic exhaust emissions (Figure 12) (Spassov *et al.*, 2004).

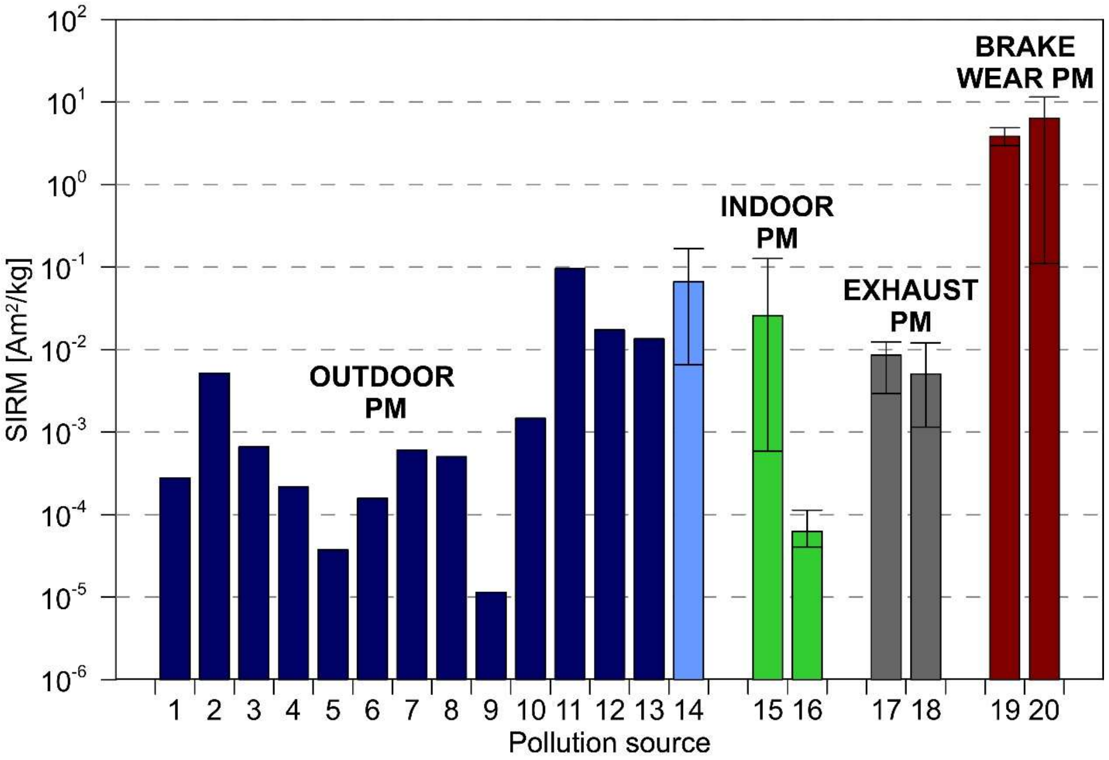

Figure 11. Saturation magnetic remanence (SIRM) for indoor and outdoor PM (adapted from Halsall *et al.* (2008) and Hansard *et al.* (2012)), exhaust and brake-wear emissions (Gonet *et al.*, 2021b): 1, wood fired boiler; 2, coal fired boiler; 3, gas/oil boiler; 4, oil fired boiler; 5, gas kettle incinerator; 6, coal fired power station; 7, gas/oil power station; 8, graphite plant; 9, smelting plant; 10, coke; 11, sinter; 12, BOS slag; 13, iron ore pellets; 14, roadside filters from Halsall *et al.* (2008); 15, indoor filters from Halsall *et al.* (2008); 16, printer dust; 17, diesel emissions from Gonet *et al.* (2021b); 18, gasoline emissions from Gonet *et al.* (2021b); 19, airborne brake-wear emissions, from Gonet *et al.* (2021a); and 20, non-airborne brake emissions, from Gonet *et al.* (2021a).

Conventional, elemental analysis of Fe, which is present in high concentrations at urban roadsides (see previous sections) cannot differentiate between its different vehicular sources. In contrast, magnetic methods of PM analysis can distinguish between different Fe minerals and oxidation states (Fe^{2+} vs Fe^{3+}), information of particular potential value regarding Fe-bearing NP toxicity and human health impacts (see Section 1.13. Specific toxicity of iron-bearing nanoparticles). Moreover, given distinctive magnetic fingerprints from different PM sources, combining elemental and magnetic analyses may enable more accurate and precise source apportionment (cf. Figure 12).

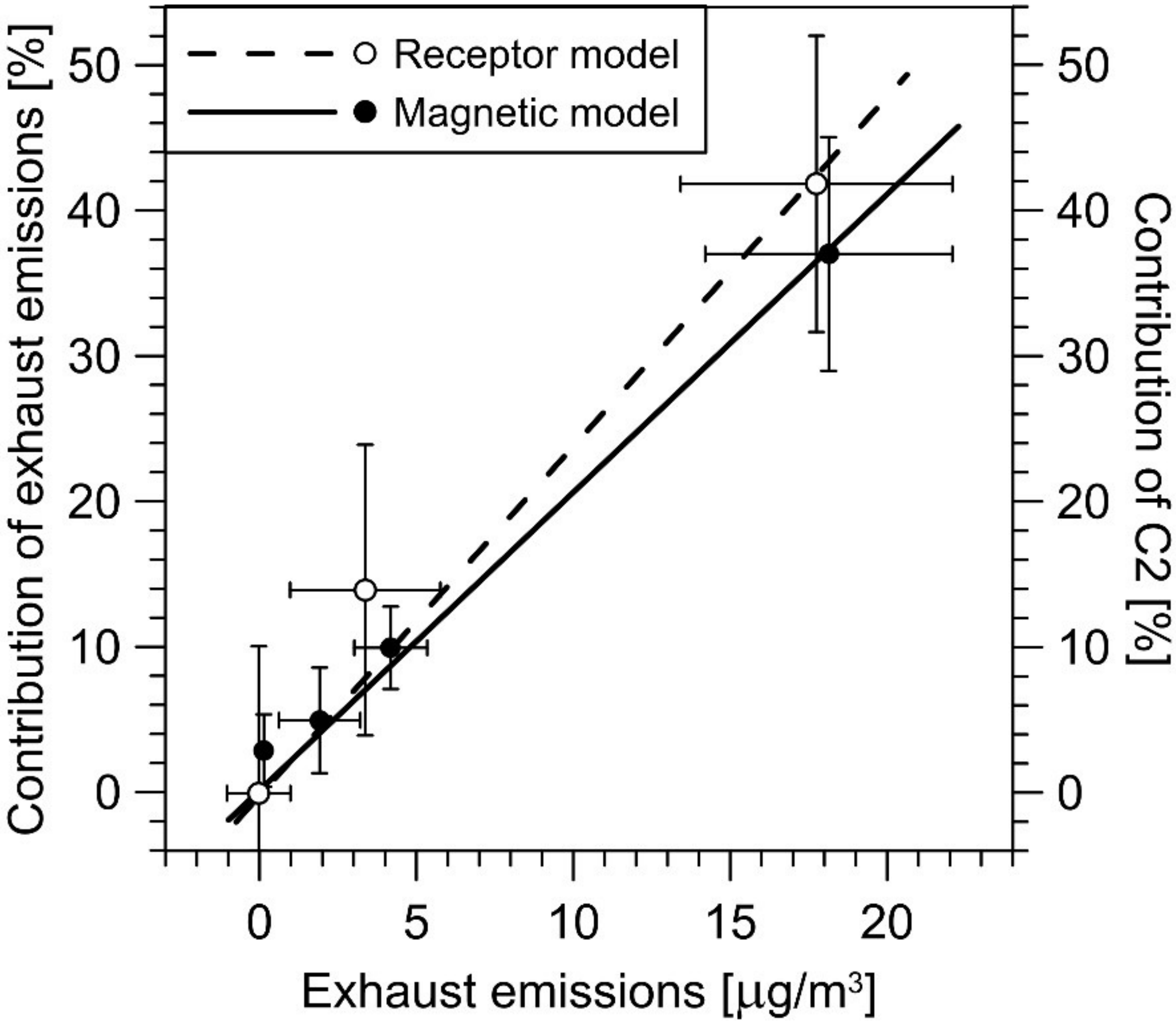

Figure 12. Absolute and relative contributions of exhaust emissions to PM_{10} at several sites in Switzerland. Open circles and dashed best-fit line refer to the receptor model (chemically estimated PM_{10} mass contribution of exhaust emissions). Solid dots and the solid best-fit line refer to the magnetic model, where component C2 (identified using magnetic component analysis) corresponded to exhaust emissions (adapted from Spassov *et al.* (2004)).

1.13. Specific toxicity of Fe-bearing nanoparticles

Exposure to airborne Fe-bearing NPs may be particularly hazardous to human health due to their high bioreactivity and potential toxicity, combined with their abundance in the urban environment. Numerous studies have shown that Fe plays an important role in the generation and pathogenicity of ROS (Ghio *et al.*, 1992; Dusseldorp *et al.*, 1995; Gilmour *et al.*, 1996; Donaldson *et al.*, 1997; Valavanidis *et al.*, 2000; Aust *et al.*, 2002; Ghio & Cohen, 2005; Li & Reichmann, 2016; Pelclova *et al.*, 2016; Moretti *et al.*, 2019). Dusseldorp *et al.* (1995) found that airborne Fe was associated with exacerbation of some respiratory symptoms. Fe-rich particles have been shown to generate ROS and provoke an inflammatory response (Aust *et al.*, 2002). These findings are supported by the results obtained by Pelclova *et al.* (2016) who found elevated oxidative stress markers in exhaled breath condensate of workers exposed to NPs during Fe oxide pigment production (see also Appendix A: Table A5).

The presence in the human brain specifically of magnetite, a strongly magnetic, mixed Fe^{2+}/Fe^{3+} oxide, is important because it has been causally linked with neurodegenerative diseases. Magnetite in brain tissue has been observed to be directly associated with AD plaques (e.g. Collingwood & Dobson, 2006; Quintana *et al.*, 2006; Plascencia-Villa *et al.*, 2016) and correlated (albeit with rather small sample size) with the incidence of AD (Hautot *et al.*, 2003; Pankhurst *et al.*, 2008). Neuropathological changes associated with AD include the formation of senile plaques, containing amyloid-*β* fibrils. When associated with redox-active transition metal ions, such as the Fe^{2+} ions contained within magnetite, amyloid-*β* can generate damaging ROS, directly contributing to oxidative brain damage, a key early feature of AD (e.g. Castellani *et al.*, 2007; Allsop *et al.*, 2008; Tabner *et al.*, 2010). *In vitro* experimental data additionally show that magnetite acts synergistically to enhance the toxicity of amyloid-*β* (Allsop *et al.*, 2008; Teller *et al.*, 2015). Moreover, higher concentrations of magnetite have been also detected in brain tumor tissue, in meningioma (Kobayashi *et al.*, 1997; Brem *et al.*, 2006) and in diseased hippocampal tissues (Dobson & Grassi, 1996), compared to healthy brain tissue.

In vitro studies on A549 human epithelial cells have shown that exposure to magnetite (Fe_3O_4) leads to acute cytotoxic effects and generation of ROS (Könczöl *et al.*, 2011). In the case of the NP fraction (< 0.1 μm), the health response (DNA damage) was more severe than with larger particles (0.2 – 10 μm) (Könczöl *et al.*, 2013). Assessment of the 'theranostic' use of SP iron oxide nanoparticles (SPIONs) has also shown that exposure to these particles can lead to toxic effects, including DNA damage, ROS generation, chromosome condensation, formation of apoptotic bodies, inflammation, impaired mitochondrial function and membrane leakage of lactate dehydrogenase (e.g. Apopa *et al.*, 2009; Naqvi *et al.*, 2010; Singh *et al.*, 2010; Feng *et al.*, 2018; see also Appendix A: Table A5).

Fe^{2+} is toxic as it may cause the generation of ROS via the Fenton reaction (Smith *et al.*, 1997):

$$H_2O_2 + Fe^{2+} \rightarrow OH^{\cdot} + OH^{-} + Fe^{3+} \qquad (1)$$

The hydroxyl radical ($OH^{\cdot}$) is especially dangerous in brain tissue as it might cause oxidative stress, which is a hallmark of neurodegenerative diseases like AD (e.g. Castellani *et al.*, 2007; Allsop *et al.*, 2008; Tabner *et al.*, 2010). Until recently, the magnetite particles found in the human brain were assumed to be entirely of *in situ*, biogenic origin (Kirschvink *et al.*, 1992; Schultheiss-Grassi *et al.*, 1999). It has been suggested that the normal processes for safe storage (within ferritin cores) and transport of the brain Fe become dysfunctional as a result of neurodegeneration (e.g. Castellani *et al.*, 2007). However, Maher *et al.* (2016) identified, for the first time, the abundant presence in the human brain of externally-derived, magnetite pollution NPs. These magnetite NPs displayed a range of particles sizes (from ~10 to 150 nm), were frequently rounded or even spherical, and often associated with other 'exotic' transition metal NPs, containing Pt, Ni, Co, and Cu. Some have fused surface crystallites that would be very difficult to reconcile with *in situ*, low temperature growth or dissolution formation processes.

Thus, airborne magnetic pollution NPs may pose a threat to human health due to their bioreactivity, their ability to penetrate every organ, including the brain, their link with neurodegenerative diseases and their abundance in the urban atmosphere.

1.14. Perspectives and outlook

Many studies have identified adverse health effects associated with exposure to particulate air pollution (e.g. Calderón-Garcidueñas *et al.*, 2002; Beelen *et al.*, 2014). Traffic-derived emissions are a major source of urban PM, constituting up to 80% of airborne concentrations of PM in the urban environment (Pant & Harrison, 2013). Hence, improved understanding of the biological interactions induced in the human body by traffic-derived PM is of critical importance for identifying their specific pathways of impact, and relative priority in terms of their abatement and/or mitigation.

Metal-bearing NPs may be especially hazardous to human health. Studies on mouse models and human epithelial cells have demonstrated the detrimental impact of NPs (e.g. Donaldson *et al.*, 2005; Oberdörster *et al.*, 2005), with Fe-bearing NPs of particular potential hazard (e.g. Gilmour *et al.*, 1996; Valavanidis *et al.*, 2000). Combustion- and friction heating-derived, Fe-bearing NPs found in human brain (Maher *et al.*, 2016) are especially worrisome, due to the high redox activity of magnetite and its potential association with neurodegenerative diseases, such as Alzheimer's or Parkinson's diseases (Smith *et al.*, 1997; Maher *et al.*, 2016; Plascencia-Villa *et al.*, 2016). Given the abundant occurrence of Fe-bearing NPs in the environment (indoor and outdoor), workplace, and in biomedical applications, and the inconsistency of the data reporting their effects on biological systems, more systematic studies on nano-sized, Fe-bearing particles are needed in order to define their toxic potential.

Traffic-related air pollution has been shown to be associated with respiratory, cardiovascular and neurological problems (e.g. Calderón-Garcidueñas *et al.*, 2002; Hoek *et al.*, 2013). However, little is known about long-term health effects of ambient NPs. Recently, studies have examined regression models of health outcomes and the spatial distribution of NPs (e.g. Hoek *et al.*, 2011; Weichenthal *et al.*, 2016a; 2016b; 2017a; 2017b; Van Nunen *et al.*, 2017). These models can be useful in the assessment of chronic health effects of NPs using population-based cohorts. Ostro *et al.* (2015) observed statistically significant associations between ischemic heart disease (IHD) mortality and both $PM_{2.5}$ and $PM_{0.1}$ fractions. Moreover, some specific components were observed to be independently associated with IHD mortality, including gasoline/diesel emissions and metals (Fe and Cu) (Ostro *et al.*, 2015). The results of Weichenthal *et al.* (2017b) suggest that exposure to ambient NPs is directly associated with the incidence of prostate cancer. Bai *et al.* (2018) found that chronic exposure to NPs may increase the incidence of hypertension and diabetes. Land use regression models can potentially be used, along with actual NP concentration measurements, as a basis for an assessment of human chronic exposures to NPs. Interestingly, Weichenthal *et al.* (2017a) did not observe evidence of positive associations between modelled long-term NP exposure and the incidence of respiratory disease.

It is worth emphasizing that humans are variably exposed not to a single, individual traffic-related source of particulates, but to a complex mixture of them. Some of the deleterious effects of particular particles/compounds can be accelerated by the presence of others. For example, adverse effects (for instance, lipid peroxidation in brain tissue) of Fe-bearing particles (for instance, from brake-wear) are promoted by the presence of Al (for instance, from tire wear or natural, soil dust) (Campbell *et al.*, 2004). Although increasing numbers of epidemiological studies have identified associations between exposure to traffic-derived air pollution and detrimental health impacts, the specific mechanisms of these associations remain imperfectly understood.

Furthermore, PM composition is variable not only from city to city but also within cities, such that different populations are exposed to different pollution mixes. Hence, the impacts of exposure to PM on human health likely also differ by location.

Exhaust emissions have been legally regulated for over 25 years (e.g. in EU since 1992, in USA since 1994, in India since 1991) (DieselNet. Engine & Emission Technology Website). Initially, only the mass of CO (carbon monoxide), HC (hydrocarbons; in USA), NO_X (nitrogen oxides; in EU and USA), PM (in EU and USA), and NMHC (non-methane hydrocarbons; in USA) was limited. Subsequently, more parameters have been covered by these regulations, e.g. mass of VOC (volatile organic compounds) and PN (particle number) (DieselNet. Engine & Emission Technology Website). It seems highly probable that legal regulation concerning brake-wear emissions will be introduced in the near future, especially given their increasing importance as exhaust emissions decline with electrification of vehicle fleets. Given the growing evidence that Fe-bearing NPs may constitute a particular hazard to human health, regulation to limit these Fe-rich, strongly magnetic emissions may also become important and urgent, on an international scale.

Contributions of authors

Tomasz Gonet: Conceptualization, Writing – original draft, Writing - review & editing. **Barbara A. Maher**: Conceptualization, Supervision, Writing - review & editing.

Chapter Two: Brake-wear emissions – literature review

2.1. Traffic-derived PM emissions in the urban environment

Urban airborne PM is a complex mixture of emissions originated from a wide variety of natural (e.g. soil-derived or marine dust) and anthropogenic (e.g. traffic, biomass burning, train, aircraft or shipping emissions) sources. Traffic-derived emissions are often a dominant source of urban PM, especially at the roadside, constituting up to 80% of airborne concentrations of ambient PM_{10} (e.g. Thorpe & Harrison, 2008; Belis *et al.*, 2013; Pant & Harrison, 2013). Traffic-related PM includes engine exhaust emissions, i.e. diesel- and petrol-engine tailpipe emissions; and non-exhaust emissions, i.e. brake, tyre and road wear emissions, and resuspension of the roadside dust. Although the concentrations of exhaust emissions have decreased significantly in the last 20 years due to the more and more stringent legislation, non-exhaust emissions are currently unregulated. Yet non-exhaust emissions presently constitute a similar or even higher proportion of urban PM_{10} concentrations, compared to exhaust emissions (Figure 13) (e.g. Bukowiecki *et al.*, 2009a; Lawrence *et al.*, 2013; Denier van der Gon *et al.*, 2018; Piscitello *et al.*, 2021).

Legal regulations regarding harmful levels of air pollutants usually concern mass-based metrics, e.g. WHO outdoor air quality 24-hour mean limit values of 50 $\mu g/m^3$ for PM_{10} (particles with aerodynamic diameter smaller than 10 μm), or 25 $\mu g/m^3$ for $PM_{2.5}$ (particles with aerodynamic diameter smaller than 2.5 μm) (WHO, 2016). Such metrics are often dominated by larger particles (< 1 μm) because UFPs contribute very little to the total particle mass. Conversely, UFPs often predominate number-normalised PSDs and they are usually monitored as particle number concentrations (PNCs). In urban environments, UFPs are ubiquitous, albeit in spatially and temporally variable concentrations, depending on the proximity to major roads, traffic characteristics, local road structure and topography, time of the day, weather conditions and season (e.g. Rakowska *et al.*, 2014; Jeong *et al.*, 2015; Pasquier & André, 2017; Agudelo-Castañeda *et al.*, 2019). Although higher UFP levels (PNC > 30,000 $\#/cm^3$) are usually found in the close proximity to major roads (usually within 50 – 100 m of the road), UFPs are also present in residential areas, usually in lower concentrations (PNC < 15,000 $\#/cm^3$) (e.g. Kumar *et al.*, 2012; Jeong *et al.*, 2015; Hama *et al.*, 2017; Simon *et al.*, 2017).

Estimation of source apportionment of urban PM is challenging and variable between different studies (see also Section 1.11. Source apportionment of roadside-derived PM). Brake-wear PM has been reported to contribute ~11% – 21% to total PM_{10} mass (Bukowiecki *et al.*, 2009a; Lawrence *et al.*, 2013) and ~1.7% to PNC (Harrison *et al.*, 2011) in roadside environments.

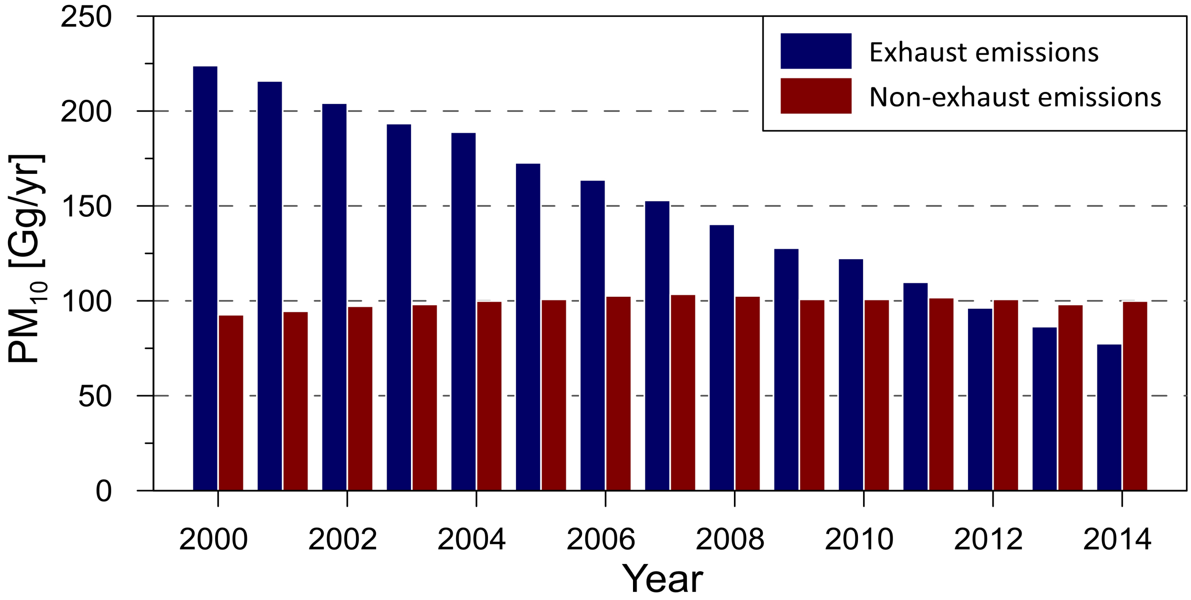

Figure 13. PM_{10} emissions from vehicle exhaust and non-exhaust sources for EU15, Norway and Switzerland (adapted from Denier van der Gon *et al.*, 2018).

2.2. Friction materials

PSD and chemical composition of brake-wear dust are complex and depend on temperature and other environmental conditions, the shape of brake pad, sliding speed, pressure, and chemical and physical properties of the friction couple (brake disc and brake pad). Currently, brake discs in passenger cars are usually made of cast iron. Brake pads typically consist of the following components (Eriksson *et al.*, 1999; Wang & Chung, 2013; JRC, 2014):

a) Fibres – providing mechanical stability. They usually contain various metals, carbon, glass or/and Kevlar.
b) Fillers – reducing the cost and improving manufacturability. Barite, calcite, magnetite and/or mica are commonly used.

c) Binders – maintaining structural integrity under mechanical and thermal stresses. Phenolic resins are widely used.
d) Additives – determining the frictional properties of brake pads. They comprise a mixture of lubricants (such as graphite) for decreasing the friction coefficient, and abrasives (such as Al oxide or Fe oxides), for increasing the friction coefficient and maintaining cleanliness between contact surfaces.

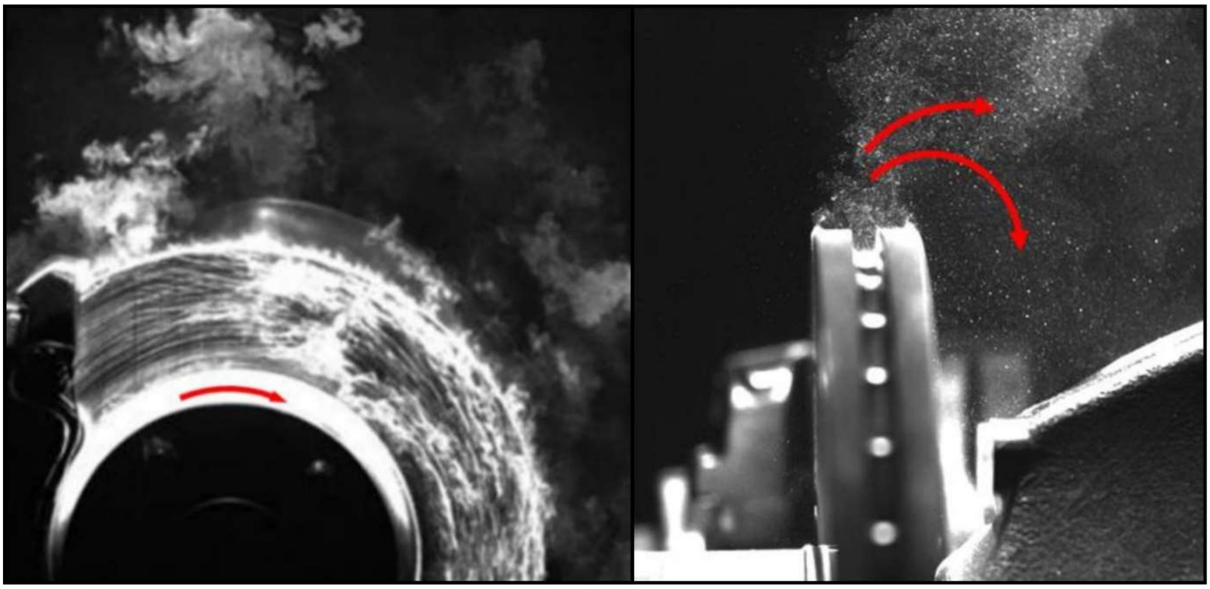

Figure 14. Particle injection and distribution (laser illuminated plane) in a vehicle braking system (adapted from Augsburg & Hesse, 2020).

Several thousand different raw materials have been used to produce brake pads by automotive manufacturers (Hulskotte *et al.*, 2014). Brake pads are typically categorised into three main types: semi-metallic (SM), low-metallic (LM) and non-asbestos organic (NAO) (Table 1). NAO brake pads are widely used in the Japanese market (a 2005-2010 survey; Hagino *et al.*, 2016) and in North America, while LM pads are more common in Europe. During braking, pad and disc materials are subjected to various chemical and mechanical processes and consequently, the structure and composition of the brake-wear dust are different from those of the original braking materials (Österle *et al.*, 2001; Kukutschová *et al.*, 2009; Kukutschová & Filip, 2018).

Table 1. Characteristics of main types of brake pads (Chan & Stachowiak, 2004).

Type of brake pad	Ingredients	Characteristics
Semi-metallic (SM)	Predominantly metallic – steel fibres	Highest durability, higher wear of disc than NAO
Low-metallic (LM)	Mixture of organic and metallic components	Higher friction performance than NAO, high durability
Non-asbestos organic (NAO)	Predominantly organic compounds, mineral fibres, graphite	Relatively softer than LM and SM, lower friction performance than LM and SM, sensitive to elevated temperature

2.3. Experiments and studies

Studies of brake-wear emissions are usually done in one of three ways. Firstly, pin-on-disc machines are used (e.g. Mosleh *et al*., 2004; Wahlström *et al*., 2010a; Nosko & Olofsson, 2017a; Tarasiuk *et al*., 2020). These are small-scale laboratory tests where pin samples of brake pads are pressed against the rotating disc. The second method is to use full-scale dynamometer testing (e.g. Sanders *et al*., 2003; Kukutschová *et al*., 2009; 2010; 2011; Aranganathan *et al*., 2016; Mamakos *et al*., 2019), which is more expensive but simulates the braking system and real-world conditions in a more robust and realistic manner. Finally, some researchers (e.g. Wahlström *et al*., 2010b; Harrison *et al*., 2012; Wahlström & Olofsson, 2014) have conducted field studies addressing the indirect detection of brake-wear emissions. Laboratory tests do not imitate real-world conditions perfectly but have the advantage of full control over experimental braking conditions. However, the variability of dynamometer testing procedures used worldwide represents a confounding factor in such tests (Table 2). Mass, number and composition of brake-wear emissions vary notably, depending on several dynamometer cycle parameters, e.g. temperature, speed, rate of deceleration (see also Section 2.7. Quantification of brake-wear emissions). On the other hand, the interpretation of field studies is more complicated due to numerous sources of roadside PM and the lack of a compelling and unambiguous method of assessing the contribution of brake-wear emissions to total atmospheric PM. For these reasons, the combination of laboratory dynamometer tests and field studies may be the most reliable approach to quantify airborne particle emission from brake-wear.

Table 2. Examples of the parameters used during various dynamometer cycles.

Reference	Temperature [°C]	Sliding speed [km/h]	Deceleration [m/s^2]
Garg *et al*. (2000)	100, 200, 300, 400	< 65	2.9
Sanders *et al*. (2003)	< 200	< 89	0.6 – 1.6
Kukutschová *et al.* (2009)	121 – 426	< 96	1.5 – 9.1
Hagino *et al*. (2015)	< 100	20, 40, 60	0.5 – 3.0
Hagino *et al*. (2016)	< 100	< 88	0.2 – 1.2
Perricone *et al.* (2017)	100 – 200	50, 80, 100	2.5 – 3.9

2.4. Chemical composition of brake-wear emissions

Garg *et al.* (2000) reported that brake-wear debris contains primarily carbonaceous and metal-bearing components. Fe is usually observed to be a dominant metal, sometimes constituting even more than 50 wt.% of all emissions (Sanders *et al.*, 2003; Adachi and Tainosho, 2004; Kukutschová & Filip, 2018). Figure 5 shows a TEM image and electron diffraction intensity data for ultrafine brake-wear particles collected during a dynamometer test. These data show that the brake-wear UFPs contain magnetite and elemental Fe (Kukutschová *et al*., 2010). The coarse fraction of brake-wear emissions (Figure 15) also contains Ba, Cu, Sb, Mg, Si and S. Other Fe oxides, including haematite, wüstite and maghemite, have also been observed in the ultrafine fraction of brake-wear emissions (e.g. Hinrichs *et al*., 2011a, 2011b; Peikertová *et al*., 2013; Verma *et al*. 2016). Although Fe-rich particles have been found in brake-wear particles in several studies (e.g. Sanders *et al.*, 2003; Kukutschová *et al*., 2010; 2011; Hinrichs *et al*., 2011a; 2011b; Hagino *et al*., 2016; Sanderson *et al*., 2016; Verma *et al*., 2016), little attention has yet been devoted to the identification of their properties (phase/mineralogical composition, concentrations of particular phases) or their potential health impact. In terms of elemental composition, besides Fe, brake dust emissions also contain a wide range of other elements, including Cu, C, Ba, Sb, Si, Al, Mo, S, Sn, Cd, Cr, Pb, Zr, Ti and Zn (e.g. Mosleh *et al*., 2004; Kukutschová *et* al., 2011; Peikertová *et* al., 2013; Kazimirova *et al*., 2016; Verma *et* al., 2016; Nosko & Olofsson, 2017b).

Some authors also emphasise the importance of organic brake-wear products (Gadd & Kennedy, 2000; Garg *et* al., 2000; Malachová *et al.*, 2016; Plachá *et al.*, 2017). Garg *et al.* (2000) suggested that hydrocarbon emissions could account for a significant amount of the post-braking mass loss, especially at higher (300 – 400ºC) temperatures. Malachová *et al.* (2016) studied non-airborne brake-wear originating from a friction couple of cast iron disc and LM brake pad, and found a great variety of organic compounds, with some of them being toxic, mutagenic and carcinogenic (e.g. fluoranthene, ethanone, benzophenone). Plachá *et al.* (2017) tested low-metallic brake pads in a dynamometer and found a number of organic compounds (including phenolic, aromatic aldehydes, S- and N-containing organic substances) in brake-wear debris. In that work, only one model of a LM brake pad was analysed. Further studies of various types of brake pads are needed in order to achieve greater understanding of the environmental and health hazards of organic brake-wear emissions.

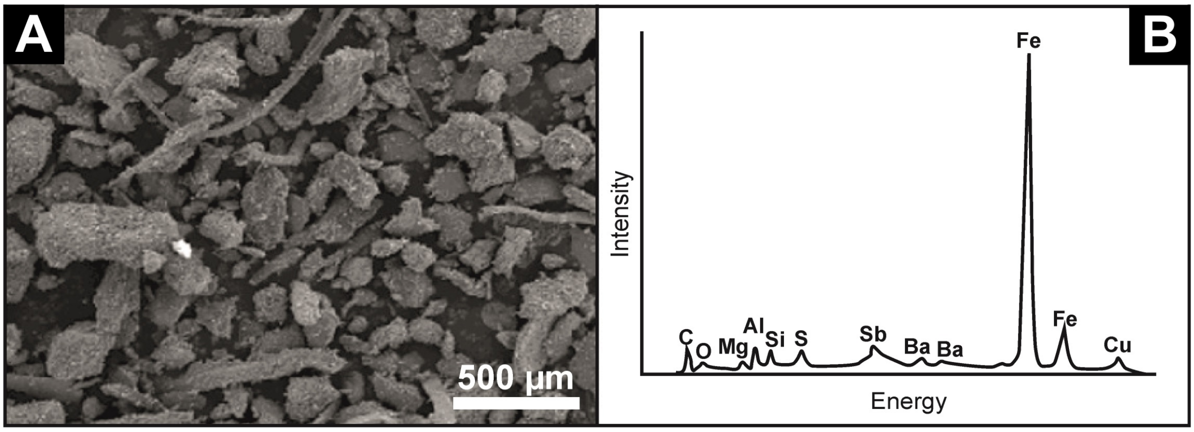

Figure 15. SEM image of coarse fraction of brake-wear debris (A) and SEM-EDX spectrograph of total area of coarse fraction of debris (B) (Kukutschová *et al.*, 2009).

2.5. Particle size distribution of brake-wear emissions

Generally, brake-wear mass increases with increasing temperature of brake pad/disc (Figure 16; Garg *et al.*, 2000; Filip *et al.*, 2002; Nisko & Olofsson, 2017; Niemann *et al.*, 2020). Below 200ºC, the abrasive processes dominate and larger (> 1 µm) wear particles are mostly generated. At higher temperatures (> 160 – 190ºC), the concentration of smaller particles (< 0.1 µm) increases considerably due to evaporation, condensation and aggregation processes (Garg *et* al., 2000; Kukutschová *et al.*, 2010; 2011; Verma *et al.* 2016; Piscitello *et al.*, 2021). Several studies observed that there is a critical temperature at which the ultrafine particle emission rate increases by 4 – 6 orders of magnitude, probably due to the decomposition of organic/inorganic binders (Ramousse *et al.*, 2001; Kukutschová *et al.*, 2011). It usually lies in the range between 160ºC and 240ºC (Nosko *et al.*, 2015; 2017; Alemani *et al.*, 2016; 2018; Perricone *et al.*, 2018; Farwick zum Hagen *et al.*, 2019b; Mathissen *et al.*, 2019; Niemann *et al.*, 2020). This critical temperature is lower than the decomposition temperature of the raw binder materials (~250 – 300ºC). Although the integral disc temperature is usually lower than ~130 – 155ºC in real-world conditions (Mathissen *et al.*, 2018; Farwick zum Hagen *et al*, 2019a), the local surface temperature in so-called 'hot spots' might be notably higher, resulting in the prolific generation of UFPs (Niemann *et al.*, 2020).

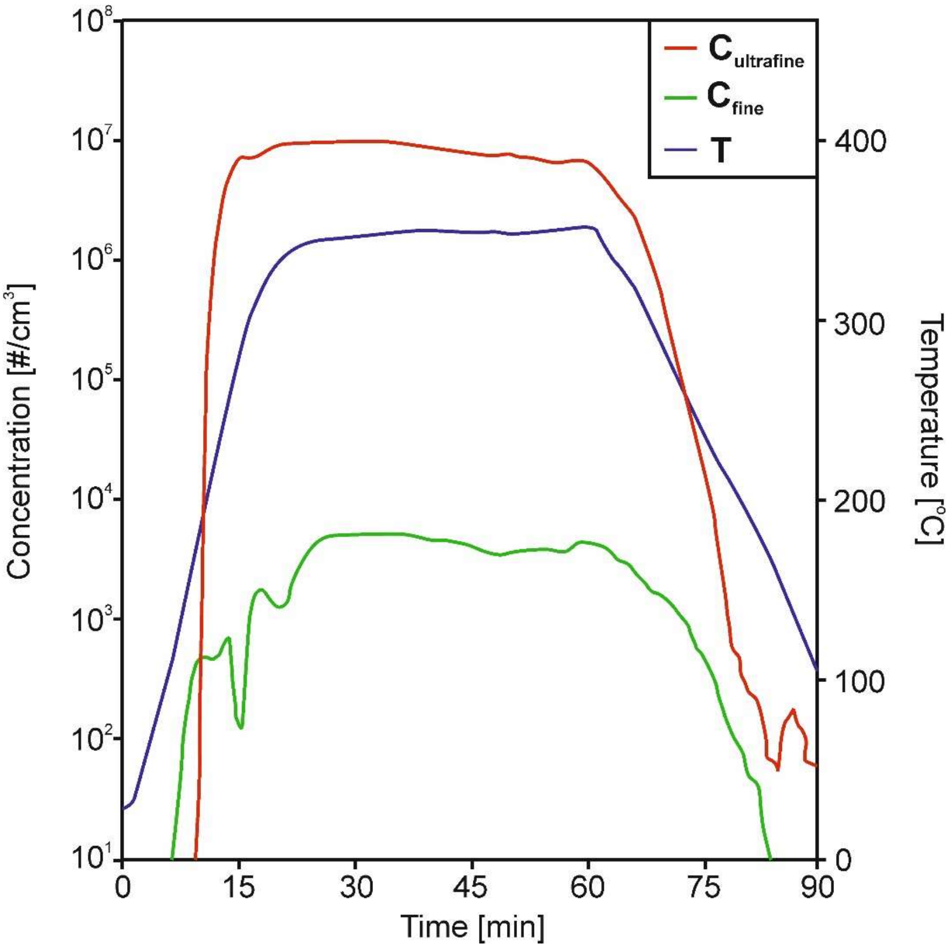

Figure 16. Particle number concentrations C_{fine} (0.1 – 10 μm), $C_{ultrafine}$ (< 0.1 μm) and temperature (T) vs. time during the dynamometer test (Nosko & Olofsson, 2017a).

In terms of mass-based metrics (e.g. PM_{10}), larger grains (> ~1 μm) dominate in total brake-wear emissions, usually with a unimodal mass-normalised PSD and peak ~2 μm – 6 μm (Sanders *et al.*, 2003; Iijima *et al.*, 2007; 2008; Kukutschová *et al.*, 2011; Harrison *et al.*, 2012; Grigoratos & Martini, 2015). Conversely, as shown by several studies, the number concentration of UFPs emitted is usually higher (by several orders of magnitude) compared to larger (> 0.1 μm) particles (e.g. Kukutschová *et al.*, 2011; Sanderson *et al.*, 2016; Verma *et al.*, 2016; Nosko & Olofsson 2017a). Appendix A: Table A6 shows total particle number and mass of brake dust emissions obtained with the ELPI+ impactor (DEKATI, Finland) during a dynamometer test (Verma *et al.* 2016). Each stage corresponds to different mean aerodynamic diameter (D_i). The ultrafine fraction (< 0.1 μm) constitutes > 90% of total particle number. Similar results were obtained by Garg *et al.* (2000); they reported that most particles emitted were smaller than 30 nm (see also Figure 3).

2.6. Tracers of brake-wear emissions

Quantification of brake-wear emissions in the environment presents serious challenges due not only to variability of braking conditions, but also the great diversity of friction materials used for manufacturing brake pads. Sternbeck *et al.* (2002) proposed a Cu:Sb mass ratio of 4.6 ± 2.3 in airborne PM as a diagnostic criterion for brake-wear emissions. However, further studies (Figure 17; Table 3) reported substantial differences in the ratio (from 1.3 up to 10.0) probably due to various compositions of the friction couple and contributions of metals from other sources. Moreover, Sb has been found in diesel exhaust emissions (Wang *et al.*, 2003); another confounding factor in source apportionment analysis. It is also important to note that modern brake pads often do not contain Sb (due to health concerns) so the value of the Cu:Sb ratio as a brake-wear indicator will increasingly decline.

Other studies (Adachi & Tainosho, 2004; Schauer *et al.*, 2006; Hjortenkrans *et al.*, 2007; Tanner *et al.*, 2008; Dongarrá *et al.*, 2009; Gietl *et al.*, 2010; Keuken *et al.*, 2010; Amato *et al.*, 2011; Harrison *et al.*, 2012; Lawrence *et al.*, 2013) have suggested that Ba and Cu can be used as tracers of brake-wear debris. Ba seems especially promising because barite ($BaSO_4$) is usually added to brake pads both as a filler and stabiliser of the friction layer and this usage is unlikely to be changed in the near future. Beddows *et al.* (2016) used aerosol time-of-flight mass spectrometry (ATOFMS) to detect brake-wear emissions and showed that the presence of the [$^{-88}FeO_2$], [^{138}Ba] and [^{154}Ba] peaks can be used as a proxy for brake-wear debris. It should, however, be emphasised that brake-wear compositions both vary between individual countries, and are likely to change in the future. Hence, local conditions need to be taken into account in attempting to achieve quantification of brake-wear emissions (Beddows *et al.*, 2016).

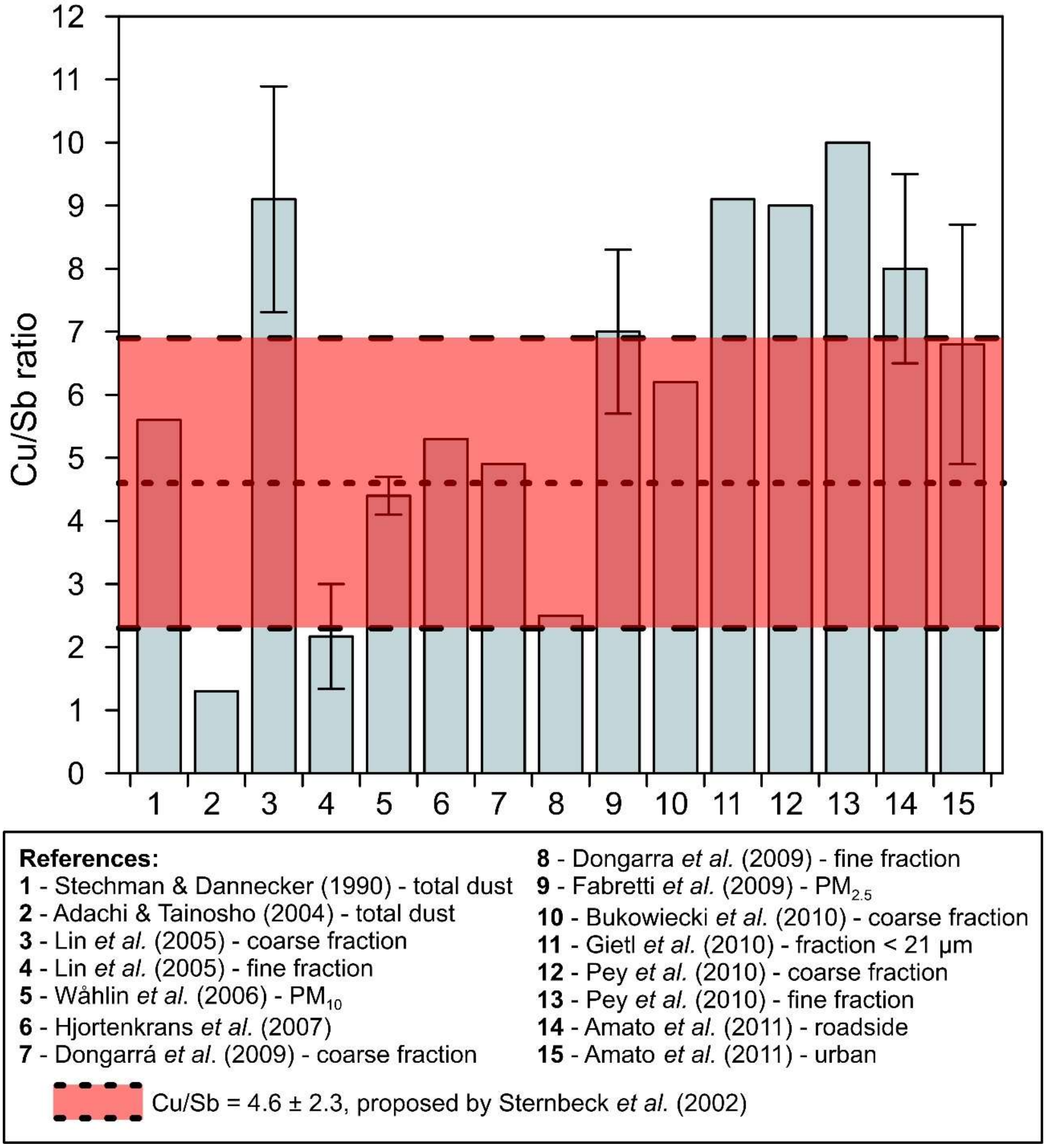

Figure 17. Cu:Sb mass ratio of brake-wear particles in ambient PM reported in the literature.

2.7. Quantification of brake-wear emissions

Several authors have attempted to quantify brake-wear emissions (Table 3). This task has proved challenging and therefore reported emission factors (EFs) are highly variable between different studies, depending on the friction materials (see Section 2.2. Friction materials), measurement method, laboratory/field equipment and braking conditions (see

Section 2.3. Experiments and studies), local road structure and topography (e.g. proximity to traffic lights), and normalisation method (Table 3).

From dynamometer studies, reported EFs for PM_{10} emitted by vehicle brake systems varied from 7 mg/stop/brake (Sanders *et al.*, 2003) to 46.4 mg/stop/brake (Perricone *et al.*, 2017) for LM brake pads, and from 1.5 mg/stop/brake (Sanders *et al.*, 2003) to 9.2 mg/stop/brake (Perricone *et al.*, 2017) for NAO brake pads. Normalised by the mileage, it ranged from 5.6 mg/km/car (field study; Farwick zum Hagen *et al.*, 2019a) to 21 mg/km/car for LM brake pads (dynamometer, Park *et al.*, 2021), and from 0.04 mg/km/car (dynamometer; Hagino *et al.*, 2016) to 8.8 mg/km/car (dynamometer; Garg *et al.*, 2000) for NAO brake pads (Table 3). The discrepancies between different studies are probably a consequence of different braking conditions applied in the dynamometer tests (or field studies). For example, Perricone *et al.* (2017) used higher deceleration rates (up to 0.40 g) compared to Sanders *et al.* (2003) (up to 0.16 g). Moreover, Perricone *et al.* (2017) used slightly higher sliding speed (up to 100 km/h) and temperature (up to 200°C) compared to Sanders *et al.* (2003) (up to 89 km/h and 177°C) (Table 2).

It is important to note that brake systems with NAO pads have been reported consistently to generate lower mass of PM_{10} (Table 3). In terms of particle number, however, Perricone *et al.* (2017) observed that the NAO brake pad emitted much higher particle numbers than the LM pad (153×10^{10} particles/stop/brake and up to 91×10^{10} particles/stop/brake, respectively). Similar results were obtained by Alemani *et al.* (2016) who observed that a NAO brake pad emitted higher number of brake-wear particles than the LM pad, even at temperatures below the transition temperature (160 – 190°C) (see also discussion in Section 2.5. Particle size distribution of brake-wear emissions). However, in a recent dynamometer study, Park *et al.* (2021) reported that LM brake pads emitted somewhat higher particle number, compared to NAO, i.e. $\sim 2.3 \times 10^{10} - 4.7 \times 10^{10}$ particles/km/car for LM, and $\sim 0.8 \times 10^{10} - 3.1 \times 10^{10}$ particles/km/car for NAO. Since particle number and/or surface area (rather than particle mass) might be relevant regarding pulmonary, cardiovascular and neurological health (e.g. Oberdörster, 2001; Oberdörster *et al.*, 2005; Nel *et al.*, 2006; Maher, 2019), the particle number emitted from brake systems should be taken into consideration in each study of brake-wear emissions.

Table 3. Overview of studies quantifying brake-wear emissions. Brake pads: NAO – non-asbestos organic, LM – low-metallic; SM -semi-metallic.

Reference	Brake pad type	PM$_{10}$	PM$_{2.5}$	PM$_{0.1}$
Garg *et al.* (2000)	NAO [dynamometer]	3.2 – 8.8 mg/km/car	2.7 – 7.5 mg/km/car	1.0 – 2.9 mg/km/car
Hagino *et al.* (2016)	NAO [dynamometer]	0.04 – 1.20 mg/km/car	-	-
Park *et al.* (2021)	LM [dynamometer]	11 – 21 mg/km/car	2.6 – 5.3 mg/km/car	-
	NAO [dynamometer]	1 – 5 mg/km/car	0.4 – 2.4 mg/km/car	
Abu-Allaban *et al.* (2003)	Various [field study]	0 – 80 mg/km/car	0 – 5 mg/km/car	-
Bukowiecki *et al.* (2010)	Various [field study]	~15 mg/km/car	-	-
Farwick zum Hagen *et al.* (2019a)	LM [field study]	5.6 – 8.4 mg/km/car	-	-
Iijima *et al.* (2008)	NAO [dynamometer]	5.8 mg/braking/car	3.9 mg/braking/car	-
Hagino *et al.* (2015)	NAO [dynamometer]	0.024 – 0.056 mg/braking/car	-	-
Sanders *et al.* (2003)	LM [dynamometer]	7.0 mg/stop/brake	-	-
	SM [dynamometer]	1.7 mg/stop/brake		
	NAO [dynamometer]	1.5 mg/stop/brake		
Perricone *et al.* (2017)	LM [dynamometer]	14.5 – 46.4 mg/stop/brake	-	-
	NAO [dynamometer]	8.5 – 9.2 mg/stop/brake		

The quantification of brake-wear emissions in urban environments presents many challenges, one issue comprising the varied measurement set-ups used in different studies. The large discrepancies in EFs show the difficulty inherent to selection of appropriate braking cycles for dynamometer studies. Over the last few years, the JRC (Joint Research Centre, European Commission) has been working on establishing a dynamometer braking cycle which better reflects real-world conditions. They proposed a dynamometer cycle based on Worldwide Harmonised Light-Duty Vehicles Test Procedure (WLTP), a large database consisting of in-use driving data from five different regions (EU, USA, India, Korea and Japan) with a total mileage of almost 750,000 km (Mathissen *et al.*, 2018). Although the concentrations of brake-wear emissions in urban air are expected to be highly variable depending on the road proximity, weather conditions, local topography, and frequency of braking events (e.g. due to traffic-control lights), the dynamometer cycle proposed by the JRC group was designed to represent average braking conditions and it is expected to be used by European Union in legislation concerning the limitation of brake-wear emissions, likely to be introduced in the near future.

2.8. Health impact of brake-wear emissions

Brake systems release large amounts of brake-wear particles to the atmosphere each year. It was estimated that in Stockholm, Sweden passenger cars emit ~45 t/year of brake-wear particles (Westerlund, 2001). Several studies have assessed the toxicity of brake-wear emissions *in vitro* and *in vivo*. It has been observed that the exposure to brake dust results in toxic and mutagenic effects, including generation of ROS, chromosomal damage, heightened proinflammatory response, reduced cell viability, cell morphology alterations and damage to tight junctions (Gasser *et al.*, 2009; Kukutschova *et al.*, 2009; Denier van der Gon *et al.*, 2013; Zhao *et al.*, 2015; Malachova *et al.*, 2016; Kazimirova *et al.*, 2016; Barosová *et al.*, 2018; Puisney *et al.*, 2018; Rajhelová *et al.*, 2019; Selley *et al.*, 2020).

It is interesting to note that particulate matter derived from events leading to a complete stop provoke more adverse effects than less severe braking events (Gasser *et al.*, 2009). Barosová *et al.* (2018) found that brake-wear particles originated from an LM pad did not activate a biological response while a sample from an NAO formula invoked an inflammatory response, reduced cell viability and altered cell morphology in a human 3D multicellular model consisting of human A549 epithelial cells and human primary immune cells. These studies showed that biological responses depend both on the friction couple formulation and braking conditions. Another problematic issue is the assessment of realistic dose of exposure to brake emissions (Barosová *et al*., 2018; Gerlofs-Nijland *et al*., 2019) as the estimations of the brake-wear contribution to roadside PM vary across such a wide range (cf. Section 1.11. Source apportionment of roadside-derived PM and Section 2.7. Quantification of brake-wear emissions).

At the roadside, various metals (e.g. Fe, Cu, Ba, Al, Sb, Mn, Ni and Zn) (Gao *et al*., 2020) are emitted abundantly from car brake systems (Thorpe & Harrison, 2008; Kukutschová *et al.,* 2010; 2011; Peíkertová *et al.,* 2013; Straffelini *et al.,* 2015; Peíkertová & Filip, 2016; Verma *et al.,* 2016; Kukutschová & Filip, 2018). These high concentrations of various metals (e.g. up to ~50 wt.% Fe, ~18 wt.% Cu, and ~13 wt.% Ba) (Iijima *et al*., 2007; Kukutschová & Filip, 2018) in brake-wear emissions might be of significance regarding potential health impacts. Transition metals, such as Cu, Fe or Mn, can catalyse ROS production (Smith *et al.,* 1997; Allsop *et al.,* 2008; Charrier & Anastasio, 2011; Tabner *et al.,* 2010; Li & Reichmann, 2016; Gao *et al.,* 2020). Moreover, mixture of metals (e.g. Fe and Cu) can act synergistically to promote damage caused by excess oxidative stress (Charrier & Anastasio, 2011).

Exogeneous, rounded/spherical UFPs (< ~150 nm) of metal-rich composition (especially Fe-rich) have been reported in frontal cortex and brainstem tissues (Maher *et al*., 2016; Calderón-Garcidueñas *et al*., 2020), heart (Calderón-Garcidueñas *et al*., 2019b; Maher *et al*., 2020), human serum and pleural effusions (Lu *et al*., 2020), placenta (Bové *et al*., 2019; Liu *et al*., 2021) and amniotic fluid (Barošová *et al*, 2015). These UFPs have been associated with biological dysfunction, including misfolded proteins, neurites and mitochondrial damage in the brainstem (Calderón-Garcidueñas *et al*., 2020), and mitochondrial damage and ventricular up-regulation in the heart (Calderón-Garcidueñas *et al*., 2019b; Maher *et al*., 2020).

Most brake-wear-based toxicological studies have so far been carried out on human bronchial/lung epithelial cells. Given the abundant presence of brake-wear particles in the environment, predominance of UFPs (99% of PNC < 200 nm; cf. Figure 3), high concentrations of Fe and its reported association with neurodegenerative (see Section 1.13. Specific toxicity of Fe-bearing nanoparticles) and cardiovascular diseases (Maher *et al*., 2020), investigations of the potential impacts of human exposure to brake emissions on cardiovascular and neurological health are both an important and timely task.

Chapter Three: Methodology

In total, 166 particulate samples have been measured and analysed within this thesis, including:

a) 13 total (swept or vacuumed from the pavement/road surfaces) dust samples, from roadside and urban background locations in Lancaster and Birmingham, U.K.;
b) 11 engine-exhaust PM samples (7 diesel-engine tailpipe emissions and 4 petrol-engine tailpipe emissions samples);
c) 140 samples of size-fractionated brake-wear PM, emitted from a low-metallic brake pads worn against a cast iron disc;
d) 2 samples of non-airborne (swept from the floor of the dynamometer) brake-wear PM, emitted from a low-metallic brake pad worn against a cast iron disc.

All 140 size-fractionated brake-wear PM samples were collected using a full-scale brake dynamometer (Link M2800) at VŠB – Technical University of Ostrava, Czech Republic. The dynamometer was equipped with an environmental chamber, with cooling airflow of 2500 m^3/h around the brake system. A Dekati ELPI+ impactor was used to collect brake-derived primary particles directly in the dynamometer chamber, on Al foils, in 14 size fractions, from 0.016 μm up to 10 μm. Additionally, the non-airborne fraction was also collected (swept from the floor of the dynamometer chamber after the test cycle).

A wide variety of analytical procedures and methods have been used to evaluate magnetic properties, chemical composition, morphology, structure and particle size distribution of PM emissions and urban dust. Room-temperature, remanence-based magnetic measurements (i.e., IRM, ARM, AF demagnetisation) were conducted at the Centre for Environmental Magnetism and Palaeomagnetism, Lancaster University, U.K. Low-temperature (room temperature down to 77 K) magnetic measurements were carried out at the Centre for Science at Extreme Conditions, University of Edinburgh, U.K. Electron microscopy (SEM and TEM) was used to image and analyse the brake-wear PM at the Research Institute of Biomolecular and Chemical Engineering, University of Pannonia, Veszprém, Hungary.

Details of sample collection, preparation and analytical procedures are provided in the research papers presented in chapters four and five, and Appendix A: Section A1: Analytical techniques and methods used in this thesis.

Chapter Four (Paper II): Source apportionment of magnetite particles in roadside airborne particulate matter

4.1. Abstract

Exposure to airborne particulate matter (PM) is associated with pulmonary, cardiovascular and neurological problems. Magnetite, a mixed Fe^{2+}/Fe^{3+} oxide, is ubiquitous and abundant in PM in urban environments, and might play a specific role in both neurodegeneration and cardiovascular diseases. We collected samples of vehicle exhaust emissions, and of heavily-trafficked roadside and urban background dusts from Lancaster and Birmingham, U.K. Then, we measured their saturation magnetic remanence and used magnetic component analysis to separate the magnetite signal from other contributing magnetic components. Lastly, we estimated the contributions made by specific traffic-related sources of magnetite to the total airborne magnetite in the roadside environment. The concentration of magnetite in exhaust emissions is much lower (3 – 14 x lower) than that in heavily-trafficked roadside PM. The magnetite concentration in petrol-engine exhaust emissions is between ~0.06 and 0.12 wt.%; in diesel-engine exhaust emissions ~0.08 – 0.18 wt.%; in background dust ~0.05 – 0.20 wt.% and in roadside dust ~0.18 – 0.95 wt.%. Here, we show that vehicle brake-wear is responsible for between ~68 and 85% of the total airborne magnetite at the two U.K. roadside sites. In comparison, diesel-engine exhaust emissions account for ~7% – 12%, petrol-engine exhaust emissions for ~2% – 4%, and background dust for 6% – 10%. Thus, vehicle brake-wear is by far the most dominant source of airborne magnetite in the roadside environment at the two sites examined. Given the potential risk posed, post-inhalation, by ultrafine magnetite and co-associated transition metal-rich particles to human cardiovascular and neurological health, the high magnetite content of vehicle brake-wear might need to be reduced in order to mitigate such risk, especially for vulnerable population groups.

Published:

Gonet, T.; Maher, B. A.; Kukutschová, J. Source apportionment of magnetite particles in roadside airborne particulate matter. *Science of the Total Environment* **2021**, 752, 141828.

4.2. Introduction

Exposure to increased concentrations of particulate air pollution has been associated with increased morbidity and mortality worldwide (e.g. Dockery *et al.*, 1993; Laden *et al.,* 2000; Zanobetti *et al.,* 2002; Brook *et al.*, 2010; Ostro *et al.*, 2015; Burnett *et al.*, 2018; Ho *et al.,* 2018; WHO, 2018; Malik *et al.,* 2019; Miller & Newby, 2019). Both acute and chronic exposure to coarse (CP; 2.5 µm – 10 µm), fine (FP; 0.1 µm – 2.5 µm) and ultrafine (UFP; < 0.1 µm) particulate matter is associated with various pulmonary, cardiovascular and neurological problems (Calderón-Garcidueñas *et al.,* 2002; Pope & Dockery, 2006; Hoek *et al.,* 2013; Beelen *et al.*, 2014; Costa *et al.*, 2014; Weichenthal *et al.*, 2017a; Liu *et al.*, 2018; Malik *et al.,* 2019; Maher *et al.*, 2020). For example, epidemiological data have shown that living in proximity to heavy traffic is associated with cognitive and behavioural impairments (Suglia *et al.,* 2007; Chen & Schwartz, 2009; Power *et al.,* 2011; Ailshire & Crimmins, 2014; Sunyer *et al.,* 2015; Kilian & Kitazawa, 2018; Zhang *et al.,* 2018a), and higher incidence of dementia, Alzheimer's disease, Parkinson's disease and multiple sclerosis (Jung *et al.,* 2015; Wu *et al.,* 2015; Oudin *et al.,* 2016; Chen *et al.,* 2017a; Kilian & Kitazawa, 2018; Peters *et al.,* 2019; Yuchi *et al.,* 2020).

Metal-bearing FPs and UFPs might be especially hazardous to human health (Ferin *et al.,* 1992; Seaton *et al.*, 1995; Gilmour *et al.,* 1996; 1997; Stone *et al.,* 1998; Donaldson *et al.,* 2002; Brook *et al.,* 2010; Maher, 2019; Weichenthal *et al.,* 2020) due to their abundance in urban environments, bioreactivity, small size and ability to reach all major organs of the human body (e.g. Nel *et al.,* 2006; Sanderson *et al.,* 2014; 2016; Maher *et al.,* 2016; Bové *et al.,* 2019; Calderón-Garcidueñas *et al.,* 2019b; Maher *et al.,* 2020). Of the potentially bioreactive, transition metals, Fe present in FPs and UFPs might play a particularly important role in the adverse impacts of airborne PM on human health (Donaldson *et al.,* 1997; Dusseldorp *et al.,* 1995; Valavanidis *et al.,* 2000; Ghio & Cohen, 2005; Maher *et al.,* 2016; González-Maciel *et al.,* 2017; Gonet & Maher, 2019; Maher, 2019). Those Fe-bearing particles which are smaller than ~200 nm can enter both the heart (Calderón-Garcidueñas *et al.,* 2019b; Maher *et al.,* 2020) via the circulation, and the brain, directly, via olfactory and/or trigeminal nerves, bypassing the blood-brain barrier (Oberdörster *et al.,* 2004; Maher *et al.,* 2016) (Figure 18).

When inside the brain, Fe in its reduced form (Fe^{2+}) is toxic to cells, catalysing the formation of reactive oxygen species (ROS) via the Fenton reaction (Smith *et al.,* 1997). Magnetite, a mixed Fe^{2+}/Fe^{3+} oxide ($(Fe^{3+})_{tet}[Fe^{2+}+Fe^{3+}]_{oct}O_4$) has been found directly associated with senile plaques and amyloid-β fibrils in an AD brain (Collingwood & Dobson, 2006; Quintana *et al.,* 2006; Plascencia-Villa *et al.,* 2016). Dissolution of magnetite (and other co-associated Fe-rich UFPs) in the brain might be a source of labile, unregulated Fe^{2+} (Maher, 2019; Van de Walle *et al.*, 2019), inducing oxidative stress and contributing directly to Alzheimer-like neurodegeneration changes (Smith *et al.,* 1997; Castellani *et al.,* 2007; Allsop *et al.,* 2008; Tabner *et al.,* 2010; Wu *et al.,* 2013; Coccini *et al*., 2017; Maher, 2019). Not only may magnetite UFPs be toxic on their own, but they are also often co-associated with other bioreactive metals, including Cr, Cu, Mn, Ni, Pb, Ti, Al and Zn (Spassov *et al.,* 2004; Chen *et al.,* 2006; Kim *et al.,* 2007; Maher *et al*., 2016; Yang *et al.,* 2016; Hofman *et al*., 2020), and surface-adsorbed organic species, including polycyclic aromatic hydrocarbons (PAHs) (Lehndorff & Schwark, 2004; Halsall *et al.,* 2008).

In the urban environment, Fe-bearing (and specifically magnetite-rich) FPs and UFPs are emitted by a wide variety of vehicle-derived sources, including exhaust emissions (both petrol and diesel), brake-wear, tyre/road surface wear emissions and resuspension of roadside dust (Thorpe & Harrison, 2008; Gonet & Maher, 2019). Although there have been several studies focusing on the source apportionment of CPs, FPs and UFPs (e.g. Bukowiecki *et al.,* 2009a; Harrison *et al.,* 2012; Lawrence *et al*., 2013; Hama *et al.,* 2017), relatively little attention has yet been paid to the magnetic properties of exhaust and brake-wear emissions, and there has been no source apportionment of potentially toxic magnetite particles in airborne PM.

The aim of this study is to quantify the contributions from different traffic-derived sources to total airborne magnetite particles at the roadside and to identify the major source(s) of magnetite in the roadside environment. Firstly, we measured the saturation magnetic remanence (SIRM) of petrol- and diesel-engine exhaust emissions, and of urban background and urban roadside dust in two contrasting U.K. cities, Lancaster, northwest England (population ~148,000) and Birmingham, central England (population ~2.6 million). Then, we used magnetic methods to deconvolve the contributing magnetic components in order to separate the signal from magnetite, and finally, estimated the contributions made by specific traffic-related sources of magnetite to the total airborne magnetite in the roadside environment in Lancaster and Birmingham, U.K.

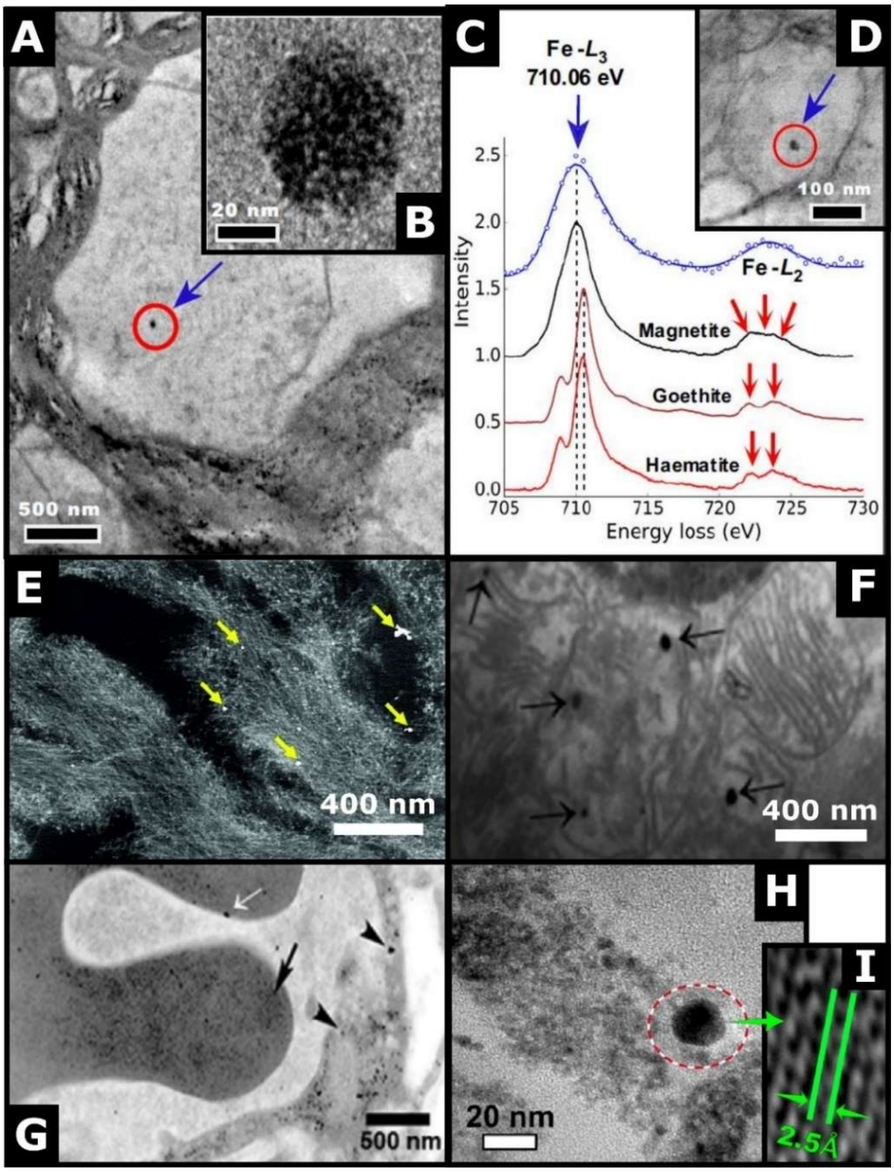

Figure 18. Transmission electron microscopy (TEM) images of metal-bearing UFPs found in the human brain and heart: (A) and (D) magnetite UFPs in frontal cortex brain tissue (Maher *et al.,* 2016); (B) magnification of magnetite particle shown in (A) (Maher *et al*., 2016); (C) electron energy loss spectra (in black) for the rounded particle shown in (D) and for standard Fe oxide species (Maher *et al.,* 2016); (E) magnetite UFPs (yellow arrows) in AD amyloid plaques in the human brain (Plascencia-Villa *et al.,* 2016); (F) electron-dense UFPs in the left ventricle from a 37 years old male (Calderón-Garcidueñas *et al.,* 2019b); (G) electron-dense UFPs inside caveolae (arrowhead), and in the red blood cells (black and white arrows) in the human heart (Calderón-Garcidueñas *et al.,* 2019b); (H) aggregated UFPs of magnetite/maghemite in the human heart, with the lattice spacing of 2.5 Å (Calderón-Garcidueñas *et al.,* 2019b); (I) magnification of the magnetite/maghemite particle shown in (H) (Calderón-Garcidueñas *et al.,* 2019b).

4.3. Methods

4.3.1. Collection of petrol and diesel exhaust emissions, and roadside and background dust

Exhaust PM samples were collected by attaching a PTFE filter to the tailpipe of an idling vehicle. The diesel exhaust samples D1 – D3 were collected from a Volkswagen Transporter tailpipe, and D4 – D7 from a Mercedes-Benz Sprinter. The petrol-derived exhaust samples P1 and P2 were collected from a Saab 9-3 tailpipe; samples P3 and P4 from a BMW E39. In total, 4 petrol and 7 diesel exhaust emission samples were collected. The samples were collected for either 30 min or, to increase magnetic signal-to-noise ratio, for 60 min.

Five sites were selected for the sampling of the roadside and background dust in two contrasting U.K. cities: 1 background and 2 roadside sites in Lancaster, and 1 background and 1 roadside site in Birmingham (Table 4). A map with the sites' locations is shown Appendix A: Figure A12. In total, 13 dust samples were collected at heavily-trafficked roadside and urban background sites in Lancaster and Birmingham, U.K. (Table 4; see also Appendix A: Figure A12). Eight roadside dust samples were collected at two heavily-trafficked roadside sites (Cable Street and Dalton Square; Appendix A: Figure A12) in Lancaster, U.K., by using a vacuum cleaner on the pavement surface or by sweeping. All samples were collected as close to the street as possible (i.e. < 0.5 m). Additionally, an urban 'background' dust sample was collected from the suburban area, close to Bailrigg House at Lancaster University campus (Table 4; Appendix A: Figure A12). Hereafter, the bulk roadside dust samples collected in Lancaster and Birmingham are called 'total roadside dust'. Sweeping is a commonly used method of collecting total urban dust (e.g. Marié *et al.,* 2010; Yang *et al.,* 2016; Dytłow *et al.,* 2019).

Four dust samples were collected in Birmingham, U.K. (Table 4), Two samples (R1 and R2) were collected in close proximity (i.e. < 0.5 m) to the heavily-trafficked A38 road (Appendix A: Figure A12), close to the Bristol Road Observation Site and entrance of the University of Birmingham. Two urban 'background' samples (B1 and B2) were collected in the vicinity of the Birmingham Air Quality Site (previously known as Birmingham Observatory Super Site), close to Elms Road (Table 4; Appendix A: Figure A12).

Background dust samples (BG in Lancaster, and B1 – B2 in Birmingham; Table 4) were collected from sites located far (> 300 m) from major roads. These samples represent a mixture of local, soil-derived dust and regional, anthropogenic and natural PM, without a significant contribution from traffic-related sources. Conversely, the roadside dust samples (A1 – A6 and C1 – C2 in Lancaster, and R1 – R2 in Birmingham; Table 4) were collected from the very close proximity of major roads (< 0.5 m) and consist of a mixture of both traffic- and non-traffic-derived PM.

Table 4. Details on the collected dust samples at heavily trafficked roadside and urban background sites in Lancaster and Birmingham, U.K.

City	Sample type	Site	Sample name	Collection method
Lancaster	heavily trafficked roadside	(road A6) Cable Street ~12,000 vehicles/day	A1	Sweeping
			A2	Sweeping
			A3	Vacuum cleaner
			A4	Sweeping
			A5	Sweeping
			A6	Vacuum cleaner
		(road A6) Dalton Square ~12,000 vehicles/day	C1	Sweeping
			C2	Vacuum cleaner
	urban background	Bailrigg House	BG	Vacuum cleaner
Birmingham	heavily trafficked roadside	(road A38) Bristol Road Observation site ~32,000 vehicles/day	R1	Sweeping
			R2	Vacuum cleaner
	urban background	Birmingham Air Quality Site	B1	Sweeping
			B2	Vacuum cleaner

No metal tools were used throughout the field and laboratory work, to avoid potential contamination of the samples. For sweeping, a nylon brush and plastic scoop were used. For vacuuming, an Evertop cordless handheld mini vacuum cleaner (with a plastic trash bin) was used. Brush, scoop and vacuum cleaner were thoroughly cleaned before each use, to preclude any potential contamination. All samples were first dried for 24h in a room with controlled temperature (20ºC) and humidity (50%), and subsequently weighed, with a Mettler AT250 balance (accuracy of 0.00001 g). Each measurement was repeated 3 times.

4.3.2. Magnetic measurements

Magnetic remanence measurements were made at the Centre for Environmental Magnetism and Palaeomagnetism, Lancaster University, U.K. Saturation isothermal remanent magnetisation (SIRM), was imparted at room temperature to all samples at 1 Tesla (T) (Newport Instruments electromagnet), and measured with a 2G RAPID cryogenic magnetometer (noise level ~10^{-11} Am^2).

For the purpose of magnetic component analysis, detailed alternating field (AF) demagnetisation of SIRM was conducted (in 69 steps, up to 240 milliTesla, mT), following Egli (2003, 2004a, 2004b, 2004c). Whereas this author proposed AF demagnetisation of anhysteretic remanent magnetisation (ARM), we measured and AF demagnetised SIRMs due to a weak ARM signal in the finer size-fractions (< ~0.3 μm) of brake-wear and exhaust emissions, and to avoid any potential influence of magnetic interactions (Maher, 1988). For weaker samples (SIRM < 10^{-8} Am^2), we repeated the measurements up to 6 times to increase the signal-to-noise ratio. In order to identify the magnetic components contributing to the sample SIRMs, we used the CODICA & GECA software (Egli, 2003), kindly provided by Dr. R. Egli. Each SIRM component is characterised by three parameters: i) the median destructive field of SIRM (MDF_{IRM}) – i.e. the field required to demagnetise 50% of SIRM; ii) the dispersion parameter (s), a parameter related to the standard deviation of the coercivity distribution; and iii) the magnetic concentration (c_m), the contribution of a specific component to the total SIRM.

Magnetite concentrations in the samples were estimated based on SIRM values for sized, synthetic magnetite powders spanning from < 0.1 μm to 10 μm (Maher, 1988). To cover all particle size possibilities, we have made these estimates based on 3 possible magnetite grain size ranges: (i) < 0.1 μm (average SIRM ~7.5 Am^2/kg), (ii) 0.1 – 1 μm (average SIRM ~5.0

Am^2/kg) and (iii) 5 – 10 μm (average SIRM ~11.0 Am^2/kg). Haematite concentrations were also estimated based on data for synthetic haematite particles (Maher *et al.*, 2004), using an SIRM value for haematite powders ~100 nm in size (0.18 Am^2/kg).

4.3.3. Source apportionment of airborne magnetite at the roadside

We assumed that total concentration of airborne magnetite in PM at the roadside (m_R, in wt.%) is a sum of magnetite contributions from background dust (representing soil- and regional industry-derived PM), from diesel- and petrol-engine exhaust emissions, and from brake-wear emissions:

$$m_R = m_{BG} + m_D + m_P + m_{BR} \tag{1}$$

where:

m_{BG} – magnetite contribution of background dust (in wt.%),

m_D – magnetite contribution of diesel-engine exhaust emissions (in wt.%),

m_P – magnetite contribution of petrol-engine exhaust emissions (in wt.%),

m_{BR} – magnetite contribution of brake-wear emissions (in wt.%).

Magnetite contributions of background dust (m_{BG}), diesel- (m_D) and petrol-engine (m_P) exhaust emissions can be estimated based on their measured concentrations of magnetite (see Section 4.3.2. Magnetic measurements) multiplied by the reported contributions of these PM sources to total PM_{10} at the roadside. We consider 2 options: the first based on the PMF-based source apportionment of PM_{10} by Bukowiecki *et al.* (2009a); the second based on the PCA-based source apportionment of PM_{10} by Lawrence *et al.* (2013) (Table 5). As Bukowiecki *et al.* (2009a) did not distinguish between diesel- and petrol-engine exhaust emissions, we additionally consider 2 other scenarios: (a) all exhaust emissions are diesel-derived, and (b) all exhaust emissions are petrol-derived. It is obvious that the real situation in cities is within the range between these two scenarios.

The contribution of brake-wear to total magnetite (m_{BR}) can be estimated as:

$$m_{BR} = m_R - (m_{BG} + m_D + m_P) \tag{2}$$

Finally, the contributions of background dust (m_{BG}), brake-wear (m_{BR}), and diesel- (m_D) and petrol-engine (m_P) exhaust emissions are expressed as a percentage of the total measured magnetite concentration in PM at the roadside (m_R).

Table 5. Contributions of traffic-derived PM sources to total PM_{10} at the roadside.

Source	Bukowiecki *et al.* (2009a)	Lawrence *et al.* (2013)
Resuspension	38%	27%
Diesel exhaust emissions	41%	21%
Petrol exhaust emissions		12%

4.4. Results

4.4.1. Concentration of ferromagnetic grains in PM emissions at the roadside

For the vehicle-sourced PM, SIRM values for exhaust-emitted PM range from ~$5.1 \cdot 10^{-3}$ Am^2/kg (petrol-fuelled car) to ~$8.6 \cdot 10^{-3}$ Am^2/kg (diesel-fuelled car). In contrast, the roadside dust at densely trafficked sites in Lancaster and Birmingham displays SIRM values of $23 \cdot 10^{-3}$ Am^2/kg – $55 \cdot 10^{-3}$ Am^2/kg for Lancaster and $37 \cdot 10^{-3}$ Am^2/kg – $71 \cdot 10^{-3}$ Am^2/kg for Birmingham. These roadside dust SIRM values are 3 – 14 times higher than those for exhaust emissions, suggesting that, in addition to any tailpipe emissions, roadside dust contains a significant portion of strongly-magnetic particles from non-exhaust sources.

4.4.2. Magnetic component analysis for vehicle exhaust emissions

Measured SIRM values and subsequent AF demagnetisation of the samples enabled the separation of the signal from magnetite (using magnetic component analysis) and estimation of its mass concentrations in exhaust (both diesel and petrol), and in roadside and background dust. Magnetic component analysis revealed the presence of 2 components (CE_1 and CE_2) in the petrol-derived exhaust emissions and 3 components (CE_1, CE_2 and CE_3) in the diesel-vehicle exhaust emissions (Figure 19; Table 6; see Section 4.3.2. Magnetic measurements for a detailed description of the methodology of magnetic component analysis).

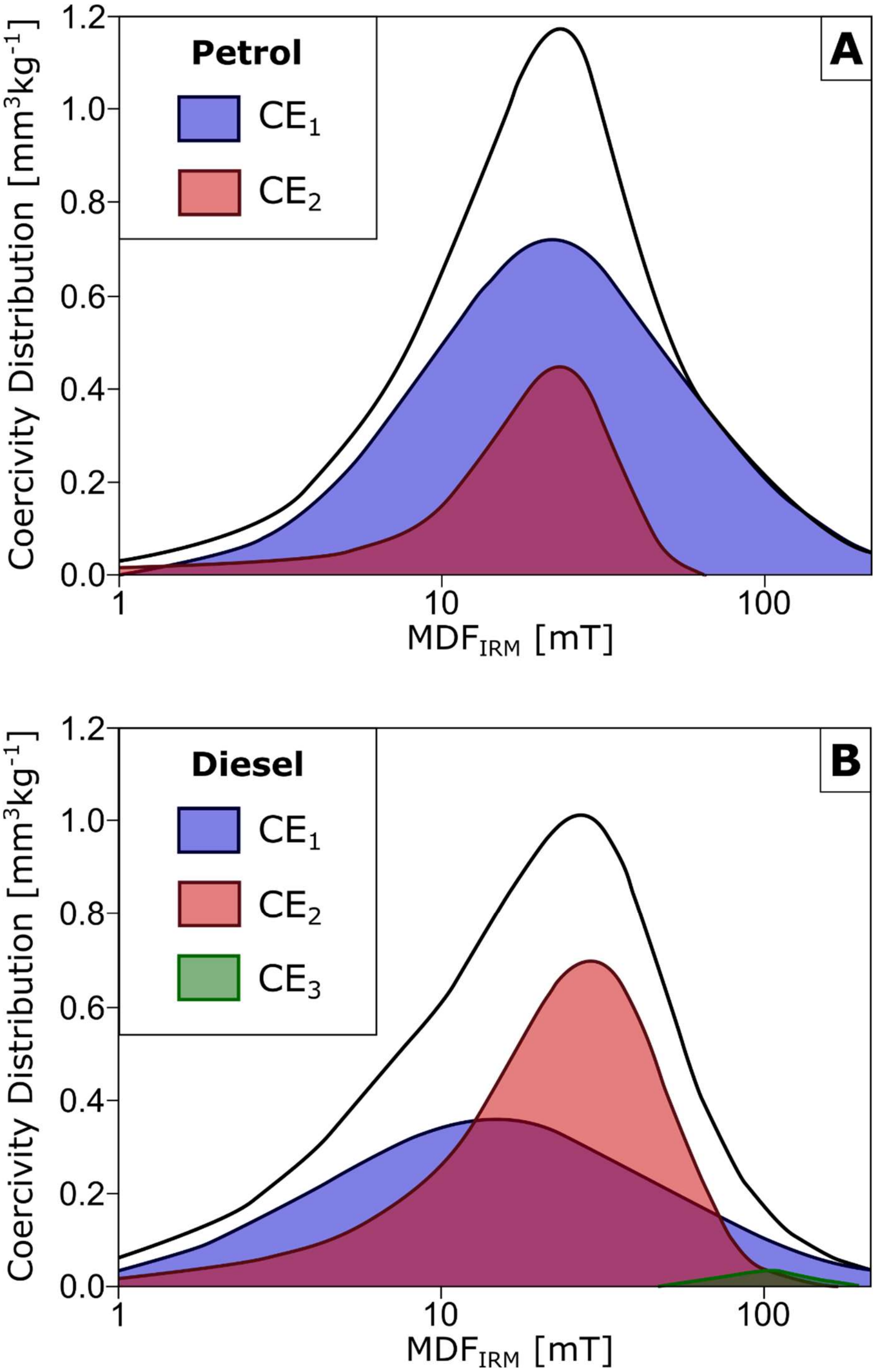

Figure 19. Examples of coercivity distributions for petrol- (A) and diesel- (B) exhaust emissions, with 3 deconvolved magnetic components (CE$_1$, CE$_2$ and CE$_3$).

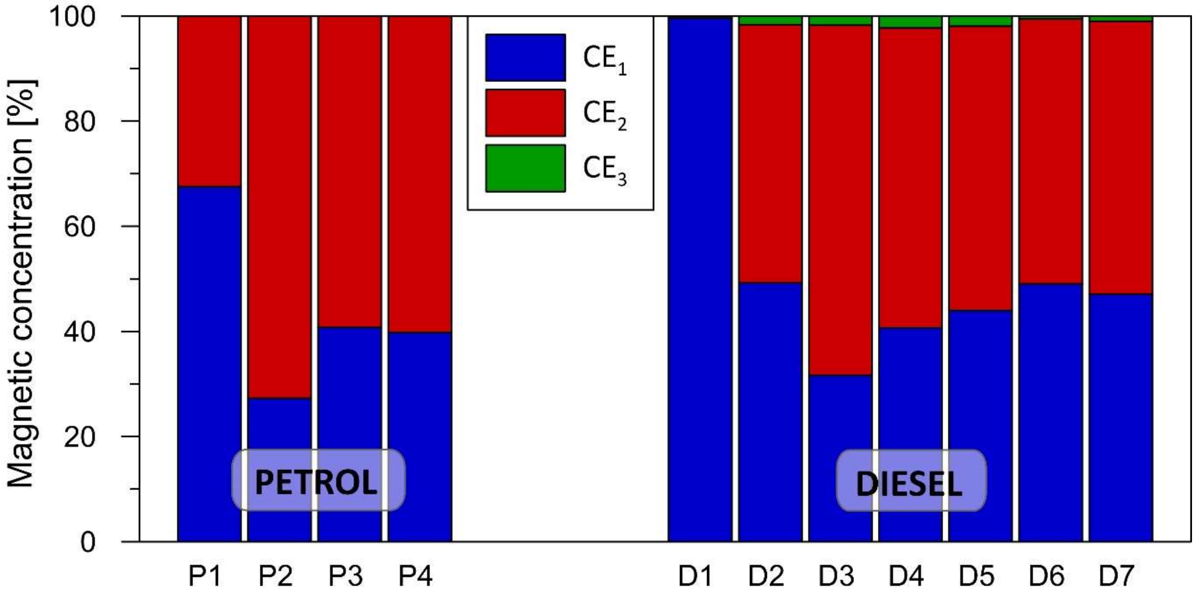

Figure 20. Magnetic concentration (contribution to total SIRM) of 3 magnetic components for 4 petrol- and 7 diesel-engine exhaust samples.

Components CE_1 and CE_2 have low MDF_{IRM} values of 19 mT and 24 mT for the petrol vehicles, and 17 mT and 20 mT for the diesel, respectively. Both components thus reflect the presence of magnetically 'soft' (i.e. easily demagnetised) minerals, probably magnetite and/or maghemite. Additionally, a magnetically 'hard' component (CE_3) was observed for the diesel exhaust emissions (Figure 19B; Table 6), with an MDF_{IRM} of 92 mT, probably corresponding to haematite (Maher *et al.*, 2004). The magnetic concentration (c_m; contribution to total SIRM) of component CE_3 is ~1.3%, which indicates haematite mass concentrations of ~0.09 wt.% (Maher *et al.*, 2004). This haematite-like component was not observed in the petrol-derived exhaust emissions.

Both components CE_1 and CE_2, found in the exhaust (both petrol and diesel) emissions, reflect magnetically-soft phases, and have similar MDF_{IRM} and distribution parameters (s) (Table 6). They probably reflect similar mixtures of magnetite of different grain sizes and/or a mixture of magnetite/maghemite. Considering both magnetically-soft components (CE_1 and CE_2) as magnetite and as 3 potential size ranges (< 0.1 µm, 0.1 – 1.0 µm and 5 – 10 µm) of magnetite (see Section 4.3.2. Magnetic measurements), we estimate the magnetite concentration to be between 0.06 and 0.12 wt.% (average of 0.09 wt.%) for petrol-derived exhaust emissions, and 0.08 to 0.18 wt.% (average of 0.13 wt.%) for diesel-derived exhaust emissions.

Table 6. Average parameters of the magnetic components identified in exhaust (petrol and diesel) emissions, roadside and 'background' dust in Lancaster and Birmingham. MDF_{IRM} – median destructive field of SIRM; s – distribution parameter; c_m – magnetic concentration (contribution to total SIRM).

Exhaust emissions										
Samples	**Number of samples**	**Component CE_1**			**Component CE_2**			**Component CE_3**		
		MDF_{IRM} [mT]	**s [-]**	**c_m [%]**	**MDF_{IRM} [mT]**	**s [-]**	**c_m [%]**	**MDF_{IRM} [mT]**	**s [-]**	**c_m [%]**
Petrol	4	19 ± 2	0.57 ± 0.17	43.8 ± 16.9	24 ± 4	0.43 ± 0.12	56.2 ± 16.9	-	-	-
Diesel	7	17 ± 4	0.59 ± 0.13	51.6 ± 22.0	20 ± 5	0.47 ± 0.22	47.1 ± 21.4	92 ± 14	0.16 ± 0.03	1.3 ± 0.8

Roadside dust										
Samples	**Number of samples**	**Component CD_1**			**Component CD_2**			**Component CD_3**		
		MDF_{IRM} [mT]	**s [-]**	**c_m [%]**	**MDF_{IRM} [mT]**	**s [-]**	**c_m [%]**	**MDF_{IRM} [mT]**	**s [-]**	**c_m [%]**
Roadside dust in Lancaster	8	5 ± 3	0.46 ± 0.10	35.3 ± 18.8	21 ± 3	0.29 ± 0.04	54.9 ± 18.5	70 ± 14	0.21 ± 0.09	9.8 ± 5.2
Roadside dust in Birmingham	2	4 ± 1	0.46 ± 0.06	25.8 ± 11.6	19 ± 1	0.26 ± 0.01	62.4 ± 9.9	57 ± 14	0.25 ± 0.05	11.8 ± 1.8
Background dust in Lancaster	1	2	0.42	12.4	22	0.32	73.9	79	0.19	13.7
Background dust in Birmingham	2	7 ± 1	0.43 ± 0.04	34.2 ± 0.6	23 ± 1	0.26 ± 0.01	46.7 ± 1.2	83 ± 1	0.29 ± 0.02	19.1 ± 1.8

4.4.3. Magnetic component analysis for roadside and background dust

For both heavily-trafficked roadside and urban background dust in Lancaster and Birmingham, 3 magnetic components (CD_1, CD_2 and CD_3) were identified from their SIRM demagnetisation behaviour (Figure 21, Figure 22; Table 6). Component CD_1 has the lowest MDF_{IRM}: 5 mT (Lancaster) and 4 mT (Birmingham) for the roadside dust; and 2 mT (Lancaster) and 7 mT (Birmingham) for the background dust (Table 6). Component CD_2 has higher MDF_{IRM} values, ranging from 19 mT to 23 mT. This component appears magnetically similar to the magnetic component CE_2 identified in the petrol- and diesel-derived exhaust emissions (Figure 19; Figure 21; Table 6). Hence, in both the exhaust emissions and roadside dust, two components (CE_1 and CE_2 in exhaust emissions, and CD_1 and CD_2 in roadside dust) reflect the presence of magnetically-soft phases, probably magnetite, maghemite, a mixture of these two minerals, or metallic Fe.

In order to estimate the magnetite-like concentrations in the roadside dust, we consider the full range of possible scenarios: (a) that component CD_1 corresponds to magnetite and component CD_2 corresponds to maghemite (it is unlikely for component CD_2 to reflect metallic Fe due to its relatively high MDF_{IRM}); (b) that component CD_2 corresponds to magnetite and component CD_1 corresponds to maghemite or metallic Fe; and (c) that both components CD_1 and CD_2 correspond to magnetite. Based on these 3 possible mineralogical scenarios, and in combination with the 3 possible average SIRM values (7.5 Am^2/kg, 5.0 Am^2/kg and 11.0 Am^2/kg) which encompass all 3 potential magnetite particle size ranges (< 0.1 μm, 0.1 – 1.0 μm and 5 – 10 μm) of magnetite (see Section 4.3.2. Magnetic measurements), we estimate the magnetite concentration to be between 0.18 and 0.63 wt.% in the roadside dust from Lancaster and between 0.32 and 0.95 wt.% from Birmingham. The estimated magnetite concentration in the background dust varies between 0.05 and 0.18 wt.% in Lancaster, and between 0.05 and 0.20 wt.% in Birmingham. The concentrations of metallic Fe in the roadside dust are relatively low in both Lancaster (~0.015 wt.%) and Birmingham (~0.016 wt.%).

Component CD_3 in the roadside and background dusts, characterised by notably higher MDF_{IRM} values of between 57 mT and 83 mT (Table 6), probably corresponds to haematite (Maher *et al.*, 2004). The magnetic concentration (c_m) of component CD_3 varies from 9.8% to 13.7% in Lancaster and from 11.8% to 19.1% in Birmingham (Figure 22; Table 6), which corresponds to haematite concentrations of between 0.1 and 3.8 wt.% in Lancaster and 1.2 to 5.1 wt.% in Birmingham (Maher *et al.*, 2004). The higher haematite concentrations in

Birmingham might reflect the haematite contribution from the local Triassic sandstone in windblown dust.

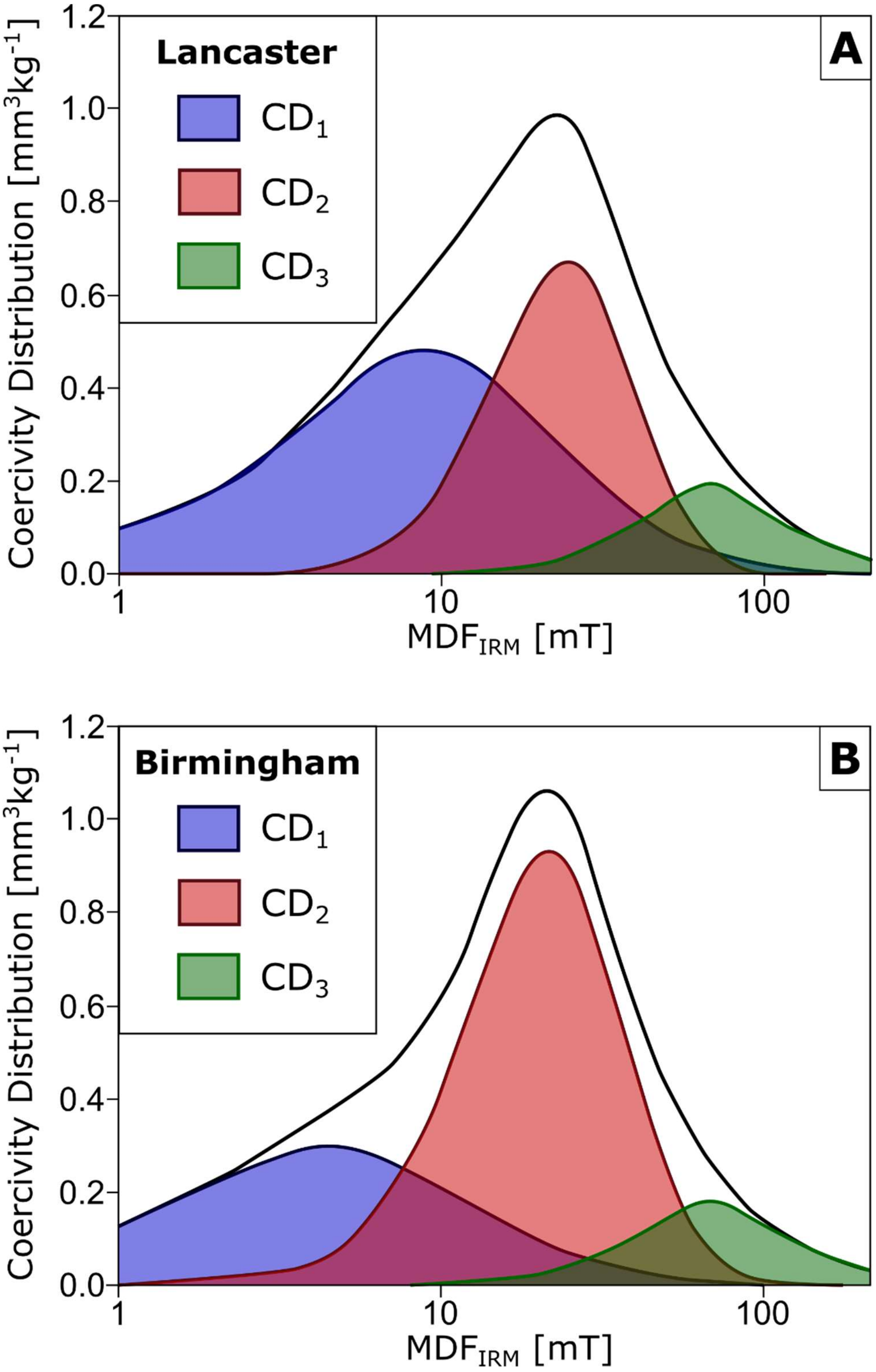

Figure 21. Examples of magnetic coercivity distribution for roadside dust samples from Lancaster (A) and Birmingham (B), with 3 identified magnetic components (CD_1, CD_2 and CD_3).

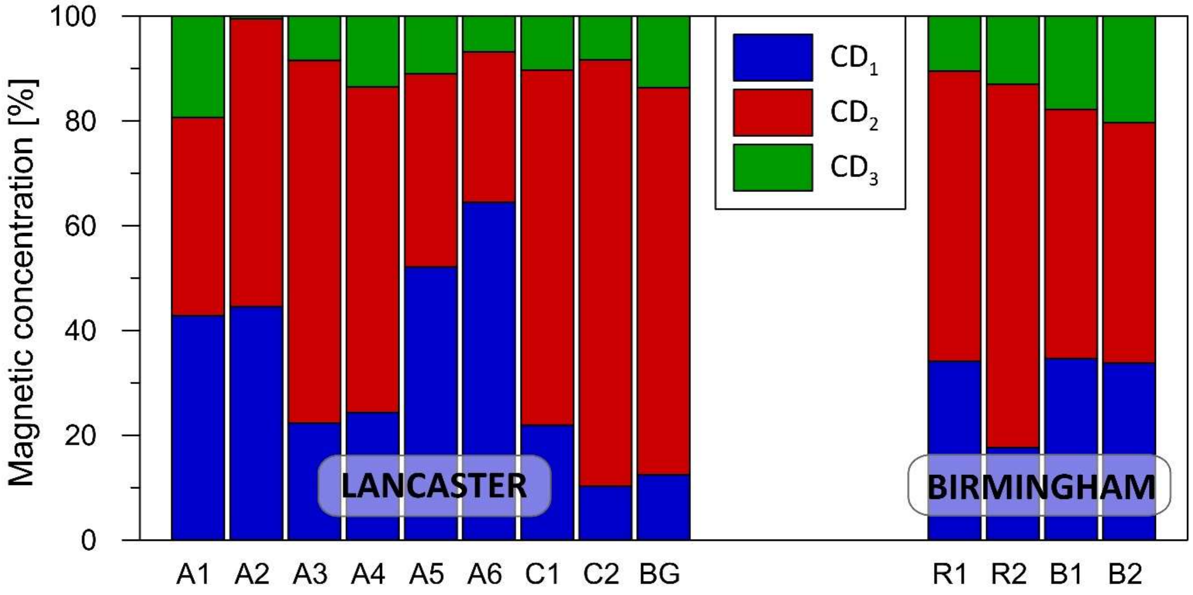

Figure 22. Magnetic concentration (contribution to total SIRM) of 3 magnetic components for total roadside dust from Lancaster (A1-A6 and C1-C2 – heavily-trafficked roadside, BG – urban background) and Birmingham (R1 and R2 – heavily-trafficked roadside, B1 and B2 – urban background).

4.4.4. Source apportionment of magnetite in roadside airborne PM

Magnetic component analysis of the SIRM demagnetisation behaviour of these traffic-related PM samples enables identification and quantification of the presence in each sample of 2 components dominated by magnetically-soft minerals (magnetite/maghemite) and 1 magnetically-hard, haematite-like component. By subtracting the haematite signal from the total SIRM, we can estimate the magnetite concentrations in these exhaust (petrol and diesel) emissions, and the heavily trafficked roadside and urban background dusts, taking into account 3 possible scenarios (see Section 4.4.3. Magnetic component analysis for roadside and background dust). The magnetite concentration in the petrol-engine exhaust emissions is between ~0.06 and 0.12 wt.%, and in diesel emissions between ~0.08 and 0.18 wt.%. In urban background dust, the magnetite concentration is estimated as ~0.05 – 0.18 wt.% (in Lancaster) and ~0.05 – 0.20 wt.% (in Birmingham). In heavily trafficked roadside dust, the estimated magnetite concentration is between ~0.18 and 0.63 wt.% (in Lancaster) and ~0.32– 0.95 wt.% (in Birmingham).

Quantification of the contributions made by different traffic-related sources to total PM mass is challenging, and estimates are notably variable between different studies (Ketzel *et al.*, 2007; Viana *et al.*, 2008; Bukowiecki *et al.*, 2009a; Harrison *et al.*, 2011; 2012; Lawrence *et al.*, 2013; Vu *et al.*, 2015; Squizzato *et al.*, 2016; Crilley *et al.*, 2017). For a tunnel in Hatfield, U.K., Lawrence *et al.* (2013) used principal component analysis (PCA) and multiple linear regression analysis, and estimated that petrol-engine exhaust emissions contributed 12%, diesel-engine exhaust emissions 21%, road surface 11%, resuspension of roadside dust 27% and brake-wear 11% of total PM_{10} mass. Another traffic source-specific study, of roadside PM in a street canyon in Zurich, Switzerland, indicated that exhaust emissions (petrol + diesel), resuspension and brake-wear are responsible for 41%, 38% and 21% of total traffic-derived PM_{10} mass, respectively (Bukowiecki *et al.*, 2009a). The latter source apportionment was based on elemental composition of PM_{10} and positive matrix factorization (PMF).

Based on these two source apportionment studies (Bukowiecki *et al.*, 2009a; Lawrence *et al.*, 2013) and our estimations of the magnetite concentrations, it is possible to quantify the contributions of specific, traffic-derived PM sources to the total magnetite content in airborne roadside airborne PM mass (see Section 4.3.3. Source apportionment of airborne magnetite at the roadside). We selected these 2 source apportionment studies because they both distinguished between different exhaust and non-exhaust (brake-wear, tyre-wear, road-wear and resuspension) PM sources.

Based on the PM_{10} source apportionment provided by Lawrence *et al.* (2013), we estimate that in Lancaster, the average contributions of background dust, petrol-fuelled and diesel-fuelled exhaust emissions to magnetite PM concentrations are 7%, 4% and 12%, respectively (Figure 23; Table 7). Thus, the great majority (~77%) of the roadside magnetite particles in Lancaster, U.K. can be attributed to brake-wear. In Birmingham, the average contributions are 6% for background dust, 2% for petrol-fuelled exhaust emissions, 7% for diesel exhaust emissions and 85% for brake-wear (Figure 23; Table 7). Based on the PM_{10} source apportionment made by Bukowiecki *et al.* (2009a), similar contributions are estimated: 10% from background dust; 22% from exhaust emissions (i.e. petrol + diesel); and 68% for brake-wear in Lancaster; and, in Birmingham, 7% from background dust, 13% from exhaust (petrol + diesel) and 80% from brake-wear (Table 7).

Table 7. Average contributions of background dust, diesel- and petrol-engine exhaust, and brake-wear emissions to the total airborne magnetite in the roadside environment in Lancaster and Birmingham, U.K. (based on PM_{10} source apportionment by Lawrence *et al.* (2013) and Bukowiecki *et al.* (2009a)).

Based on PM_{10} source apportionment by Lawrence *et al.* (2013)		
PM emissions	**Lancaster average (min – max)**	**Birmingham average (min – max)**
Brake-wear	77% (63% – 90%)	85% (79% – 91%)
Diesel	12% (3% – 21%)	7% (2% – 12%)
Petrol	4% (1% – 8%)	2% (1% – 4%)
Background dust	7% (6% – 8%)	6% (5% – 6%)
Based on PM_{10} source apportionment by Bukowiecki *et al.* (2009a)		
PM emissions	**Lancaster average (min – max)**	**Birmingham average (min – max)**
Brake-wear	68% (48% – 88%)	80% (71% – 89%)
Exhaust (petrol and diesel)	22% (4% – 41%)	13% (2% – 23%)
Background dust	10% (8% – 11%)	7% (6% – 8%)

4.5. Discussion

Globally, air pollution is responsible for approximately 7 million deaths annually (WHO, 2018). Exposure to urban PM causes a variety of health problems, including respiratory, cardiovascular and neurological impairments (e.g. Calderón-Garcidueñas *et al.*, 2008a; 2019b; Rückerl *et al.*, 2011; Guxens & Sunyer, 2012; Liu *et al.*, 2018; Maher *et al.*, 2020).

Air pollution is a complex mixture of natural and anthropogenic components, including both industry- and traffic-derived emissions. Chemical mass balance (CMB), principal component analysis (PCA) and positive matrix factorization (PMF) are most commonly used methods in the studies of source apportionment of PM_{10} in urban environments (e.g. Viana *et al.*, 2008; Harrison *et al.*, 2011; Lawrence *et al.*, 2013). Because Fe-bearing FPs and UFPs might be especially hazardous to neurological health and magnetite, as a mixed Fe^{2+}/Fe^{3+} oxide, might play a specific role in Alzheimer-like pathology (Maher, 2019), we have focused here on magnetite concentrations in urban airborne PM, rather than on source apportionment of urban PM in general.

Airborne Fe-bearing PM usually occurs as complex mixtures of magnetite (Fe_3O_4), haematite (α-Fe_2O_3) and maghemite (γ-Fe_2O_3), with some metallic Fe (α-Fe) also reported (Muxworthy *et al.*, 2002; Halsall *et al.*, 2008; Maher *et al.*, 2008; Mitchell & Maher, 2009; Hansard *et al.*, 2011; Sanderson *et al.*, 2016; Dytłow *et al.*, 2019; Górka-Kostrubiec *et al.*, 2019). Conventional, elemental analysis of PM is unable to distinguish between the different Fe-bearing minerals/phases contained in urban PM. Conversely, magnetic methods have proved effective in distinguishing between different Fe forms (e.g. Muxworthy *et al.*, 2002; Hansard *et al.*, 2012; Górka-Kostrubiec *et al.*, 2019). Hence, we used a combination of reported PM_{10} source apportionment studies and magnetic methods to estimate the contributions of specific, traffic-related sources to the total airborne magnetite in the roadside environment in Lancaster and Birmingham, U.K.

The saturation magnetic remanence (SIRM) represents the total ferromagnetic content of a sample. SIRM values for the total roadside dust collected at heavily-trafficked sites varied between $23 \cdot 10^{-3}$ Am^2/kg and $55 \cdot 10^{-3}$ Am^2/kg in Lancaster, and $37 \cdot 10^{-3}$ Am^2/kg and $71 \cdot 10^{-3}$ Am^2/kg in Birmingham. These values fall within the range of SIRM values obtained for urban and suburban airborne PM collected on filters in Lancaster ($7 \cdot 10^{-3}$ Am^2/kg – $167 \cdot 10^{-3}$ Am^2/kg) (Halsall *et al.*, 2008). The high variability of SIRMs shows that the concentration of ferromagnetic grains can significantly vary at the local scale in city environments, being heavily influenced by emissions source(s), its proximity, weather conditions and dominant transport directions.

Similar SIRM values have been reported for roadside PM in other cities in Europe, e.g. in Antwerp, Belgium ($34 \cdot 10^{-3}$ Am^2/kg – $95 \cdot 10^{-3}$ Am^2/kg for roadside PM_{10}) (Hofman *et al.*, 2020) and Munich, Germany ($32 \cdot 10^{-3}$ Am^2/kg – $44 \cdot 10^{-3}$ Am^2/kg for airborne roadside PM) (Muxworthy *et al.*, 2003). Some authors obtained somewhat higher SIRMs for roadside dust (total suspended particles), e.g. up to $549 \cdot 10^{-3}$ Am^2/kg in Shanghai, China (Shu *et al.*, 2001) or even up to $700 \cdot 10^{-3}$ Am^2/kg in Tamil Nadu State, India (Gargiulo *et al.*, 2016), indicating greater contributions of highly magnetic industrial-, domestic- and traffic-related PM emissions to total roadside PM in these latter areas.

Emissions of magnetite particles from both diesel- (Abdul-Razzaq & Gautam, 2001; Liati *et al.*, 2015) and petrol-engine (Zajzon *et al.*, 2013) exhaust emissions have been reported previously. Here, for the first time, we have quantified the concentration of magnetite in exhaust emissions. The SIRM values measured here for both petrol- (~$5.1 \cdot 10^{-3}$ Am^2/kg) and diesel-engine (~$8.6 \cdot 10^{-3}$ Am^2/kg) exhaust emissions indicate that the magnetite concentrations in diesel- and petrol-derived exhaust emissions are similar, ~0.08 – 0.18 wt.% and 0.06 – 0.12 wt.%, respectively. It is notable that these estimated magnetite concentrations are markedly lower than those of our roadside dust samples.

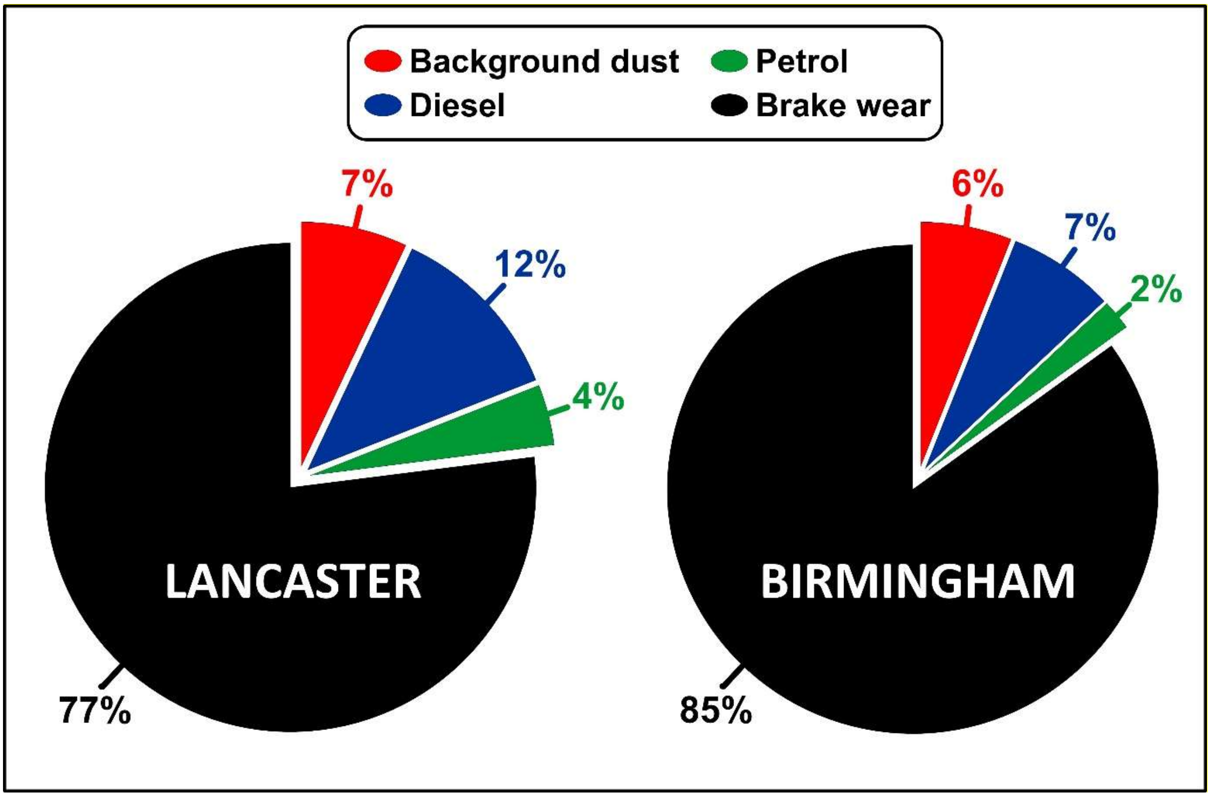

Figure 23. Average contributions of background dust, diesel, petrol and brake-wear emissions to the total airborne magnetite in the roadside environment in Lancaster and Birmingham (based on Lawrence *et al.* (2013)).

In terms of the magnetic mineralogy of the exhaust-derived PM, our magnetic component analysis reveals a difference between diesel- and petrol-fuelled emissions. While 2 magnetite-like phases were evident in both petrol and diesel emissions, a haematite-like phase appeared present only in the diesel exhaust emissions (Figure 19; Figure 20). At room temperature, haematite particles > ~30 nm can contribute to the measured remanence. Haematite nanoparticles of 10 – 60 nm in size were previously reported in petrol-engine exhaust by Zajzon *et al.* (2013). Due to thermal agitation of their magnetic moments, haematite grains < ~30 nm are unable to retain magnetic remanence at room temperature (Maher *et al.*, 2004). It is probable that most haematite particles in petrol-engine exhaust emissions are smaller than ~30 nm, and consequently, they are magnetically 'invisible' to remanence analysis at room temperature. Addition of low temperature-measuring capability in the RAPID 2G cryogenic magnetometry system would be valuable in providing such data for future PM source apportionment.

Here, magnetic component analysis also enabled differentiation between different Fe-bearing minerals and quantification of the magnetite concentrations in each of the studied samples. Magnetite constitutes an estimated content of between ~0.06 and 0.12 wt.% of petrol-engine exhaust emissions, ~0.08 and 0.18 wt.% of diesel-engine exhaust emissions, ~0.05 and 0.20 wt.% of background dust, and ~0.18 and 0.95 wt.% of roadside dust (in Lancaster and Birmingham).

Based on published PM_{10} source apportionment studies (Bukowiecki *et al.*, 2009a; Lawrence *et al.*, 2013) and our magnetite concentration estimates, we quantified the contributions made by specific sources to total magnetite mass in roadside airborne PM. The source apportionment of magnetite is similar for Lancaster and Birmingham (Figure 23; Table 7). Brake-wear-derived magnetite predominates, constituting 68% – 77% of total magnetite in roadside airborne PM in Lancaster, and 80% – 85% in Birmingham. Petrol-engine exhaust emissions account for ~4% of total magnetite in Lancaster and ~2% in Birmingham. Diesel-engine exhaust emissions contribute ~12% of total magnetite in Lancaster and ~7% in Birmingham. Background dust is responsible for 7% – 10% of total magnetite in the roadside environment in Lancaster and 6% – 7% in Birmingham (Figure 23; Table 7). The contribution of brake-wear emissions is higher in Birmingham, compared to Lancaster, which is probably related to the specificity of the sampling sites, i.e. the Birmingham site is located in close proximity (10 – 15 m) to traffic lights, while the Lancaster site is further away from traffic lights, and very often affected by traffic jams, which generate more exhaust emissions. It is especially noteworthy that vehicle brake systems appear to be by far the most dominant source of airborne magnetite in all the considered scenarios, i.e. different grain sizes of magnetite, possibility of the presence of other magnetic phases (maghemite and/or metallic Fe), and in two different cities in the U.K. These results are in line with laboratory measurements of brake-wear emissions (collected using a dynamometer) showing that SIRM values for brake-derived PM is 100 – 10,000 times higher, compared to other outdoor PM sources (Gonet & Maher, 2019).

These results independently accord with a recent study by Winkler *et al.* (2020), who used a combination of magnetic and microscopic methods to study airborne PM accumulated by lichens exposed to air pollution in Milan, Italy. The authors observed a correlation (R^2 of 0.36 – 0.76) between magnetic susceptibility and concentrations of Fe, Cu and Sb in the lichen samples, and a close resemblance between magnetic properties of the lichen samples and brake-wear emissions; and thus concluded that brake-wear emissions might be the main source of the airborne particles accumulated by lichens.

PM emissions from tyre/road surface wear were not considered in this study. The magnetic contribution from these sources is unlikely to be more than a few percent at most since Fe-bearing FPs and UFPs constitute less than ~2.5 wt.% of tyre/road surface wear emissions (Gonet & Maher, 2019 and references therein). Even with addition of tyre-derived magnetite to the source apportionment, brake-wear will still constitute by far the most important source of airborne magnetite at the roadside at these two U.K. sites.

The number of samples used in this study is not very high (in total, 24 samples). Yet our SIRM values for urban PM in Lancaster fall within the SIRM range previously reported (Halsall *et al.*, 2008), although the latter range is broader than the one obtained in this study, i.e. $7 \cdot 10^{-3}$ Am^2/kg – $167 \cdot 10^{-3}$ Am^2/kg in Halsall *et al.* (2008) vs $23 \cdot 10^{-3}$ Am^2/kg – $55 \cdot 10^{-3}$ Am^2/kg in this study. If we used the highest reported SIRM value ($167 \cdot 10^{-3}$ Am^2/kg) as the SIRM for Lancaster's roadside dust, and the lowest value ($7 \cdot 10^{-3}$ Am^2/kg) as the SIRM for its background dust, we would obtain an even higher contribution from brake systems (> 90%) to the total magnetite in roadside PM in Lancaster.

So far, there have been no studies reporting SIRM for urban dust in Birmingham. However, Shilton *et al.* (2005) studied magnetic properties of urban street dust in Wolverhampton and Dudley, U.K., cities located near (15 – 20 km) to our sampling sites in Birmingham. The authors reported SIRMs of ~$12 \cdot 10^{-3}$ Am^2/kg for background dust (residential area in Dudley), and ~$47 \cdot 10^{-3}$ Am^2/kg (maximum of ~$100 \cdot 10^{-3}$ Am^2/kg for a site with a high proportion of bus traffic) for roadside PM collected by a heavily-trafficked street in Wolverhampton. Here, for our Birmingham dusts, we obtained very similar SIRM values for both the background (~$12 \cdot 10^{-3}$ Am^2/kg) and the roadside (~$54 \cdot 10^{-3}$ Am^2/kg) samples. As in the Lancaster case (above), if we used Shilton *et al.*'s (2005) SIRM values (i.e., $47 \cdot 10^{-3}$ Am^2/kg for all Wolverhampton roads; $100 \cdot 10^{-3}$ Am^2/kg for the Lichfield Road bus route) in our source apportionment estimations, we would obtain similar or even higher contributions of brake-derived magnetite to total magnetite in roadside airborne PM, compared to our 2019 sampling and analysis.

Millions of people spend hours commuting and moving through urban environments every day, experiencing both acute and chronic exposures to damaging levels of air pollutants, including FPs and UFPs of magnetite and other reactive metal compounds. For UFPs of ~20 nm in size, the olfactory deposition rate in humans has been modelled as ~0.1% (Garcia *et al.*, 2015). Given our estimated magnetite concentration in roadside dust of between ~0.18 wt.% and 0.95 wt.%, we can then estimate the exposure to which an urban commuter is exposed every year. Assuming: 1 hour of commuting every day, 5 days/week, 12 months/year; PM_{10} level of 50 $\mu g/m^3$; breathing rate of 0.54 m^3/h (Zhou & Levy, 2008); grain size of 20 – 30 nm (the mean diameter of magnetite UFPs found at the Birmingham roadside (Sanderson *et al.*, 2016)); an urban-dweller could be exposed to olfactory deposition of 174 million – 3.1 billion magnetite UFPs every year. Given the potential link between exposure to magnetite and other Fe-rich UFPs and neurodegenerative disease (including Alzheimer's disease) (Maher, 2019), and the fact that > 70% of airborne roadside magnetite originates from vehicle brake systems (Figure 23; Table 7), it seems prudent to consider this information in designing any future legislation limiting brake-wear emissions. Specifically, the number of magnetite and other Fe-rich particles emitted by friction processes occurring in vehicle brake systems should be reduced, especially, for example, by limiting or banning the use of magnetite powders as fillers in brake pads.

This source apportionment of magnetite in roadside airborne PM has important implications for magnetic biomonitoring studies. Our estimates show that brake-derived magnetite constitutes > 70% of total airborne magnetite at the roadside of Lancaster and Birmingham, U.K. Brake emissions might thus dominate the magnetic properties of roadside dust and consequently hinder information about other vehicle- and industry-derived pollutants. Consequently, caution may be necessary when interpreting magnetic data for PM collected on filters, tree leaves or other sensors because they might reflect predominantly the properties of brake-wear emissions.

4.6. Conclusions

The concentration of magnetite in vehicle exhaust emissions was found to be consistently low compared with the magnetite concentration in heavily-trafficked urban roadside PM. The magnetite concentration is between ~0.06 and 0.12 wt.% in petrol-engine exhaust emissions; ~0.08 – 0.18 wt.% in diesel-engine exhaust emissions; ~0.05 – 0.20 wt.% in background dust, and 0.18 – 0.95 wt.% in roadside dust.

Rather than exhaust emissions, vehicle brake-wear is the major source of airborne magnetite at the present day at the roadside in two contrasting U.K. cities (Lancaster and Birmingham); contributing between ~68% and 85% of the total airborne magnetite in the roadside environment, followed by diesel exhaust emissions (~7% – 12%), petrol exhaust emissions (~2% – 4%) and background dust (~6% – 10%).

Caution appears necessary when interpreting magnetic biomonitoring data because magnetic properties of roadside PM might often be dominated by magnetic properties of brake emissions and information regarding other vehicle- and/or industry-derived pollutants might thus be obscured.

Finally, particulate pollution levels (especially FP and UFP numbers) vary enormously at the local scale in city environments, being heavily influenced by particulate source, source proximity, weather conditions and dominant transport directions. At the individual level, careful selection of time and route of commuting, avoiding highly polluted areas, can reduce personal exposure to potentially toxic particles rich in Fe and other co-associated transition metals, capable of inducing high oxidative potential and resultant oxidative stress. In terms of toxicity, human health outcomes can be dominated even by metal species of moderate oxidative potential if, like Fe, they are the species emitted in the greatest abundance and, critically, in the case of UFPs, number concentrations.

Contributions of authors

Tomasz Gonet: Conceptualization, Data curation, Writing – original draft, Writing - review & editing. **Barbara A. Maher**: Conceptualization, Supervision, Writing - review & editing**. Jana Kukutschová**: Conceptualization, Supervision.

Chapter Five (Paper III): Size-resolved quantitative evaluation of the magnetic mineralogy of airborne brake-wear particulate emissions

5.1. Abstract

Exposure to particulate air pollution has been associated with a variety of respiratory, cardiovascular, and neurological problems, resulting in increased morbidity and mortality worldwide. Brake-wear emissions are one of the major sources of metal-rich airborne particulate pollution in roadside environments. Of potentially bioreactive metals, Fe (especially in its ferrous form, Fe^{2+}) might play a specific role in both neurological and cardiovascular impairments. Here, we collected brake-wear particulate emissions using a full-scale brake dynamometer, and used a combination of magnetic measurements and electron microscopy to make quantitative evaluation of the magnetic composition and particle size of airborne emissions originating from passenger car brake systems. Our results show that the concentrations of Fe-rich magnetic grains in airborne brake-wear emissions are very high (i.e. ~100 – 10,000 × higher), compared to other types of particulate pollutants produced in most urban environments. From magnetic component analysis, the average magnetite mass concentration in total PM_{10} of brake emissions is ~20.2 wt.% and metallic Fe ~1.6 wt.%. Most brake-wear airborne particles (> 99% of particle number concentration) are smaller than 200 nm. Using low-temperature magnetic measurements, we observed a strong superparamagnetic signal (indicative of ultrafine magnetic particles, < ~30 nm) for all of the analysed size fractions of airborne brake-wear particles. Transmission electron microscopy independently shows that even the larger size fractions of airborne brake-wear emissions dominantly comprise agglomerates of UFPs (< 100 nm). Such UFPs likely pose a threat to neuronal and cardiovascular health after inhalation and/or ingestion. The observed abundance of ultrafine magnetite particles (estimated to constitute ~7.6 wt.% of $PM_{0.2}$) might be especially hazardous to the brain, contributing both to microglial inflammatory action and excess generation of reactive oxygen species.

Published:

Gonet, T.; Maher, B. A.; Nyirő-Kósa, I.; Pósfai, M.; Vaculík, M.; Kukutschová, J. Size-resolved, quantitative evaluation of the magnetic mineralogy of airborne brake-wear particulate emissions. *Environmental Pollution* **2021**, 288, 117808.

5.2. Introduction

Exposure to airborne particulate matter (PM) has been associated with both acute and chronic health problems. Coarse (10 – 2.5 µm), fine (2.5 – 0.1 µm) and ultrafine (< 0.1 µm) particles have been linked to impairment of pulmonary, cardiovascular and neurological health (Calderón-Garcidueñas *et al*., 2002; Pope & Dockery, 2006; Hoek *et al.,* 2013; Beelen *et al.,* 2014; Weichenthal *et al*., 2017a; Peters *et al.,* 2019; Maher *et al*., 2020, Shi *et al*., 2020). For example, epidemiological studies have shown a link between living close to heavy traffic (and consequently, chronic exposure to raised airborne PM concentrations) with higher incidence of dementia (Jung *et al.,* 2015; Wu *et al*., 2015; Oudin *et al.,* 2016; Chen *et al.,* 2017a), and cognitive and behavioural deficits (Suglia *et al*., 2007; Chen & Schwartz, 2009; Sunyer *et al.,* 2015; Zhang *et al.,* 2018a; Calderón-Garcidueñas *et al*., 2019a; Iaccarino *et al*., 2020). Exposure to PM is also linked to pre-term birth and low birth weight (e.g. Stieb *et al*., 2012; Lamichhane *et al.,* 2015; Li *et al.,* 2017).

UFPs might be especially hazardous to human health for several reasons. They (i) are abundant in the urban air (Putaud *et al.,* 2010; Sanderson *et al*., 2014; Yang *et al.,* 2016); (ii) can be suspended in the atmosphere for longer and consequently, transported over greater distances, compared to coarse particles; (iii) are able to penetrate easily into the indoor environment; (iv) have the ability to reach almost all organs in the human body, including the liver (Oberdörster *et al.,* 2002; Miller *et al*., 2017), placenta (Bové *et al.,* 2019; Liu *et al.,* 2021) and amniotic fluid (Barošová *et al*., 2015), heart (Calderón-Garcidueñas *et al.,* 2019b; Maher *et al.,* 2020), and central nervous system (Tjälve *et al.,* 1996; Oberdörster *et al.,* 2004; Elder *et al.*, 2006; Geiser & Kreyling, 2010; Maher *et al*., 2016); (v) have a larger surface area per unit mass, compared to coarse particles; and (vi) can be highly bioreactive (Donaldson *et al.,* 2001; Nel *et al*., 2006; Maher *et al.,* 2016).

Exposure to Fe-bearing UFPs might play a specific role in adverse health effects (Maher *et al*., 2016; 2020). Labile, bioreactive Fe^{2+} (a specific component within magnetite ($Fe_3O_4 = FeO \cdot Fe_2O_3$, a mixed Fe^{2+}/Fe^{3+} oxide), for example), can be toxic to living cells; it can catalyse excess production of reactive oxygen species and has been linked with neurodegenerative changes similar to those occurring in Alzheimer's disease (Smith *et al.,* 1997; Wu *et al.,* 2013; Coccini *et al.,* 2017; Maher, 2019). Fe-bearing UFPs may be toxic on their own but also often co-associate with other transition and heavy metals, including Cr, Cu, Mn, Ni, Pb, Zn (Spassov *et al.,* 2004; Chen *et al.,* 2006; Kim *et al.,* 2007; Maher *et al.,* 2016;

Yang *et al.,* 2016; Hofman *et al.,* 2020) and organic species, including PAHs (Lehndorff & Schwark, 2004; Halsall *et al.,* 2008).

In the urban environment, a great variety of both vehicular and non-vehicular sources of Fe-bearing UFPs has been identified, including exhaust emissions, brake-wear, tyre-wear, resuspension of roadside dust, underground, rail and tram systems, aircraft and shipping emissions, welding fumes, waste incineration, biomass burning, construction, demolition, power plants and cigarette smoking (e.g. Thorpe & Harrison, 2008; Salma *et al.,* 2009; Kumar *et al.,* 2013; Gonet & Maher, 2019). However, estimation of the contributions made by specific sources to total airborne PM or PNC (particle number concentration) has proved challenging, and variable between different studies (e.g. Viana *et al.,* 2008; Bukowiecki *et al.,* 2009a; Harrison *et al.,* 2011; 2012; Lawrence *et al*., 2013; Beddows *et al*., 2015; Crilley *et al*., 2017; Conte & Contini, 2019). Although the concentrations of gaseous and particulate engine exhaust emissions have been decreasing notably in the last 20 years, due to increasingly stringent legislation, non-exhaust emissions are currently unregulated and presently constitute a similar or even higher proportion of urban PM_{10} (PM with an aerodynamic diameter < 10 μm) concentrations, compared to exhaust emissions (e.g. Lawrence *et al.,* 2013; Denier van der Gon *et al.,* 2018; Conte & Contini, 2019).

One of the major sources of airborne, Fe-bearing UFPs in the roadside environment is brake emissions (Gonet & Maher, 2019). Although source apportionment estimates differ, brake-wear PM has been reported to contribute more to total PM_{10} mass (~11% – 21%; Bukowiecki *et al.,* 2009a; Lawrence *et al.,* 2013) than to particle number (~1.7%; Harrison *et al.,* 2011) at the roadside.

The emission of solid (non-volatile) brake-derived components depends on the braking conditions but in real-world conditions, they usually exceed 75 wt.% of total brake emissions (Sanders *et al.,* 2002; Roubicek *et al.,* 2008). Fe is frequently the dominant metal in non-volatile brake-wear PM (arising from conventional low-metallic brake pads and cast iron discs), often constituting ~50% of the total mass of particles emitted from brake systems (Sanders *et al.,* 2003; Adachi & Tainosho, 2004; Kukutschová *et al.,* 2011). The number-normalised PSD of brake emissions is usually dominated by fine and ultrafine fractions, with UFPs (< 0.1 μm) constituting up to 95% of total particle number (Garg *et al.,* 2000; Sanders *et al.,* 2003; Verma *et al.,* 2016). Since UFPs constitute the vast majority of brake-wear particle numbers, and Fe is the dominant metal of those emissions, brake-derived dust might thus be a major source of urban airborne Fe-bearing UFPs (Gonet & Maher, 2019).

Fe in brake emissions has been found in various forms: magnetite (Fe_3O_4), maghemite (γ-Fe_2O_3), haematite (α-Fe_2O_3), wüstite (FeO) and metallic Fe (α-Fe) (e.g. Kukutschová & Filip, 2018). Little attention has yet been paid to the mass concentrations of specific magnetic phases/minerals. In terms of potential association with neurodegeneration and Alzheimer's disease, the oxidation state of Fe (e.g. metallic Fe, Fe^0; ferrous Fe, Fe^{2+}; ferric Fe, Fe^{3+}) may be critical (Smith *et al.,* 1997; Collingwood & Dobson, 2006; Castellani *et al.,* 2007; Pankhurst *et al.,* 2008; Plascencia-Villa *et al.,* 2016; Maher *et al.,* 2016; Maher, 2019). Hence, quantitative evaluation of the magnetic mineralogy of roadside, traffic-derived UFPs, and especially, of the concentration and particle size distribution of Fe^{2+}-bearing magnetite, may be particularly important in the context of human health hazard.

Here, we use a combination of magnetic component analysis of room- and low-temperature magnetic measurements, and scanning and transmission electron microscopy to obtain quantitative evaluation of the mineralogy and particle size of magnetically-ordered particles within airborne PM emissions originating from automotive brake systems.

5.3. Methods

5.3.1. Brake-wear generation, braking cycle and particulate matter sampling

Brake-wear emission tests were performed using a full-scale brake dynamometer (Link M2800) at VŠB – Technical University of Ostrava, Czech Republic. The dynamometer was equipped with an environmental chamber, with cooling airflow of 2500 m^3/h around the brake system. Commercially available low-metallic brake pads, a cast iron brake disc and hardware of a mid-size passenger car were used, during the ISO26867 brake cycle simulating friction behaviour at different speeds and brake pressures. The composition of the brake pad was analysed using X-ray diffraction (XRD). The dynamometer test was conducted 4 times and results for the 4 sets of collected samples were averaged, i.e. the particle size distributions (Figure 24A), IRMs (Figure 25), magnetic component analysis, and estimated mass concentrations of magnetite, metallic Fe and haematite. The same brake pad/disc system was used 4 times (each time a new set of brake pads was used).

A Dekati ELPI+ impactor was used to collect brake-derived primary particles directly in the dynamometer chamber, on Al foils, in 14 stages (size fractions), from 0.016 µm to 10 µm (Appendix A: Table A9). Additionally, the non-airborne fraction, swept from the floor of the dynamometer chamber after the test cycle, was also collected (hereafter called 'non-airborne brake emissions').

All Al foils were weighed before and after the dynamometer tests, and the difference treated as the mass of the collected brake-derived particles. The mass measurements were made using a Mettler Toledo XP6U/M ultra-micro balance with accuracy of 0.1 µg.

Number-normalised PSD was estimated based on the masses of particles collected on each foil and average effective density of airborne brake-derived particles emitted by a low-metallic brake pad (0.75 g/cm^3), from Nosko & Olofsson (2017a).

5.3.2. Magnetic measurements and electron microscopy

Brake-wear emissions were analysed by magnetic remanence measurements conducted at room temperature at the Centre for Environmental Magnetism and Palaeomagnetism, Lancaster University, U.K.; and at low temperature (down to 77 K) at the Centre for Science at Extreme Conditions, University of Edinburgh, U.K.

To obtain independent information on the composition, structure, morphology and particle size of the brake-wear particles, we used scanning (SEM) and transmission (TEM) electron microscopy to image and analyse the particles directly at the Research Institute of Biomolecular and Chemical Engineering, University of Pannonia, Veszprém, Hungary. Two units of the aluminium foil with the deposited particles (stage 10 with nominal particle size of 1.6 µm and stage 11 with nominal particle size of 2.5 µm) were analysed with SEM and TEM. The particle size given by the manufacturer (DEKATI) is an average size of particles collected by a certain stage (size fraction). The actual size distribution of the particles collected by each stage can vary across a wide range (e.g. Pagels *et al.,* 2005; Noël *et al.,* 2013), e.g. for the nominal size fraction of 3.0 µm, the particle size ranges from 0.2 µm up to even >10 µm (Pagels *et al.,* 2005).

Details of all of the sample preparation and analytical procedures are provided in the Appendix A: Sections A4 – A6).

5.4. Results

5.4.1. Particle size distribution

The PSD of the airborne brake-wear emissions is shown in Figure 24A in terms of both mass and number. UFPs (< 0.1 µm) contribute very little to the mass-based metrics, but account for > 99% of the total number of emitted brake-derived particles. Conversely, the mass-normalised PSD is dominated (> 90%) by particles bigger than 1 µm (Figure 24A). Similar results have been obtained elsewhere (Garg *et al.,* 2000; Verma *et al.*, 2016; Nosko & Olofsson, 2017b).

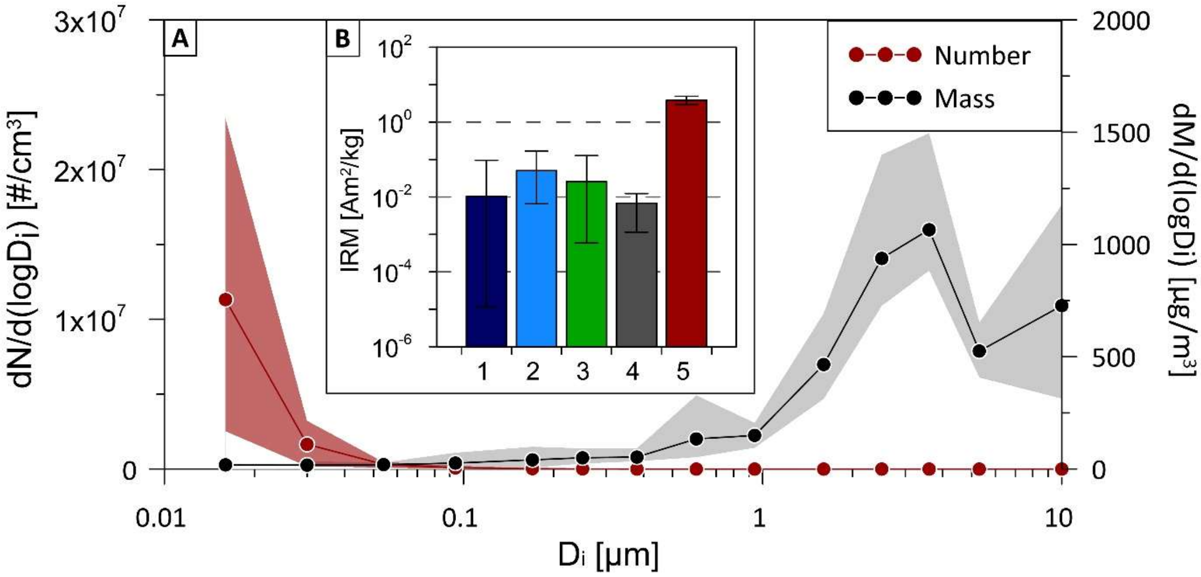

Figure 24. (A) Average mass- and number-normalised particle size distributions for the analysed brake emissions. M – particle mass; N – particle number; D_i – average grain size; the shaded areas represent the minimum and maximum levels of particle mass/number observed in the 4 dynamometer experiments. (B) IRM imparted at 1 T at room temperature at the Centre for Environmental Magnetism & Palaeomagnetism, Lancaster University, for (1) outdoor PM sources (Hansard *et al.,* 2012), (2) roadside PM in Lancaster (Halsall *et al.,* 2008; Gonet *et al.,* 2021b), (3) indoor PM (Halsall *et al.,* 2008), (4) engine exhaust PM (Gonet *et al.,* 2021b) and (5) airborne brake-wear PM (low-metallic brake pad/cast iron disc; this study).

5.4.2. Magnetic content of brake emissions

Figure 24B shows the room-temperature magnetic remanence (IRM, acquired at 1T) for various types of PM emissions measured in our laboratory, including indoor and outdoor PM, exhaust emissions and brake-wear (Gonet & Maher, 2019; Gonet *et al.*, 2021b). The IRM of a material depends on the concentration of magnetic grains, and their magnetic mineralogy and/or grain size distribution. Here, our analysed range of airborne particles display IRM values of between $\sim 0.01 \cdot 10^{-3}$ Am^2/kg and $\sim 95.8 \cdot 10^{-3}$ Am^2/kg for outdoor PM sources; between $\sim 0.06 \cdot 10^{-3}$ Am^2/kg and $\sim 8.32 \cdot 10^{-3}$ Am^2/kg for indoor PM sources; and for engine exhaust emissions between $\sim 5.1 \cdot 10^{-3}$ Am^2/kg (gasoline emissions) and $\sim 8.6 \cdot 10^{-3}$ Am^2/kg (diesel emissions).

In stark contrast, the IRM values for our brake-wear particles are 100 – 10,000 times higher; reaching average values of $\sim 3{,}383 \cdot 10^{-3}$ Am^2/kg for the airborne fraction (PM_{10}) and $\sim 8{,}891 \cdot 10^{-3}$ Am^2/kg for the non-airborne fraction. IRM values for airborne brake emissions were similar for all 4 sampling cycles, varying between $2{,}963 \cdot 10^{-3}$ Am^2/kg and $3{,}800 \cdot 10^{-3}$ Am^2/kg.

In comparison, IRMs for roadside PM, both the airborne fraction (pumped air samples, Lancaster, U.K.; Halsall *et al.*, 2008) and total roadside dust (dust swept from roadside surfaces), fall in the lower range between exhaust emissions (and other PM sources) and brake emissions (low-metallic brake pad/cast iron disc), reaching levels of $\sim 66.5 \cdot 10^{-3}$ Am^2/kg and $\sim 34.8 \cdot 10^{-3}$ Am^2/kg for airborne and total roadside PM, respectively (cf. Figure 24B).

For the size-fractionated brake emissions (Figure 25), IRM decreases with decreasing particle size from $> 3{,}000 \cdot 10^{-3}$ Am^2/kg for particle sizes ~1.6 – 10 µm (stages 10 – 14) to $< 500 \cdot 10^{-3}$ Am^2/kg for particle sizes ~0.016 – 0.054 µm (stages 1 – 3). This trend most probably reflects lower concentrations of both magnetite and magnetic Fe (cf. Appendix A: Figure A5 and discussion on the mass concentrations of magnetite and metallic Fe with particle size in Section 5.5. Discussion (Paper III)).

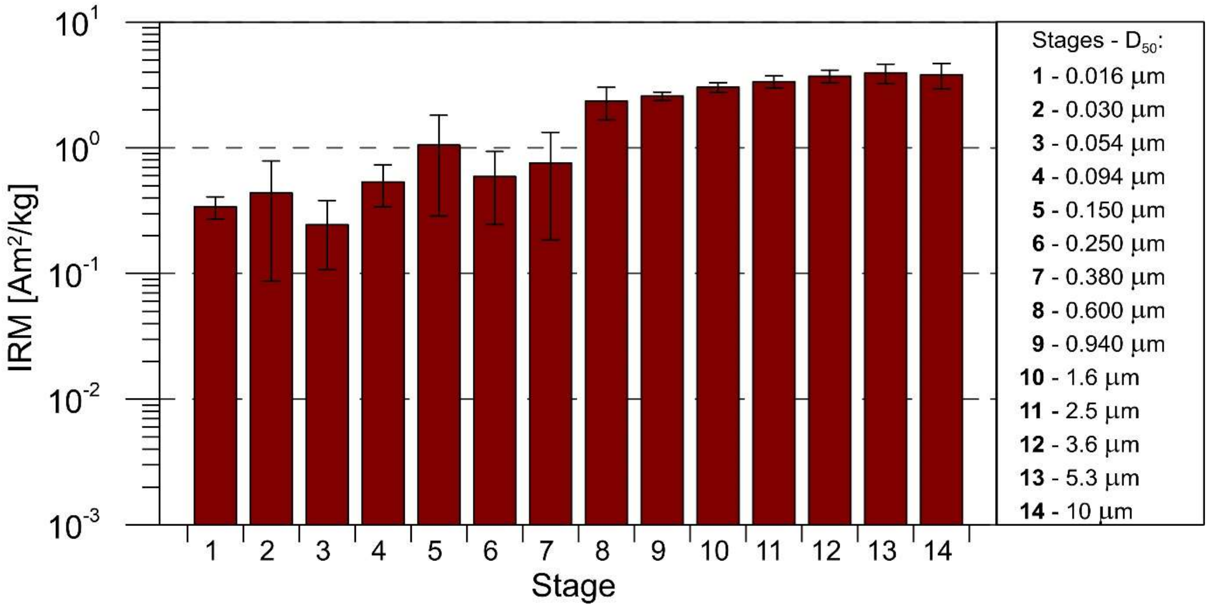

Figure 25. Average isothermal remanent magnetisation (IRM), imparted at 1 T at room temperature, for size-fractionated brake-wear emissions from low-metallic brake pads collected in 4 dynamometer sampling cycles.

5.4.3. Magnetic component unmixing

Each magnetic phase is characterised by several parameters, including the median destructive field of the IRM (MDF_{IRM}, indicating how easily a sample can be demagnetised); and a dispersion parameter (describing the level of scattering around the mean MDF_{IRM}). Detailed AF demagnetisation of IRM allowed identification of 3 magnetic components (C1, C2 and C3) in the brake emissions (Appendix A: Section A5). Two of these identified components are magnetically 'soft', i.e., they demagnetise at low AF values (MDF_{IRM} of 12 mT and 28 mT for C1 and C3, respectively), and one (C2) is magnetically 'hard', having distinctly higher MDF_{IRM} (81 mT). The dispersion parameter is lowest for C2 (~0.16), higher for C3 (~0.31) and highest for C1 (~0.40). On average, magnetic component C1 contributes ~37.6% to total IRM, component C2 accounts for ~5.6%, and C3 for ~56.8% of total IRM (Appendix A: Table A1). These 'magnetic' contributions can be used for estimation of mass concentrations of specific magnetic minerals/phases, i.e. magnetite, haematite and metallic Fe (see Section 5.5. Discussion (Paper III)).

5.4.4. Low-temperature magnetic measurements

Our low-temperature magnetic remanence measurements identify, first, magnetic transitions diagnostic of different minerals and particle sizes (see also Appendix A: Section A9). Specifically, the Morin transition, a first order magnetic transition in haematite, is visible at ~210 – 220 K, and the Verwey transition, diagnostic of the presence of magnetite, is seen at ~100 – 150 K (Figure 26A). The Verwey transition for the measured brake-wear samples is not sharp, reflecting either very small grain size (close to the stable single domain/superparamagnetic boundary, ~30 nm), non-stoichiometry of magnetite, and/or substitutions of Fe by other metals (e.g. Özdemir *et al.,* 1993). A relatively low Verwey transition temperature ($T_V < 100$ K) also suggests the presence of ultrafine grains of magnetite/maghemite (Özdemir & Dunlop, 2010; Özdemir *et al.,* 1993).

The low-temperature measurements also show sharp increase in magnetic remanence with cooling (Figure 26B), reflecting the magnetic 'blocking in' of ultrafine (< ~30 nm), superparamagnetic (SP) grains, which were magnetically unstable at room temperature through thermal agitation. To quantify the SP contribution, we estimated ΔM (Figure 26B), compared to the total IRM (at 5 T and 77 K), for the selected samples. Counter-intuitively, ΔM seems to decrease with decreasing particle size, reaching 44% – 46% for stages 13, 11 and 7 (~5.3 µm, ~2.5 µm and ~0.380 µm, respectively), and declining to 32% for stage 3 (~0.054 µm) and 28% for stage 1 (~0.016 µm). This behaviour might reflect: (1) agglomeration of SP grains and/or their adherence to bigger particles, and hence their effective assignment as larger particles (i.e. collected in the larger particle stages) by the impactor, and/or (2) the presence of SP, oxidised rims around larger magnetic grains. The latter has been suggested by Özdemir *et al.* (1993), Sagnotti *et al.* (2009) and Sagnotti & Winkler (2012).

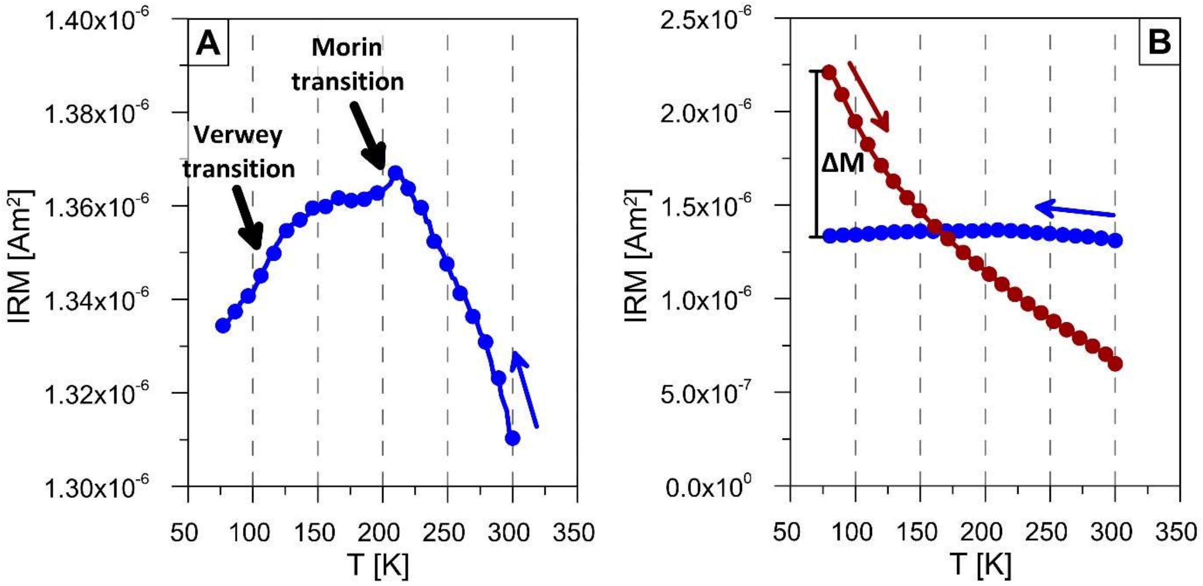

Figure 26. Low-temperature measurements for stage 11 (~2.5 μm) brake-wear emissions: (A) zero-field changes in IRM during cooling, after acquisition of IRM (at 5 T) at room temperature; and (B) the same cooling changes (blue curve) and zero-field changes of IRM while heating after acquisition of IRM (at 5 T) at 77K (red curve). ΔM reflects the contribution of superparamagnetic grains.

5.4.5. Scanning (SEM) and transmission (TEM) electron microscopy

Two brake-wear samples (stage 10 with particle size of ~1.6 μm and stage 11 with particle size of ~2.5 μm) were analysed using SEM and TEM. Figure 27 shows an overview SEM image of brake-wear particulate emissions (stage 11, ~2.5 μm). The sample is dominated by agglomerates of UFPs (one of which is marked '1'), with smaller numbers of larger grains with smooth surfaces and sharp edges (marked '2'). The larger, sharp-edged particles were also observed in our previous study (Kukutschová *et al.,* 2011). The size of the UFP agglomerates and the smooth, larger grains ranges between ~0.8 μm and 9 μm. Both agglomerates and larger grains have similar elemental composition, typical of brake emissions, with Fe, C and O being dominant, and with smaller amounts of Cu, Al, Si, S, Sn, Mg, P and Cr (EDS spectra in Figure 27).

Sb has sometimes been reported in brake-wear emissions and even suggested as a brake-wear tracer (e.g. Sternbeck *et al.,* 2002; Bukowiecki *et al.,* 2009b). In our brake-wear PM, we did not detect Sb (unsurprisingly, given its trace concentrations in the commercial brake pad used here, see Appendix A: Figure A2).

The TEM images show that the agglomerates comprise prolific numbers of UFPs ~10 nm – 50 nm in size (Figure 28 and Figure 29; see also Appendix A: Section A10). Elemental analysis using EDS in STEM mode showed the presence of C, O and Fe, with variable but typically lower concentrations of various other elements, including Mg, Al, Si, S, Ti, Cr, Cu, Zn and Sn (Figure 28). The distributions of these minor elements are not uniform over entire agglomerates; for example, Ti, Cr and Cu occur in specific nanoparticles within the agglomerate shown in Figure 28C. In terms of mineralogy, the agglomerates are dominantly composed of magnetite (Figure 28A and Figure 29) and haematite (Figure 29A), often covered with a thin shell composed of layers of graphitic/amorphous carbon (Figure 29A). Although it is challenging to quantify the concentration of haematite using TEM, it appears to be present in lower concentration than magnetite.

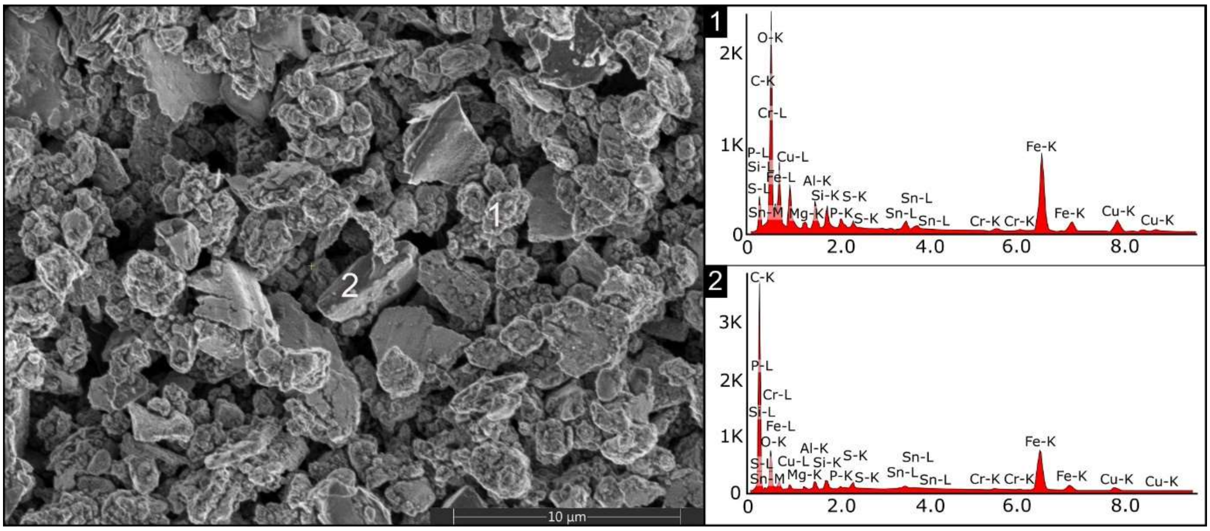

Figure 27. An overview SEM image of the stage 11 (~2.5 µm) size fraction of brake-wear emissions; EDS spectra for (1) an UFP agglomerate and (2) a large grain with smooth surface and sharp edges.

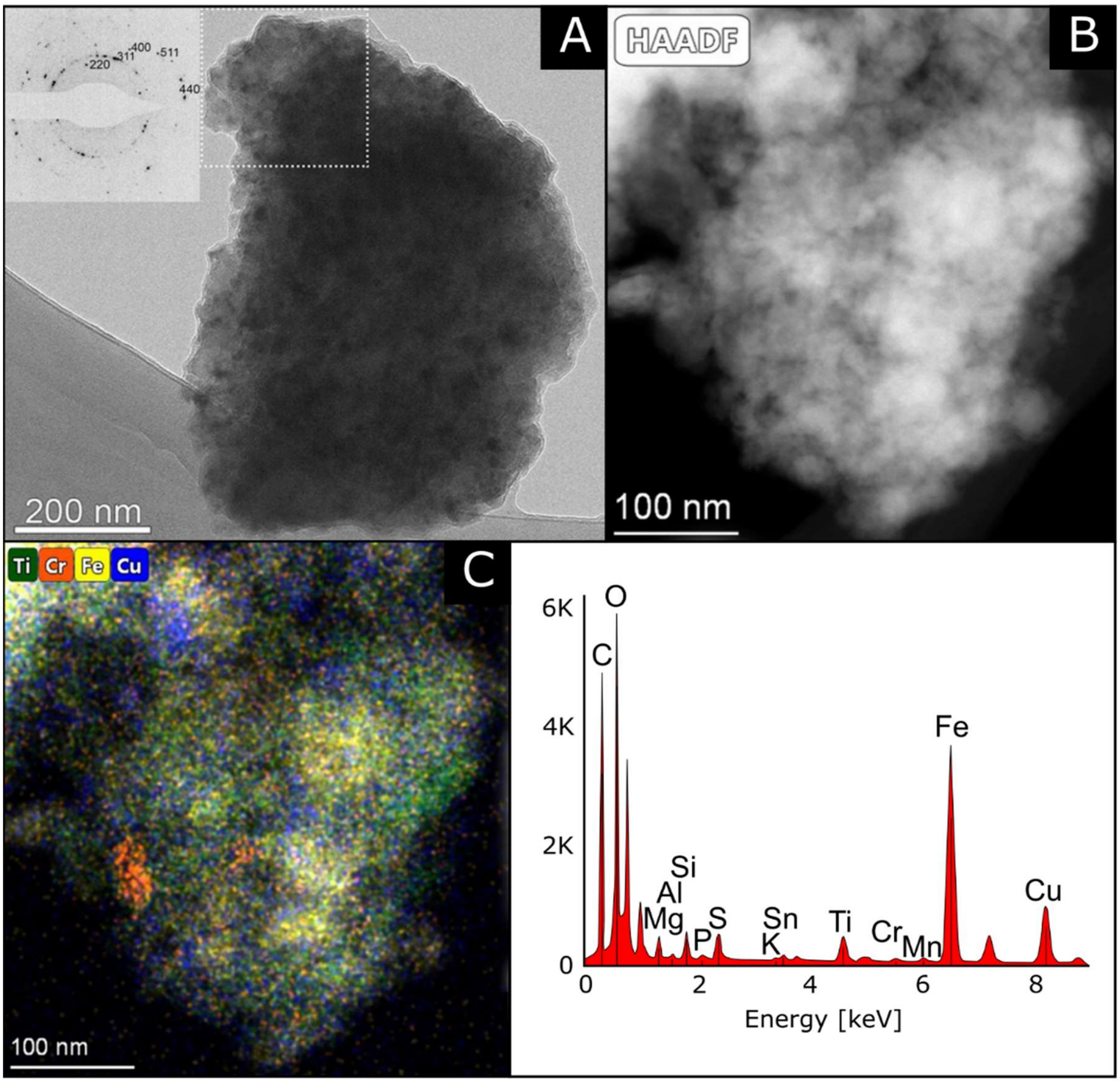

Figure 28. (A) TEM image of an UFP agglomerate with associated selected-area electron diffraction (SAED) pattern corresponding to an ensemble of randomly oriented magnetite nanocrystals; (B) high-angle annular dark-field (HAADF) image of an UFP agglomerate found in the sample of stage 10 (~1.6 µm), (C) its EDS elemental map obtained in scanning transmission mode (STEM), showing the distributions of Cr, Fe, Cu and Ti, and EDS spectra showing elemental composition.

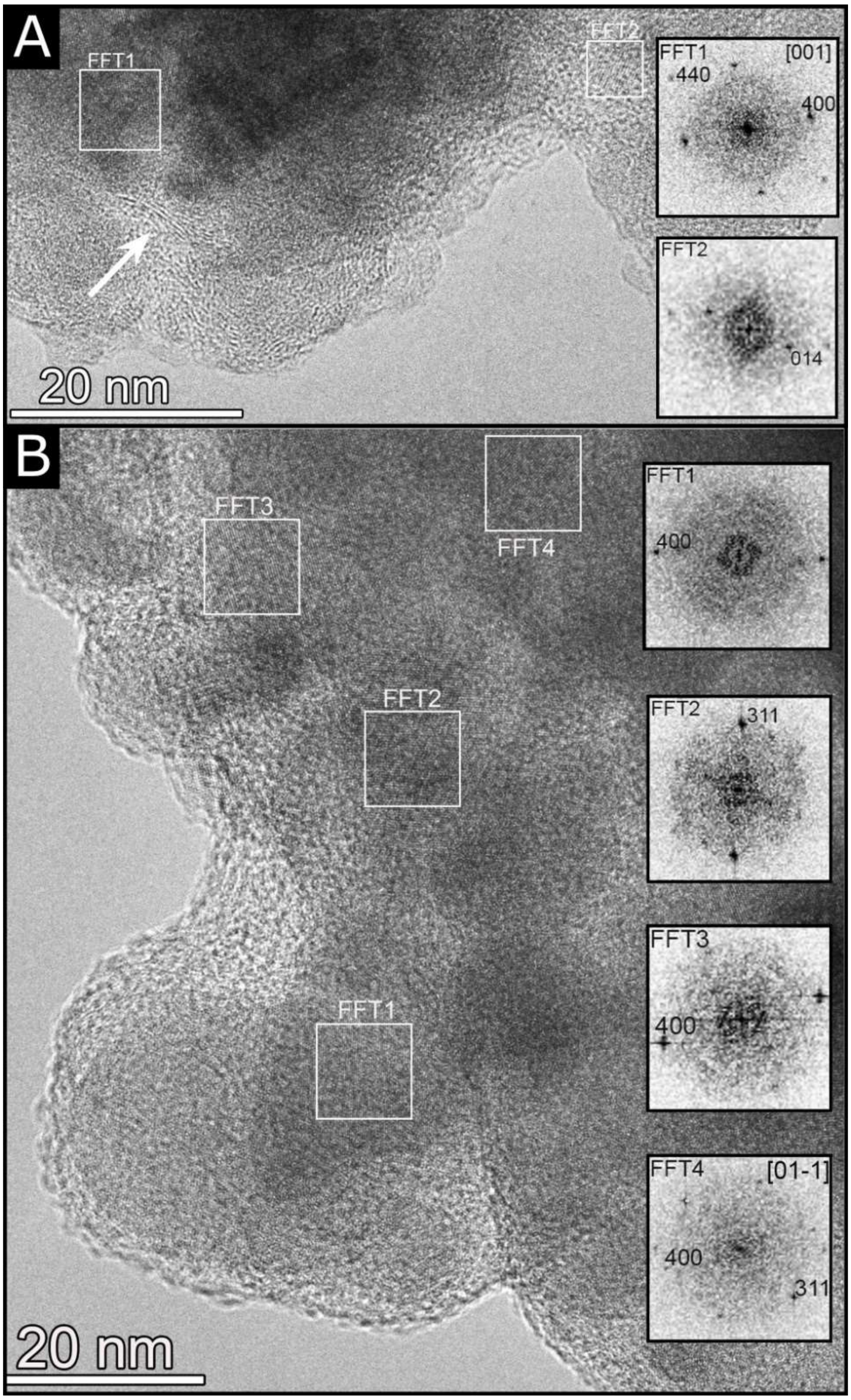

Figure 29. Structural analysis of iron oxide nanoparticles using TEM. (A) high-resolution (HRTEM) image of an UFP agglomerate found in the stage 11 (~2.5 μm) sample, with associated fast Fourier transforms (FFTs) of the indicated particle regions, containing reflections corresponding to periodicities in magnetite (FFT1) and haematite (FFT2); the arrow marks several layers of graphite/amorphous carbon with periodicity of 3.6 Å, similar to typical periodicities observed in atmospheric soot; (B) HRTEM image of an UFP agglomerate with associated FFTs obtained from specific particle regions, showing reflections consistent with lattice spacings in magnetite (stage 10, ~1.6 μm).

5.5. Discussion

Our results show that the concentrations of Fe-rich magnetic grains in airborne brake-wear emissions are very high (∼100 – 10,000 times higher), compared to other types of particulate pollutants produced in most urban environments (Figure 24B). Chronic exposure at the roadside or in-cabin to such high magnetite concentrations is especially worrisome because of the association of Fe-bearing (and especially magnetite) UFPs with the excess production of ROS in the brain, neurodegeneration and Alzheimer's disease (e.g. Plascencia-Villa *et al.*, 2016; Coccini *et al.,* 2017; Maher, 2019). In addition to roadside environments with frequent braking (e.g. close to traffic-control lights or speed bumps), Fe-rich UFPs occur in high concentrations in other environments, including underground subway/train stations (Moreno *et al.,* 2015) and areas affected by airborne emissions from iron-/steelworks (Li *et al.,* 2021).

The oxidation state of Fe in airborne PM appears important in terms of its health hazard (e.g. Smith *et al.,* 1997; Maher, 2019). Surface coatings (e.g. graphite/amorphous carbon) (Figure 29A) of UFPs might also change the uptake, distribution, clearance and toxicity of Fe-rich UFPs (e.g. Singh *et al.,* 2010; Feng *et al.,* 2018). Most brake-wear studies, however, have so far focused on mass and/or number concentrations of brake-wear emissions (e.g. Perricone *et al.,* 2017; Alemani *et al.,* 2018; Matějka *et al.,* 2020); few have analysed the elemental composition of the emitted particles (e.g. Menapace *et al.,* 2020), and almost none have studied the phase composition of the released particles. Given that magnetite contains Fe^{2+}, reportedly toxic to human cells through its catalysis of the Fenton reaction (e.g. Smith *et al.*, 1997), and that UFPs constitute the majority of brake-wear particles (both as discrete particles (collected by ultrafine size fractions of the impactor; Figure 24A) and agglomerates (collected by larger size fractions of the impactor; Figures 27 – 29)), a thorough, size-resolved evaluation of elemental, mineralogical and structural composition of airborne brake-wear emissions may be critical for further assessment of potential health impact.

Several different magnetic phases have been reported previously in brake emissions: haematite, magnetite, maghemite, wüstite and metallic Fe (e.g. Kukutschová & Filip, 2018). Here, we identified 3 magnetic components in brake emissions (cf. Appendix A: Section A5). No component can correspond to wüstite as its Neél temperature is 200 – 210 K (Cornell & Schwertman, 2003) so it does not carry magnetic remanence at room temperature (∼290 K). Moreover, the Neél temperature of wüstite was not observed on the heating curve from 77 K to room temperature (Figure 26B), excluding its presence in our analysed brake-wear samples.

The magnetic 'hardness' (high MDF_{IRM} of 81 mT) of component C2 suggests that it represents haematite. Haematite has previously been observed in other brake-wear studies (using Raman microspectroscopy, TEM/EDS and XRD) (review in Kukutschová & Filip (2018)). The presence of haematite in our dynamometer-generated brake-wear samples from low-metallic brake pads is evident from the Morin transition in the cooling curves (Figure 26A). Based on MDF_{IRM} data for synthetic haematite and our measured MDF_{IRM} of ~81 mT, C2 corresponds to haematite grains of ~120 nm in diameter (cf. Appendix A: Section A5). Based on IRM data for pure, synthetic haematite powders (see Appendix A: Section A5) (Maher *et al.,* 2004), it is possible to estimate mass concentrations (wt.%) of this mineral in the analysed samples. Hence, we estimate the average haematite mass concentration to be ~54.6 wt.% in the PM_{10} of airborne brake-wear emissions. However, due to haematite's low IRM (~25 – 60 times lower than that of magnetite, and ~450 times lower than of metallic Fe; cf. Appendix A: Table A2) and very low contribution to total IRM (~5.6%; Appendix A: Table A1), the inherent uncertainty of this estimated haematite mass concentration is very high, reaching levels up to ±32.8 wt.% (see Appendix A: Section A8 for more details). Although haematite was observed in TEM analysis (Figure 29A), its concentration appears much less than the 50 wt.% estimated using magnetic component analysis. It is, therefore, highly likely that the haematite mass concentration is magnetically over-estimated here.

Since the Verwey transition was observed in the cooling curve (Figure 26A), at least one of the 'soft' magnetic components (with relatively low MDF_{IRM} of 12 mT (C1) or 28 mT (C3)) comprises magnetite. Component C3 probably represents magnetite due to its higher MDF_{IRM} (28 mT for C3 vs 12 mT for C1; Appendix A: Table A1). Based on magnetic contributions from magnetic component analysis and average IRMs for sized magnetite particles (Maher, 1988), we can estimate the mass concentration of magnetite (see Appendix A: Section A5 for more details on the estimation). On average, the mass concentration of magnetite is ~20.2 wt.% of the total PM_{10} of brake emissions (~18.5 wt.% in $PM_{2.5}$ and ~7.6 wt.% in $PM_{0.2}$) (see Appendix A: Section A8 for details on the error estimations). It is likely that component C3 reflects a partially oxidised (maghemitised) magnetite, with a high contribution of SP grains, as indicated by the low-temperature magnetic properties (Figure 26). Magnetite has been observed, but not quantified, previously in brake-wear emissions (from low-metallic brake pad/cast iron disc) (Kukutschová *et al.,* 2010, 2011; Peikertová *et al.,* 2013; Verma *et al.,* 2016; Kukutschová & Filip, 2018).

The remaining component, C1, probably corresponds to metallic Fe, as indicated by high-temperature changes in magnetic susceptibility (Appendix A: Section A7). Its concentration is ~1.6 wt.% (see also Appendix A: Section A8 for the estimation uncertainties and Appendix A: Section A5 for details on the estimation).

The mass concentrations of all three magnetic phases generally decline with decreasing particle size (Appendix A: Figure A5). Magnetite concentrations reach levels ~20 wt.% for particles > 0.600 μm and decrease to 2 – 15 wt.% for particles < 0.380 μm. Metallic Fe content ranges between ~2.0 wt.% for size fractions > 1.6 μm and < 0.5 wt.% for particles < 0.400 μm. The physical and chemical processes occurring within brake systems while braking are complex, abrupt, and irregular (e.g. Kukutschová *et al.,* 2009; Lee & Filip, 2013; Nosko *et al.,* 2015; Kukutschová & Filip, 2018). Magnetic particles can be released from the magnetite filler that is often added to brake pads as solid lubricant, Fe/steel fibres used as reinforcing constituents (Jang, 2013; Kukutschová & Filip, 2018), and/or the cast iron brake disc. The XRD spectrum for the brake pad used in this study showed the presence of various phases of Fe, including metallic Fe (α-Fe), Fe oxides (magnetite/maghemite) and Fe oxide-hydroxides (Appendix A: Figure A2). The 3-component magnetic composition of Fe-bearing particles we identify in our brake-wear emissions may reflect either or both the release of abraded particles from the brake pad and friction-derived modification of particles through increasing stages of oxidation, from metallic Fe (in both brake pad and disc), through magnetite (potentially partially oxidised/mixed with maghemite), and finally to haematite.

Although brake systems are designed to abrade friction materials of brake pads and discs, our data show that high-temperature oxidation, evaporation and condensation processes are also important, creating very high numbers of discrete, rounded/spherical UFPs, which can subsequently be released to the atmosphere both as discrete UFPs (> 99% of PNC; Figure 24) and as agglomerates of UFPs (dominating larger size fractions; Figures 27 – 29). Interestingly, some authors have observed PM emissions (both solid and semi-volatile) from braking systems even without applying brakes, presumably due to similar evaporation/condensation processes (Wahlström & Olofsson, 2014; Hagino *et al.,* 2015; 2016; Ma *et al.,* 2020). These processes depend on the friction materials, braking conditions (e.g. braking frequency, applied pressure, air humidity), and even the age of the friction materials (due to rust). In general, below ~200°C, the abrasive processes usually dominate and larger (> 1 μm) wear particles are mostly emitted. At higher temperatures (> 160°C – 190°C), the concentration of UFPs (< 0.1 μm) increases considerably due to high-temperature oxidation, evaporation and condensation processes (e.g.

Garg *et al.*, 2000, Kukutschová *et al.,* 2010; 2011; Verma *et al*., 2016; Piscitello *et al.,* 2021). These ultrafine particles subsequently agglomerate and form larger aggregates, such as these observed in our SEM/TEM images (Figures 27 – 29 and Appendix A: Section A10). Importantly, only impactors/particle sizers (e.g. ELPI+, OPS and/or SMPS) are conventionally used to evaluate particle size distributions of brake-wear emissions. Without further analysis (e.g. using SEM and/or TEM), it is impossible to distinguish between discrete larger grains and agglomerates of UFPs, since both of these are classified as 'large' particles by an impactor/particle sizer. Hence, in many studies the presence of agglomerated ultrafine particles in coarse fractions is not analysed or discussed whatsoever.

The magnetic properties of brake-wear emissions deposited on vehicle wheel rims have been investigated in several studies (Sagnotti *et al.,* 2009; Chaparro *et al.,* 2010; Marié *et al.,* 2010; Sagnotti & Winkler, 2012). Chaparro *et al.* (2010), for example, observed IRM of these wheel deposits to be between $570 \cdot 10^{-3}$ Am^2/kg and $1{,}201 \cdot 10^{-3}$ Am^2/kg, substantially lower than the IRMs of the non-airborne brake-wear we obtained here ($\sim 8{,}891 \cdot 10^{-3}$ Am^2/kg). These previous studies suggested that brake-wear PM is dominated by magnetic grains > 0.1 μm or even > 1 μm (albeit with uncertainty regarding any SP fraction) (Sagnotti *et al.,* 2009; Chaparro *et al.,* 2010; Marié *et al.,* 2010; Sagnotti & Winkler, 2012). However, our results, based on size-fractionated airborne brake emissions, show high IRMs for all collected size fractions, including those smaller than 0.1 μm (Figure 25). This discrepancy probably reflects different methods of sample collection. Here, we collected particles which had originated from the friction couple (brake pad/cast iron disc), during braking, using a full-scale dynamometer and one formulation of brake pads; and analysed the magnetic properties of this size-fractionated brake-wear. Most UFPs emitted from car braking systems probably do not settle on the wheel rim, but are released to the roadside air. It is also likely that PM samples settled on wheel rims, contain, besides highly magnetic brake-wear particles, some portion of tyre-wear, roadside and soil-derived resuspended PM, which display lower IRMs (cf. Figure 24B and Paper II). Thus, the wheel-deposited PM mixture has lower magnetic content than our 'pure' brake-wear particles. The age of brake pads might also be important. In the dynamometer experiments, we used a new set of brake pads and discs, whereas car brake pads often rust as they age. As rust is a mixture of hydrous Fe oxides and Fe oxide-hydroxides (rather than 'pure', well-crystalline Fe oxides, e.g. highly magnetic magnetite), the measured IRM of such 'aged' brake emissions will be lower compared to 'new' friction materials from dynamometer experiments. Vehicle-derived rust might contribute to the ferrihydrite reported by Pattammattel *et al.* (2021)

in roadside PM analysed in Los Angeles, USA. Moreover, wheel rim-deposited PM might oxidise with residence time in the urban air (metallic Fe oxidising to magnetite/maghemite, and then into haematite). Each oxidation stage will decrease the final, measured IRM value of such deposited material.

Various studies show the abundant presence of Fe-bearing UFPs in roadside PM (e.g. Ntziachristos *et al.,* 2007; Sanderson *et al.,* 2014; 2016; Yang *et al.,* 2016; Gonet & Maher, 2019; Long *et al.,* 2020; Zhang *et al.,* 2020). Magnetic data for roadside PM have also shown the presence of ultrafine, SP grains (< ~30 nm) in roadside air pollution (e.g. Muxworthy *et al.,* 2002; 2003; Sagnotti *et al.,* 2006; 2009). However, SP grains could occur as discrete ultrafine grains and/or as oxidized rims around larger particles, arising from cracking of cation-deficient coatings of the unoxidised core (Özdemir *et al.,* 1993; Muxworthy *et al.,* 2002; 2003; Sagnotti *et al.,* 2009, Sagnotti & Winkler, 2012; Rea-Downing *et al.,* 2020). Indeed, specifically for particulate brake-wear emissions, magnetic studies have provided contradictory data on the presence of discrete ultrafine SP grains versus SP oxidised rims around larger magnetic grains (Sagnotti *et al.,* 2009; Sagnotti & Winkler, 2012). Our low-temperature (77 K) magnetic measurements identify that the SP contribution to total magnetic remanence of brake emissions varies from ~25% to 45%. In contrast, Marié *et al.* (2010) obtained very low values (0.0 – 0.8%) of frequency dependence of magnetic susceptibility ($\kappa_{fd\%}$) for brake-wear. This parameter is sensitive to the presence of SP grains and is usually higher than ~5 – 6% in the presence of SP grains (Dearing *et al.,* 1996). Here, we also obtained low $\kappa_{fd\%}$, ranging between 0.5% and 3.4% (data not shown). To resolve these apparently contradictory magnetic data, we used, besides low-temperature magnetic measurements, an independent analytical approach, TEM.

Our TEM analysis shows that agglomerated UFPs dominate even the larger size fractions (~1.6 – 2.5 μm) of brake-wear emissions, consistent with our previous study (Kukutschová *et al.,* 2011). These aggregates comprise rounded/spherical particles ~10 nm – 50 nm in size, abundant in Fe oxides, with smaller concentrations of Al, Cu, Si, Sn, Mg, Cr, Mn and Zn, in places surrounded by or embedded in C (Figures 27 – 29 and Appendix A: Section A10). The presence of C is probably a product of the oxidative wear of phenolic resin, used in brake pads as a binder (Filip *et al.,* 2002; Kukutschová & Filip, 2018). Liati *et al.* (2019) found brake-derived agglomerates of UFPs, with similar rounded/spherical morphology and elemental composition to our agglomerates (Figures 27 – 29 and Appendix A: Section A10). We did not observe SP oxidised rims using TEM, and the presence of such prolific numbers of agglomerated, magnetic UFPs can readily account for the observed SP behaviour, i.e. the large increase in IRM at 77 K (Figure 26B).

Interestingly, we observed measurable magnetic remanence for all size fractions, including those smaller than 30 nm (stages 1 and 2 in Figure 25). Theoretically, magnetite grains < 30 nm, haematite < 27 nm and metallic Fe < 8 nm should not hold any magnetic remanence at room temperature due to thermal agitation of their moments, hence resulting in SP behaviour (Dunlop, 1973; Özdemir *et al.,* 1993; Bødker & Mørup, 2000; Pankhurst *et al.,* 2008). Magnetic component analysis suggests that metallic Fe is responsible for only ~36% of IRM for stages 1 and 2 (< 30 nm; Appendix A: Figure A3); hence, the measurable IRM of these ultrafine particle size fractions likely reflects magnetic interactions of SP grains of magnetite, resulting in collective SD-like behaviour. Similar effects were observed by Radhakrishnamurty *et al.* (1973) and Maher (1988). This collective, SD-like behaviour might also explain the low values of frequency dependent magnetic susceptibility for brake-wear emissions obtained in our study, and by Marié *et al.* (2010).

The very strongly magnetic nature of brake-derived PM also has important consequences for interpreting magnetic monitoring studies, regarding the properties and sources of the magnetic PM deposited on biological surfaces (e.g. see review by Hofman *et al.* (2017)). Sagnotti *et al.* (2009) and Sagnotti & Winkler (2012) compared the magnetic properties of roadside PM, petrol, diesel, and brake emissions. They noted close resemblance between the magnetic properties of brake emissions and the roadside PM accumulated on air filters and roadside leaves. This now appears unsurprising, given that brake-derived magnetite might constitute 68 – 85% of total airborne magnetite in the roadside environment, as estimated in our recent study (Gonet *et al.,* 2021b). Moreover, the presence of brake-derived metallic Fe might be another confounding factor.

Air pollution in urban environments occurs in spatially and temporally variable concentrations, changing from country to country, town to town, even from one side of the street to another (Matzka & Maher, 1999). Locally, air pollution levels depend on the proximity to major roads, traffic characteristics, local road structure and topography, time of the day, weather conditions and season (e.g. Jeong *et al.,* 2015; Pasquier & André, 2017). Specifically, high concentrations of brake-wear emissions are expected in proximity to traffic-control lights (or speed bumps), or where traffic jams are frequent, and braking (and accelerating) is repetitive. At such sites, co-association between brake-derived PM and engine exhaust emissions might explain the correlation between concentration-dependent magnetic parameters (e.g. IRM) and exhaust-related metals (e.g. Pb) (Maher *et al.,* 2008), even though the magnetic properties of roadside PM might be dominated by brake-wear emissions, rather than by engine-exhaust PM (Gonet *et al.,* 2021b). However, at other heavily polluted urban sites (e.g. close to highways where engine exhaust emissions dominate), brake-derived PM is likely to occur in low (or sometimes negligible) concentrations due to rather sporadic braking.

Indeed, this inter-correlation between the concentrations of different traffic-related sources of PM in some sites (e.g. close to traffic lights) and lack of such correlation at other sites (e.g. close to freeways) might be a key reason why source apportionment of different traffic-derived sources of PM in urban environments is challenging and variable between different studies and sampling sites (e.g. Bukowiecki *et al.,* 2009a; Harrison *et al.,* 2011; 2012; Lawrence *et al.,* 2013). Thus, careful selection of different types of roadside sampling sites is essential for characterising and quantifying different roadside PM sources, and resultant human exposure levels to those different sources.

Notably, over 99% of the PNC of our solid (non-volatile) brake-wear particles is smaller than ~200 nm (Figure 24). Moreover, even larger particle collection stages are dominated by agglomerates of UFPs ~10 nm – 50 nm in diameter (Figures 27 – 29), which, depending on particle/cell interactions, have the potential to release millions of discrete UFPs inside the human body. Such small particles have been shown to reach almost all major organs, including the brain; the latter accessible directly by inhalation via the olfactory bulb (Oberdörster *et al.,* 2004; Maher *et al.,* 2016), and/or indirectly through ingestion/swallowing and transfer via the gut wall and neuroenteric system (Calderón-Garcidueñas *et al.,* 2020), and/or via the systemic circulation. The presence of magnetite, Fe- and other metal-rich air pollution UFPs has been demonstrated recently in the blood serum, and pleural effusions, of residents living in Beijing, China (Lu *et al.,* 2020).

Maher *et al.* (2016) and Calderón-Garcidueñas *et al.* (2020) observed exogenous, rounded/spherical UFPs (usually < 150 nm) of Fe-rich composition, including magnetite, in frontal cortex and brainstem tissues, similar to those found in the brake emissions in this (Figure 28 and Figure 29) and previous studies (Kukutschová *et al.,* 2010). Exogenous, carbon- and Fe-rich UFPs have also been found in other human tissues, including heart (Calderón-Garcidueñas *et al.,* 2019b; Maher *et al.,* 2020), human serum and pleural effusions (Lu *et al.,* 2020), placenta (Bové *et al.,* 2019; Liu *et al.,* 2021) and amniotic fluid (Barošová *et* *al.,* 2015). These UFPs are usually associated both with other metals (e.g., Al, Ca, Ce, Co, Cr, Cu, Mn, Ni, Pt, Ti, Sn and Zn) (Barošová *et al*., 2015; Maher *et al.,* 2016; Bové *et al.,* 2019; Calderón-Garcidueñas *et al.,* 2019b; 2020; Lu *et al.,* 2020; Liu *et al*., 2021) and with evidence of biological dysfunction, e.g. misfolded proteins, neurites and mitochondrial damage in the brainstem (Calderón-Garcidueñas *et al.,* 2020), and mitochondrial damage and ventricular up-regulation in the heart (Calderón-Garcidueñas *et al.,* 2019b; Maher *et al.,* 2020).

In the roadside environment, various toxic metals (e.g. Al, Ba, Cu, Fe or Mn) (Gao *et al.,* 2020), and especially potentially neurotoxic magnetite, originate abundantly from brake-wear (Thorpe & Harrison, 2008; Kukutschová *et al.,* 2010; 2011; Peíkertová *et al.,* 2013; Straffelini *et al.,* 2015; Peíkertová & Filip, 2016; Verma *et al.,* 2016; Kukutschová & Filip, 2018; Gonet *et al.,* 2021b). Both Fe and Cu might catalyse ROS production (Smith *et al.,* 1997; Allsop *et al*., 2008; Charrier & Anastasio, 2011; Tabner *et al.,* 2010; Li & Reichmann, 2016; Gao *et al*., 2020). Further, mixtures of metals (e.g. Fe and Cu) can act synergistically to promote oxidative cell damage (Charrier & Anastasio, 2011). Exposure to Ba, found in human amniotic fluid (Barošová *et al*., 2015), might additionally lead to cardiovascular, renal, metabolic, neurological and mental disorders (e.g. Kravchenko *et al*., 2014). Hence, brake-wear particulate emissions, rich in potentially toxic metals and organic matter, might exert adverse impacts on various human organs, including the brain, at every life stage, from foetal to adult.

In vitro and *in vivo* studies of the pulmonary and cardiovascular toxicity of brake-wear PM (both 'airborne' and 'non-airborne' fractions) show that brake emissions can cause oxidative stress and chromosomal damage, invoke pro-inflammatory responses and increase ROS production (Gasser *et al*., 2009; Kukutschová *et al*., 2009; Zhao *et al.,* 2015; Kazimirova *et al*., 2016; Malachova *et al.,* 2016; Barosova *et al*., 2018; Puisney *et al*., 2018; Rajhelová *et al*., 2019; Selley *et al*., 2019). Given the predominance of UFPs (99% of PNC < 200 nm; Figure 24) in brake-wear emissions, our identification of high concentrations of magnetite in $PM_{0.2}$ (~7.6 wt.%) and its reported association with neurodegenerative diseases, it seems both timely and important for the neurotoxic potential of the specific components of brake-wear emissions to be investigated in detail. Indeed, the impacts of Fe and other transition metals in airborne PM are likely under-estimated in such studies at present, due to assay-induced metal precipitation/immobilization, e.g. in phosphate-buffered systems (Reed *et al.,* 2021).

The ISO26867 dynamometer cycle, used in this study, is an established and commonly used brake dynamometer cycle in mechanical and tribological studies of brake systems. It covers a wide variety of driving and braking conditions, including, among others, harsh braking events which likely happen only episodically in urban areas. This cycle might thus not be fully representative for urban driving. Brake pad/disc temperature is a critical parameter in terms of the release of ultrafine particles. During the ISO26867 cycle, this temperature can reach levels higher than these usually occurring when driving in cities (e.g. Nosko *et al.,* 2015; 2017; Perricone *et al.,* 2017; Alemani *et al.,* 2018). Follow-up magnetic, elemental and morphological analyses of brake-wear emissions, using a less severe brake cycle (e.g. the WLTP-based cycle proposed by Mathissen *et al.* (2018)) would be valuable for further characterising and understanding the generation and concentration of brake-derived UFPs.

In this study, we tested and analysed PM emissions from an example of a brake system for a middle-size passenger car, commercially-available and widely-used on the European market. Although the range of friction materials used on the global market is very wide (e.g. Hulskotte *et al.*, 2014), our magnetic and compositional data are generally in line with other studies of brake-wear emissions. The three magnetic phases observed in this study (i.e. magnetite, haematite and metallic Fe) have been reported (but not quantified) by other authors (e.g. Peikertová *et al.,* 2013; Verma *et al.,* 2016; Kukutschová & Filip, 2018). Our SEM/TEM analyses showed the presence of Fe, C and O, with lower concentrations of Cu, Al, Si, S, Sn, Mg, P and Cr (cf. Figure 27 and Figure 28). All these elements have been commonly observed in brake-wear emissions (e.g. review in Kukutschová & Filip (2018)). Hence, our results seem to be representative for commonly used friction materials.

5.6. Conclusions

Combining magnetic component analysis (based on magnetic remanence), low-temperature and high-field magnetic measurements, and electron microscopy enabled, for the first time, size-resolved quantitative evaluation of the magnetic mineralogy of airborne brake-wear emissions.

We observed three magnetic phases: haematite, magnetite, and metallic Fe. From the magnetic component analysis, the average magnetite concentration in total PM_{10} of brake emissions is ~20.2 wt.%, metallic Fe ~1.6 wt.%, and haematite ~54.6 wt.%. The haematite concentration is likely magnetically over-estimated (high uncertainty being associated with its much lower IRM compared with magnetite and metallic Fe).

Most brake-wear particles (> 99% of PNC) are smaller than 200 nm. Brake-wear emissions exhibit a strong superparamagnetic signal, reflecting the presence of very high numbers of UFPs < ~30 nm in size. Even the larger brake-wear PM size fractions are dominated by agglomerates of ultrafine, superparamagnetic grains, which explains their low-temperature increase in IRM. Depending on interactions between these agglomerates and potential biological targets, release of discrete UFPs might result in chronic supply of toxic metal-bearing UFPs to all major organs of the body. Such UFPs likely pose a threat to neuronal and cardiovascular health after inhalation and/or ingestion. The concentration of magnetite in brake-wear particle sizes smaller than 200 nm ($PM_{0.2}$) is estimated to be ~7.6 wt.%. Magnetite particles < 200 nm might be especially hazardous to the brain and the heart, contributing both to microglial inflammatory action, and catalysis of the Fenton reaction, leading to excess ROS production and cell damage due to oxidative stress.

Given this predominance of UFPs in non-volatile brake-wear emissions, high concentrations of magnetite in $PM_{0.2}$, and the reported association between excess Fe and neurodegenerative diseases, the neurotoxic potential of brake-wear emissions warrants detailed investigation. We hypothesise that chronic exposure to such particles can plausibly account for the observed PM dose/response relationships reported for cardiovascular disease, and for neurodegenerative diseases, including Alzheimer's and Parkinson's disease.

Finally, based on current knowledge, it is evident that particulate emissions generated by wear of brake pads/discs can be controlled by modification of brake pad formulation and/or brake pads/disc coatings. However, great care is required in order to avoid the risk of exchanging one health hazard (e.g. asbestos used in brake formulations before ~1990) for another (e.g. cytotoxic metal-rich UFPs). Another potentially effective strategy to limit brake emissions is the replacement of standard, friction brakes by regenerative brake systems, increasingly implemented by manufacturers of electric vehicles.

Contributions of authors

Tomasz Gonet: Conceptualization, Data curation, Writing – original draft, Writing - review & editing. **Barbara A. Maher**: Conceptualization, Supervision, Writing - review & editing**. Ilona Nyirő-Kósa**: Data curation, Writing - review & editing. **Mihály Pósfai:** Writing - review & editing, Supervision. **Miroslav Vaculík:** Data curation. **Jana Kukutschová**: Conceptualization, Supervision.

Chapter Six: General discussion

6.1. Paper I: Airborne, vehicle-derived Fe-bearing nanoparticles in the urban environment – A review

Air pollution is currently the largest environmental cause of mortality worldwide, being responsible for an estimated 9 million premature deaths yearly (cf. Figure 30) (Landrigan *et al.*, 2018; HEI, 2020). The consequent economic burden of air pollution is thus very high. Pollution-related worldwide welfare losses have been estimated to amount US$4.6 trillion every year (Landrigan *et al.*, 2018). In urban environments, population exposure to PM is inevitable. Over the last few decades, the proportion of people living in cities has been rising consistently, and it is expected to keep increasing in the foreseeable future (e.g. Our World in Data, 2017; UN, 2018). It is thus increasingly important to identify the sources of urban air pollution and mitigate its negative health effects.

UFPs (< 0.1 µm) might pose a specific hazard to human health. They are abundant and pervasive in urban environments and, due to their small size, they are able to penetrate deeply into human body and access all major organs, including the heart (Calderón-Garcidueñas *et al.*, 2019b; Maher *et al.,* 2020) and brain (Oberdörster *et al.,* 2004; Maher *et al.,* 2016; Calderón-Garcidueñas *et al.*, 2020). These UFPs are usually rich in potentially cytotoxic metals (e.g. Fe, Al, Ca, Ce, Co, Cr, Cu, Mn, Ni, Pt, Ti, Sn and Zn) (Barošová *et al.,* 2015; Maher *et al.,* 2016; Bové *et al.*, 2019; Calderón-Garcidueñas *et al.,* 2019b; 2020; Lu *et al.,* 2020; Liu *et al.*, 2021) and might pose a threat to respiratory, cardiovascular and neurological health.

Such metal-rich (especially Fe-rich) UFPs have been found in the human heart and associated with ventricular up-regulation (Calderón-Garcidueñas *et al.,* 2019b; Maher *et al.*, 2020). They have also been reported to reach the brain (Oberdörster *et al.,* 2004; Maher *et al.,* 2016; Calderón-Garcidueñas *et al.*, 2020), either via systemic circulation (Lu *et al.*, 2020) and/or axonal pathways (Maher *et al.*, 2016; Calderón-Garcidueñas *et al.,* 2020). Magnetite ($Fe_3O_4 = FeO{\cdot}Fe_2O_3$) UFPs might pose a specific hazard to neurological health (e.g. Maher, 2019). The presence of this highly magnetic, mixed Fe^{2+}/Fe^{3+} oxide in the brain has been directly associated with senile plaques and amyloid-*β* fibrils, the hallmarks of Alzheimer's disease (Collingwood & Dobson, 2006; Quintana *et al.*, 2006; Plascencia-Villa *et al.*, 2016). Moreover, magnetite UFPs present in urban environments are usually co-associated with other potentially cytotoxic metals, including Cr, Cu, Mn, Ni, Pb, Ti, Al and Zn (e.g. Spassov *et al.*, 2004; Yang *et al.,* 2016; Hofman *et al.*, 2020), and surface-adsorbed organic species, including PAHs (Lehndorff and Schwark, 2004; Halsall *et al.*, 2008).

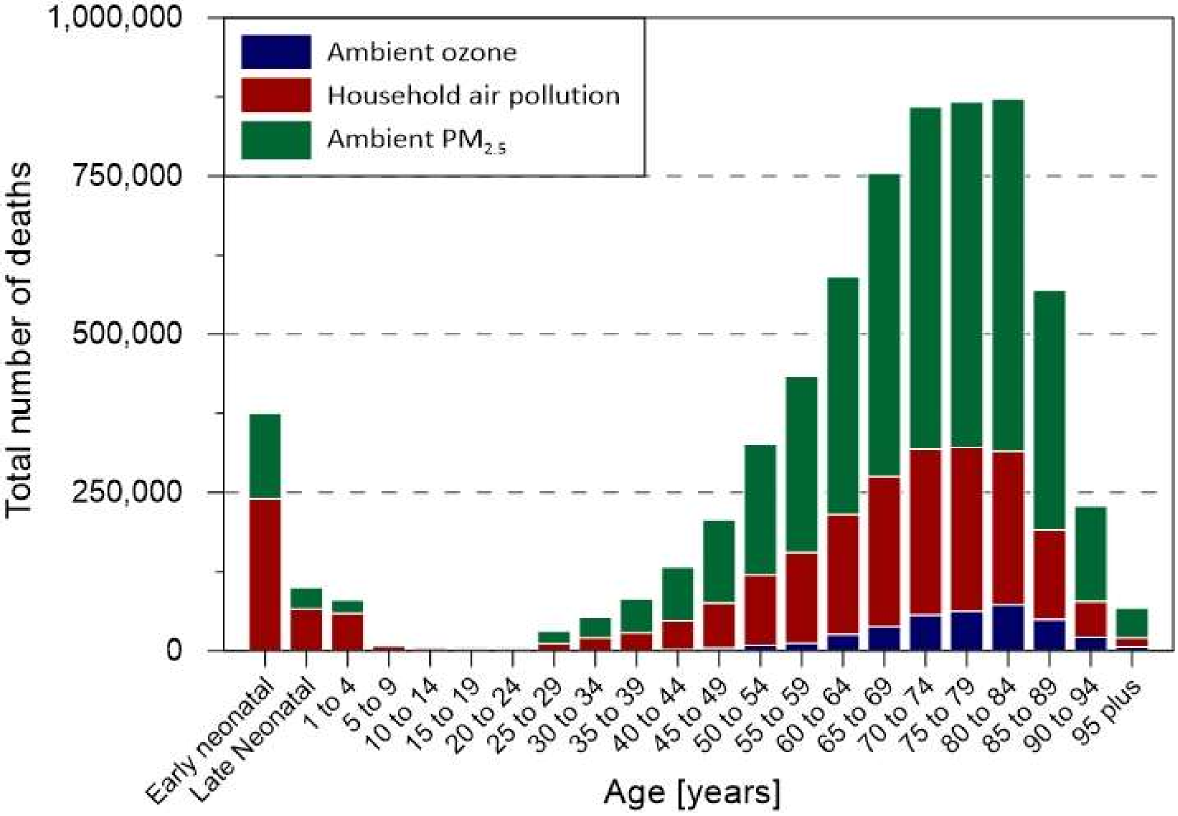

Figure 30. Distribution of global deaths in 2019 attributable to $PM_{2.5}$, ozone, and household air pollution by age (years, except early neonatal [0 to 6 days] and late neonatal [7 to 27 days]) (adapted from HEI, 2020).

Paper I examines the current knowledge regarding vehicle-derived Fe-bearing UFPs in urban environments, and identifies 7 such sources, including engine exhaust emissions (both petrol and diesel), brake-wear, tire and road-wear, resuspension of the roadside dust, underground, train and tram emissions, aircraft and shipping emissions. This review paper is focused on the chemical and mineralogical composition of Fe-bearing UFPs, their particle size distribution, and potential hazard to human health.

Car brake systems were identified as one of the main sources of Fe-bearing UFPs in urban environments, especially at the roadside, and in the proximity to traffic-control lights (or speed bumps), where braking is frequent and repetitive. In Europe, so-called 'low-metallic' brake pads (and cast iron discs) are predominantly used (see also Section 2.2. Friction materials). The term ‘low-metallic’ is a commonly used name for brake pads comprising a mixture of organic and metallic components, as opposed to non-asbestos organic (NAO) brake pads (used more commonly on the Asian and American markets) consisting of minor or trace amounts of metals (e.g. Chan & Stachowiak, 2004; Hulskotte *et al.*, 2014). Given the relatively high concentrations of metals in brake pads (~50 wt.%) and discs (> 90 wt.%) in Europe (Chan & Stachowiak, 2004; Hulskotte *et al.*, 2014), brake systems might be one of the main sources of metal-rich (and specifically Fe-rich) UFPs at the roadside (see also Paper II and the next section).

6.2. Paper II: Source apportionment of magnetite particles in roadside airborne particulate matter

In Paper I, brake-wear PM emissions were identified as one of the major sources of airborne magnetite particles in the urban environment. The main goal of the Paper II was to quantify the contribution of brake-wear (and other traffic sources) to total airborne magnetite in the roadside environment. For this purpose, magnetic properties of roadside PM at both roadside and urban background sites in Lancaster and Birmingham, U.K. (Appendix A: Figure A12) were evaluated. Additionally, petrol- and diesel-engine exhaust PM samples were collected and analysed.

The concentrations of magnetic grains (as measured by SIRM) in engine exhaust emissions (from both patrol- and diesel-fuelled cars) are 3 – 14 times lower than these in roadside PM in Lancaster and Birmingham, U.K. Magnetic component analysis enabled the identification of magnetite, and estimation of its mass concentrations in the collected samples. In engine exhaust emissions, magnetite mass concentrations varied between ~0.09 wt.% for petrol-derived PM and ~0.13 wt.% for diesel-derived PM. These values are significantly lower than those for roadside PM (0.18 – 0.63 wt.% in Lancaster, and 0.32 – 0.95 wt.% in Birmingham), suggesting that, in addition to engine exhaust emissions, there is another notable traffic-derived source of airborne magnetite at the roadside.

Based on these estimations and source apportionment of PM_{10} at the roadside (Bukowiecki *et al.*, 2009; Lawrence *et al.*, 2013), the contributions made by specific sources to the total airborne magnetite are estimated. Brake-wear was found to be the dominant source, contributing between ~68% and ~85% of the total magnetite at the two U.K. roadside sites. In contrast, diesel-engine exhaust emissions are responsible for ~7% – 12%, petrol-engine exhaust emissions for ~2% – 4%, and background dust for ~6% – 10% of the total airborne magnetite (Figure 23).

The strongly magnetic signature of brake-wear emissions has important implications for magnetic biomonitoring studies. At many roadside sites (especially close to traffic-control lights and speed bumps, or where traffic jams are frequent), brake-derived (rather than exhaust-derived) magnetite might dominate magnetic properties of roadside PM, and consequently hinder information about other sources of particulate pollution. Caution appears necessary when selecting sampling sites and interpreting magnetic biomonitoring data.

6.3. Paper III: Size-resolved quantitative evaluation of the magnetic mineralogy of airborne brake-wear particulate emissions

Paper II showed that brake-wear is responsible for ~68% – 85% of total airborne magnetite at the roadside at the two U.K. roadside sites. Paper III examines morphological, elemental, and magnetic properties of dynamometer-generated, size-resolved brake-wear emissions, with a special focus on quantitative evaluation of magnetic mineralogy of brake-derived PM.

During braking, pads are pressed against the disc, and this process inevitably results in the emission of worn particles. As conventional low-metallic brake pads used in Europe usually contain 20 – 50 wt.% of Fe and brake discs (usually made of cast iron) > 90 wt.% of Fe (Hulskotte *et al.*, 2014), it comes as no surprise that the resultant brake-wear PM is Fe-rich and highly magnetic. The concentration of magnetic grains (as measured by SIRM) in brake-derived PM_{10} is ~100 – 10,000 times higher, compared to other outdoor and indoor PM sources (cf. Figure 11 and Figure 24B). The combination of magnetic component analysis, high- and low-temperature magnetic measurements, and TEM allowed the identification and quantification of magnetite (~20.2 wt.%) and metallic Fe (~1.6 wt.%) in brake-derived PM_{10}.

Most of the brake-wear PM (> 99% of PNC) was found to be smaller than 200 nm, and importantly, even larger fractions were dominated by agglomerated rounded/spherical UFPs ~10 – 50 nm in size, rich in Fe^{2+}-bearing magnetite and potentially cytotoxic elements, including Al, Cr, Cu, S, Si, Sn, Ti and Zn. After the release from car brake systems, such particles can be easily inhaled/ingested by humans, and access all major organs, including heart and brain. Depending on the particle-cell interactions, the abundant brake-derived agglomerates might provide a chronic supply of potentially toxic metal-rich UFPs to major organs in the human body.

The presence of prolific numbers of agglomerated UFPs in larger size fractions (e.g. ~2.5 μm) demonstrates that conventional analysis of brake-wear PM emissions using impactors/particle sizers should be complemented by additional analytical tools (e.g. electron microscopy) in order to evaluate the presence of agglomerated UFPs classified as 'large' by an impactor/particle sizer.

Although there have been several *in vitro* and *in vivo* studies on toxicity of brake-wear emissions (e.g. Gasser *et al*., 2009; Puisney *et al*., 2018; Selley *et al*., 2020), none of them evaluated potential cardiac or neurological impairments associated with the exposure to brake-derived PM. Given the predominance of UFPs (both as discrete particles and agglomerates) and high concentrations of metals in brake-derived UFPs, it seems both timely and important for the cardio- and neurotoxic potential of brake-wear emissions to be explored in detail.

Chapter Seven: Conclusions and Prospects for Future Work

Conclusions

There is a growing body of evidence that urban UFPs can pose a specific threat to human health. Due to their small size, they can reach not only the lungs, but also almost all major organs in the human body, including brain, heart, human serum and pleural effusions, placenta and amniotic fluid.

Although UFPs are pervasive in urban environments, their concentrations very spatially and temporally, depending on local topographic and traffic conditions. Hence, the individual selection of commuting routes and times, potentially avoiding heavy traffic, might significantly reduce personal exposure to UFPs.

Given abundance of various cytotoxic metals (and organic species) in urban UFPs and inevitable human exposure to such particles, it is increasingly important to identify and quantify the sources of metal-rich UFPs, and to mitigate their potential impact on pulmonary, cardiovascular and neuronal health.

The abundant presence of magnetite UFPs in urban environments might be of importance due to their reported association with neurodegeneration and Alzheimer's disease. As reviewed in Paper I, there is a wide variety of urban sources of Fe-bearing UFPs, including vehicle- (including engine-exhaust emissions, brake-wear, tyre-wear, road surface-wear, resuspension of the roadside dust, aircraft, shipping, underground, tram, and rail emissions) and non-vehicle-derived (including welding fumes, laser printers, biomass burning, construction, demolition, power plants and cigarette smoking) sources.

In roadside environments, brake-wear might be the dominant source of potentially neurotoxic magnetite, constituting ~68% – 85% of total airborne magnetite. Consequently, caution seems necessary when interpreting magnetic biomonitoring studies because magnetic properties might be often dominated by brake-derived magnetite, and the information regarding other PM sources might be hindered.

Most of the brake-derived PM is smaller than 100 nm, both as discrete particles and agglomerates. Depending on the particle-cell interactions, these agglomerates might provide a chronic supply of cytotoxic metals to human body.

On average, the mass concentration of magnetite was found to be ~20.2 wt.% in PM_{10}, ~18.5 wt.% in $PM_{2.5}$, and ~7.6 wt.% in $PM_{0.2}$ of dynamometer-generated brake-wear PM emissions. Given the abundance of magnetite in brake-derived PM, and the predominance of UFPs in brake-wear emissions (both as discrete particles and agglomerates), exposure to brake-derived PM might be hazardous to major organs in the human body, including brain and heart.

Prospectively, the legislation, likely to be introduced in the future to limit brake-wear emissions in Europe, should encompass not only general mass- (e.g. PM_{10}) and number-based (e.g. PNC) metrics, but also potentially cytotoxic components within brake emissions, e.g. magnetite, Cu and/or Sb.

Such legal emission limits will most likely force the manufacturers to seek new solutions and friction materials to reduce the emissions from car brake systems. Great care is required to avoid replacing one health hazard (e.g. asbestos-based brake pads used before ~1990) for another (e.g. cytotoxic metal-rich UFPs).

Prospects for future work

In paper III, a set of low-metallic brake pads and cast iron discs (a friction couple predominantly used in Europe) were tested. For full understanding of the brake-derived PM generation, a further analysis would be needed, including more low-metallic and non-asbestos organic brake pads (more commonly utilised on American and Asian markets). Ideally, these dynamometer experiments would encompass a very wide spectrum of braking conditions, both mild and harsh. It could be carried out, for example, by testing a dynamometer braking cycles such as ISO26867 or SAE J2522, and dividing them into several sections, separating mild braking events (e.g. with applied pressure < 20 bar) from severe ones (e.g. with applied pressure > 20 bar). Given the predominance of UFPs in brake-wear PM, both as discrete particles and agglomerates (cf. Paper III), these future studies of brake-wear PM emissions should include not only impactors/particle sizers, but also electron microscopy, for full understanding of the particle size distribution, concentrations, and generation processes of brake-derived PM, especially in the ultrafine range.

From the perspective of the automotive industry, it would be desirable to test various friction materials in a dynamometer, using the WLTP-based brake cycle proposed by

Mathissen *et al.* (2018), for the optimal estimation of emission factors for brake-derived PM. This dynamometer cycle will probably be used in the legislation regarding the limitation of brake-derived particulate pollution, likely to be introduced in the near future.

In dynamometer studies, new sets of brake pads and discs are conventionally used. However, car brake pads often rust as they age, and this process might have important implications regarding the mineralogical composition of the brake-wear PM occurring in urban environments (cf. Section 5.5. Discussion (Paper III)). Additional dynamometer studies, comparing 'aged' and 'new' brake-derived PM would shed some light on that issue, particularly in the context of the oxidation state of brake-derived, Fe-rich UFPs and their health relevance.

In another study (Hammond *et al.*, in prep.), we analysed toxicity (cell viability, ROS generation, and inflammatory response) of roadside UFPs (from Lancaster, Birmingham and Mexico City) in human lung cells, and found that the UFPs induce oxidative and inflammatory responses in *in vitro* lung cells. Urban UFPs are a complex mixture of multiple traffic- and non-traffic-derived components. Further toxicity assays, analysing biological effects of specific exhaust (diesel- and petrol-engine) and non-exhaust (i.e. brake-wear, tyre-wear, and road surface-wear) UFP sources might provide more definite answers which UFP sources/compounds are the most hazardous to human health. It would be also desirable to assess the potential synergistic effects of these traffic-derived UFP sources.

Most toxicological studies of brake-wear PM have been so far carried out on lung/bronchial epithelial cells (or animals). Given that brake-derived PM might be dominated by UFPs < 100 nm (cf. Paper III) and that they can reach all major organs in the human body (including the heart and brain), potential cardiotoxic and neurotoxic effects of brake-wear UFPs warrant thorough investigation.

In vitro toxicity assays usually evaluate the effects of acute exposure to potential toxicants. There have been multiple epidemiological studies assessing the impact of chronic exposure to, for example, PM_{10}, $PM_{2.5}$, UFPs, NO_X or noise, yet none of them have considered magnetite particles, especially in the ultrafine fraction. The addition of magnetite concentrations in such epidemiological analyses might shed some light on the potential neurological (and cardiovascular) problems associated with chronic exposure to Fe^{2+}-bearing UFPs.

This thesis is focused on outdoor sources of Fe-rich PM. However, highly magnetic PM also occurs in the indoor environment. In another study (Maher *et al.*, 2021), we found a negative association between open fire usage (and hence the exposure to the emitted PM) and cognitive function, using individual-level data of nearly seven thousand older people from The Irish Longitudinal Study on Aging (TILDA). It would be desirable to widen the scope of this research, by both follow-up epidemiological and toxicological studies, focusing on potential health hazard posed by particulate pollution emitted by various indoor sources, e.g. cooking and/or cleaning.

There is growing body of evidence that UFPs can reach not only lungs, but also all major organs in the human body, including heart and brain. In the latter case, it has become evident that there are multiple pathways of entry. UFPs can cross the gas-blood barrier in lungs, enter the bloodstream, and access the brain via systemic circulation. Moreover, UFPs can be translocated via axonal pathways by inhalation via the olfactory bulb, and through ingestion/swallowing and transfer via the gut wall and neuroenteric system. In Appendix B: Paper IV, we hypothesise that metal-rich (and specifically Fe-rich) UFPs can also enter the brain via the taste nerve pathway (VII and IX cranial nerves), and this process might plausibly account for the reported elevated incidence of neurodegeneration-related deaths among bank tellers (in a cohort who died between 1992 and 1998). Detailed investigations, potentially including electron microscopy imaging of the human tongue and brain tissue, might aid understanding this axonal pathway of UFPs, and evaluate the efficiency of the UFP transfer to different parts of the human brain. Furthermore, given the scale and costs of neurodegenerative disease on the international scale, detailed studies of newly-developing occupational groups being potentially at risk of high exposure to Fe-rich UFPs seem both important and timely.

REFERENCES

1. Aarnio, P.; Yli-Tuomi, T.; Kousa, A.; Mäkelä, T.; Hirsikko, A.; Hämeri, K.; Räisänen, M.; Hillamo, R.; Koskentalo, T.; Jantunen, M. The concentrations and composition of and exposure to fine particles ($PM_{2.5}$) in the Helsinki subway system. *Atmos. Environ.* **2005**, *39*, 5059-5066.
2. Abbasi, S.; Jansson, A.; Sellgren, U.; Olofsson, U. Particle emissions from rail traffic: A literature review. *Crit. Rev. Environ. Sci. Technol.* **2013**, *43*, 2511-2544.
3. Abbasi, S.; Olander, L.; Larsson, C.; Olofsson, U.; Jansson, A.; Sellgren, U. A field test study of airborne wear particles from a running regional train. *Proc. IMechE* **2011**, *226*(F), 95-109.
4. Abdul-Razzaq, W.; Gautam, M. Discovery of magnetite in the exhausted material from a diesel engine. *Appl. Phys. Lett.* **2001**, *78*(14), 2018-2019.
5. Abu-Allaban, M.; Gillies, J. A.; Gertler, A. W.; Clayton, R.; Proffitt. Tailpipe, resuspended road dust, and brake-wear emission factors from on-road vehicles. *Atmos. Environ.* **2003**, *37*, 5283-5293.
6. Adachi, K.; Tainosho, Y. Characterization of heavy metal particles embedded in tire dust. *Environ. Int.* **2004**, *30*, 1009-1017.
7. Agrawal, H.; Malloy, Q. G. J.; Welch, W. A.; Miller, J. W.; Cocker, D. R., III. In-use gaseous and particulate matter emissions from a modern ocean going container vessel. *Atmos. Environ.* **2008**, *42*, 5504-5510.
8. Agudelo-Castañeda, D. M.; Teixeira, E. C.; Braga, M.; Rolim, S. B. A.; Silva, L.F.O.; Beddows, D. C. S.; Harrison, R. M.; Querol, X. cluster analysis of urban ultrafine particles size distribution. *Atmos. Pollut. Res.* **2019**, *10*, 45-52.
9. Aguilar Reyes, B.; Mejía, V.; Goguitchaichvili, A.; Escobar, J.; Bayona, G.; Bautista, F.; Morales, J. C.; Ihl, T. J. Reconnaissance environmental magnetic study of urban soils, dust and leaves from Bogotá, Colombia. *Stud. Geophys. Geod.* **2013**, *57*, 741-754.
10. Aguilar Reyes, B.; Ruiz, R. C.; Martínez-Cruz, J.; Bautista, F.; Gogoitchaichvili, A.; Carvallo, C.; Morales, J. *Ficus benjamina* leaves as indicator of atmospheric pollution: a reconnaissance study. *Stud. Gephys. Geod.* **2012**, *56*, 879-887.
11. Ailshire, J. A.; Crimmins, E. M. Fine particulate matter air pollution and cognitive function among older US adults. *Am. J. Epidemiol.* **2014**, *180*(4), 359-366.
12. Alam, M. S.; Zeraati-Rezaei, S.; Stark, C. P.; Liang, Z.; Xu, H.; Harrison, R. M. The characterisation of diesel exhaust particles – composition, size distribution and partitioning. *Faraday Discuss.* **2016**, *189*, 69-84.
13. Alemani, M.; Nosko, O.; Metinoz, I.; Olofsson, U. A study of emission of airborne wear particles from car brake friction pairs. *SAE Int. J. Mater. Manf.* **2016**, *9*(1), 147-157.
14. Alemani, O.; Wahlström, J.; Olofsson, U. On the influence of car brake system parameters on particulate matter emissions. *Wear* **2018**, *396-397*, 67-74.
15. Allen, J. O.; Alexandrova, O.; Kaloush, K. E. *Tire wear emissions for asphalt rubber and Portland cement concrete pavement surfaces. Final report.* Arizona Dept. of Transportation: Arizona, 2006.
16. Allsop, D.; Mayes, J.; Moore, S.; Masad, A.; Tabner, B. J. Metal-dependent generation of reactive oxygen species from amyloid proteins implicated in neurodegenerative disease. *Biochem. Soc. Trans.* **2008**, *36*, 1293-1298.
17. Amato, F.; Moreno, T.; Pandolfi, M.; Querol, X.; Alastuey, A.; Delgado, A.; Pedrero, M.; Cots, N. Concentrations, sources and geochemistry of airborne particulate matter at a major European airport. *J. Environ. Monit.* **2010**, *12*, 854-862.
18. Amato, F.; Pandolfi, M.; Moreno, T.; Furger, M.; Pey, J.; Alastuey, A.; Bukowiecki, N.; Prevot, A. S. H.; Baltensperger, U.; Querol, X. Sources and variability of inhalable road dust particles in three European cities. *Atmos. Environ.* **2011**, *45*, 6777-6787.
19. Amin, N.; Arajs, S. Morin temperature of annealed submicronic α-Fe_2O_3 particles. *Phys. Rev. B* **1987**, *35*(10), 4810-4811.
20. Antonini, J. M.; Taylor, M. D.; Zimmer, A. T.; Roberts, J. R. Pulmonary responses to welding fumes: Role of metal constituents. *J. Toxicol. Environ. Health A* **2003**, *67*, 233-249.

21. Apopa, P. L.; Qian, Y.; Shao, R.; Guo, N. L.; Schwegler-Berry, D.; Pacurari, M.; *et al*. Iron oxide nanoparticles induce human microvascular endothelial cell permeability through reactive oxygen species production and microtubule remodeling. *Part. Fibre Toxicol.* **2009**, *6*(1).
22. Aranganathan, N.; Mahale, V.; Bijwe, J. Effects of aramid fiber concentration on the friction and wear characteristics of non-asbestos organic friction composites using standardized braking tests. *Wear* **2016**, *354-355*, 69-77.
23. Augsburg, K.; Hesse, D. Comparative study of brake particle emissions. *11. Internationales AVL Forum Abgas- und Partikelemissionen* (conference paper), **2020**.
24. Aust, A. E.; Ball, J. C.; Hu, A. A.; Lighty, J. S.; Smith, K. R.; Straccia, A. M.; Veranth, J. M.; Young, W. C. Particle characteristics responsible for effects on human lung epithelial cells. Research report of *Health Effects Institute* **2002**, *110*, 1-77.
25. Bagley, S. T.; Baumgard, K. J.; Gratz, L. D.; Johnson, J. H.; Leddy, D. G. Characterization of fuel and aftertreatment device effects on diesel emissions. Research report of *Health Effects Institute* **1996**, *76*, 1-75.
26. Bai, L.; Hatzopoulou, M.; Jerrett, M.; Kwong, J. C.; Burnett, R. T.; van Donkelaar, A.; Copes, R.; Martin, R. V.; van Ryswyk, K.; Lu, H.; Kopp, A.; Weichenthal, S. Exposure to ambient ultrafine particles and nitrogen dioxide and incident hypertension and diabetes. *Epidemiol.* **2018**, *29*(3), 323-332.
27. Barima, Y. S. S.; Angaman, D. M.; N'Gouran, K. P.; Koffi, N. A.; Kardel, F.; De Cannière, C.; Samson, R. Assessing atmospheric particulate matter distribution based on saturation isothermal remanent magnetization of herbaceous and tree leaves in a tropical urban environment. *Sci. Total Environ.* **2014**, *470-471*, 975-982.
28. Barošová, H.; Chortarea, S.; Peikertová, P.; Clift, M. J. D.; Petri-Fink, A.; Kukutschová, J.; Rothen-Rotishauser, B. Biological response of an in vitro human 3D lung cell model exposed to brake-wear debris varies based on brake pad formulation. *Arch. Toxicol.* **2018**, *92*, 2339-2351.
29. Barošová, H.; Dvořáčková, J.; Motyka, O.; Mamulová Kutláková, K.; Peikertová, P.; Rak, J.; Bielniková, H.; Kukutschová, J. Metal-based particles in human amniotic fluids of foetuses with normal karyotype and congenital malformation – a pilot study. *Environ. Sci. Pollut. Res.* **2015**, *22*(10), 7582-7589.
30. Barregard, L.; Sällsten, G.; Gustafson, P.; Andersson, L.; Johansson, L.; Basu, S.; Stigendal, L. Experimental exposure to wood-smoke particles in healthy humans: Effects on markers of inflammation, coagulation, and lipic peroxidation. *Inhal. Toxicol.* **2006**, *18*, 845-853.
31. Barrett, S. R. H.; Britter, R. E.; Waitz, I. A. Global mortality attributable to aircraft cruise emissions. *Environ. Sci. Technol.* **2010**, *44*, 7736-7742.
32. Bateson, T. F.; Schwarz, J. Children's response to air pollution. *J. Toxicol. Environ. Health A* **2008**, *71*, 238-243.
33. Beard, J. L.; Connor, J. R.; Jones, B. C. Iron in the brain. *Nutr. Rev.* **1993**, *51*(6), 157-170.
34. Beddows, D. C. S.; Dall'Osto, M.; Harrison, R. M. Cluster analysis of rural, urban and curbside atmospheric particle size data. *Environ. Sci. Technol.* **2009**, *43*, 4694-4700.
35. Beddows, D. C. S.; Dall'Osto, M.; Olatunbosun, O. A.; Harrison, R. M. Detection of brake-wear aerosol time-of-flight mass spectrometry. *Atmos. Environ.* **2016**, *129*, 167-175.
36. Beddows, D. C. S.; Harrison, R. M.; Green, D. C.; Fuller, G. W. Receptor modelling of both particle composition and size distribution from a background site in London, UK. *Atmos. Chem. Phys.* **2015**, *15*, 10107-10125.
37. Beelen, R.; Raaschou-Nielsen, O.; Stafoggia, M.; Jovanovic Andersen, Z.; Weinmayr, G.; Hoffmann, B.; *et al*. Effects of long-term exposure to air pollution on natural-cause mortality: an analysis of 22 European cohorts within the multicentre ESCAPE project. *Lancet* **2014**, *383*, 785-795.
38. Belis, C. A.; Karagulian, F.; Larsen, B. R.; Hopke, P. K. Critical review and meta-analysis of ambient particulate matter source apportionment using receptor models in Europe. *Atmos. Environ.* **2013**, *69*, 94-108.
39. Bell, M. L.; Ebisu, K.; Belanger, K. Ambient air pollution and low birth weight in Connecticut and Massachusetts. *Environ. Health Perspect.* **2007**, *115*(7), 1118-1124.

40. Biswas, S.; Fine, P. M.; Geller, M. D.; Hering, S. V.; Sioustas, C. Performance evaluation of a recently developed water-based condensation particle counter. *Aerosol Sci. Technol.* **2005**, *39*, 419-427.
41. Block, M.L.; Calderón-Garcidueñas, L. Air pollution: Mechanisms of neuroinflammation & CNS disease. *Trends Neurosci.* **2009**, *32*(9), 506-516.
42. Bødker, F.; Mørup, S. Size dependence of the properties of hematite nanoparticles. *Europhys. Lett.* **2000**, *52*(2), 217-223.
43. Bové, H.; Bongaerts, E.; Slenders, E.; Bijnens, E. M.; Saenen, N. D.; Gyselaers, W.; Van Eyken, P.; Plusquin, M.; Roeffaers, M. B. J.; Ameloot, M.; Nawrot, T. S. Ambient black carbon particles reach the fetal side of human placenta. *Nat. Commun.* **2019**, *10*, 3866.
44. Brackx, M.; Van Wittenberghe, S.; Verhelst, J.; Scheunders, P.; Samson, R. Hyperspectral leaf reflectance of *Carpinus betulus L.* samplings for urban air quality estimation. *Environ. Pollut.* **2017**, *220*, 159-167.
45. Braun, A.; Huggins, F. E.; Kelly, K. E.; Mun, B. S.; Ehrlich, S. N.; Huffman, G. P. Impact of ferrocene on the structure of diesel exhaust soot as probed with wide-angle X-ray scattering and C(1s) NEXAFS spectroscopy. *Carbon* **2006**, *44*, 2904-2911.
46. Brem, F.; Hirt, A. M.; Winklhofer, M.; Frei, K.; Yonekawa, Y.; Wieser, H.-G.; Dobson, J. Magnetic iron compounds in the human brain: a comparison of tumour and hippocampal tissue. *J.R. Soc. Interface* **2006**, *3*, 833-841.
47. Brito, J. M.; Belotti, L.; Toledo, A. C.; Antonangelo, L.; Silva, F. S.; Alvim, D. S.; Andre, P. A.; Saldiva, P. H. N.; Rivero, D. H. R. F. Acute cardiovascular and inflammatory toxicity induced by inhalation of diesel and biodiesel exhaust particles. *Toxicol. Sci.* **2010**, *116*(1), 67-78.
48. Brook, J. R.; Graham, L.; Charland, J. P.; Cheng, Y.; Fan, X.; Lu, G.; Li, S. M.; Lillyman, C.; MacDonald, P.; Caravaggio, G.; MacPhee, J. A. Investigation of the motor vehicle exhaust contribution to primary fine particle organic carbon in urban air. *Atmos. Environ.* **2007**, *41*, 119-135.
49. Brook, R.D.; Rajagopalan, S.; Pope, A. C., III; Brook, J. R.; Bhatnagar, A.; Diez-Roux, A. V.; Holguin, F.; Hong, Y.; Luepker, R.V.; Mittleman, M. A.; Peters, A.; Siscovick, D.; Smith Jr, S. C.; Whitsel, L.; Kaufman, J. D. Particulate matter air pollution and cardiovascular disease. An update to the scientific statement from the American Heart Association. *Circulation* **2010**, *121*, 2331-2378.
50. Brown, D. M.; Stone, V.; Findlay, P.; MacNee, W.; Donaldson, K. Increased inflammation and intracellular calcium caused by ultrafine carbon black is independent of transition metals or other soluble components. *Occup. Environ. Med.* **2000**, *57*, 685-691.
51. Bućko, M. S.; Magiera, T.; Johanson, B.; Petrovský, E.; Pesonen, L. J. Identification of magnetic particulates in road dust accumulated on roadside snow using magnetic, geochemical and micro-morphological analyses. *Environ. Pollut.* **2011**, *159*, 1266-1276.
52. Bućko, M. S.; Mattila, O.-P.; Chrobak, A.; Ziółkowski, G.; Johanson, B.; Čuda, J.; Filip, J.; Zbořil, R.; Pesonen, L. J.; Leppäranta, M. Distribution of magnetic particulates in a roadside snowpack based on magnetic, microstructural and mineralogical studies. *Geophys. J. Int.* **2013**, *195*, 159-175.
53. Bukowiecki, N.; Gehrig, R.; Hill, M.; Lienemann, P.; Zwicky, C. N.; Buchmann, B.; Weingartner, E.; Baltensperger, U. Iron, manganese and copper emitted by cargo and passenger trains in Zürich (Switzerland): Size-segregated mass concentrations in ambient air. *Atmos. Environ.* **2007**, *41*, 878-889.
54. Bukowiecki, N.; Gehrig, R.; Lienemann, P.; Hill, M.; Figi, R.; Buchmann, B.; Furger, M.; Richard, A.; Mohr, C.; Weimer, S.; Prévôt, A.; Baltensperger, U. PM10 emission factors of abrasion particles from road traffic. Schweiz, Eidgenoss, **2009a**, p. 1268.
55. Bukowiecki, N.; Lienemann, P.; Hill, M.; Figi, R.; Richard, A.; Furger, M.; Rickers, K.; Falkenberg, G.; Zhao, Y.; Cliff, S. S.; Prevot, A. S. H.; Baltensperger, U.; Buchmann, B.; Gehrig, R. Real-world emission factors for antimony and other brake-wear related trace elements: Size-segregated values for light and heavy duty vehicles. *Environmental Science & Technology* **2009b**, *43*, 8072-8078.

56. Bukowiecki, N.; Lienemann, P.; Hill, M.; Furger, M.; Richard, A.; Amato, F.; Prévôt, A. S. H.; Baltensperger, U.; Buchmann, B.; Gehrig, R. PM_{10} emission factors for non-exhaust particles generated by road traffic in an urban street canyon and along a freeway in Switzerland. *Atmos. Environ.* **2010**, *44*, 2330-2340.
57. Burnett, R.; Chen, H.; Szyszkowicz, M.; Fann, N.; Hubbell., B.; Pope III, C. A.; *et al.* Global estimates of mortality associated with long-term exposure to outdoor fine particulate matter. *PNAS* **2018,** *115*(38), 9592-9597.
58. Burtscher, H.; Schüepp, K. The occurrence of ultrafine particles in the specific environment of children. *Paediatr. Respir. Rev.* **2012**, *13*, 89-94.
59. Buseck, P. R.; Adachi, K. Nanoparticles in the atmosphere. *Elements* **2008**, *4*, 389-394.
60. Cacciotolo, M.; Wang, X.; Driscoll, I.; Woodward, N.; Saffari, A.; Reyes, J.; Serre, M. L.; Vizuete, W.; Sioutas, C.; Morgan, T. E.; Gatz, M.; Chui, H. C.; Shumaker, S. A.; Resnick, S. M.; Espeland, M. A.; Finch, C. E.; Chen, J. C. Particulate air pollutants, APOE alleles and their contributions to cognitive impairment in older women and to amyloidogenesis in experimental models. *Transl. Psychiatry* **2017**, *7*, e1022.
61. Calderón-Garcidueñas, L.; Azzarelli, B.; Acuna, H.; Garcia, R.; Gambling, T. M.; Osnaya, N.; Monroy, S.; Del Rosario Tizapantzi, M.; Carson, J. L.; Villareal-Calderón, A.; Rewcastle, B. Air pollution and brain damage. *Toxicol. Pathol.* **2002**, *30*(3), 373-389.
62. Calderón-Garcidueñas, L.; Mukherjee, P. S.; Kulesza, R. J.; Torres-Jardón, R.; Hernández-Luna, J.; Ávila-Cervantes, R.; Macías-Escobedo, E.; González-González, O.; González-Maciel, A.; García-Hernández, K.; Hernández-Castillo, A.; Research UVM Group, Villareal-Ríos, R. Mild cognitive impairment and dementia involving multiple cognitive domains in Mexican urbanities. *J. Alzheimer Dis.* **2019a**, *68*(3), 1113-1123.
63. Calderón-Garcidueñas, L.; González-Maciel, A.; Mukherjee, P. S.; Reynoso-Robles, R.; Pérez-Guillé, B.; Gaynosso-Chávez, C.; Torres-Jardón, R.; Cross, J. V.; Ahmed, I. A. M.; Karloukovski, V. V.; Maher, B. A. Combustion- and friction-derived magnetic air pollution nanoparticles in human hearts. *Environ. Res.* **2019b**, *176*, 108567.
64. Calderón-Garcidueñas, L.; González-Maciel, A.; Reynoso-Robles, R.; Hammond, J.; Kulesza, R.; Lachmann, I.; Torres-Jardón, R.; Mukherjee, P.S.; Maher, B.A. Quadruple abnormal protein aggregates in brainstem pathology and exogenous metal-rich magnetic nanoparticles. The substantia nigrae is a very early target in young urbanities and the gastrointestinal tract likely a key brainstem portal. *Environ. Res.* **2020**, *191*, 110139.
65. Calderón-Garcidueñas, L.; Kavanaugh, M.; Block, M.; D'Angiulli, A.; Delgado-Chávez, R.; Torres-Jardón, R.; González-Maciel, A.; Reynoso-Robles, R.; Osnaya, N.; Villareal-Calderón, R.; Gou, R.; Hua, Z.; Zhu, H.; Perry, G.; Diaz, P. Neuroinflammation, hyperphosphorylated tau, diffuse amyloid plaques, and down-regulation of the cellular prion protein in air pollution exposed children and young adults. *J. Alzheimers Dis.* **2012**, *28*, 93-107.
66. Calderón-Garcidueñas, L.; Reed, W.; Maronpot, R. R.; Henríquez-Roldán, C.; Delgado-Chavez, R.; Calderón-Garcidueñas, A.; Dragustinovis, I.; Franco-Lira, M.; Aragón-Flores, M.; Solt, A. C.; Altenburg, M.; Torres-Jardón, R.; Swenberg, J. A. Brain inflammation and Alzheimer's-like pathology in individuals exposed to severe air pollution. *Toxicol. Pathol.* **2004**, *32*, 650-658.
67. Calderón-Garcidueñas, L.; Reynoso-Robles, R.; Vargas-Martínez, J.; Gómez-Maqueo-Chew, A.; Pérez-Guillé, B.; Mukherjee, P. S.; Torres-Jardón, R.; Perry, G.; Gónzalez-Maciel, A. Prefrontal white matter pathology in air pollution exposed Mexico City young urbanities and their potential impact on neurovascular unit dysfunction and the development of Alzheimer's disease. *Environ. Res.* **2016**, *146*, 404-417.
68. Calderón-Garcidueñas, L.; Serrano-Sierra, A.; Torres-Jardón, R.; Zhu, H.; Yuan, Y.; Smith, D.; Delgado-Chávez, R.; Cross, J. V.; Medina-Cortina, H.; Kavanaugh, M.; Guilarte, T. R. The impact of environmental metals in young urbanities' brains. *Exp. Toxicol. Pathol.* **2013**, *65*(5), 503-511.
69. Calderón-Garcidueñas, L.; Solt, A. C.; Henríquez-Roldán, C.; Torres-Jardón, R.; Nuse, B.; Herritt, L.; Villareal-Calderón, R.; Osnaya, N.; Stone, I.; García, R.; Brooks, D. M.; González-Maciel, A.; Reynoso-Robles, R.; Delgado-Chávez, R.; Reed, W. Long-term air pollution exposure is associated with neuroinflammation, an altered innate immune response, disruption of

the blood-brain barrier, ultrafine particulate deposition, and accumulation of amyloid β-42 and α-synuclein in children and young adults. *Toxicol. Pathol.* **2008a**, *36*, 289-310.

70. Calderón-Garcidueñas, L.; Villareal-Calderón, R.; Valencia-Salazar, G.; Henríquez-Roldán, C.; Gutiérrez-Castrellón, P.; Torres-Jardón, R.; Osnaya-Brizuela, N.; Romero, L.; Torres-Jardón, R.; Solt, A.; Reed, W. Systematic inflammation, endothelial dysfunction, and activation in clinically healthy children exposed to air pollutants. *Inhal. Toxicol.* **2008b**, *20*, 499-506.
71. Camatini, M.; Crosta, G. F.; Dolukhanyan, T.; Sung, C.; Giuliani, G.; Corbetta, G. M.; Cencetti, S.; Regazzoni, C. Microcharacterization and identification of tire debris in heterogeneous laboratory and environmental specimens. *Mater. Charact.* **2001**, *46*, 271-283.
72. Campbell, A.; Becaria, A.; Lahiri, D. K.; Sharman, K.; Bondy, S. C. Chronic exposure to aluminum in drinking water increases inflammatory parameters selectively in the brain. *J. Neurosci. Res.* **2004**, *75*, 565-572.
73. Cao, L.; Appel, E.; Hu, S.; Ma, M. An economic passive sampling method to detect particulate pollutants using magnetic measurements. *Environ. Pollut.* **2015**, *205*, 97-102.
74. Cass, G.R.; Hughes, L. A.; Bhave, P.; Kleeman, M. J.; Allen, J. O.; Salmon, L. G. The chemical composition of atmospheric ultrafine particles. *Phil. Trans. R. Soc. Lond. A* **2000**, *358*, 2581-2592.
75. Castanheiro, A.; Samson, R.; De Wael, K. Magnetic- and particle-based techniques to investigate metal deposition on urban green. *Sci. Total Environ.* **2016**, *571*, 594-602.
76. Castellani, R. J.; Moreira, P. I.; Liu, G.; Dobson, J.; Perry, G.; Smith, M. A.; Zhu, X. Iron: The redox-active center of oxidative stress in Alzheimer disease. *Neurochem. Res.* **2007**, *32*, 1640-1645.
77. Cavallo, D.; Ursini, C. L.; Carelli, G.; Iavicoli, I.; Ciervo, A.; Perniconi, B.; Rondinone, B.; Gismondi, M.; Iavicoli, S. Occupational exposure in airport personnel: Characterization and evaluation of genotoxic and oxidative effects. *Toxicol.* **2006**, *223*, 26-35.
78. Cernuschi, S.; Giugliano, M.; Ozgen, S.; Consonni, S. Number concentration and chemical composition of ultrafine and nanoparticles from WTE (waste to energy) plants. *Sci. Total Environ.* **2012**, *420*, 319-326.
79. Chan, D.; Stachowiak, G. W. Review of automotive brake friction materials. *Proc. IMechE Pard D: J. Automobile Engineering* **2004**, *218*(9), 953-966.
80. Chaparro, M. A. E.; Chaparro, M. A. E.; Castañeda Miranda, A. G.; Böhnel, H. N.; Sinito, A. M. An interval fuzzy model for magnetic biomonitoring using the specie *Tillandsia recurvata L. Ecol. Indic.* **2015**, *54*, 238-245.
81. Chaparro, M. A. E.; Marié, D. C.; Gogorza, C. S. G.; Navas, A.; Sinito, A. M. Magnetic studies and scanning electron microscopy – X-ray energy dispersive spectroscopy analyses of road sediments, soils and vehicle-derived emissions. *Stud. Geophys. Geod.* **2010**, *54*, 633-650.
82. Charrier, J. G.; Anastasio, C. Impacts of antioxidants on hydroxyl radical production from individual and mixed transition metals in a surrogate lung fluid. *Atmos. Environ.* **2011**, *45*, 7555-7562.
83. Chen, G.; Huey, L. G.; Trainer, M.; Nicks, D.; Corbett, J.; Ryerson, T.; *et al.* An investigation of the chemistry of ship emission plumes during ITCT 2002. *J. Geophys. Res.* **2005**, *110*(D10S90).
84. Chen, H.; Kwong, J. C.; Copes, R.; Tu, K.; Villeneuve, P. J.; van Donkelaar, A.; Hystad, P.; Martin, R. V.; Murray, B.J.; Jessiman, B.; Wilton, A. S.; Kopp, A.; Burnett, R. T. Living near major roads and the incidence of dementia, Parkinson's disease, and multiple sclerosis: a population-based study. *Lancet* **2017a**, *389*(10070), 718-726.
85. Chen, J.; Li, C.; Ristovski, Z.; Milic, A.; Gu, Y.; Islam, M. S.; Wang, S.; Hao, J.; Zhang, H.; He, C.; Guo, H.; Fu, H.; Miljevic, B.; Morawska, L.; Thai, P.; LAM, Y.-F.; Pereira, G.; Ding, A.; Huang, X.; Dumka, U. C. A review of biomass burning: Emissions and impacts on air quality, health and climate in China. *Sci. Total Environ.* **2017b**, *579*, 1000-1034.
86. Chen, A.; Liang, H.; Liu, J.; Ou, L.; Wei, L.; Wu, J.; Lai, X.; Han, X.; Shao, L. Central neurotoxicity induced by the instillation of ZnO and TiO2 nanoparticles through the taste nerve pathway. Nanomedicine (Lond) **2017c**, *12*(20), 2453-2470.
87. Chen, J.; Wang, W.; Liu, H.; Ren, L. Determination of road dust loadings and chemical characteristics using resuspension. *Environ. Monit. Assess.* **2012**, *184*, 1693-1709.

88. Chen, J.; Zheng, H.; Wang, W.; Liu, H.; Lu, L.; Bao, L.; Ren, L. Resuspension method for road surface dust collection and aerodynamic size distribution characterization. *China Part.* **2006**, *4*(6), 300-303.
89. Chen, J.-C.; Schwartz, J. Neurobehavioral effects of ambient air pollution on cognitive performance in US adults. *Neurotoxicology* **2009**, *30*, 231-239.
90. Chen, J.-C.; Wang, X.; Wellenius, G. A.; Serre, M. L.; Driscoll, I.; Casanova, R.; McArdle, J. J.; Manson, J. E.; Chui, H. C.; Espeland M. A. Ambient air pollution and neurotoxicity on brain structure: evidence from Women's Health Initiative Memory Study. *Ann. Neurol.* **2015**, *78*, 466-476.
91. Chen, R.; Yin, H.; Cole, I.S.; Shen, S.; Zhou, X.; Wang, Y.; Tang, S. Exposure, assessment and health hazards of particulate matter in metal additive manufacturing: A review. *Chemosphere* **2020**, *259*, 127452.
92. Chen, X.; Mao, S.S. Titanium dioxide nanomaterials: Synthesis, properties, modifications, and applications. *Chem. Rev.* **2007**, *107*, 2891-2959.
93. Cheng, H.; Saffari, A.; Sioutas, C.; Forman, H. J.; Morgan, T. E.; Finch, C. E. Nanoscale particulate matter from urban traffic rapidly induces oxidative stress and inflammation in olfactory epithelium with concomitant effects on brain. *Environ. Health Perspect.* **2016**, *124*(10), 1537-1546.
94. Cheung, K. L.; Ntziachristos, L.; Tzamkiozis, T.; Schauer, J. J.; Samaras, Z.; Moore, K. F.; Sioutas, C. Emissions of particulate trace elements, metals and organic species from gasoline, diesel, and biodiesel passenger vehicles and their relation to oxidative stress. *Aerosol Sci. Technol.* **2010**, *44*(7), 500-513.
95. Coccini, T.; Caloni, F.; Cando, L. J. R.; De Simone, U. Cytotoxicity and proliferative capacity impairment induced on human brain cell cultures after short- and long-term exposure to magnetite nanoparticles. *J. Appl. Toxicol.* **2017**, *37*, 361-373.
96. Cohen, D.E.; Kim, R.H. The legacy of the Radium Girls. *JAMA Dermatology* **2017**, *153*(8), 801.
97. Collingwood, J.; Dobson, J. Mapping and characterization of iron compounds in Alzheimer's tissue. *J. Alheimers Dis.* **2006**, *10*, 215-222.
98. Conte, M.; Contini, D. Size-resolved particle emission factors of vehicular traffic derived from urban eddy covariance measurements. *Environ. Pollut.* **2019**, 251, 830-838.
99. Corbett, J. J.; Koehler, H. W. Updated emissions from ocean shipping. *J. Geophys. Res.* **2003**, *108*(D20), 4650.
100. Corbett, J. J.; Winebrake, J. J.; Green, E. H.; Kasibhatla, P.; Eyring, V.; Lauer, A. Mortality from ship emissions: A global assessment. *Environ. Sci. Technol.* **2007**, *41*, 8512-8518.
101. Corbin, J. C.; Mensah, A. A.; Pieber S. M.; Orasche, J.; Michalke, B.; Zanatta, M.; *et al.* Trace metals in soot and $PM_{2.5}$ from heavy-fuel-oil combustion in a marine engine. *Environ. Sci. Technol.* **2018**, *52*, 6714-6722.
102. Cornell, R. M.; Schwertmann, U. Electronic, electric and magnetic properties and colour. [In:] *The iron oxides: Structure, Properties, Reactions, Occurrences and Uses*, by Cornell, R. M.; Schwertmann, U. WILEY-VCH Verlag GmbH & Co. KGaA, **2003**, Weinheim.
103. Costa, L. G.; Cole, T. B.; Coburn, J.; Chang, Y.-C.; Dao, K.; Roque, P. Neurotoxicants are in the air: Convergence of human, animal, and *in vitro* studies on the effects of air pollution on the brain. *BioMed Res. Int.* **2014**, *736385*.
104. Costa, L. G.; Manzo, L. *Occupational Neurotoxicology*. CRC Press, Boca Raton, Boston, London, New York, Washington, D.C., **1998**.
105. Crilley, L. R.; Lucarelli, F.; Bloss, W. J.; Harrison, R. M.; Beddows, D. C.; Calzolai, G.; Nava, S.; Valli, G.; Bernardoni, V.; Vecchi, R. Source apportionment of fine and coarse particles at a roadside and urban background site in London during the 2012 summer ClearfLo campaign. *Environ. Pollut.* **2017**, *220*, 766-778.
106. Cyrys, J.; Pitz, M.; Heinrich, J.; Wichmann, H.-E.; Peters, A. Spatial and temporal variation of particle number concentration in Augsburg, Germany. *Sci. Total Environ.* **2008**, *401*, 168-175.
107. Dahl, A.; Gharibi, A.; Swietlicki, E.; Gudmundsson, A.; Boghard, M.; Ljungman, A.; Blomqvist, G.; Gustafsson, M. Traffic-generated emissions of ultrafine particles from pavement-tire interface. *Atmos. Environ.* **2006**, *40*, 1314-1323.

108. Dall'Osto, M.; Beddows, D. C. S.; Gietl, J. K.; Olatunbosom, O. A.; Yang, X.; Harrison, R. M. Characteristics of tyre dust in polluted air: Studies by single particle mass spectrometry (ATOFMS). *Atmos. Environ.* **2014**, *94*, 224-230.
109. Davila, A. F.; Rey, D.; Mohamed, K.; Rubio, B.; Guerra, A. P. Mapping the sources of urban dust in a coastal environment by measuring magnetic parameters of *Platanus hispanica* leaves. *Environ. Sci. Technol.* **2006**, *40*, 3922-3928.
110. Dearing, J. A.; Dann, R. J. L.; Hay, K.; Lees, J. A.; Loveland, P. J.; Maher, B. A.; O'Grady, K. Frequency-dependent susceptibility measurements of environmental materials. *Geophys. J. Int.* **1996**, *124*, 228-240.
111. Demirdjian, B.; Ferry, D.; Suzanne, J.; Popovicheva, O. B.; Persiantseva, N. M.; Shonija, N. K. Heterogeneities in the microstructure and composition of aircraft engine combustor soot: Impact on the water uptake. *J. Atmos. Chem.* **2007**, *56*, 83-103.
112. Denier van der Gon, H. A. C.; Gerlofs-Nijland, M. E.; Gehrig, R.; Gustafsson, M.; Janssen, N.; Harrison, R. M.; Hulskotte, J.; Johansson, C.; Jozwicka, M.; Keuken M.; Krijgsheld, K.; Ntziachristos, L.; Riediker, M.; Cassee, F. R. The policy relevenace of wear emissions from road transport, now and in the future – An international workshop report and consensus statement. *J. Air. Waste Manag. Assoc.* **2013**, *63*(2): 136-149.
113. Denier van der Gon, H.; Hulskotte, J.; Jozwicka, M.; Kranenburg, R.; Kuenen, J.; Visschedijk, A. European emission inventories and projections for road transport non-exhaust emissions. Analysis of consistency and gaps in emission inventories from EU member states. In *Non-exhaust emissions. An urban air quality problem for public health; Impact and mitigation measures*; Amato, F., Ed.; Academic Press, **2018**.
114. DieselNet. Engine & emission technology online. https://www.dieselnet.com/ (accessed Jun 10, 2019).
115. Dobson, J. Magnetic iron compounds in neurological disorders. *Ann. N.Y. Acad. Sci.* **2004**, *1012*, 183-192.
116. Dobson, J.; Grassi, P. Magnetic properties of human hippocampal tissue – evaluation of artefact and contamination sources. *Brain Res. Bull.* **1996**, *39*(4), 255-259.
117. Dockery, D. W.; Pope III, A.; Xu, X.; Spengler, J. D.; Ware, J. H.; Fay, M. E.; Ferris, B. G. Jr.; Speizer, F. E. An association between air pollution and mortality in six U.S. cities. *N. Engl. J. Med.* **1993**, *329*(24), 1753-1759.
118. Donaldson, K.; Brown, D. M.; Mitchell, C.; Dineva, M.; Beswick, P. H.; Gilmour, P.; MacNee, W. Free radical activity of PM_{10}: Iron-mediated generation of hydroxyl radicals. *Environ. Health Prospect.* **1997**, *105*, 1285-1289.
119. Donaldson, K.; Brown, D.; Clouter, A.; Duffin, R.; MacNee, W.; Renwick, L.; Tran, L.; Stone, V. The pulmonary toxicity of ultrafine particles. *J. Aerosol Med.* **2002**, *15*(2), 213-220.
120. Donaldson, K.; Li, X. Y.; MacNee, W. Ultrafine (nanometre) particle mediated lung injury. *J. Aerosol Sci.* **1998**, *29*(5/6), 553-560.
121. Donaldson, K.; Stone, V.; Clouter, A.; Renwick, L.; MacNee, W. Ultrafine particles. *Occup. Environ. Med.* **2001**, *58*, 211-216.
122. Donaldson, K.; Tran, L.; Jimenez, L. A.; Duffin, R.; Newby, D. E.; Mills, N.; MacNee, W.; Stone, V. Combustion-derived nanoparticles: A review of their toxicology following inhalation exposure. *Part. Fibre Toxicol.* **2005**, *2*(10).
123. Dongarrá, G.; Manno, E.; Varrica, D. Possible markers of traffic-related emissions. *Environ. Monit. Assess.* **2009**, *154*, 117-125.
124. Doty, R. L. The olfactory vector hypothesis of neurodegenerative disease: Is it viable? *Ann. Neurol.* **2008**, *63*, 7-15.
125. Dunlop, D. J. Superparamagnetic and single-domain threshold sizes in magnetite. *J. Gephys. Res.* **1973**, *78*(11), 1780-1793.
126. Duong, T. T. T.; Lee, B.-K. Determining contamination level of heavy metals in road dust from busy traffic areas with different characteristics. *J. Environ. Manage.* **2011**, *92*, 554-562.
127. Dusseldorp, A.; Kruize, H.; Brunekreef, B.; Hofschreuder, P.; de Meer, G.; van Oudvorst, A. B. Associations of PM10 and airborne iron with respiratory health of adults living near a steel factory. *Am. J. Respir. Crit. Care Med.* **1995**, *152*, 1932-1939.

128. Dytłow, S.; Górka-Kostrubiec, B. Effective and universal tool for evaluating heavy metals – passive dust samplers. *Environ. Pollut.* **2019**, *247*, 188-194.
129. Dytłow, S.; Winkler, A.; Górka-Kostrubiec, B.; Sagnotti, L. Magnetic, geochemical and granulometric properties of street dust from Warsaw (Poland). *J. Appl. Geophys.* **2019**, *169*, 58-73.
130. Egli, R. Analysis of the field dependence of remanent magnetization curves. *J. Geophys. Res.* **2003**, *108*(B2), 2081.
131. Egli, R. Characterization of individual rock magnetic components by analysis of remanence curves. 1. Unmixing natural sediments. *Stud. Geophys. Geod.* **2004a**, *48*, 391-446.
132. Egli, R. Characterization of individual rock magnetic components by analysis of remanence curves. 2. Fundamental properties of coercivity distributions. *Phys. Chem. Earth* **2004b**, *29*, 851-867.
133. Egli, R. Characterization of individual rock magnetic components by analysis of remanence curves. 3. Bacterial magnetite and natural processes in lakes. *Phys. Chem. Earth* **2004c**, *29*, 869-884.
134. El Haddad, I.; Marchand, N.; Dron, J.; Temime-Roussel, B.; Quivet, E.; Wortham, H.; Jaffrezo, J. L.; Baduel, C.; Voisin, D.; Besombes, J. L.; Gille, G. Comprehensive primary particulate organic characterization of vehicular exhaust emissions in France. *Atmos. Environ.* **2009**, *43*, 6190-6198.
135. Elder, A.; Gelein, R.; Silva, V.; Feikert, T.; Opanashuk, L.; Carter, J.; Potter, R.; Maynard, A.; Ito, Y.; Finkelstein, J.; Oberdörster, G. Translocation of inhaled ultrafine manganese oxide particles to the central nervous system. *Environ. Health Perspect.* **2006**, *114*(8), 1172-1178.
136. Ema, M.; Naya, M.; Horimoto, M.; Kato, H. Developmental toxicity of diésel exhaust: A review of studies in experimental animals. *Reprod. Toxicol.* **2013**, *42*, 1-17.
137. Endresen, Ø. Sørgård, E.; Sundet, J. K.; Dalsøren, S. B.; Isaksen, I. S. A.; Berglen, T. F.; Gravir, G. Emission from international sea transportation and environmental impact. *J. Geophys. Res.* **2003**, *108*(D17), 4560.
138. Eom, H.-J.; Jung, H.-J.; Sobanska, S.; Chung, S.-G.; Son, Y.-S.; Kim, J.-C.; Sunwoo, Y.; Ro, C.-U. Iron speciation of airborne subway particles by the combined use of Energy Dispersive Electron Probe X-ray microanalysis and Raman microspectrometry. *Anal. Chem.* **2013**, *85*, 10424-10431.
139. Eriksson, M.; Bergman, F.; Jacobson, S. Surface characterisation of brake pads after running under silent and squealing conditions. *Wear* **1999**, *232*, 163-167.
140. Evans, A.; Evans, R. The composition of a tyre: Typical components. Report of the Waste & Resources Action Programme. Banbury, UK, **2006**.
141. Eyring, V.; Isaksen, I. S. A.; Berntsen, T.; Collins, W. J.; Corbett, J. J.; Endresen, O.; Grainger, R. G.; Moldanova, J.; Schlager, H.; Stevenson, D. S. Transport impacts on atmosphere and climate: Shipping. *Atmos. Environ.* **2010**, *44*, 4735-4771.
142. Fabretti, J.-F.; Sauret, N.; Gal, J.-F.; Maria, P.-C.; Schärer, U. Elemental characterization and source identification of $PM_{2.5}$ using positive matrix factorization: the Malraux road tunnel, Nice, France. *Atmos. Res.* **2009**, *94*(2), 320-329.
143. Farwick zum Hagen, F. H.; Mathissen, M.; Grabiec, T.; Hennicke, T.; Rettig, M.; Grochowicz, J.; Vogt, R.; Benter, T. On-road vehicle measurements of brake-wear particle emissions. *Atmos. Environ.* **2019a**, *217*, 116943.
144. Farwick zum Hagen, F. H.; Mathissen, M.; Grabiec, T.; Hennicke, T.; Rettig, M.; Grochowicz, J.; Vogt, R.; Benter, T. Study of brake-wear particle emissions: Impact of braking and cruising conditions. *Environ. Sci. Technol.* **2019b**, *53*, 5143-5150.
145. Feng, Q.; Liu, Y.; Huang, J.; Chen, K.; Huang, J.; Xiao, K. Uptake, distribution, clearance, and toxicity of iron oxide nanoparticles with different sizes and coatings. *Sci. Rep.* **2018**, *8*(2082).
146. Ferin, J.; Oberdörster, G.; Penney, D. P. Pulmonary retention of ultrafine and fine particles in rats. *Am. J. Respir. Cell Mol. Biol.* **1992**, *6*, 535-542.
147. Ferin, J.; Oberdörster, G.; Soderholm, S. C.; Gelein, R. Pulmonary tissue access of ultrafine particles. *J. Aerosol Med.* **1991**, *4* (1), 57-68.
148. Filip, P.; Weiss, Z.; Rafaja, D. On friction layer formation in polymer matrix composite materials for brake applications. *Wear* **2002**, *252*, 189-198.

149. Filippelli, G. M.; Laidlaw, M. A. S.; Latimer, J. C.; Raftis, R. Urban lead poisoning and medical geology: Un unfinished story. *GSA Today* **2005**, *15*(1), 4-11.
150. Fine, P.; Polidori, A.; Teffera, S. *General aviation airport air monitoring study*; Final Report for the U.S. Environmental Protection Agency, Region IX: San Francisco, **2010**.
151. Flanders, P. J. Collection, measurements, and analysis of airborne magnetic particulates from pollution in the environment (invited). *J. Appl. Phys.* **1994**, *75*, 5931-5936.
152. Foitzik, M.-J.; Unrau, H.-J.; Gauterin, F.; Dörnhöfer, J.; Koch, T. Investigation of ultra fine particulate matter emission of rubber tires. *Wear* **2018**, *394-395*, 87-95.
153. Fulper, C. R.; Kishan, S.; Baldauf, R. W.; Sabisch, M.; Warila, J.; Fujita, E. M.; Scarbro, C.; Crews, W. S.; Snow, R.; Gabele, P.; Santos, R.; Tierney, E.; Cantrell, B. Methods of characterizing the distribution of exhaust emissions from light-duty, gasoline-powered motor vehicles in the U.S. fleet. *J. Air & Waste Manage. Assoc.* **2010**, *60*, 1376-1387.
154. Funari, V.; Mantovani, L.; Vigliotti, L.; Tribaudino, M.; Dinelli, E.; Braga, R. Superparamagnetic iron oxides nanoparticles from municipal solid waste incinerators. *Sci. Total. Environ.* **2018**, *621*, 687-696.
155. Gadd, J.; Kennedy, P. Preliminary examination of organic compounds present in tyres, brake pads and road bitumen in New Zealand. *Kingett Mitchell Limited* **2000**.
156. Gao, D.; Ripley, S.; Weichenthal, S.; Pollitt, K. J. G. Ambient particulate matter oxidative potential: Chemical determinants, associated health effects, and strategies for risk management. *Free Radic. Biol. Med.* **2020**, *151*, 7-25.
157. Garcia, G. J. M.; Schroeter, J. D.; Kimbell, J. S. Olfactory deposition of inhaled nanoparticles in humans. *Inhal. Toxicol.* **2015**, *27*(8), 394-403.
158. Garg, B. D.; Cadle, S. H.; Mulawa, P. A.; Groblicki, P. J.; Laroo, C.; Parr, G. A. Brake-wear particulate matter emissions. *Environ. Sci. Technol.* **2000**, *34*(21), 4463-4469.
159. Gargiulo, J. D.; Kumar, R. S.; Chaparro, M. A. E.; Chaparo, M. A. E.; Natal, M.; Rajkumar, P. Magnetic properties of air suspended particles in thirty eight cities from south India. *Atmos. Pollut. Res.* **2016**, *7*, 626-637.
160. Gasser, M.; Riediker, M.; Mueller, L.; Perrenoud, A.; Blank, F.; Gehr, P.; Rothen-Rotishauser, B. Toxic effects of brake-wear particles on epithelial lung cells *in vitro*. *Pert. Fibre Toxicol.* **2009**, *6*(30).
161. Gauderman, W. J.; Vora, H.; McConnell, R.; Berhane, K.; Gilliland, F.; Thomas, D.; Lurmann, F.; Avol, E.; Kunzli, N.; Jerrett, M.; Peters, J. Effect of exposure to traffic on lung development from 10 to 18 years of age: a cohort study. *Lancet* **2007**, *369*, 571-577.
162. Gautam, P.; Blaha, U.; Appel, E. Magnetic susceptibility of dust-loaded leaves as a proxy of traffic-related heavy metal pollution in Kathmandu city, Nepal. *Atmos. Environ.* **2005**, *39*, 2201-2211.
163. Gehrig, R.; Hill, M.; Lienemann, P.; Zwicky, C. N.; Bukowiecki, N.; Weingartner, E.; Baltensperger, U.; Buchmann, B. Contribution of railway traffic to local PM10 concentrations in Switzerland. *Atmos. Environ.* **2007**, *41*, 923-933.
164. Geiser, M.; Kreyling, W. G. Deposition and biokinetics of inhaled nanoparticles. *Part. Fibre Toxicol.* **2010**, *7*(2).
165. Gerlofs-Nijland, M. E.; Bokkers, B. G. H.; Sachse, H.; Reijnders, J. J. E.; Gustafsson, M.; Boere, A. J. F.; Fokkens, P. F. H.; Leseman, D. L. A. C.; Augsburg, K.; Cassee, F. R. Inhalation toxicity profiles of particulate matter: a comparison between brake-wear with other sources of emission. *Inhal. Toxicol.* **2019**, *31*(3), 89-98.
166. Ghio, A. J.; Cohen, M. D. Disruption of iron homeostasis as a mechanism of biologic effect by ambient air pollution particles. *Inhal. Toxicol.* **2005**, *17*, 709-716.
167. Ghio, A. J.; Kennedy, T. P.; Whorton, A. R.; Crumbliss, A. L.; Hatch, G. E.; Hoidal, J. R. Role of surface complexed iron in oxidant generation and lung inflammation induced by silicates. *Am. J. Physiol.* **1992**, *263*, 511-518.
168. Gietl, J. K.; Lawrence, R.; Thorpe, A. J.; Harrison, R. M. Identification of brake-wear particles and derivation of a quantitative tracer for brake dust at a major road. *Atmos. Environ.* **2010**, *44*, 141-146.

169. Gilmour, P. S.; Brown, D. M.; Beswick, P. H.; Benton, E.; MacNee, W.; Donaldson, K. Surface free radical activity of PM_{10} and ultrafine titanium dioxide: a unifying factor in their toxicity? *Ann. Occup. Hyg.* **1997**, *41* (1), 32-38.
170. Gilmour, P. S.; Brown, D. M.; Lindsay, T. G.; Beswick, P. H.; MacNee, W.; Donaldson, K. Adverse health effects of PM_{10} particles: involvement of iron in generation of hydroxyl radical. *Occup. Environ. Med.* **1996**, *53*, 817-822.
171. Gilmour, P.; Brown, D. M.; Beswick, P. H.; Benton, E.; MacNee, W.; Donaldson, K. Surface free radical activity from PM_{10} and ultrafine titanium dioxide: A unifying factor in their toxicity? *The Ann Occup. Hyg.* **1997**, *41*(suppl. 1), 32-38.
172. Ginsberg, G. L.; Perkovich Foos, B.; Firestone, M. P. Review and analysis of inhalation dosimetry methods for application to children's risk assessment. *J. Toxicol. Environ. Health A* **2005**, *68*, 573-615.
173. Gminski, R.; Decker, K.; Heinz, C.; Seidel, A.; Könczöl, M.; Goldenberg, E.; Grobéty, B.; Ebner, W.; Gieré, R.; Mersch-Sundermann, V. Genotoxic effects of three selected black toner powders and their dimethyl sulfoxide extracts in cultured human epithelial A549 lung cells *in vitro*. *Environ. Mol. Mutagen.* **2011**, *52*, 296-309.
174. Goddu, S. R.; Appel, E.; Jordanova, D.; Wehland, F. Magnetic properties of road dust from Visakhapatnam (India) – relationship to industrial pollution and road traffic. *Phys. Chem. Earth* **2004**, *29*, 985-995.
175. Goldstein, A.; Soroka, Y.; Frušić-Zlotkin, M.; Popov, I.; Kohen, R. High resolution SEM imaging of gold nanoparticles in cells and tissues. *J. Microsc.* **2014**, *256*(3), 237-347.
176. Gómez-Paccard, M.; McIntosh, G.; Villasante, V.; Osete, M. L.; Rodriguez-Fernández, J.; Gómez-Sal, J. C. Low-temperature and high magnetic field measurements of atmospheric particulate matter. *J. Magn. Magn. Mater.* **2004**, *272-276*, 2420-2421.
177. Gonet, T.; Maher, B. A. Airborne, Vehicle-derived Fe-bearing nanoparticles in the urban environment: A review. *Environ. Sci. Technol.* **2019**, *53*, 9970-9991.
178. Gonet, T.; Maher, B. A.; Nyirő-Kósa, I.; Pósfai, M.; Vaculík, M.; Kukutschová, J. Size-resolved, quantitative evaluation of the magnetic mineralogy of airborne brake-wear particulate emissions. *Environ. Pollut.* **2021a**, *288*, 117808.
179. Gonet, T.; Maher, B. A.; Kukutschová, J. Source apportionment of magnetite particles in roadside particulate matter. *Sci. Total Environ.* **2021b**, *752*, 141828.
180. González, Y.; Rodríguez, S. A comparative study on the ultrafine particle episodes induced by vehicle exhaust: A crude oil refinery and ship emissions. *Atmos. Res.* **2013**, *120-121*, 43-54.
181. González, Y.; Rodríguez, S.; García, J. C. G.; Trujillo, J. L.; García, R. Ultrafine particles pollution in urban coastal air due to ship emissions. *Atmos. Environ.* **2011**, *45*, 4907-4914.
182. González-Maciel, A.; Reynoso-Robles, R.; Torres-Jardón, R.; Mukherjee, P. S.; Calderón-Garcidueñas, L. Combustion-derived nanoparticles in key brain target cells and organelles in young urbanities: Culprit hidden in plain sight in Alzheimer's disease development. *J. Alzheimer Dis.* **2017**, *59*(1), 189-208.
183. Górka-Kostrubiec, B.; Król, E.; Jeleńska, M. Dependence of air pollution on meteorological conditions based on magnetic susceptibility measurements: a case study from Warsaw. *Stud. Geophys. Geod.* **2012**, *56*, 861-877.
184. Górka-Kostrubiec, B.; Szczapaniak-Wnuk, I. Magnetic study of a mixture of magnetite and metallic iron in indoor dust samples. *Air Qual. Atmos. Health* **2017**, *10*(1), 105-116.
185. Górka-Kostrubiec, B.; Werner, T.; Dytłow, S. Szczepaniak-Wnuk, I.; Jeleńska, M.; Hanc-Kuczkowska, A. Detection of metallic iron in urban dust by using high-temperature measurements supplemented with microscopic observations and Mössbauer spectra. *J. Appl. Geophys.* **2019**, *166*, 89-102.
186. Grigoratos, T.; Martini, G. Brake-wear particle emissions: a review. *Environ. Sci. Pollut. Res.* **2015**, *22*, 2491-2504.
187. Gualtieri, M.; Andrioletti, M.; Mantecca, P.; Vismara, C.; Camatini, M. Impact of tire debris on *in vitro* and *in vivo* systems. *Part. Fibre Toxicol.* **2005**, *2*(1).
188. Gunderman, R. B.; Gonda, A. S. Radium Girls. *Radiol.* **2015**, *274*(2), 314-318.
189. Gustafsson, M.; Blomqvist, G.; Gudmundsson, A.; Dahl, A.; Swietlicki, E.; Bohgard, M.; Lindbom, J.; Ljungman, A. Properties and toxicological effects of particles from the interaction

between tires, road pavement and winter traction material. *Sci. Total Environ.* **2008**, *393*, 226-240.

190. Gustafsson, M.; Blomqvist, G.; Swietlicki, E.; Dahl, A.; Gudmundsson, A. Inhalable railroad particles at ground level and subterranean stations – Physical and chemical properties and relation to train traffic. *Transp. Res. D* **2012**, *17*, 277-285.
191. Guxens, M.; Sunyer, J. A review of epidemiological studies on neuropsychological effects of air pollution. *Swiss Med Wkly* **2012**, *141*, w13322.
192. Hagino, H.; Oyama, M.; Sasaki, S. Airborne brake-wear particle emission due to braking and accelerating. *Wear* **2015**, *334-335*, 44-48.
193. Hagino, H.; Oyama, M.; Sasaki, S. Laboratory testing of airborne brake-wear particle emissions using a dynamometer system under urban city driving cycles. *Atmos. Environ.* **2016**, *131*, 269-278.
194. Hall, G. S.; Chambliss, C. R. Nondestructive multi-elemental analyses of current-size United States federal reserve notes by energy dispersive X-ray fluorescence. *Appl. Spectrosc.* **2004**, *58*(11), 1334-1340.
195. Halsall, C. J.; Maher, B. A.; Karloukovski, V. V.; Shah, P.; Watkins, S. J. A novel approach to investigating indoor/outdoor pollution links: Combined magnetic and PAH measurements. *Atmos. Environ.* **2008**, *42*, 8902-8909.
196. Hama, S. M. L.; Cordell, R. L.; Monks, P. S. Quantifying primary and secondary source contributions to ultrafine particles in the UK urban background. *Atmos. Environ.* **2017**, *166*, 62-78.
197. Hammond, J.; Maher, B. A.; Gonet, T., *et al*. Cytotoxic, inflammatory, and oxidative stress responses to urban nanoparticulate roadside dust from the UK and Mexico in the human epithelial lung cells [**in prep.**].
198. Hanesch, M.; Scholger, R. Mapping of heavy metal loadings in soils by means of magnetic susceptibility measurements. *Environ. Geol.* **2002**, *42*, 857-870.
199. Hanesch, M.; Scholger, R.; Rey, D. Mapping dust distribution around an industrial site by measuring magnetic parameters of tree leaves. *Atmos. Environ.* **2003**, *37*, 5125-5133.
200. Hansard, R.; Maher, B. A.; Kinnersley, R. Biomagnetic monitoring of industry-derived particulate pollution. *Environ. Pollut.* **2011**, *159*, 1673-1681.
201. Hansard, R.; Maher, B. A.; Kinnersley, R. P. Rapid magnetic biomonitoring and differentiation of atmospheric particulate pollutants at the roadside and around two major industrial sites in the U.K. *Environ. Sci. Technol.* **2012**, *46*, 4403-4410.
202. Harris, S. J.; Maricq, M. M. Signature size distributions for diesel and gasoline engine exhaust particulate matter. *Aerosol Sci.* **2001**, *32*, 749-764.
203. Harrison, R. M.; Beddows, D. C. S.; Dall'Osto, M. PMF analysis of wide-range particle size spectra collected on a major highway. *Environ. Sci. Technol.* **2011**, *45*, 5522-5528.
204. Harrison, R. M.; Jones, A. M.; Gietl, J.; Yin, J.; Green, D. C. Estimation of the contributions of brake dust, tire wear, and resuspension to nonexhaust traffic particles derived from atmospheric measurements. *Environ. Sci. Technol.* **2012**, *46*, 6523-6529.
205. Harrison, R. M.; Masiol, M.; Vardoulakis, S. Civil aviation, air pollution and human health. *Environ. Res. Lett.* **2015**, *10*, 041001.
206. Harrison, R. M.; Shi, J. P.; Xi, S.; Khan, A.; Mark, D.; Kinnersley, R.; Yin, J. Measurement of number, mass and size distribution of particles in the atmosphere. *Phil. Trans. R. Soc. Lond. A* **2000**, *358*, 2567-2580.
207. Harrison, R. M.; Yin, J.; Mark, D.; Stedman, J.; Appleby, R. S.; Booker, J.; Moorcroft, S. Studies of the coarse particle (2.5-10 μm) component un UK urban atmospheres. *Atmos. Environ.* **2001**, *35*, 3667-3679.
208. Hautot, D.; Pankhurst, Q. A.; Khan, N.; Dobson, J. Preliminary evaluation of nanoscale biogenic magnetite in Alzheimer's disease brain tissue. *Proc. R. Soc. Lond. B* **2003**, *270*, S62-S64.
209. Hawkes, P. W.; Spence, J. C. H. *Springer Handbook of Microscopy*. Springer, Switzerland, **2019**.
210. Hays, M. D.; Cho, S.H.; Baldauf, R.; Schauer, J. J.; Shafer, M. Particle size distributions of metal and non-metal elements in an urban near-highway environment. *Atmos. Environ.* **2011**, *45*, 925-934.

211. He, R.-W.; Shirmohammadi, F.; Gerlofs-Nijland, M. E.; Sioutas, C.; Cassee, F. R. Pro-inflammatory responses to $PM_{0.25}$ from airport and urban traffic emissions. *Sci. Total. Environ.* **2018**, *640-641*, 997-1003.
212. Healy, R. M.; Hellebust, S.; Kourtchev, I.; Allanic, A.; O'Connor, I. P.; Bell, J. M.; Healy, D. A.; Sodeau, J. R.; Wenger, J. C. Source apportionment of $PM_{2.5}$ in Cork Harbour, Ireland using a combination of single particle mass spectrometry and quantitative semi-continuous measurements. *Atmos. Chem. Phys.* **2010**, *10*, 9596-9613.
213. Healy, R. M.; O'Connor, I. P.; Hellebust, S.; Allanic, A.; Sodeau, J. R.; Wenger, J. C. Characterisation of single particles from in-port ship emissions. *Atmos. Environ.* **2009**, *43*, 6408-6414.
214. HEI Panel on the health effects of traffic-related air pollution. Traffic-related air pollution: A critical review of the literature on emissions, exposure, and health effects. *HEI Special Report* **2010**. Health Effects Institute, Boston, MA.
215. HEI State of Global Air 2020. *HEI Special Report* **2020**. Health Effects Institute, Boston, MA.
216. Hinrichs, R.; Soares, M. R. F.; Lamb, R. G.; Soares, M. R. F.; Vasconcellos, M. A. Z. Phase characterization of debris generated in brake pad coefficient of friction tests. *Wear* **2011a**, *270*, 515-519.
217. Hinrichs, R.; Vasconcellos, M. A. Z.; Österle, W.; Prietzel, C. A TEM snapshot of magnetite formation in brakes: The role of the disc's cast iron graphite lamellae in third body formation. *Wear* **2011b**, *270*, 365-370.
218. Hjortenkrans, D. S. T.; Bergbäck, B. G.; Häggerud, A. V. Metal emissions from brake linings and tires: Case studies of Stockholm, Sweden 1995/1998 and 2005. *Environ. Sci. Technol.* **2007**, *41*, 5224-5230.
219. Ho, H. C.; Wong, M. S.; Yang, L.; Shi, W.; Yang, J.; Bilal, M.; Chan, T.-C. Spatiotemporal influence of temperature, air quality, and urban environment on cause-specific mortality during hazy days. *Environ. Int.* **2018**, *112*, 10-22.
220. Hoek, G.; Beelen, R.; Kos, G.; Dijkema, M.; van der Zee, S.; Fischer, P. H.; Brunekreef, B. Land use regression model for ultrafine particles in Amsterdam. *Environ. Sci. Technol.* **2011**, *45*, 622-628.
221. Hoek, G.; Krishnan, R. M.; Beelen, R.; Peters, A.; Ostro, A.; Brunekreef, B.; Kaufman, J. D. Long-term air pollution exposure and cardio-respiratory mortality: a review. *Environ. Health* **2013**, *12*(43).
222. Hoffmann, V.; Knab, M.; Appel, E. Magnetic susceptibility mapping of roadside pollution. *J. Geochem. Explor.* **1999**, *66*, 313-326.
223. Hofman, J.; Castanheiro, A.; Nuyts, G.; Joosen, S.; Spassov, S.; Blust, R.; De Wael, K.; Lenaerts, S.; Samson, R. Impact of urban street canyon architecture on local atmospheric pollutant levels and magneto-chemical PM_{10} composition: An experimental study in Antwerp, Belgium. *Sci. Total Environ.* **2020**, *712*, 135534.
224. Hofman, J.; Lefebvre, W.; Janssen, S.; Nackaerts, R.; Nuyts, S.; Mattheyses, L.; Samson, R. Increasing the spatial resolution of air quality assessments in urban areas: A comparison of biomagnetic monitoring and urban scale modelling. *Atmos. Environ.* **2014a**, *92*, 130-140.
225. Hofman, J.; Maher, B. A.; Muxworthy, A. R.; Wuyts, K.; Castanheiro, A.; Samson, R. Biomagnetic monitoring of atmospheric pollution: A review of magnetic signatures from biological sensors. *Environ. Sci. Technol.* **2017**, *51*, 6648-6664.
226. Hofman, J.; Stokkaer, I.; Snauwaert, L.; Samson, R. Spatial distribution assessment of particulate matter in an urban street canyon using biomagnetic leaf monitoring of tree crown deposited particles. *Environ. Pollut.* **2013**, *183*, 123-132.
227. Hofman, J.; Wuyts, K.; Van Wittenberghe, S.; Brackx, M.; Samson, R. On the link between biomagnetic monitoring and leaf-deposited dust load of urban trees: Relationships and spatial variability of different particle size fractions. *Environ. Pollut.* **2014b**, *189*, 63-72.
228. Hofman, J.; Wuyts, K.; Van Wittenberghe, S.; Samson, R. On the temporal variation of leaf magnetic parameteras: Seasonal accumulation of leaf-deposited and leaf-encapsulated particles of a roadside tree crown. *Sci. Total Environ.* **2014c**, *493*, 766-772.

229. Hosiokangas, J.; Ruuskanen, J.; Pekkanen, J. Effects of soil dust episodes and mixed fuel sources on source apportionment of PM10 particles in Kuopio, Finland. *Atmos. Environ.* **1999**, *33*, 3821-3829.
230. Hosseini, S.; Li, Q.; Cocker, D.; Weise, D.; Miller, A.; Shrivastava, M.; Miller, J. W.; Mahalingam, S.; Princevac, M.; Jung, H. Particle size distributions from laboratory-scale biomass fires using fast response instruments. *Atmos. Chem. Phys.* **2010**, *10*, 8065-8076.
231. Hu, S. Y.; Duan, X. M.; Shen, M. J.; Blaha, U.; Roesler, W.; Yan, H. T.; Appel, E.; Hoffman, V. Magnetic response to atmospheric heavy metal pollution recorded by dust-loaded leaves in Shougang industrial area, western Beijing. *Chin. Sci. Bull.* **2008**, *53*(10), 1555-1564.
232. Hu, S.; Fruin, S.; Kozawa, K.; Mara, S.; Winer, A. M.; Paulson, S. E. Aircraft emission impacts in a neighborhood adjacent to a general aviation airport in Southern California. *Environ. Sci. Technol.* **2009**, *43*, 8039-8045.
233. Hu, X.-F.; Su, Y.; Ye, R.; Li, X.-Q.; Zhang, G.-L. Magnetic properties of the urban soils in Shanghai and their environmental implications. *Catena* **2007**, *70*, 428-436.
234. Hulskotte, J. H. J.; Roskam, G. D.; Denier van der gon, H. A. C. Elemental composition of current automotive braking materials and derived air emission factors. *Atmos. Environ.* **2014**, *99*, 436-445.
235. Iaccarino, L.; La Joie, R.; Lesman-Segev, O. H.; Lee, E.; Hanna, L.; Allen, I. E.; Hillner, B. E.; Siegel, B. A.; Whitmer, R. A.; Carrillo, M. C.; Gatsonis, C.; Rabinovici, G. D. Association between ambient air pollution and amyloid positron emission tomography positivity in older adults with cognitive impairment. *JAMA Neurol.* **2020**, *78*(2), 197-207.
236. Iijima, A.; Sato, K.; Yano, K.; Kato, M.; Kozawa, K.; Furuta, N. Emission factor for antimony in brake abrasion dust as one of the major atmospheric antimony sources. *Environ. Sci. Technol.* **2008**, *42*, 2937-2942.
237. Iijima, A.; Sato, K.; Yano, K.; Tago, H.; Kato, M.; Kimura, H.; Furuta, N. Particle size and composition distribution analysis of automotive brake abrasion dusts for the evaluation of antimony sources of airborne particulate matter. *Atmos. Environ.* **2007**, *41*, 4908-4919.
238. Imhof, D.; Weingartner, E.; Prévôt, A. S. H.; Ordóñez, C.; Kurtenbach, R.; Wiesen, P.; Rodler, J.; Sturm, P.; McCrae, I.; Ekström, M.; Baltensperger, U. Aerosol and NO_x emission factors and submicron particle number size distributions in two road tunnels with different traffic regimes. *Atmos. Chem. Phys.* **2006**, *6*, 2215-2230.
239. Isakson, J.; Persson, T. A.; Selin Lindgren, E. Identification and assessment of ship emissions and their effects in the harbour of Göteborg, Sweden. *Atmos. Environ.* **2001**, *35*, 3659-3666.
240. Jalava, P. I.; Salonen, R. O.; Nuutinen, K.; Pennanen, A. S.; Happo, M. S.; Tissari, J.; Frey, A.; Hillamo, R.; Jokiniemi, J.; Hirvonen, M.-R. Effect of combustion condition on cytotoxic and inflammatory activity of residential wood combustion particles. *Atmos. Environ.* **2010**, *44*, 1691-1698.
241. Jang, H. Brake friction materials. In *Encyclopedia of Tribology*; Wang, Q. J.; Chung, Y.-W., Eds.; Springer: New York, Heidelberg, Dordrecht, London, **2013**; pp. 263-273.
242. Janssen, N.A.H.; Yang, A.; Strak, M.; Steenhof, M.; Hellack, B.; Gerlofs-Nijland, M. E.; Kuhlbusch, T.; Kelly, F.; Harrison, R.; Brunkreef, B.; Hoek, G.; Cassee, F. Oxidative potential of particulate matter collected at sites with different source characteristics. *Sci. Total Environ.* **2014**, *472*, 572-581.
243. Jeleńska, M.; Górka-Kostrubiec, B.; Werner, T.; Kądziałko-Hofmokl, M.; Szczepaniak-Wnuk, I.; Gonet, T.; Szwarczewski, P. Evaluation of indoor/outdoor urban air pollution by magnetic, chemical and microscopic studies. *Atmos. Pollut. Res.* **2017**, *8*, 754-766.
244. Jeong, C.-H.; Evans, G. J.; Healy, R. M.; Jadidian, P.; Wentzell, J.; Liggio, J.; Brook, J. R. Rapid physical and chemical transformation of traffic-related atmospheric particles near a highway. *Atmos. Pollut. Res.* **2015**, *6*, 662-672.
245. Jones, A. M.; Harrison, R. M. Emission of ultrafine particles from the incineration of municipal solid waste: A review. *Atmos. Environ.* **2016**, *140*, 519-528.
246. Jordanova, D.; Jordanova, N.; Lanos, P.; Petrov, P.; Tsacheva, T. Magnetism of outdoor and indoor settled dust and its utilization as a tool for revealing the effect of elevated particulate air pollution on cardiovascular mortality. *Geochem. Geophys. Geosyst.* **2012**, *13*, Q08Z49.

247. Jordanova, D.; Petrov, P.; Hoffman, V.; Gocht, T.; Panaiotu, C.; Tsacheva, T.; Jordanova, N. Magnetic signature of different vegetation species in polluted environment. *Stud. Gephys. Geod.* **2010**, *54*, 417-442.
248. Jordanova, N. V.; Jordanova, D. V.; Veneva, L.; Yorova, K.; Petrovský, E. Magnetic response of soils and vegetation to heavy metal pollution – A case study. *Environ. Sci. Technol.* **2003**, *37*, 4417-4424.
249. JRC, **2014**. *Non-exhaust traffic related emissions. Brake and tyre wear PM*. JRC Science and policy reports.
250. Jung, C.-R.; Lin, Y.-T.; Hwang, B.-F. Ozone, particulate matter, and newly diagnosed Alzheimer's disease: A population-based cohort study in Taiwan. *J. Alzheimers Dis.* **2015**, *44*, 573-584.
251. Jung, H.-J.; Kim, B.; Malek, M. A.; Koo, Y. S.; Jung, J. H.; Son, Y.-S.; Kim, J.-C.; Kim, H.; Ro, C.-U. Chemical speciation of size-segregated floor dusts and airborne magnetic particles collected at underground subway stations in Seoul, Korea. *J. Hazar. Mater.* **2012**, *213-214*, 331-340.
252. Juwono, A. M.; Johnson, G. R.; Mazaheri, M.; Morawska, L.; Roux, F.; Kitchen, B. Investigation of the airborne submicrometer particles emitted by dredging vessels using a plume capture method. *Atmos. Environ.* **2013**, *73*, 112-123.
253. Kam, W.; Liacos, J. W.; Schauer, J. J.; Delfino, R. J.; Sioustas, C. Size-segregated composition of particulate matter (PM) in major roadways and surface streets. *Atmos. Environ.* **2012**, *55*, 90-97.
254. Kam, W.; Ning, Z.; Shafer, M. M.; Schauer, J. J.; Sioustas, C. Chemical characterization and redox potential of coarse and fine particulate matter (PM) in underground and ground-level rail systems of the Los Angeles Metro. *Environ. Sci. Technol.* **2011**, *45*, 6769-6776.
255. Kang, S.; Hwang, H.; Park, Y.; Kim, H.; Ro, C.-U. Chemical compositions of subway particles in Seoul, Korea determined by a quantitative single particle analysis. *Environ. Sci. Technol.* **2008**, *42*, 9051-9057.
256. Kardel, F.; Wuyts, K.; De Wael, K.; Samson, R. Biomonitoring of atmospheric particulate pollution via chemical composition and magnetic properties of roadside tree leaves. *Environ. Sci. Pollut. Res.* **2018**, *25*, 25994-26004.
257. Kardel, F.; Wuyts, K.; Maher, B. A.; Hansard, R.; Samson, R. Leaf saturation isothermal remanent magnetization (SIRM) as a proxy for particulate matter monitoring: Inter-species differences and in-season variation. *Atmos. Environ.* **2011**, *45*, 5164-5171.
258. Kardel, F.; Wuyts, K.; Maher, B. A.; Samson, R. Intra-urban spatial variation of magnetic particles: Monitoring via leaf saturation isothermal remanent magnetisation (SIRM). *Atmos. Environ.* **2012**, *55*, 111-120.
259. Karjalainen, P.; Pirjola, L.; Heikkilä, J.; Lähde, T.; Tzamkiozis, T.; Ntziachristos, L.; Keskinen, J.; Rönkkö, T. Exhaust particles of modern gasoline vehicles: A laboratory and on-road study. *Atmos. Environ.* **2014**, *97*, 262-270.
260. Karlsson, H. L.; Holgersson, Å.; Möller, L. Mechanisms related to the genotoxicity of particles in the subway and from other sources. *Chem. Res. Toxicol.* **2008**, *21*, 726-731.
261. Karlsson, H. L.; Ljungman, A. G.; Lindbom, J.; Möller, L. Comparison of genotoxic and inflammatory effects of particles generated by wood combustion, a road simulator and collected from street and subway. *Toxicol. Lett.* **2006**, *165*, 203-211.
262. Karlsson, H. L.; Nilsson, L.; Möller, L. Subway particles are more genotoxic than street particles and induce oxidative stress in cultured human lung cells. *Chem. Res. Toxicol.* **2005**, *18*, 19-23.
263. Kazimirova, A.; Peikertova, P.; Barancokova, M.; Staruchova, M.; Tulinska, J.; Vaculik, M.; Vavra, I.; Kukutschova, J.; Filip, P.; Dusinska, M. Automotive airborne brake-wear debris nanoparticles and cytokinesis-block micronucleus assay in peripheral blood lymphocytes: A pilot study. *Environ. Res.* **2016**, *148*, 443-449.
264. Ketzel, M.; Omstedt, G.; Johansson, C.; Düring, I.; Pohjola, M.; Oettl, D.; Gidhagen, L.; Wåhlin, P.; Lohmeyer, A.; Haakana, M.; Berkowicz, R. Estimation and validation of $PM_{2.5}$/PM_{10} exhaust and non-exhaust emission factors for practical street pollution modelling. *Atmos. Environ.* **2007**, *41*, 9370-9385.

265. Keuken, M.; Denier van der Gon, H.; van der Valk, K. Non-exhaust emissions of PM and the efficiency of emission reduction by road sweeping and washing in the Netherlands. *Sci. Total Environ.* **2010**, *408*, 4591-4599.

266. Keuken, M. P.; Henzing, J. S.; Zandveld, P.; van den Elshout, S.; Karl, M. Dispersion of particle numbers and elemental carbon from road traffic, a harbour and an airstrip in the Netherlands. *Atmos. Environ.* **2012**, *54*, 320-327.

267. Kilian, J.; Kitazawa, M. The emerging risk of exposure to air pollution on cognitive decline and Alzheimer's disease – Evidence from epidemiological and animal studies. *Biomed. J.* **2018**, *41*, 141-162.

268. Kim, K. Y.; Kim, Y. S.; Roh, Y. M.; Lee, C. M.; Kim, C. N. Spatial distribution of particulate matter (PM_{10} and $PM_{2.5}$) in Seoul Metropolitan Subway stations. *J. Hazard. Mater.* **2008**, *154*, 440-443.

269. Kim, W.; Doh, S.-J.; Park, Y.-H.; Yun, S.-T. Two-year magnetic monitoring in conjunction with geochemical and electron microscopic data of roadside dust in Seoul, Korea. *Atmos. Environ.* **2007**, *41*, 7627-7641.

270. Kirschvink, J. L.; Kobayashi-Kirschvink, A.; Woodford, B. J. Magnetite biomineralization in the human brain. *Proc. Natl. Acad. Sci. USA* **1992**, *89*, 7683-7687.

271. Klepeis, N. E.; Nelson, W. C.; Ott, W. R.; Robinson, J. P.; Tsang, A. M.; Switzer, P.; Behar, J. V.; Hern, S. C.; Engelmann, W. H. The National Human Activity Pattern Survey (NHAPS): a resource for assessing exposure to environmental pollutants. *J. Expo. Anal. Environ. Epidemiol.* **2001**, *11*, 231-252.

272. Knibbs, L. D.; Cole-Hunter, T.; Morawska, L. A review of commuter exposure to ultrafine particles and its health effects. *Atmos. Environ.* **2011**, *45*, 2611-2622.

273. Kobayashi, A.; Yamamoto, N.; Kirschvink, J. Studies of inorganic crystals in biological tissue: Magnetite in human tumor. *J. Jpn. Soc. Powder Powder Metall* **1997**, *44*, 294-300.

274. Könczöl, M.; Ebeling, S.; Goldenberg, E.; Treude, F.; Gminski, R.; Gieré, R.; Grobéty, B.; Rothen-Ruthishauser, B.; Merfort, I.; Mersch-Sundermann, V. Cytotoxicity and genotoxicity of size-fractionated iron oxide (magnetite) in A549 human lung epithelial cells: Role of ROS, JNK, and NF-κB. *Chem. Res. Toxicol.* **2011**, *24*, 1460-1475.

275. Könczöl, M.; Weiss, A.; Stangenberg, E.; Gminski, R.; Garcia-Käufer, M.; Gieré, R.; Merfort, I.; Mersch-Sundermann, V. Cell-cycle changes and oxidative stress response to magnetite in A549 human lung cells. *Chem. Res. Toxicol.* **2013**, *26*, 693-702.

276. Kravchenko, J.; Darrah, T. H.; Miller, R. K.; Lyerly, H. K.; Vengosh, A. A review of the health impacts of barium from natural and anthropogenic exposure. *Environ. Geochem. Health* **2014**, *36*, 797-814.

277. Kreyling, W. G.; Semmler, M.; Möller, W. Dosimetry and toxicology of ultrafine particles. *J. Aerosol Med.* **2004**, *17*(2), 140-152.

278. Kukutschová, J.; Filip, P. Review of brake-wear emissions: A review of brake emission measurement studies: Identification of gaps and future needs. In *Non-exhaust emissions*; Amato, F., Ed.; Academic Press: **2018**; pp 123-146.

279. Kukutschová, J.; Moravec, P.; Tomášek, V.; Matéjka, V.; Smolík, J.; Schwarz, J.; Seidlerová, J.; Šafářová, K.; Filip, P. On airborne nano/micro-sized wear particles released from low-metallic automotive brakes. *Environ. Pollut.* **2011**, *159*, 998-1006.

280. Kukutschová, J.; Roubíček, V.; Malachová, K.; Pavlíčková, Z.; Holuša, R.; Kubačková, J.; Mička, V.; MacCrimmon, D.; Filip, P. Wear mechanism in automotive brake materials, wear debris and its potential environmental impact. *Wear* **2009**, *267*, 807-817.

281. Kukutschová, J.; Roubíček, V.; Mašláň, M.; Jančík, D.; Slovák, V.; Malachová, K.; Pavlíčková, Z.; Filip, P. Wear performance and wear debris of semimetallic automotive brake materials. *Wear* **2010**, *268*, 86-93.

282. Kumar, P.; Fennell, P.; Langley, D.; Britter, R. Pseudo-simultaneous measurements for the vertical variation of coarse, fine and ultrafine particles in an urban street canyon. *Atmos. Environ.* **2008**, *42*, 4304-4319.

283. Kumar, P.; Morawska, L.; Harrison, R. M. Nanoparticles in European cities and associated health impacts. In *Urban air quality in Europe*, Viana, M., Ed.; Springer-Verlag Berlin Heidelberg, **2012**.
284. Kumar, P.; Pirjola, L.; Ketzel, M.; Harrison, R. M. Nanoparticle emissions from 11 non-vehicle exhaust sources – A review. *Atmos. Environ.* **2013**, *67*, 252-277.
285. Kumata, H.; Yamada, J.; Masuda, K.; Takada, H.; Sato, Y.; Sakurai, T.; Fujiwara, K. Benzothiazolamines as tire-derived molecular markers: Sorptive behavior in Street runoff and application to source apportioning. *Environ. Sci. Technol.* **2002**, *36*, 702-708.
286. Künzi, L.; Krapf, M.; Daher, N.; Dommen, J.; Jeannet, N.; Schneider, S.; Platt, S.; Slowik, J. G.; Baumlin, N.; Salathe, M.; Prévôt, A. S. H.; Kalberer, M.; Strähl, C.; Dümbgen, L.; Sioutas, C.; Baltensperger, U.; Geiser, M. Toxicity of aged gasoline exhaust particles to normal and diseased airway epithelia. *Sci. Rep.* **2015**, *5*(11801).
287. Kupiainen, K. J.; Tervahattu, H.; Räisänen, M.; Mäkelä, T.; Aurela, M.; Hillamo, R. Size and composition of airborne particles from pavement wear, tires, and traction sanding. *Environ. Sci. Technol.* **2005**, *39*, 699-706.
288. Laden, F.; Neas, L. M.; Dockery, D. W.; Schwartz, J. Association of fine particulate matter from different sources with daily mortality in six U.S. cities. *Environ. Health Perspect.* **2000**, *108*(10), 941-947.
289. Lamberg, H.; Nuutinen, K.; Tissari, J.; Ruusunen, J.; Yli-Pirilä, P.; Sippula, O.; Tapainen, M.; Jalava, P.; Makkonen, U.; Teinilä, K.; Saarnio, K.; Hillamo, R.; Hirvonen, M.-R.; Jokiniemi, J. Physicochemical characterization of fine particles from small-scale wood combustion. *Atmos. Environ.* **2011**, *45*, 7635-7643.
290. Lamichhane, D. K.; Leem, J.-H.; Lee, J.-Y.; Kim, H.-C. A meta-analysis of exposure to particulate matter and adverse birth outcomes. *Environ. Health and Toxicol.* **2015**, *30*, e2015011.
291. Landrigan, P. J.; Fuller, R.; Acosta, N. J. R.; Adeyi, O.; Arnold, R.; *et al.* The *Lancet* Comission on pollution and health. *Lancet* **2018**, *391*, 462-512.
292. Lawrence, S.; Sokhi, R.; Ravindra, K.; Mao, H.; Prain, H. D.; Bull, I. D. Source apportionment of traffic emissions of particulate matter using tunnel measurements. *Atmos. Environ.* **2013**, *77*, 548-557.
293. Lee, P. W.; Filip, P. Friction and wear of Cu-free and Sb-free environmental friendly automotive brake materials. *Wear* **2013**, *302*, 1404-1413.
294. Lee, B. E.; Ha, E. H.; Park, H. S.; Kim, Y. J.; Hong, Y. C.; Kim, H.; Lee, J. T. Exposure to air pollution during different gestational phases contributes to risks of low birth weight. *Hum. Reprod.* **2003**, *18*(3), 638-643.
295. Lee, D.; Miller, A.; Kittelson, D.; Zachariah, M. R. Characterization of metal-bearing diesel nanoparticles using single-particle mass spectrometry. *Aerosol Sci.* **2006**, *37*, 88-110.
296. Lee, H.; Namgung, H.-G.; Kwon, S.-B. Effect of train velocity on the amount of airborne wear particles generated from wheel-rail contacts. *Wear* **2018a**, *414-415*, 296-302.
297. Lee, Y.; Choi, K.; Jung, W.; Versoza, M. E.; Barabad, M. L. M.; Kim, T.; Park, D. Generation characteristics of nanoparticles emitted from subways in operation. *Aerosol Air Qual. Res.* **2018b**, *18*, 2230-2239.
298. Lehndorff, E.; Schwark, L. Biominitoring of air quality in the Cologne Conurbation using pine needles as a passive sampler – Part II: polycyclic aromatic hydrocarbons (PAH). *Atmos. Environ.* **2004**, *38*, 3793-3808.
299. Lehndorff, E.; Urbat, M.; Schwark, L. Accumulation histories of magnetic particles on pine needles as function of air quality. *Atmos. Environ.* **2006**, *40*, 7082-7096.
300. Lelièvre, C. P.; Magnani, G.; Ramaroson, R.; Gouriou, F.; Talbaut, M.; Fréjafon, E.; Schuermann, G.; Schaefer, K.; Cornier, I.; Emeis, S.; Vannier, F.; Paux, E.; Copalle, A. Air quality and engine emission at Paris CDG airport during AIRPUR field campaigns. In *Air Pollution*; Longhurst, J. W. S.; Brebbia, C. A., Eds.; WIT Transactions on Ecology and the Environment, **2006.**
301. Leng, X.; Qian, X.; Yang, M.; Wang, C.; Li, H.; Wang, J. Leaf magnetic properties as a method for predicting heavy metal concentrations in $PM_{2.5}$ using support vector machine: A case study in Nanjing, China. *Environ. Pollut.* **2018**, *242*, 922-930.
302. Levy, B. S.; Nassetta, W. J. Neurologic effects of manganese in humans: A review. *Int. J. Occup. Environ. Health* **2003**, *9*, 153-163.

303. Li, C.; Li, X.; Suzuki, A. K.; Zhang, Y.; Fujitani, Y.; Nagaoka, K.; Watanabe, G.; Taya, K. Effects of exposure to nanoparticle-rich diesel exhaust on pregnancy in rats. *J. Reprod. Develop.* **2013**, *59*(2), 145-150.
304. Li, K.; Reichmann, H. Role of iron in neurodegenerative diseases. *J. Neural. Transm.* **2016**, *123*, 389-399.
305. Li, X. Y.; Gilmour, P. S.; Donaldson, K.; MacNee, W. Free radical activity and pro-inflammatory effects of particulate air pollution (PM_{10}) in vivo and in vitro. *Thorax* **1996**, *51*, 1216-1222.
306. Li, X.; Huang, S.; Jiao, A.; Yang, X.; Yun, J.; Wang, Y.; Xue, X.; Chu, Y.; Liu, F.; Liu, Y.; Ren, M.; Chen, X.; Li, N.; Lu, Y.; Mao, Z.; Tian, L.; Xiang, H. Association between ambient fine particulate matter and preterm birth or term low birth weight: An updated systematic review and meta-analysis. *Environ. Pollut.* **2017**, *227*, 596-605.
307. Li, S.; Zhang, B.; Wu, D.; Li, Z.; Chu, S.-Q.; Ding, X.; Tang, X.; Chen, J.; Li, Q. Magnetic particles unintentionally emitted from anthropogenic sources: Iron and steel plants. *Environ. Sci. Technol. Lett.* **2021**, *8*(4), 295-300.
308. Liang, H.; Chen, A.; Lai, X.; Liu, J.; Wu, J.; Kang, Y.; Wang, X.; Shao, L. Neuroinflammation is induced by tongue-instilled ZnO nanoparticles via Ca^{2+}-dependent NF-κB and MAPK pathways. *Part. Fibre Toxicol.* **2018**, *15*(39).
309. Liati, A.; Pandurangi, S. S.; Boulouchos, K.; Schreiber, D.; Dasilva, Y. A. R. Metal nanoparticles in diesel exhaust derived by in-cylinder melting of detached engine fragments. *Atmos. Environ.* **2015**, *101*, 34-40.
310. Liati, A.; Schreiber, D.; Dasilva, Y. A. R.; Eggenschwiler, D. Ultrafine particle emissions from modern gasoline and diesel vehicles: An electron microscopic perspective. *Environ. Pollut.* **2018**, *239*, 661-669.
311. Liati, A.; Schreiber, D.; Eggenschwiler, P. D.; Dasilva, Y. A. R. Metal particle emissions in the exhaust stream of diesel engines: An electron microscopy study. *Environ. Sci. Technol.* **2013**, *47*, 14495-14501.
312. Liati, A.; Schreiber, D.; Lugovyy, D.; Gramstat, S.; Dimopoulos Eggenschwiler, P. Airborne particulate matter emissions from vehicle brake in micro- and nano-scales: Morphology and chemistry by electron microscopy. *Atmos. Environ.* **2019**, *212*, 281-289.
313. Liati, A.; Spiteri, A.; Eggenschwiler, P. D.; Vogel-Schäuble, N. Microscopic investigation of soot and ash particulate matter derived from biofuel and diesel: implications for the reactivity of soot. *J. Nanopart. Res.* **2012**, *14*(1224).
314. Lin, C.-C.; Chen, S.-J.; Huang, K.-L.; Hwang, W.-I.; Chang-Chien, G.-P.; Lin, W.-Y. Characteristics of metals in nano-ultrafine/fine/coarse particles collected beside a heavily trafficked road. *Environ. Sci. Technol.* **2005**, *39*(21), 8113-8122.
315. Lindbom, J.; Gustafsson, M.; Blomqvist, G.; Dahl, A.; Gudmundsson, A.; Swietlicki, E.; Ljungman, A. G. Exposure to wear particles generated from studded tires and pavement induces inflammatory cytokine release from human macrophages. *Chem. Res. Toxicol.* **2006**, *19*, 521-530.
316. Lindbom, J.; Gustafsson, M.; Blomqvist, G.; Dahl, A.; Gudmundsson, A.; Swietlicki, E.; Ljungman, A. G. Wear particles generated from studded tires and pavement induces inflammatory reactions in mouse macrophage cells. *Chem. Res. Toxicol.* **2007**, *20*, 937-946.
317. Liu, J.-Y.; Hsiao, T.-C.; Lee, K.-Y.; Chuang, H.-C.; Cheng, T.-J.; Chuang, K.-J. Association of ultrafine particles with cardiopulmonary health among adult subjects in the urban areas of northern Taiwan. *Sci. Total Environ.* **2018**, *627*, 211-215.
318. Liu, N. M.; Miyashita, L.; Maher, B. A.; McPhail, G.; Jones, C. J. P.; Barratt, B.; Thangaratinam, S.; Karloukovski, V.; Ahmed, I. A.; Aslam, Z.; Grigg, J. Evidence for the presence of air pollution nanoparticles in placental tissue cells. *Sci. Total Environ.* **2021**, *751*, 142235.
319. Lombaert, K.; Morel, S.; Le Moyne, L.; Adam, P.; Tardieu de Maleissye, J.; Amouroux, J. Nondestructive analysis of metallic elements in diesel soot collected on filter: Benefits of laser induced breakdown spectroscopy. *Plasma Chem. Plasma P.* **2004**, *24*(1), 41-56.
320. Long, X.; Luo, Y.-H.; Zhang, Z.; Zheng, C.; Zeng, C.; Bi, Y.; Zhou, C.; Rittmann, B. E.; Waite, T. D.; Herckes, P.; Westerhoff, P. The nature and oxidative reactivity of urban magnetic nanoparticle dust provide new insights into potential neurotoxicity studies. *Environ. Sci. Technol.* **2020**, *54*, 10599-10609.

321. Lough, G. C.; Schauer, J. J.; Park, J.-S.; Shafer, M. M.; Deminter, J. T.; Weinstein, J. P. Emissions of metals associated with motor vehicle roadways. *Environ. Sci. Technol.* **2005**, *39*, 826-836.
322. Loxham, M.; Cooper, M. J.; Gerlofs-Nijland, M. E.; Cassee, F. R.; Davis, D. E.; Palmer, M. R.; Teagle, D. A. H. Physicochemical characterization of airborne particulate matter at a mainline underground railway station. *Environ. Sci. Technol.* **2013**, *47*, 3614-3622.
323. Loxham, M.; Morgan-Walsch, R. J.; Cooper, M. J.; Blume, C.; Swindle, E. J.; Dennison, P. W.; Howarth, P. H.; Cassee, F. R.; Teagle, D. A. H.; Palmer, M. R.; Davis, D. E. The effects on bronchial epithelial mucociliary cultures of coarse, fine, and ultrafine particulate matter from an underground railway station. *Toxicol. Sci.* **2015**, *145*(1), 98-107.
324. Lu, D.; Luo, Q.; Chen, R.; Zhuansun, Y.; Jiang, J.; Wang, W.; Yang, X.; Zhang, L.; Liu, X.; Li, F.; Liu, Q.; Jiang, G. Chemical multi-fingerprinting of exogenous ultrafine particles in human serum and pleural effusion. *Nat. Commun.* **2020**, *11*, 2564.
325. Ma, J.; Olofsson, U.; Lyu, Y.; Wahlström, J.; Åström, A. H.; Tu, M. A comparison of airborne particles generated from disk brake contacts: Induction versus frictional heating. *Tribol. Lett.* **2020**, *68*, 38.
326. Magiera, T.; Strzyszcz, Z.; Kapicka, A.; Petrovsky, E. Discrimination of lithogenic and anthropogenic influences on topsoil magnetic susceptibility in Central Europe. *Geoderma* **2006**, *130*, 299-311.
327. Maher, B. A. Airborne magnetite- and iron-rich pollution nanoparticles: Potential neurotoxicants and environmental risk factors for neurodegenerative disease, including Alzheimer's disease. *J. Alzheimer Dis.* **2019**, *71*(2), 361-375.
328. Maher, B. A. Magnetic properties of some synthetic sub-micron magnetites. *Geophys. J.* **1988**, *94*, 83-96.
329. Maher, B. A. Rain and dust: Magnetic records of climate and pollution. *Elements* **2009**, *5*, 229-234.
330. Maher, B. A.; Ahmed, I. A. M.; Karloukovski, V.; MacLaren, D. A.; Foulds, P. G.; Allsop, D.; Mann, D. M. A.; Torres-Jardón, R.; Calderón-Garcidueñas, L. Magnetite pollution nanoparticles in the human brain. *PNAS* **2016**, *113* (39), 11797-10801.
331. Maher, B. A.; González-Maciel, A.; Reynoso-Robles, R.; Torres-Jardón, R.; Calderón-Garcidueñas, L. Iron-rich air pollution nanoparticles: An unrecognised environmental risk factor for myocardial mitocondrial dysfunction and cardiac oxidative stress. *Environ. Res.* **2020**, *188*, 109816.
332. Maher, B. A.; Karloukovski, V. V.; Mutch, T. J. High-field remanence properties of synthetic and natural submicrometre haematites and goethites: significance for environmental contexts. *Earth Planet. Sci. Lett.* **2004**, *226*, 491-505.
333. Maher, B. A.; Moore, C.; Matzka, J. Spatial variation in vehicle-derived metal pollution identified by magnetic and elemental analysis of roadside tree leaves. *Atmos. Environ.* **2008**, *42*, 364-373.
334. Maher, B. A.; O'Sullivan, V.; Feeney, J.; Gonet, T.; Kenny, R. A. Indoor particulate air pollution from open fires and the cognitive function of older people. *Environ. Res.* **2021**, *192*, 110298.
335. Maher B. A., Thompson R., **1999**. *Quaternary Climates, Environments and Magnetism.* Cambridge University Press, New York, USA.
336. Malachova, K.; Kukutschova, J.; Rybkova, Z.; Sezimova, H.; Placha, D.; Cabanova, K.; Filip, P. Toxicity and mutagenicity of low-metallic automotive brake pad materials. *Ecotoxicol. Environ. Saf.* **2016**, *131*, 37-44.
337. Malik, A. O.; Jones, P. G.; Chan, P. S.; Peri-Okonny, P. A.; Hejjaji, V.; Spertus, J. A. Association of long-term exposure to particulate matter and ozone with health status and mortality in patients after myocardial infarction. *Circ-Cardiovasc. Qual.* **2019**, *12*, e005598.
338. Mamakos, A.; Arndt, M.; Hesse, D.; Augsburg, K. Physical characterization of brake-wear particles in a PM_{10} dilution tunnel. *Atmos.* **2019**, *10*, 639.
339. Maricq, M. M. Chamical characterization of particulate emissions from diesel engines: A review. *Aerosol Sci.* **2007**, *38*, 1079-1118.
340. Marié, D. C.; Chaparro, M. A. E.; Gogorza, C. S. G.; Navas, A.; Sinito, A. M. Vehicle-derived emissions and pollution on the road Autovia 2 investigated by rock-magnetic parameters: A case study from Argentina. *Stud. Gephys. Geod.* **2010**, *54*, 135-152.

341. Martuzevicius, D.; Kliucininkas, L.; Prasauskas, T.; Krugly, E.; Kauneliene, V.; Strandberg, B. Resuspension of particulate matter and PAHs from street dust. *Atmos. Environ.* **2011**, *45*, 310-317.
342. Masiol, M.; Harrison, R. M. Aircraft engine exhaust emissions and other airport-related contributions to ambient air pollution: A review. *Atmos. Environ.* **2014**, *95*, 409-455.
343. Masiol, M.; Harrison, R. M.; Vu, T. V.; Beddows, D. C. S. Sources of sub-micrometre particles near a major international airport. *Atmos. Chem. Phys.* **2017**, *17*, 12379-12403.
344. Masiol, M.; Vu, T. V.; Beddows, D. C. S.; Harrison, R. M. Source apportionment of wide range particle size spectra and black carbon collected at the airport of Venice (Italy). *Atmos. Environ.* **2016**, *139*, 56-74.
345. Matějka, V.; Perricone, G.; Vlček, J.; Olofsson, U.; Wahlström, J. Airborne wear particle emissions produced during the dyno bench tests with a slag containing semi-metallic brake pads. *Atmosphere* **2020**, *11*, 1220.
346. Mathissen, M.; Grigoratos, T.; Lahde, T.; Vogt, R. Brake-wear particle emissions of a passenger car measured on a chassis dynamometer. *Atmosphere* **2019**, *10*, 556.
347. Mathissen, M.; Grochowicz, J.; Schmidt, C.; Vogt, R.; Farwick zum Hagen, F. H.; Grabiec, T.; Steven, H.; Grigoratos, T. A novel real-world braking cycle for studying brake-wear particles. *Wear* **2018**, *414-415*, 219-226.
348. Mathissen, M.; Scheer, V.; Vogt, R.; Benter, T. Investigation on the potential generation of ultrafine particles from the tire-road interface. *Atmos. Environ.* **2011**, *45*, 6172-6179.
349. Matzka, J.; Maher, B. A. Magnetic biomonitoring of roadside tree leaves: identification of spatial and temporal variations in vehicle-derived particulates. *Atmos. Environ.* **1999**, *33*, 4565-4569.
350. Mazaheri, M.; Bostrom, T. E.; Johnson, G. R.; Morawska, L. Composition and morphology of particle emissions from in-use aircraft during takeoff and landing. *Environ. Sci. Technol.* **2013**, *47*, 5235-5242.
351. Mazaheri, M.; Johnson, G. R.; Morawska, L. An inventory of particle and gaseous emissions from large aircraft thrust engine operations at an airport. *Atmos. Environ.* **2011**, *45*, 3500-3507.
352. McIntosh, G.; Gómez-Paccard, M.; Osete, M. L. The magnetic properties of particles deposited on *Platanus x hispanica* leaves in Madrid, Spain, and their temporal and spatial variations. *Sci. Total Environ.* **2007**, *382*, 135-146.
353. McClean, R. G.; Kean, W. F. Contributions of wood ash magnetism to archaeomagnetic properties of fire pits and hearts. *Earth Planet. Sci. Lett.* **1993**, *119*, 387-394.
354. Menapace, C.; Mancini, A.; Federici, M.; Straffelini, G.; Gialanella, S. Characterization of airborne wear debris produced by brake pads pressed against HVOF-coated discs. *Friction* **2020**, *8*(2), 421-432.
355. Mehran, Q. M.; Fazal, M. A.; Bushroa, A. R.; Rubaiee, S. A critical review on physical vapour deposition coatings applied on different engine components. *Crit. Rev. Solid State Mater. Sci.* **2018**, *43*(2), 158-175.
356. Midander, K.; Elihn, K.; Wallén, A.; Belova, L.; Karlsson, A.-K. B.; Wallinder, I. O. Characterisation of nano- and micron-sized airborne and collected subway particles, a multi-analytical approach. *Sci. Total Environ.* **2012**, *427-428*, 390-400.
357. Milani, M.; Pucillo, F. P.; Ballerini, M.; Camatini, M.; Gualtieri, M.; Martino, S. First evidence of tire debris characterization at the nanoscale by focused ion beam. *Mater. Charact.* **2004**, *52*, 283-288.
358. Miller, A.; Ahlstrand, G.; Kittelson, D.; Zachariah, M. The fate of metal (Fe) during diesel combustion: Morphology, chemistry, and formation pathways of nanoparticles. *Combust. Flame* **2007**, *149*, 129-143.
359. Miller, M. R.; Newby, D. E. Air pollution and cardiovascular disease: car sick. *Cardiovasc. Res.* **2019**, *cvz228*.
360. Miller, M. R.; Raftis, J. B.; Langrish, J. P.; McLean, S. G.; Samutrtai, P.; Connell, S. P.; Wilson, S.; Vesey, A. T.; Fokkens, P. H. B.; Boere, A. J. F.; Krystek, P.; Campbell, C. J.; Hadoke, P. W. F.; Donaldson, K.; Cassee, F. R.; Newby, D. E.; Duffin, R.; Mills, N. L. Inhaled nanoparticles accumulate at sites of vascular disease. *ACS Nano* **2017**, *11*, 4542-4552.
361. Mitchell, R.; Maher, B. A. Evaluation and application of biomagnetic monitoring of traffic-derived particulate pollution. *Atmos. Environ.* **2009**, *43*, 2095-2103.

362. Mitchell, R.; Maher, B. A.; Kinnersley, R. Rates of particulate pollution deposition onto leaf surfaces: Temporal and inter-species magnetic analyses. *Environ. Pollut.* **2010**, *158*, 1472-1478.
363. Mohai, P.; Kweon, B.-S.; Lee, S.; Ard, K. Air pollution around schools is linked to poorer student health and academic performance. *Health Aff.* **2011**, *30*(5), 852-862.
364. Moldanová, J.; Fridell, E.; Popovicheva, O.; Demirdjian, B.; Tishkova, V.; Faccinetto, A.; Focsa, C. Characterisation of particulate matter and gaseous emissions from a large ship diesel engine. *Atmos. Environ.* **2009**, *43*, 2632-2641.
365. Moldanová, J.; Fridell, E.; Winnes, H.; Holmin-Fridell, S.; Boman, J.; Jedynska, A.; Tishkova, V.; Demirdjian, B.; Joulie, S.; Bladt, H.; Ivleva, N. P.; Niessner, R. Physical and chemical characterisation of PM emissions from two ships operating in European Emission Control Areas. *Atmos. Meas. Tech.* **2013**, *6*, 3577-3596.
366. Morawska, L.; He, C.; Johnson, G.; Jayaratne, R.; Salthammer, T.; Wang, H.; Uhde, E.; Bostrom, T.; Modini, R.; Ayoko, G.; McGarry, P.; Wensing, M. An investigation into the characteristics and formation mechanisms of particles originating from the operation of laser printers. *Environ. Sci. Technol.* **2009**, *43*, 1015-1022.
367. Moreno, E.; Sagnotti, L.; Dinarés-Turell, J.; Winkler, A.; Cascella, A. Biomonitoring of traffic air pollution in Rome using magnetic properties of tree leaves. *Atmos. Environ.* **2003**, *37*, 2967-2977.
368. Moreno, T.; de Miguel, E. Improving air quality in subway systems: An overview. *Environ. Pollut.* **2018**, *239*, 829-831.
369. Moreno, T.; Kelly, F. J.; Dunster, C.; Oliete, A.; Martins, V.; Reche, C.; Minguillón, M. C.; Amato, F.; Capdevila, M.; de Migueal, E.; Querol, X. Oxidative potential of subway $PM_{2.5}$. *Atmos. Environ.* **2017a**, *148*, 230-238.
370. Moreno, T.; Martins, V.; Querol, X.; Jones, T.; BéruBé, K.; Minguillón, M. C.; Amato, F.; Capdevila, M.; de Miguel, E.; Centelles, S.; Gibbons, W. A new look at inhalable metalliferous airborne particles on rail subway platforms. *Sci. Total Environ.* **2015**, *505*, 367-375.
371. Moreno, T.; Querol, X.; Martins, V.; Minguillón, M. C.; Reche, C.; Ku, L. H.; Eun, H. R.; Ahn, K. H.; Capdevila, M.; de Miguel, E. Formation and alteration of airborne particles in the subway environment. *Environ. Sci.: Processes Impacts* **2017b**, *19*, 59-64.
372. Moretti, S.; Smets, W.; Hofman, J.; Mubiana, K. V.; Oerlemans, E.; Vandenheuvel. D.; Samson, R.; Blust, R.; Lebeer, S. Human inflammatory response of endotoxin affected by particulate matter-bound transition metals. *Environ. Pollut.* **2019**, *244*, 118-126.
373. Morris, W. A.; Versteeg, J. K.; Bryant, D. W.; Legzdins, A. E.; McCarry, B. E.; Marvin, C. H. Preliminary comparisons between mutagenicity and magnetic susceptibility of respirable airborne particulate. *Atmos. Environ.* **1995**, *29*(23), 3441-3450.
374. Morrow, P.E. Possible mechanisms to explain dust overloading of the lungs. *Fundam. Appl. Toxicol.* **1988**, *10*, 369-384.
375. Mosleh, M.; Blau, P. J.; Dumitrescu, D. Characteristics and morphology of wear particles from laboratory testing of disk brake materials. *Wear* **2004**, *256*, 1128-1134.
376. Mousavi, A.; Sowlat, M. H.; Hasheminassab, S.; Polidori, A.; Shafer, M. M.; Schauer, J. J.; Sioutas, C. Impact of emissions from the Ports of Los Angeles and Long Beach on the oxidative potential of ambient $PM_{0.25}$ measured across the Los Angeles County. *Sci. Total Environ.* **2019**, *651*, 638-647.
377. Mugica-Álvarez, V.; Figueroa-Lara, J.; Romero-Romo, M.; Sepúlveda-Sánchez, J.; López-Moreno, T. Concentrations and properties of airborne particles in the Mexico City subway system. *Atmos. Environ.* **2012**, *49*, 284-293.
378. Muench, G. J.; Arajs, S.; Matijević, E. The Morin transition in small α-Fe_2O_3 particles. *Phys. Status Solidi A* **1985**, *92*, 187-192.
379. Murruni, L. G.; Solanes, V.; Debray, M.; Kreiner, A. J.; Davidson, J.; Davidson, M.; Vázquez, M.; Ozafrán, M. Concentrations and elemental composition of particulate matter in the Buenos Aires underground system. *Atmos. Environ.* **2009**, *43*, 4577-4583.
380. Muxworthy, A. R.; Matzka, J.; Davila, A. F.; Petersen, N. Magnetic signature of daily sampled urban atmospheric particles. *Atmos. Environ.* **2003**, *37*, 4163-4169.

381. Muxworthy, A. R.; Matzka, J.; Petersen, N. Comparison of magnetic parameters of urban atmospheric particulate matter with pollution and meteorological data. *Atmos. Environ.* **2001**, *35*, 4379-4386.
382. Muxworthy, A. R.; Schmidbauer, E.; Petersen, N. Magnetic properties and Mössbauer spectra of urban atmospheric particulate matter: a case study from Munich, Germany. *Geophys. I. Int.* **2002**, *150*, 558-570.
383. Namgung, H.-G.; Kim, J. B.; Kim, M.-S.; Kim. M.; Park, S.; Woo, S.-H.; Bae, G.-N.; Park, D.; Kwon, S.-B. Size distribution analysis of airborne wear particles released by subway brake system. *Wear* **2017**, *372-373*, 169-176.
384. Namgung, H.-G.; Kim, J.-B.; Woo, S.-H.; Park, S.; Kim, M.; Kim, M.-S.; Bae, G.-N.; Park, D.; Kwon, S.-B. Generation of nanoparticles from friction between railway brake disks and pads. *Environ. Sci. Technol.* **2016**, *50*, 3453-3461.
385. Nanotechnology Now Website. http://www.nanotech-now.com/news.cgi?story_id=42612 (accessed Aug 26, 2021).
386. Naqvi, S.; Samim, M.; Abdin, M. Z.; Ahmed, F. J.; Maitra, A. N.; Prashant, C. K.; Dinda, A. K. Concentration-dependent toxicity of iron oxide nanoparticles mediated by increased oxidative stress. *Int. J. Nanomedicine* **2010**, *5*, 983-989.
387. Nel, A.; Xia, T.; Mädler, L.; Li, N. Toxic potential of materials at the nanolevel. *Science* **2006**, *311* (5761), 622-627.
388. Nichols, E.; Szoeke, C.E.I.; Vollset, S.E.; Abbasi, N.; Abd-Allah, F.; Abdela, J.; Taki, M.; Aichour, E., Akinyemi, R.O. *et al.* (GBD 2016 Dementia Collaborators). Global, regional, and national burden of Alzheimer's disease and other dementias, 1990-2016: a systematic analysis for the Global Burden of Disease Study 2016. *Lancet Neurol.* **2019**, *18*, 88-106.
389. Niemann, H.; Winner, H.; Asbach, C.; Kaminski, H.; Frentz, G.; Milczarek, R. Influence of disc temperature on ultrafine, fine, and coarse particle emissions of passenger car disc brakes with organic and inorganic pad binder materials. *Atmosphere* **2020**, *11*, 1060.
390. Nieuwenhuijsen, M. J.; Gómez-Perales, J. E.; Colvile, R. N. Levels of particulate air pollution, its elemental composition, determinants and health effects in metro systems. *Atmos. Environ.* **2007**, *41*, 7995-8006.
391. Noël, A.; L'Espérance, G.; Cloutier, Y.; Plamondon, P.; Boucher, J.; Philippe, S.; Dion, C.; Truchon, G.; Zayed, J. Assessment of the contribution of electron microscopy to nanoparticle characterization sampled with two cascade impactors. *J. Occup. Environ. Hyg.* **2013**, *10*(3), 155-172.
392. Norouzi, S.; Khademi, H.; Cano, A. F.; Acosta, J. A. Biomagnetic monitoring of heavy metals contamination in deposited atmospheric dust, a case study from Isfahan, Iran. *J. Environ. Manage.* **2016**, *173*, 55-64.
393. Nosko, O.; Alemani, M.; Olofsson, U. Temperature effect on emission of airborne wear particles from car brakes. *Europe's Braking Conference and Exhibition* **2015**, *EB2015-TEF-014*.
394. Nosko, O.; Olofsson, U. Effective density of airborne wear particles from car brake materials. *J. Aerosol. Sci.* **2017a**, *107*, 94-106.
395. Nosko, O.; Olofsson, U. Quantification of ultrafine airborne particulate matter generated by the wear of car brake materials. *Wear* **2017b**, *374-375*, 92-96.
396. Nosko, O.; Vanhanen, J.; Olofsson, U. Emission of 1.3-10 nm airborne particles from brake materials. *Aerosol Sci. Technol.* **2017**, *51*(1), 91-96.
397. Ntziachristos, L.; Ning, Z.; Geller, M. D.; Sheesley, R. J.; Schauer, J. J.; Sioustas, C. Fine, ultrafine and nanoparticle trace element compositions near a major freeway with a high heavy-duty diesel fraction. *Atmos. Environ*. **2007**, *41*, 5684-5696.
398. Oberdörster, G. Pulmonary effects of inhaled ultrafine particles. *Int. Arch. Occup. Environ. Health* **2001**, *74*, 1-8.
399. Oberdörster, G.; Ferin, J.; Gelein, R.; Soderholm, S. C.; Finkelstein, J. Role oft he alveolar macrophage in lung injury: studies of ultrafine particles. *Environ. Health Perspect.* **1992**, *97*, 193-199.
400. Oberdörster, G.; Ferin, J.; Lehnert, B. E. Correlation between particle size, *in vivo* particle persistence, and lung injury. *Environ. Health Perspect.* **1994**, *102*, 173-179.

401. Oberdörster, G.; Gelein, R. M.; Ferin, J.; Weiss, B. Association of particulate air pollution and acute mortality: Involvement of ultrafine particles? *Inhal. Toxicol.* **1995**, *7*, 111-124.
402. Oberdörster, G.; Oberdörster, E.; Oberdörster, J. Nanotoxicology: An emerging discipline evolving from studies of ultrafine particles. *Environ. Health Perspect.* **2005**, *113* (7), 823-839.
403. Oberdörster, G.; Sharp, Z.; Atudorei, V.; Elder, A.; Gelein, R.; Kreyling, W.; Cox, C. Translocation of inhaled ultrafine particles to the brain. *Inhal. Toxicol.* **2004**, *16*, 437-445.
404. Oberdörster, G.; Sharp, Z.; Atudorei, V.; Elder, A.; Gelein, R.; Lunts, A.; Kreyling, W.; Cox, C. Extrapulmonary translocation of ultrafine carbon particles following whole-body inhalation exposure of rats. *J. Toxicol. Environ. Health* **2002**, *65*, 1531-1543.
405. Oeder, S.; Kanashova, T.; Sippula, O.; Sapcariu, S. C.; Streibel, T.; Arteaga-Salas, J. M.; *et al.* Particulate matter from both heavy fuel oil and diesel fuel shipping emissions show strong biological effects on human lung cells at realistic and comparable *in vitro* exposure conditions. *PLoS ONE* **2015**, *10*(6).
406. Ondráček, J.; Schwarz, J.; Ždímal, V.; Andělová, L.; Vodička, P.; Bízek, V.; Tsai, C.-J.; Chen, S.-C.; Smolík, J. Contribution of the road traffic to air pollution in the Prague city (busy speedway and suburban crossroads). *Atmos. Environ.* **2011**, *45*, 5090-5100.
407. Ostro, B.; Hu, J.; Goldberg, D.; Reynolds, P.; Hertz, A.; Bernstein, L.; Kleeman, M. J. Associations of mortality with long-term exposures to fine and ultrafine particles, species and sources: Results from the California teacher study cohort. *Environ. Health Perspect.* **2015**, *123*(6), 549-556.
408. Oudin, A.; Forsberg, B.; Nordin Adolfsson, A.; Lind, N.; Modig, L.; Nordin, M.; Nordin, S.; Adolfsson, R.; Nilsson, L.-G. Traffic-related air pollution and dementia incidence in Northern Sweden: A longitudinal study. *Environ. Health Perspect.* **2016**, *124*, 306-312.
409. Oudin, A.; Segersson, D.; Adolfsson, R.; Forsberg, B. Association between air pollution from residential wood burning and dementia incidence in a longitudinal study in Northern Sweden. *PLoS ONE* **2018**, *13*(6), e0198283.
410. Our World in Data 2017. https://ourworldindata.org/grapher/urban-and-rural-population?country=~OWID_WRL (accessed July 1, 2021).
411. Österle, W.; Deutsch, C.; Gradt, T.; Orts-Gil, G.; Schneider, T.; Dmitriev, A. I. Tribological screening tests for the selection of raw materials for automotive brake pad formulations. *Tribol. Int.* **2014**, *73*, 148-155.
412. Österle, W.; Griepentrog, M.; Gross, T.; Urban, I. Chemical and microstructural changes induced by friction and wear of brakes. *Wear* **2001**, *251*, 1469-1476.
413. Özdemir, Ö.; Banerjee, S. K. A preliminary magnetic study of soil samples from west-central Minnesota. *Earth Planet. Sci. Lett.* **1982**, *59*, 393-403.
414. Özdemir, Ö.; Dunlop, D. J. Hallmarks of maghemitization in low-temperature remanence cycling of partially oxidized magnetite nanoparticles. *J. Geophys. Res.* **2010**, *115*, B02101.
415. Özdemir, Ö.; Dunlop, D. J.; Moskowitz, B. M. The effect of oxidation on the Verwey transition in magnetite. *Gephys. Res. Lett.* **1993**, *20*(16), 1671-1674.
416. Pagels, J.; Gudmundsson, A.; Gustavsson, E.; Asking, L.; Bohgard, M. Evaluation of aerodynamic particle sizer and electrical low-pressure impactor for unimodal and bimodal mass-weighed size distributions. *Aerosol Sci. Technol.* **2005**, *39*(9), 871-887.
417. Pandey, S. K.; Tripathi, B. D.; Prajapati, S. K.; Upadhyaya, A. R.; Mishra, V. K.; Rai, P. K.; Sharma, A. P. Magnetic properties of vehicle-derived particulates and amelioration by *Ficus anfectoria*: A keystone species. *AMBIO* **2005**, *34*(8), 645-647.
418. Pandolfi, M.; Gonzalez-Castanedo, Y.; Alastuey, A.; de la Rosa, J. D.; Mantilla, E.; de la Campa, A. S.; Querol, X.; Pey, J.; Amato, F.; Moreno, T. Source apportionment of PM_{10} and $PM_{2.5}$ at multiple sites in the strait of Gibraltar by PMF: impact of shipping emissions. *Environ. Sci. Pollut. Res.* **2011**, *18*, 260-269.
419. Pankhurst, Q.; Hautot, D.; Khan, N.; Dobson, J. Increased levels of magnetic iron compounds in Alzheimer's disease. *J. Alzheimers Dis.* **2008**, *13*, 49-52.
420. Pant, P.; Harrison, R. M. Estimation of the contribution of road traffic emissions to particulate matter concentrations from field measurements: A review. *Atmos. Environ.* **2013**, *77*, 78-97.

421. Park, J.; Joo, B.; Seo, H.; Song, W.; Lee, J. J.; Lee, W. K.; Jang, H. Analysis of wear induced particle emissions from brake pads during the worldwide harmonized light vehicles test procedure (WLTP). *Wear* **2021**, *466-467*, 203539.
422. Park, R. M.; Schulte, P. A.; Bowman, J. D.; Walker, J. T.; Bondy, S. C.; Yost, M. G.; Touchstone, J. A.; Dosemeci, M. Potential occupational risks for neurodegenerative diseases. *Am. J. Ind. Med.* **2005**, *48*, 63-77.
423. Pasquier, A.; André, M. Considering criteria related to spatial variabilities for the assessment of air pollution from traffic. *Trans. Res. Proc.* **2017**, *25*, 3354-3369.
424. Pattammattel, A.; Leppert, V. J.; Aronstein, P.; Robinson, M.; Mousavi, A.; Sioutas, C.; Forman, H. J.; O'Day, P. A. Iron speciation in particulate matter ($PM_{2.5}$) from urban Los Angeles using spectro-microscopy methods. *Atmos. Environ.* **2021**, *245*, 117988.
425. Peikertova, P.; Filip, P. Influence of the automotive brake-wear debris on the environment – A review of recent research. *SAE Int. J. Mater. Manf.* **2016**, *9*(1), 133-146.
426. Peikertová, P.; Kukutschová, J.; Vávra, I.; Matějka, V.; Životský, O.; Vaculík, M.; Lee, P. W.; Filip, P. Water suspended nanosized particles released from nonairborne brake-wear debris. *Wear* **2013**, *306*, 89-96.
427. Pelclova, D.; Zdimal, V.; Kacer, P.; Fenclova, Z.; Vlckova, S.; Syslova, K.; *et al.* Oxidative stress markers are elevated in exhaled breath condensate of workers exposed to nanoparticles during iron oxide pigment production. *J. Breath Res.* **2016**, *10*, 016004.
428. Peltier, R. E.; Cromar, K. R.; Ma, Y.; Fan, Z.-H.; Lippmann, M. Spatial and seasonal distribution of aerosol chemical components in New York City: (2) Road dust and other tracers of traffic-generated air pollution. *J. Expo. Sci. Environ. Epidemiol.* **2011**, *21*, 484-494.
429. Perricone, G.; Alemani, M.; Metinöz, I.; Matějka, V.; Wahlström, J.; Olofsson, U. Towards the ranking of airborne particle emissions from car brakes – a system approach. *Proc. IMechE Pard D: J. Automobile Engineering* **2017**, *231*(6), 781-797.
430. Perricone, G.; Matějka, V.; Alemani, M.; Valota, G.; Bonfanti, A.; Ciotti, A.; Olofsson, U.; Söderberg, A.; Wahlström, J.; Nosko, O.; Straffelini, G.; Gialanella, S.; Metinoz, I. A concept for reducing PM_{10} emissions for car brakes by 50%. *Wear* **2018**, *369-397*, 135-145.
431. Peters, R.; Ee, N.; Peters, J.; Booth, A.; Mudway, I.; Anstey, K. J. Air pollution and dementia: A systematic review. *J. Alzheimer Dis.* **2019**, *70*, S145-S163.
432. Petrovský, E.; Zbořil, R.; Grygar, T. M.; Kotlík, B.; Novák, J.; Kapička, A.; Grison, H. Magnetic particles in atmospheric particulate matter collected at sites with different level of air pollution. *Stud. Geophys. Geod.* **2013**, *57*, 755-770.
433. Petzold, A.; Ström, J.; Schröder, F. P.; Kärcher, B. Carbonaceous aerosol in jet engine exhaust: emission characteristics and implications for heterogeneous chemical reactions. *Atmos. Environ.* **1999**, *33*, 2689-2698.
434. Pey, J.; Querol, X.; Alastuey, A. Discriminating the regional and urban contributions in the North-Western Mediterranean: PM levels and composition. *Atmos. Environ.* **2010**, *44*(13), 1597-1596.
435. Pieters, N.; Koppen, G.; van Poppel, M.; de Prins, S.; Cox, B.; Dons, E.; Nelen, V.; Int Panis, L.; Plusquin, M.; Schoeters, G.; Nawrot, T. S. Blood pressure and same-day exposure to air pollution at school: Associations with nano-sized to coarse PM in children. *Environ. Health Perspect.* **2015**, *123*(7), 737-742.
436. Pinkerton, K. E.; Joad, J. P. Influence of air pollution on respiratory health during perinatal development. *Clin. Exp. Pharmacol. Physiol.* **2006**, *33*, 269-272.
437. Piscitello, A.; Bianco, C.; Casasso, A.; Sethi, R. Non-exhaust traffic emissions: Sources, characterization, and mitigation measures. *Sci. Total Environ.* **2021**, *766*, 144440.
438. Plachá, D.; Vaculík, M.; Mikeska, M.; Dutko, O.; Peikertová, P.; Kukutschová, J.; Mamulová Kutláková, K.; Růžičková, J.; Tomášek, V.; Filip, P. Release of volatile organic compounds by oxidative wear of automotive friction materials. *Wear* **2017**, *376-377*, 705-716.
439. Plascencia-Villa, G.; Ponce, A.; Collingwood, J. F.; Arellano-Jiménez, M. J.; Zhu, X.; Rogers, J. T.; Betancourt, I.; José-Yamacán, M.; Perry, G. High-resolution analytical imaging and electron holography of magnetite particles in amyloid cores of Alzheimer's disease. *Sci. Rep.* **2016**, *6*, 24873.
440. Pope III, C. A.; Dockery, D. W. Health effects of fine particulate air pollution: Lines that connect. *J.Air Waste Manag. Assoc.* **2006**, *56*(6), 709-742.

441. Popovicheva, O. B.; Persiantseva, N. M.; Lukhovitskaya, E. F.; Shonija, N. K.; Zubareva, N. A.; Demirdjian, B.; Ferry, D.; Suzanne, J. Aircraft engine soot as contrail nuclei. *Geophys. Res. Lett.* **2004**, *31*.
442. Popovicheva, O.; Kireeva, E.; Persiantseva, N.; Timofeev, M.; Bladt, H.; Ivleva, N. P.; Niessner, R.; Moldanová, J. Microscopic characterization of individual particles from multicomponent ship exhaust. *J. Environ. Monit.* **2012**, *14*, 3101-3110.
443. Popovicheva, O.; Kireeva, E.; Shonija, N.; Zubareva, N.; Persiantseva, N.; Tishkova, V.; Demirdjian, B.; Moldanová, J.; Mogilnikov, V. Ship particulate pollutants: Characterization in terms of environmental implication. *J. Environ. Monit.* **2009**, *11*, 2077-2086.
444. Power, M. C.; Weisskopf, M. G.; Alexeeff, S. E.; Coull, B. A.; Spiro III, A. Traffic-related air pollution and cognitive function in a cohort of older men. *Environ. Health Perspect.* **2011**, *119*(5), 682-687.
445. Prichard, H. M.; Fisher, P. C. Identification of platinum and palladium particles emitted from vehicles and dispersed into the surface environment. *Environ. Sci. Technol.* **2012**, *46*, 3149-3154.
446. Puisney, C.; Oikonomou, E. K.; Nowak, S.; Chevillot, A.; Casale, S.; Baeza-Squiban, A.; Berret, J.-F. Brake-wear (nano)particle characterization and toxicity on wirway epithelial cells *in vitro*. *Environ. Sci.: Nano* **2018**, *5*, 1036-1044.
447. Putaud, J.-P.; Van Dingenen, R.; Alastuey, A.; Bauer, H.; Birmili, W.; *et al.* A European aerosol phenomenology – 3: Physical and chemical characteristics of particulate matter from 60 rural, urban, and kerbside sites across Europe. *Atmos. Environ*. **2010**, *44*, 1308-1320.
448. Puustinen, A.; Hämeri, K.; Pekkanen, J.; Kulmala, M.; de Hartog, J.; Meliefste, K.; ten Brink, H.; Kos, G.; Katsouyanni, K.; Karakatsani, A.; Kotronarou, A.; Kavouras, I.; Meddings, C.; Thomas, S.; Harrison, R.; Ayres, J.G.; van der Zee, S.; Hoek, G. Spatial variation of particle number and mass over four European cities. *Atmos. Environ.* **2007**, *41*, 6622-6636.
449. Quayle, B. M.; Mather, T. A.; Witt, M. L. I.; Maher, B. A.; Mitchell, R.; Martin, R. S.; Calabrese, S. Application and evaluation of biomagnetic and biochemical monitoring of the dispersion and deposition of volcanically-derived particles at Mt. Etna, Italy. *J. Volcanol. Geothem. Res.* **2010**, *191*, 107-116.
450. Querol, X.; Alastuey, A.; Ruiz, C. R.; Artiñano, B.; Hansson, H. C.; Harrison, R. M.; Buringh, E.; ten Brink, H. M.; Lutz, M.; Bruckmann, P.; Straehl, P.; Aschneider, J. Speciation and origin of PM_{10} and $PM_{2.5}$ in selected European cities. *Atmos. Environ.* **2004**, *38*, 6547-6555.
451. Querol, X.; Moreno, T.; Karanasiou, A.; Reche, C.; Alastauey, A.; Viana, M.; Font, O.; Gil, J.; de Miguel, E.; Capdevila, M. Variability of levels and composition of PM_{10} and $PM_{2.5}$ in the Barcelona metro system. *Atmos. Chem. Phys.* **2012**, *12*, 5055-5076.
452. Quintana, C.; Bellefqih, S.; Laval, J. Y.; Guerquin-Kern, J. L.; We, T. D.; Avila, J.; Ferrer, I.; Arranz, R.; Patiño, C. Study of the localization of iron, ferritin, and hemosiderin in Alzheimer's disease hippocampus by analytical microscopy at the subcellular level. *J. Struct. Boil.* **2006**, *153*, 42-54.
453. Racette, B. A.; McGee-Minnich, L.; Moerlein, S. M.; Mink, J. W.; Videen, T. O.; Perlmutter, J. S. Welding-related parkinsonism: Clinical features, treatment, and pathophysiology. *Neurology* **2001**, *56*(1), 8-13.
454. Radhakrishnamurty, C.; Sastry, N. P.; Deutsch, E. R. Ferromagnetic behaviour of interacting superparamagnetic particle aggregates in basaltic rocks. *Pramana* **1973**, *1*(2), 61-65.
455. Rai, P. K.; Chutia, B. M. Biomagnetic monitoring of atmospheric particulate pollution through roadside tree leaves in Aizawl city, Mizoram and their temporal and spatial variations. *Int. Res. J. Environ. Sci.* **2014a**, *3*(8), 46-53.
456. Rai, P. K.; Chutia, B. M.; Patil, S. K. Monitoring of spatial variations of particulate matter (PM) pollution through bio-magnetic aspects of roadside plant leaves in an Indo-Burma hot spot region. *Urban For. Urban Green.* **2014b**, *13*, 761-770.
457. Rajhelová, H.; Peikertová, P.; Čabanová, K.; Kuzníková, L.; Barabaszová, K. Č.; Mamulová Kutláková, K.; Vaculík, M.; Kukutschová, J. Determination of oxidative potential caused by brake-wear debris in non-cellular systems. *J. Nanoscience Nanotechnol.* **2019**, *19*, 2869-2875.
458. Rakowska, A.; Wong, K. C.; Townsend, T.; Chan, K. L.; Westerdahl, D.; Ng, S.; Močnik, G.; Drinovec, L.; Ning, Z. Impact of traffic volume and composition on the air quality and pedestrian exposure in urban street canyon. *Atmos. Environ.* **2014**, *98*, 260-270.

459. Ramousse, S.; Høj, J. W.; Sørensen, O. T. Thermal characterisation of brake pads. *J. Therm. Anal. Calorim.* **2001**, *64*, 933-943.
460. Ramsden, J. J. An estimate of the chronic exposure to neurotoxins of a neurologically injured pilot. *J. Biol. Phys. Chem.* **2016**, *16*(2), 95-102.
461. Ranft, U.; Schikowski, T.; Sugiri, D.; Krutmann, J.; Krämer, U. Long-term exposure to traffic-related particulate matter impairs cognitive function in the elderly. *Environ. Res.* **2009**, *109*, 1004-1011.
462. Raut, J.-C.; Chazette, P.; Fortain, A. Link between aerosol optical, microphysical and chemical measurements in an underground railway station in Paris. *Atmos. Environ.* **2009**, *43*, 860-868.
463. Rea-Downing, G.; Quirk, B. J.; Wagner, C. L.; Lippert, P. C. Evergreen needle magnetization as a proxy for particulate matter pollution in urban environments. *GeoHealth* **2020**, *4*, e2020GH000286.
464. Reche, C.; Querol, X.; Alastuey, A.; Viana, M.; Pey, J.; Moreno, T.; Rodriguez, S.; González, Y.; Fernández-Camacho, R.; Sánchez de la Campa, A. M.; de la Rosa, J.; Dall'Osto, M.; Prévôt, A. S. H.; Hueglin, C.; Harrison, R. M.; Quincey, P. New considerations for PM, black carbón and particle number concentration for air quality monitoring across different European cities. *Atmos. Chem. Phys.* **2011**, *11*, 6207-6227.
465. Reddy, C. M.; Quinn, J. G. Environmental chemistry of benzothiazoles derived from rubber. *Environ. Sci. Technol.* **1997**, *31*, 2847-2853.
466. Reed, B. E.; Yalamanchili, J.; Leach, J. B.; Hennigan, C. J. Fate of transition metals in PO_4-based in vitro assays: equilibrium modelling and macroscopic studies. *Environ. Sci.: Processes Impacts* **2021**, *23*, 160-169.
467. Rejhelová, H.; Peikertová, P.; Čabanová, K.; Kuzníková, L.; Čech Barabaszová, K., Mamulová Kutláková, K.; Vaculík, M.; Kukutschová, J. Determination of oxidative potential caused by brake-wear debris in non-cellular systems. *J. Nanosci. Nanotechnol.* **2019**, *19*, 2869-2875.
468. Revuelta, M. A.; McIntosh, G.; Pey, J.; Pérez, N.; Querol, X.; Alastuey, A. Partitioning of magnetic particles in PM_{10}, $PM_{2.5}$ and PM_1 aerosols in the urban atmosphere of Barcelona (Spain). *Environ. Pollut.* **2014**, *188*, 109-117.
469. Ripanucci, G.; Grana, M.; Vicentini, L.; Magrini, A.; Bergamashi, A. Dust in the underground railway tunnels of an Italian Town. *J. Occup. Environ. Hyg.* **2006**, *3*(1), 16-25.
470. Robert, M. A.; VanBergen, S.; Kleeman, M. J., Jakober, C. A. Size and composition distributions of particulate matter emissions: Part 1 – Light-duty gasoline vehicles. *J. Air & Waste Manage. Assoc.* **2007**, *57*, 1414-1428.
471. Rodríguez-Germade, I.; Mohamed, K. J.; Rey, D.; Rubio, B.; García, Á. The influence of weather and climate on the reliability of magnetic properties of tree leaves as proxies for air pollution monitoring. *Sci. Total Environ.* **2014**, *408-409*, 892-902.
472. Rogge, W. F.; Hildemann, L. M.; Mazurek, M. A.; Cass, G. R.; Simoneit, B. R. T. Sources of fine organic aerosol. 3. Road dust, tire debris, and organometallic brake lining dust: Roads as sources and sinks. *Environ. Sci. Technol.* **1993**, *27*, 1892-1904.
473. Rose, D.; Wehner, B.; Ketzel, M.; Engler, C.; Voigtländer, J.; Tuch, T.; Wiedensohler, A. Atmospheric number size distributions of soot particles and estimation of emission factors. *Atmos. Chem. Phys.* **2006**, *6*, 1021-1031.
474. Rouault, T. A. Systemic iron metabolism: A review and implications for brain iron metabolism. *Pediat. Neurol.* **2001**, *25*(2), 130-137.
475. Roubicek, V.; Raclavska, H.; Juchelkova, D.; Filip, P. Wear and environmental aspects of composite materials for automotive braking industry. *Wear* **2008**, *265*, 167-175.
476. Rückerl, R.; Schneider, A.; Breitner, S.; Cyrys, J.; Peters, A. Health effects of particulate air pollution: A review of epidemiological evidence. *Inhal. Toxicol.* **2011**, *23*(10), 555-592.
477. Sadeghian, M. M. Biomonitoring of particulate matter by magnetic properties of *Ulmus carpinifolia* leaves. *Afr. J. Biotechnol.* **2012**, *11*(73), 13827-13830.
478. Sagnotti, L.; Macri, P.; Egli, R.; Mondino, M. Magnetic properties of atmospheric particulate matter from automatic air sampler stations in Latium (Italy): Toward a definition of magnetic fingerprints for natural and anthropogenic PM_{10} sources. *J. Geophys. Res.* **2006**, *111*, B12S22.

479. Sagnotti, L.; Tadeucci, J.; Winkler, A.; Cavallo, A. Compositional, morphological, and hysteresis characterization of magnetic airborne particulate matter in Rome, Italy. *Geochem. Geophys. Geosyst.* **2009**, *10*, Q08Z06.
480. Sagnotti, L.; Winkler, A. On the magnetic characterization and quantification of the superparamagnetic fraction of traffic-related urban airborne PM in Rome, Italy. *Atmos. Environ.* **2012**, *59*, 131-140.
481. Saksena, S.; Quang, T. N.; Nguyen, T.; Dang, P. N.; Flachsbart, P. Commuters' exposure to particulate matter and carbon monoxide in Hanoi, Vietnam. *Transp. Res. D* **2008**, *13*, 206-211.
482. Salma, I.; Pósfai, M.; Kovács, K.; Kuzmann, E.; Homonnay, Z.; Posta, J. Properties and sources of individual particles and some chemical species in the aerosol of a metropolitan underground railway station. *Atmos. Environ.* **2009**, *43*, 3460-3466.
483. Sanders, P. G.; Dalka, T. M.; Xu, N.; Maricw, M. M.; Basch, R. H. Brake dynamometer measurements of airborne brake-wear debris. *SAE Transactions* **2002**, *111*(6), 1693-1699.
484. Sanders, P. G.; Xu, N.; Dalka, T. M.; Maricq, M. M. Airborne brake-wear debris: Size distributions, composition, and a comparison of dynamometer and vehicle tests. *Environ. Sci. Technol.* **2003**, *37*, 4060-4069.
485. Sanderson, P.; Delgado-Saborit, J. A.; Harrison, R. M. A review of chemical and physical characterisation of atmospheric metallic nanoparticles. *Atmos. Environ.* **2014**, *94*, 353-365.
486. Sanderson, P.; Su, S. S.; Chang, I. T. H.; Delgado Saborit, J. M.; Kepaptsoglou, D. M.; Weber, R. J. M.; Harrison, R. M. Characterisation of iron-rich atmospheric submicrometre particles in the roadside environment. *Atmos. Environ.* **2016**, *140*, 167-175.
487. Sant'Ovala, H.; Lacerda, M. J.; Gomes, C. Particle pollution – An environmental magnetism study using biocollectors located in northern Portugal. *Atmos. Environ.* **2012**, *61*, 340-349.
488. Sapcariu, S. C.; Kanashova, T.; Dilger, M.; Diabeté, S.; Oeder, S.; Passig, J.; *et al.* Metabolic profiling as well as stable isotope assisted metabolic and proteomic analysis of RAW 264.7 macrophages exposed to ship engine aerosol emissions: Different effects of heavy fuel oil and refined diesel fuel. *PLoS ONE* **2016**, *11*(6).
489. Saragnese, F.; Lanci, L.; Lanza, R. Nanometric-sized atmospheric particulate studied by magnetic analyses. *Atmos. Environ.* **2011**, *45*, 450-459.
490. Saxe, H.; Larsen, T. Air pollution from ships in three Danish ports. *Atmos. Environ.* **2004**, *38*, 4057-4067.
491. Schaedlich, G.; Weissflog, L.; Schuurmann, G. Magnetic-susceptibility in conifer needles as indicator of fly-ash deposition. *Fresen. Environ. Bull.* **1995**, *4*(1), 7-12.
492. Schauer, J. J.; Lough, G. D.; Shafer, M. M.; Christensen, W. F.; Arndt, M. F.; DeMinter, J. T.; Park, J.-S. Characterization of metals emitted from motor vehicles. *HEI Research report* **2006**.
493. Schindler, B. K.; Weiss, T.; Schütze, A.; Koslitz, S.; Broding, H. C.; Bünger, J.; Brüning, T. Occupational exposure of air crews to tricresyl phosphate isomers and organophosphate flame retardants after fume events. *Arch. Toxicol.* **2013**, *87*, 645-648.
494. Schultheiss-Grassi, P. P.; Wessiken, R.; Dobson, J. TEM investigations of biogenic magnetite extracted from the human hippocampus. *Biochim. Biophys. Acta* **1999**, *1426*, 212-216.
495. Seaton, A.; Cherrie, J.; Dennekamp, M.; Donaldson, K.; Hurley, J. F.; Tran, C. L. The London Underground: dust and hazards to health. *Occup. Environ. Med.* **2005**, *62*, 355-362.
496. Seaton, A.; MacNee, W.; Donaldson, K.; Godden, D. Particulate air pollution and acute health effects. *Lancet* **1995**, *345*, 176-178.
497. Selley, L.; Schuster, L.; Marbach, H.; Forsthuber, T.; Forbes, B.; Gant, T. W.; Sanderström, T.; Camiña, N.; Athersuch, T. J.; Mudway, I.; Kumar, A. Brake dust exposure exacerbates inflammation and transiently compomises phagocytosis in macrophages. *Metallomics* **2020**, *12*, 371-386.
498. Sharma, M.; Agarwal, A. K.; Bharathi, K. V. L. Characterization of exhaust particulates from diesel engine. *Atmos. Environ.* **2005**, *39*, 3023-3028.
499. Shi, J.P.; Khan, A. A.; Harrison, R. M. Measurements of ultrafine particle concentration and size distribution in the atmosphere. *Sci. Total Environ.* **1999**, *235*, 51-64.
500. Shi, L.; Yazdi, M. D.; Braun, D.; Awad, Y. A.; Wei, Y.; Liu, P.; Di, Q.; Wang, Y.; Schwartz, J.; Dominici, F.; Koiumourtzoglou, M.-A.; Zanobetti, A. Long-term effects of $PM_{2.5}$ on neurological

disorders in the American Medicare population: a longitudinal cohort study. *Lancet Planet Health* **2020**, *4*(12), E557-E565.

501. Shilton, V. F.; Booth, C. A.; Smith, J. P.; Giess, P.; Mitchell, D. J.; Williams, C. D. Magnetic properties of urban street dust and their relationship with organic matter content in the West Midlands, UK. *Atmos. Environ.* **2005**, *39*, 3651-3659.
502. Shu, J.; Dearing, J. A.; Morse, A. P.; Yu, L.; Yuan, N. Determining the sources of atmospheric particles in Shanghai, China, from magnetic and geochemical properties. *Atmos. Environ.* **2001**, *35*, 2615-1625.
503. Schulte, P. A.; Burnett, C. A.; Boeniger, M. F.; Johnson, J. Neurodegenerative diseases: Occupational occurrence and potential risk factors, 1982 through 1991. *Am. J. Pub. Health* **1996**, *86*(9), 1281-1288.
504. Shuster-Meiseles, T.; Shafer, M. M., Hoe, J.; Pardo, M.; Antkiewicz, D. S.; Schauer, J. J.; Rudich, A.; Rudich, Y. ROS-generating/ARE-activating capacity of metals in roadway particulate matter deposited in urban environment. *Environ. Res.* **2016**, *146*, 252-262.
505. Siew, S. S.; Kauppinen, T.; Kyyrönen, P.; Heikkilä, P.; Pukkala, E. Exposure to iron and welding fumes and the risk of lung cancer. *Scand. J. Work Environ. Health* **2008**, *34*(6), 444-450.
506. Simon, M. C.; Hudda, N.; Naumova, E. N.; Levy, J. I.; Brugge, D.; Durant, J. L. Comparisons of traffic-related ultrafine particle number concentrations measured in two urban areas by central, residential, and mobile monitoring. *Atmos. Environ.* **2017**, *169*, 113-127.
507. Singh, N.; Jenkins, G. J. S.; Asadi, R.; Doak, S. H. Potential toxicity of superparamagnetic iron oxide nanoparticles (SPION). *Nano Rev.* **2010**, *1*(5358).
508. Smith, M. A.; Harris, P. L. R.; Sayre, L. M.; Perry, G. Iron accumulation in Alzheimer disease is a source of redox-generated free radicals. *Proc. Natl. Acad. Sci. USA* **1997**, *94*, 9866-9868.
509. Smith, M. A.; Zhu, X.; Tabaton, M.; Liu, G.; McKeel, Jr., D. W.; Cohen, M. L.; Wang, X.; Siedlak, S. L.; Hayashi, T.; Nakamura, M.; Nunomura, A.; Perry, G. Increased iron and free radical generation in preclinical Alzheimer disease and mild cognitive impairment. *J. Alzheimers Dis.* **2010**, *19*(1), 363-372.
510. Sowards, J. W.; Lippold, J. C.; Dickinson, D. W.; Ramirez, A. J. Characterization of welding fume from SMAW electrodes – Part I. Size and mass distributions, fume generation rates, and chemistry are compared for three SMAW electrodes. *Weld. Res.* **2008**, *87*, 106-112.
511. Spassov, S.; Egli, R.; Heller, F.; Nourgaliev, D. K.; Hannam, J. Magnetic quantification of urban pollution sources in atmospheric particulate matter. *Geophys. J. Int.* **2004**, *159*, 555-564.
512. Squizzato, S.; Masiol, M.; Agostini, C.; Visin, F.; Formenton, G.; Harrison, R. M.; Rampazzo, G. Factors, origin and sources affecting PM_1 concentrations and composition at an urban background site. *Atmos. Res.* **2016**, *180*, 262-273.
513. Stechmann, H.; Donnecker, W. Characterization and source analysis of vehicle-generated aerosols. *J. Aerosol Sci.* **1990**, *21*(s1), S287-S290.
514. Sternbeck, J.; Sjödin, Å.; Andréasson, K. Metal emissions from road traffic and the influence of resuspension – results from two tunnel studies. *Atmos. Environ.* **2002**, *36*, 4735-4744.
515. Stieb, D. M.; Chen, L.; Eshoul, M.; Judek, S. Ambient air pollution, birth weight and preterm birth: A systematic review and meta-analysis. *Environ. Res.* **2012**, *117*, 100-111.
516. Stone, V.; Shaw, J.; Brown, D. M.; MacNee, W.; Faux, S. P.; Donaldson, K. The role of oxidative stress in the prolonged inhibitory effect of ultrafine carbon black on epithelial cell function. *Toxicol. In Vitro* **1998**, *12*, 649-659.
517. Straffelini, G.; Ciudin, R.; Ciotti, A.; Gialanella, S. Present knowledge and perspectives on the role of copper in brake materials and related environmental issues: A critical assessment. *Environ. Pollut.* **2015**, *207*, 211-219.
518. Streibel, T.; Schnelle-Kreis, J.; Czech, H.; Harndorf, H.; Jakobi, G.; Jokiniemi, J.; *et al*. Aerosol emissions of a ship diesel engine operated with diesel fuel of heavy fuel oil. *Environ. Sci. Pollut. Res.* **2017**, *24*, 10976-10991.
519. Su, D. S.; Müller, J.-O.; Jentoft, R. E.; Rothe, D.; Jacob, E.; Schlögl, R. Fullerene-like soot from Euro IV diesel engine: consequences for catalytic automotive pollution control. *Top. Catal.* **2004**, *30/31*, 241-245.
520. Sugamata, M.; Ihara, T.; Takano, H.; Oshio, S.; Takeda, K. Maternal diesel exhaust exposure damages newborn murine brains. *J. Health Sci.* **2006**, *52*(1), 82-84.

521. Suglia, S. F.; Gryparis, A.; Wright, R. O.; Schwartz, J.; Wright, R. J. Association of black carbon with cognition among children in a prospective birth cohort study. *Am. J. Epidemiol.* **2008**, *167*, 280-286.
522. Sunyer, J. The neurological effects of air pollution in children. *Eur. Respir. J.* **2008**, *32*, 535-537.
523. Sunyer, J.; Esnaola, M.; Alvarez-Pedrerol, M.; Forns, J.; Rivas, I.; López-Vicente, M.; Suades-González, E.; Foraster, M.; Garcia-Esteban, R.; Basagaña, X.; Viana, M.; Cirach, M.; Moreno, T.; Alastuey, A.; Sebastian-Galles, N.; Nieuwenhuijsen, M.; Querol, X. Association between traffic-related air pollution in schools and cognitive development in primary school children: A prospective cohort study. *PLoS Med.* **2015**, *12*(3), e1001792.
524. Sunyer, J.; Suades-González, E.; García-Esteban, R.; Rivas, I.; Pujol, J.; Alvarez-Pedrerol, M.; Forns, J.; Querol, X.; Basagaña, X. Traffic-related air pollution and attention in primary school children. *Epidemiology* **2017**, *28*(2), 181-189.
525. Swaiman, K. F. Hallervorden-Spatz syndrome and brain iron metabolism. *Arch. Neurol.* **1991**, *48*, 1285-1293.
526. Szönyi, M.; Sagnotti, L.; Hirt, A. M. A refined biomonitoring study of airborne particulate matter pollution in Rome, with magnetic measurements on *Quercus Ilex* tree leaves. *Gephys. J. Int.* **2008**, *173*, 127-141.
527. Szönyi, M.; Sagnotti, L.; Hirt, A. M. On leaf magnetic homogeneity in particulate matter biomonitoring studies. *Gephys. Res. Lett.* **2007**, *34*, L06306.
528. Szuszkiewicz, M.; Magiera, T.; Kapička, A.; Petrovský, E.; Grison, H.; Gołuchowska, B. Magnetic characteristics of industrial dust from different sources of emission: A case study of Poland. *J. Appl. Geophys.* **2015**, *116,* 84-92.
529. Tabner, B. J.; Mayes, J.; Allsop, D. Hypothesis: Soluble Aβ oligomers in association with redox-active metal ions are the optimal generators of reactive oxygen species in Alzheimer's disease. *Int. J. Alzheimers Dis.* **2010**, *2011*, 546380.
530. Tanner, P. A.; Ma, H.-L.; Yu, P. K. N. Fingerprinting metals in urban street dust of Beijing, Shanghai, and Hong Kong. *Environ. Sci. Technol.* **2008**, *42*, 7111-7117.
531. Tarasiuk, W.; Golak, K.; Tsybrii, Y.; Nosko, O. Correlations between the wear of car brake friction materials and airborne particle emissions. *Wear* **2020**, *456-457*, 203361.
532. Teller, S.; Tahirbegi, I. B.; Mir, M.; Samitier, J.; Soriano, J. Magnetite-Amyloid-β deteriorates activity and functional organization in an *in vitro* model for Alzheimer's disease. *Sci. Rep.* **2015**, *5*, 17261.
533. The New York City Subway System Website. https://www.ny.com/transportation/subways/ (accessed Feb 5, 2019).
534. Thompson R., Oldfield F., **1986**. *Environmental Magnetism*. Allen & Unwin, London, UK.
535. Thorpe, A.; Harrison, R. M. Sources and properties of non-exhaust particulate matter from road traffic: A review. *Sci. Total Environ.* **2008**, *400*, 270-282.
536. Timmers, V. R. J. H.; Achten, P. A. J. Non-exhaust emissions from electric vehicles. *Atmos. Environ.* **2016**, *134*, 10-17.
537. Tissari, J.; Lyyränen, J.; Hytönen, K.; Sippula, O.; Tapper, U.; Frey, A.; Saarnio, K.; Pennanen, A. S.; Hillamo, R.; Salonen, R. O.; Hirvonen, M.-R.; Jokiniemi, J. Fine particle and gaseous emissions from normal and smouldering wood combustion in a conventional masonry heater. *Atmos. Environ.* **2008**, *42*, 7862-7873.
538. Tjälve, H.; Henriksson, J.; Tallkvist, J.; Larsson, B. S.; Lindquist, N. G. Uptake of manganese and cadmium from the nasal mucosa into the central nervous system via olfactory pathways in rats. *Pharmacol. Toxicol.* **1996**, *79*, 347-356.
539. Tokarek, S.; Bernis, A. An example of particle concentration reduction in Parisian subway stations by electrostatic precipitation. *Environ. Technol.* **2006**, *27*, 1279-1287.
540. Tokyo's Metro Advertising Media Website. https://www.metro-ad.co.jp/en/ (accessed Feb 5, 2019).
541. Transport for London Website. https://tfl.gov.uk/modes/tube (accessed Feb 5, 2019).
542. UN 2018. https://www.un.org/development/desa/en/news/population/2018-revision-of-world-urbanization-prospects.html (accessed July 1, 2021).

543. Unal, A.; Hu, Y. Chang, M. E.; Odman, M. T.; Russell, A. G. Airport related emissions and impacts on air quality: Application to the Atlanta International Airport. *Atmos. Environ.* **2005**, *39*, 5787-5798.
544. Urbat, M.; Lehndorff, E.; Schwark, L. Biomonitoring of air quality in the Cologne conurbation using pine needles as a passive sampler – Part I: magnetic properties. *Atmos. Environ.* **2004**, *38*, 3781-3792.
545. Valavanidis, A.; Salika, A.; Theodoropoulou, A. Generation of hydroxyl radicals by urban suspended particulate air matter. The role of iron ions. *Atmos. Environ.* **2000**, *34*, 2379-2386.
546. Van de Walle, A.; Sangnier, A. P.; Abou-Hassan, A.; Curcio, A.; Hémadi, M.; Menguy, N.; Lalatonne, Y.; Luciani, N.; Wilhelm, C. Biosynthesis of magnetic nanoparticles from nano-degradation products revealed in human stem cells. *PNAS* **2019**, *116*(10), 4044-4053.
547. Van Nunen, E.; Vermeulen, R.; Tsai, M.-Y.; Probst-Hensch, N.; Ineichen, A.; Davey, M.; *et al.* Land use regression models for ultrafine particles in six European areas. *Environ. Sci. Technol.* **2017**, *51*, 3336-3345.
548. Van Wittenberghe, S.; Alonso, L.; Verrelst, J.; Hermans, I.; Delegido, J.; Veroustraete, F.; Valcke, R.; Moreno, J.; Samson, R. Upward and downward solar-induced chlorophyll fluorescence yield indices four tree species as indicators of traffic pollution in Valencia. *Environ. Pollut.* **2013**, *173*, 29-37.
549. Verma, P. C.; Alemani, M.; Gialanella, S.; Lutterotti, L.; Olofsson, U.; Straffelini, G. Wear debris from brake system materials: A multi-analytical characterization approach. *Tribol. Int.* **2016**, *94*, 249-259.
550. Verwey, E. J. W. Electronic conduction of magnetite (Fe_3O_4) and its transition point at low temperatures. *Nature* **1939**, *3642*, 327-328.
551. Viana, M.; Kuhlbusch, T. A. J.; Querol, X.; Alastuey, A.; Harrison, R. M.; Hopke, P. K.; Winiwarter, W.; Vallius, M.; Szidat, S.; Prévôt, A. S. H.; Hueglin, C.; Bloeman, H.; Wåhlin, P.; Vecchi, R.; Miranda, A. I.; Kasper-Giebl, A.; Maenhaut, W.; Hitzenberger, R. Source apportionment of particulate matter in Europe: A review of methods and results. *J. Aerosol Sci.* **2008**, *39*, 837-849.
552. Vu, T. V.; Delgado-Saborit, M.; Harrison, R. M. Review: Particle number size distributions from seven major sources and implications for source apportionment studies. *Atmos. Environ.* **2015**, *122*, 114-132.
553. Wåhlin, P.; Berkowicz, R.; Palmgren, F. Characterization of traffic-generated particulate matter in Copenhagen. *Atmos. Environ.* **2006**, *40*(12), 2151-2159.
554. Wahlström, J.; Olofsson, U. A field study of airborne particle emissions from automotive disc brakes. *Proc. IMechE Pard D: J. Automobile Engineering* **2014**, *229*(6): 747-757.
555. Wahlström, J.; Söderberg, A.; Olander, L.; Jansson, A.; Olofsson, U. A pin-on-disc simulation of airborne wear particles from disc brakes. *Wear* **2010a**, *268*, 763-769.
556. Wahlström, J.; Söderberg, A.; Olander, L.; Olofsson, U.; Jansson, A. Airborne wear particles from passenger car disc brakes: a comparison of measurements from field tests, a disc brake assembly test stand, and a pin-on-disc machine. *Proc. IMechE Part J: Journal of Engineering Tribology* **2010b**, *224*(2), 179-188.
557. Wang, Q. J.; Chung, Y.-W. Encyclopedia of Tribology. Springer, **2013**.
558. Wang, X.; Ding, H.; Ryan, L.; Xu, X. Association between air pollution and low birth weight: A community-based study. *Environ. Health Perspect.* **1997**, *105*(5), 514-520.
559. Wang, Y.-F.; Huang, K.-L.; Li, C.-T.; Mi, H.-H.; Luo, J.-H.; Tsai, P.-J. Emissions of fuel metals content from a diesel vehicle engine. *Atmos. Environ.* **2003**, *37*, 4637-4643.
560. Wawer, M.; Magiera, T.; Ojha, G.; Appel, E.; Bućko, M. S.; Kusza, G. Characteristics of current roadside pollution using test-monitoring plots. *Sci. Total Environ.* **2015**, *505*, 795-804.
561. Weichenthal, S.; Bai, L.; Hatzopoulou, M.; van Ryswyk, K.; Kwong, J. C.; Jerrett, M.; van Donkelaar, A.; Martin, R. V.; Burnett, R. T.; Lu, H.; Chen, H. Long-term exposure to ambient ultrafine particles and respiratory disease incidence in Toronto, Canada: a cohort study. *Environ. Health* **2017a**, *16*(64).
562. Weichenthal, S.; Lavigne, E.; Valois, M.-F.; Hatzopoulou, M.; van Ryswyk, K.; Shekarrizfard, M.; Villenueve, P. J.; Golberg, M. S.; Parent, M.-E. Spatial variations in ambient ultrafine particle

concentrations and the risk of incident prostate cancer: A case-control study. *Environ. Res.* **2017b**, *156*, 374-380.

563. Weichenthal, S.; Olaniyan, T.; Christidis, T.; Lavigne, E.; Hatzopoulou, M.; Van Ryswyk, K.; Tjepkema, M.; Burnett, R. Within-city spatial variations in ambient ultrafine particle concentrations and incident brain tumors in adults. *Epidemiol.* **2020**, *2*, 177183.
564. Weichenthal, S.; van Ryswyk, K.; Goldstein, A.; Bagg, S.; Shekkarizfard, M.; Hatzopoulou, M. A land use regression model for ambient ultrafine particles in Montreal, Canada: A comparison of linear regression and a machine learning approach. *Environ. Res.* **2016a**, *146*, 65-72.
565. Weichenthal, S.; van Ryswyk, K.; Goldstein, A.; Shekarrizfard, M.; Hatzopoulou, M. Characterizing the spatial distribution of ambient ultrafine particles in Toronto, Canada: A land use regression model. *Environ. Pollut.* **2016b**, *208*, 241-248.
566. Westerdahl, D.; Fruin, S. A.; Fine, P. L.; Sioustas, C. The Los Angeles International Airport as a source of ultrafine particles and other pollutants to nearby communities. *Atmos. Environ.* **2008**, *42*, 3143-3155.
567. Westerlund, K. G. Metal emissions from Stockholm traffic – wear of brake linings. *The Stockholm Environment and Health Protection Administration* **2001**.
568. WHO, **2016**. *Ambient (outdoor) air pollution*.
569. WHO, **2018**. *Burden of disease from the joint effects of household and ambient air pollution for 2016*.
570. WHO, **2019**. *Dementia – Fact Sheet*.
571. Wik, A.; Dave, G. Occurrence and effects of tire wear particles in the environment – A critical review and an initial risk assessment. *Environ. Pollut.* **2009**, *157*, 1-11.
572. Winkler, A.; Contardo, T.; Vannini, A.; Sorbo, S.; Basile, A.; Loppi, S. Magnetic emissions from brake-wear are the major source of airborne particulate matter bioaccumulated by lichens exposed in Milan (Italy). *Appl. Sci.* **2020**, *10*, 2073.
573. Wu, J.; Ding, T.; Sun, J. Neurotoxic potential of iron oxide nanoparticles in the rat brain striatum and hippocampus. *Neurotoxicol.* **2013**, 34, 243-253.
574. Wu, Y.-C.; Lin, Y.-C.; Yu, H.-L.; Chen, J.-H.; Chen, T.-F.; Sun, Y.; Wen, L.-L.; Yip, P.-K.; Chu, Y.-M.; Chen, Y.-C. Association between air pollutants and dementia risk in the elderly. *Alzheimers Dement. (Amst)* **2015**, *1*, 220-228.
575. Xie, S.; Dearing, J. A.; Bloemendal, J.; Boyle, J. F. Association between the organic matter content and magnetic properties in street dust, Liverpool, UK. *Sci. Total Environ.* **1999**, *241*, 205-214.
576. Xie, S.; Dearing, J. A.; Boyle, J. F.; Bloemendal, J.; Morse, A. P. Association between magnetic properties and element concentrations of Liverpool street dust and its implications. *J. Appl. Phys.* **2001**, *48*, 83-92.
577. Yang, T.; Liu, Q.; Li, H.; Zeng, Q.; Chan, L. Anthropogenic magnetic particles and heavy metals in the road dust: Magnetic identification and its implications. *Atmos. Environ.* **2010**, *44*, 1175-1185.
578. Yang, Y.; Vance, M.; Tou, F.; Tiwari, A.; Liu, M.; Hochella Jr., M. F. Nanoparticles in road dust from impervious urban surfaces: distribution, identification, and environmental implications. *Environ. Sci.: Nano* **2016**, *3*, 534-544.
579. Yin, G.; Hu, S.; Cao, L.; Roesler, W.; Appel, E. Magnetic properties of tree leaves and their significance in atmospheric particle pollution in Linfen City, China. *Chin. Geogra. Sci.* **2013**, *23*(1), 59-72.
580. Yuchi, W.; Sbihi, H.; Davies, H.; Tamburic, L.; Brauer, M. Road proximity, air pollution, noise, green space and neurologic disease incidence: a population-based cohort study. *Environmen. Health* **2020** *19*(8).
581. Zajzon, N.; Márton, E.; Sipos, P.; Kristály, F.; Németh, T.; Kis-Kovács, V.; Weiszburg, T. G. Integrated mineralogical and magnetic study of magnetic airborne particles from potential pollution sources in industrial-urban environment. *Carpath. J. Earth Env.* **2013**, *8*(1), 179-186.
582. Zanobetti, A.; Schwartz, J.; Samoli, E.; Gryparis, A.; Touloumi, G.; Atkinson, R.; *et al.* The temporal pattern of mortality responses to air pollution: A multicity assessment of mortality displacement. *Epidemiol.* **2002**, *13*, 87-93.

583. Zecca, L.; Youdim, M. B. H.; Riederer, P.; Connor, J. R.; Crichton, R. R. Iron, brain ageing and neurodegenerative disorders. *Nature Rev. Neurosci.* **2004**, *5*, 863-873.

584. Zhang, C.; Huang, B.; Li, Z.; Liu, H. Magnetic properties of high-road-side pine tree leaves in Beijing and their environmental significance. *Chin. Sci. Bull.* **2006**, *51*(24), 3041-3052.

585. Zhang, F.; Chen, Y.; Tian, C.; Wang, X.; Huang, G.; Fang, Y.; Zong, Z. Identification and quantification of shipping emissions in Bohai Rim, China. *Sci. Total Environ.* **2014**, *497-498*, 570-577.

586. Zhang, H.; Wang, S.; Hao, J.; Wan, L.; Jiang, J.; Zhang, M.; Mestl, H. E. S.; Alnes, L. W. H.; Aunan, K.; Mellouki, A. W. Chemical and size characterization of particles emitted from the burning of coal and wood in rural households in Guizhou, China. *Atmos. Environ.* **2012**, *51*, 94-99.

587. Zhang, W.; Jiang, H.; Dong, C.; Yan, Q.; Yu, L.; Yu, Y. Magnetic and geochemical characterization of iron pollution in subway dusts in Shanghai, China. *Geochem. Geophys. Geosyst.* **2011**, *12*, Q06Z25.

588. Zhang, X.; Chen, X.; Zhang, X. The impact of exposure to air pollution on cognitive performance. *PNAS* **2018a**, *115*(37), 9193-9197.

589. Zhang, D.; Zhu, Y.; Liu, L.; Ying, X.; Hsiung, C.-E.; Sougrat, R.; Li, K.; Han, Y. Atomic-resolution transmission electron microscopy of electron beam-sensitive crystalline materials. *Science* **2018b**, *359*, 675-679.

590. Zhang, Y.; Demokritou, P.; Ryan, D. K.; Bello, D. Comprehensive assessment of short-lived ROS and H_2O_2 in laser emissions: Assessing the relative contribution of metal oxides and organic constituents. *Environ. Sci. Technol.* **2019**, *53*, 7574-7583.

591. Zhang, Q.; Lu, D.; Wang, D.; Yang, X.; Zuo, P.; Yang, H.; Fu, Q.; Liu, Q.; Jiang, G. Separation and tracing of anthropogenic magnetite nanoparticles in the urban atmosphere. *Environ. Sci. Technol.* **2020**, *54*, 9274-9284.

592. Zhang, Y.; Yang, X.; Brown, R.; Yang, L.; Morawska, L.; Ristovski, Z.; Fu, Q.; Huang, C. Shipping emissions and their impacts on air quality in China. *Sci. Total Environ.* **2017**, *581-582*, 186-198.

593. Zhao, J.; Lewinski, N.; Riediker, M. Physico-chemical characterization and oxidative reactivity evaluation of aged brake-wear particles. *Aerosol Sci. Technol.* **2015**, *49*, 65-74.

594. Zhou, Y.; Levy, J. I. The impact of urban street canyons on population exposure to traffic-related primary pollutants. *Atmos. Environ.* **2008**, *42*, 3087-3098.

595. Zhu, Y.; Hinds, W. C.; Kim, S.; Sioustas, C. Concentration and size distribution of ultrafine particles near a major highway. *J. Air & Waste Manage. Assoc.* **2002**, *52*, 1032-1042.

Appendix A: Supplementary material

A1: Analytical techniques and methods used in this thesis.

In this thesis, multiple different analytical techniques and methods were used for generation, collection and analysis of PM samples. These included:

1) Brake-derived PM sample generation and collection – a full-scale brake dynamometer (Link M2800; VŠB – Technical University of Ostrava, Czech Republic) was used to generate brake-derived PM (Figure A1). Non-volatile emissions were collected using a Dekati ELPI+ impactor, on Al foils, in 14 size fractions, from 0.016 µm up to 10 µm. The details of the dynamometer setup, brake cycle and sample collection are provided in Section 5.3.1. Brake-wear generation, braking cycle and particulate matter sampling (Paper III).

Figure A1. Full-scale brake dynamometer, LINK M2800 at VŠB – Technical University of Ostrava, Czech Republic (private collection).

2) Magnetic measurements
    a) Room-temperature isothermal remanence magnetisation (IRM) – a general magnetic parameter dependent on the concentrations of magnetically-ordered grains, their grain size distribution and mineralogy. IRM and its detailed AF demagnetisation curves were used for magnetic component analysis in Papers II and III. IRM was imposed to all samples at 1 T, using a Newport Instruments electromagnet, and measured with a 2G RAPID cryogenic magnetometer at the Centre for Environmental Magnetism and Palaeomagnetism (CEMP), Lancaster University, U.K (see also Section 4.3.2. Magnetic measurements (Paper II) and Appendix A: Sections A5 and A9 for more details).
    b) Low- and high-temperature magnetic measurements – thermal changes in magnetic parameters (e.g. IRM or magnetic susceptibility) allows the identification of magnetic minerals present in a sample, as indicated by Curie/Néel temperatures and/or first order magnetic transitions (e.g. Verwey transition). Here, high-temperature (from room temperature to 700°C) changes in magnetic susceptibility were measured at the CEMP laboratory, with an AGICO KLY-3 kappabridge with a CS-3 high-temperature furnace. Low-temperature (from -196°C to room temperature) changes in IRM were conducted with an MPMS XL SQUID magnetometer (Quantum Design) at the Centre for Science at Extreme Conditions, University of Edinburgh, U.K. (Figure 26). See also Appendix A: Sections A5, A7 and A9 for more details.
    c) Susceptibility of anhysteretic remanent magnetisation (χ_{ARM}) – a parameter especially sensitive to the presence of magnetic grains ~30 – 50 nm in diameter. Here, ARM was imparted to the banknote and ink pigment samples (Paper IV) at 80 mT in 4 different DC biasing fields: 0.06 mT, 0.08 mT, 0.10 mT and 0.12 mT, and subsequently measured with a 2G RAPID cryogenic magnetometer, at the CEMP laboratory. χ_{ARM} was estimated as the slope of the ARM(DC field) linear function (see Appendix B: Materials and Methods (Paper IV)).
3) Electron microscopy – both scanning and transmission electron microscopy imaging was carried out in the Nanolab at University of Pannonia, Veszprém, Hungary (see Appendix A: Section A6 for more details on sample preparation and microscope operation settings).

d) Scanning electron microscopy (SEM) – a microscope which uses a focused beam of electrons to scan a sample surface. The electrons penetrate the sample to a depth of several micrometres, depending on the accelerating voltage and the sample density. The interaction between the electron beam and the sample surface generates various signals, providing information on the surface morphology and composition (e.g. Hawkes & Spence, 2019). Typically, the resolution of SEMs is ~20 nm but some microscopes can achieve resolutions below 1 nm (e.g. Goldstein *et al.*, 2014; Nanotechnology Now Website). Here, secondary electrons (emitted by atoms excited by the electron beam) were detected and analysed (cf. Figure 27).
    i. Energy dispersive X-ray spectroscopy (EDS or EDX) – a technique which, used together with SEM/TEM, provides information on elemental composition of a sample. After a secondary electron is emitted from a sample, the resulting electron vacancy is filled by an electron from a higher state and a photon (X-ray) is emitted (to balance the energy between the two electron's states). Each element has a characteristic X-ray energy and this can be used for the assessment of the chemical composition of a sample (c.f. Figure 27).

e) Transmission electron microscopy (TEM) – a high-resolution microscope technique in which a beam of high-energy electrons passes through a thin sample to generate an image. The interaction between the electron beam and the sample provides information on sample density, composition and crystallinity. High resolution TEMs can achieve the atomic resolution (e.g. Zhang *et al.*, 2018b) (cf. Figures 28, 29, A10 and A11).
    i. High-angle annular dark-field (HAADF) mode – a TEM method, analysing inelastically scattered electrons or thermal diffuse scattering at high angles (~50 – 200 mrad), using an annular dark-field detector. As the HAADF image intensity increases with the increasing atomic number, heavy atoms are observed brighter (cf. Figure 28 and Figure A10).
    ii. Selected-area electron diffraction (SAED) – a technique for qualitative analysis of crystal structures present in a sample. In the SAED method, a specimen is illuminated by a parallel electron beam. The electrons are diffracted (the specimen atoms act as a diffraction grating) at particular

angles, characteristic of the crystal structure of the sample. Here, this method was used to analyse the crystalline phases (here detecting magnetite and metallic-Fe (Figure 28A and Figure A11).

iii. Scanning transmission electron microscopy (STEM) – a technique of TEM, using electron optics to form a small illuminating probe which is raster-scanning across the sample. A wide variety of detectors that can be implemented in the STEM mode, including EDS (Figure 28C and Figure A10) or HAADF (Figure 28B).
iv. High resolution transmission electron microscopy (HRTEM) – an imaging mode in TEM, that allows the atomic scale study of the samples. Here, HRTEM images taken from samples were used for obtaining Fast Fourier Transforms (FFTs), basically equivalent to digitally created diffractograms identifying crystalline phases (here magnetite and haematite (Figure 29).

A2: Search strategy for literature review in Paper I: Airborne, vehicle-derived Fe-bearing nanoparticles in the urban environment.

We conducted a literature search using Web of Science and Google Scholar. Emphasis was placed on key words (including ‘pollution’, ‘pollutant’, ‘particulate matter’, ‘PM’, ‘metal’, ‘nanoparticles’, ‘ultrafine’, ‘fine’, ‘health impact’, etc.) in various combinations with ‘exhaust’, ‘tailpipe’, ‘diesel’, ‘gasoline’, ‘petrol’, ‘brake’, ‘aircraft’, ‘aeroplane’, ‘airport’; and reference lists followed from each of these topics. No time restriction for publication dates was used.

A3: Non-vehicle sources of Fe-bearing nanoparticles in the urban environment (Paper I).

Vehicles are often the major source of Fe-bearing NPs in outdoor urban environments. Although detailed discussion of non-vehicle-derived Fe-bearing NPs is beyond our scope here, some notable sources exist.

Fe is a dominant element in welding fumes (Sowards *et al.*, 2008) and associated with pulmonary problems (Antonini *et al.*, 2003b; Sowards *et al.*, 2008). Exposure to welding fumes might also be associated with Parkinson's disease (Racette *et al.*, 2001) and lung cancer (Siew *et al.*, 2008).

Fe-bearing NPs occur in stack emissions from waste incineration (Funari *et al.*, 2018). Grains smaller than 100 nm constitute > 90% of total particle number (Jones & Harrison, 2016), with Fe concentrations up to 11 wt.% (Cernuschi *et al.*, 2012). Waste incineration emissions contain a complex magnetic mixture; magnetite-like phases dominate, with smaller fractions of hematite, maghemite, wüstite and iron sulphides (Funari *et al.*, 2018). The contribution of NPs < 30 nm was observed to be ~30% of total emitted mass, which corresponds to 1000 – 7700 tonnes of Fe-bearing NPs emitted by a single municipal solid waste incineration plant yearly (Funari *et al.*, 2018). Given such high amounts of emitted Fe-bearing NPs, waste incineration should be considered as a source of hazardous air pollution.

Indoor sources of Fe-bearing NPs include laser printers (Morawska *et al.*, 2009). Printer emissions contain primarily volatile organic compounds (VOCs) with trace quantities of nano-sized Fe oxides (magnetite) and PAHs (Gminski *et al.*, 2011). Toxicological studies of the potential health effects (in cultured human epithelial lung cells *in vitro*) of black toner powders have shown high genotoxicity of those particles, probably associated with the presence of magnetite and carbon black (Gminski *et al.,* 2011). Recent study also showed that metal oxides play a critical role in the generation of short-lived ROS, which can lead to oxidative stress and inflammation in humans (Zhang *et al.*, 2019).

Biomass burning is a source of Fe-bearing NPs (indoors and outdoors). Chen *et al.* (2017b) reviewed emissions from biomass burning in China, both regionally (open field burning) and locally (indoor biomass combustion as fuel). Number PSD was unimodal (peak between 50 and 100 nm), or bimodal (both peaks < 100 nm) (Tissari *et al.*, 2008; Hosseini *et al.*, 2010; Lamberg *et al.*, 2011; Zhang *et al.*, 2012). Fe in $PM_{2.5}$ of wood combustion emissions occurs in concentrations ~0.04 wt.% (Zhang *et al.*, 2012), with evidence of Fe additionally in the ultrafine (< 100 nm) fraction (Tissari *et al.*, 2008; Lamberg *et al.*, 2011). Toxicological studies (*in vitro* and *in vivo*) show that exposure to biomass combustion emissions might cause inflammatory and cytotoxic effects (Barregard *et al*., 2006; Jalava *et al*., 2010; Chen *et al*., 2017b). A recent epidemiological study showed that $PM_{2.5}$ from residential wood burning was associated with dementia incidence in Northern Sweden (Oudin *et al*., 2018).

Summarizing available data on NP emissions from 11 non-vehicle exhaust sources, Kumar *et al*. (2013) report that construction, demolition, power plants and cigarette smoking are other sources of Fe-bearing NPs.

A4: Analytical procedures and methodology used in Paper III. Friction materials, and mass- and number-normalised PSDs.

In this study, we used low-metallic brake pads and cast iron brake disc. The term ‘low-metallic’ is a commonly used name for brake pads predominantly used on the European market (as opposed to non-asbestos organic brake pads used more commonly on the Asian and American markets). Low-metallic brake pads consist of a mixture or organic and metallic components (e.g. Chan & Stachowiak, 2004). They usually have higher friction performance and durability, but also higher emission rates, compared to the non-asbestos organic (NAO) brake pads. NAO brake pads are made of mainly organic compounds (Chan & Stachowiak, 2004).

Figure 24 shows our experimentally-obtained mass- and number-normalised PSDs. The brake-wear samples were collected with a Dekati ELPI+ impactor, on Al foils, in 14 size fractions, from 16 nm up to 10 μm. All Al foils were weighed before and after the dynamometer tests, and the difference was treated as the mass of the collected brake-derived particles. These masses were used to construct mass-normalised PSD.

Number-normalised PSD was estimated based on the masses of particles collected on each foil and average effective density of airborne brake-derived particles, calculated by Nosko & Olofsson (2017a). The authors did not show exact values of effective density for each of the size fractions in the ELPI+ Dekati impactor. However, they estimated the effective density as 0.75 ± 0.2 g/cm^3 for 6 different friction materials. They also estimated the effective density for the ultrafine (< 0.1 μm) fraction to be 0.76 ± 0.1 g/cm^3 for the same friction materials. Because these 2 effective density values are very similar, we used one density value (0.75 g/cm^3) for the whole size range analysed in our study (0.016 μm – 10 μm).

X-ray diffraction analysis for the low-metallic brake pad used in this study shows the presence of 4 dominating phases, α-Fe, Fe oxides (magnetite/maghemite), Fe oxide-hydroxides, and graphite, with minor or trace concentrations of Cu, corundum (Al_2O_3), zircon ($ZrSiO_4$), Sb oxide (SbO_2), and sulphides, including stibnite (Sb_2S_3), Sn sulphide (Sn_3S_4), berndtite (SnS_2) and ottemannite (Sn_2S_3) (Figure A2).

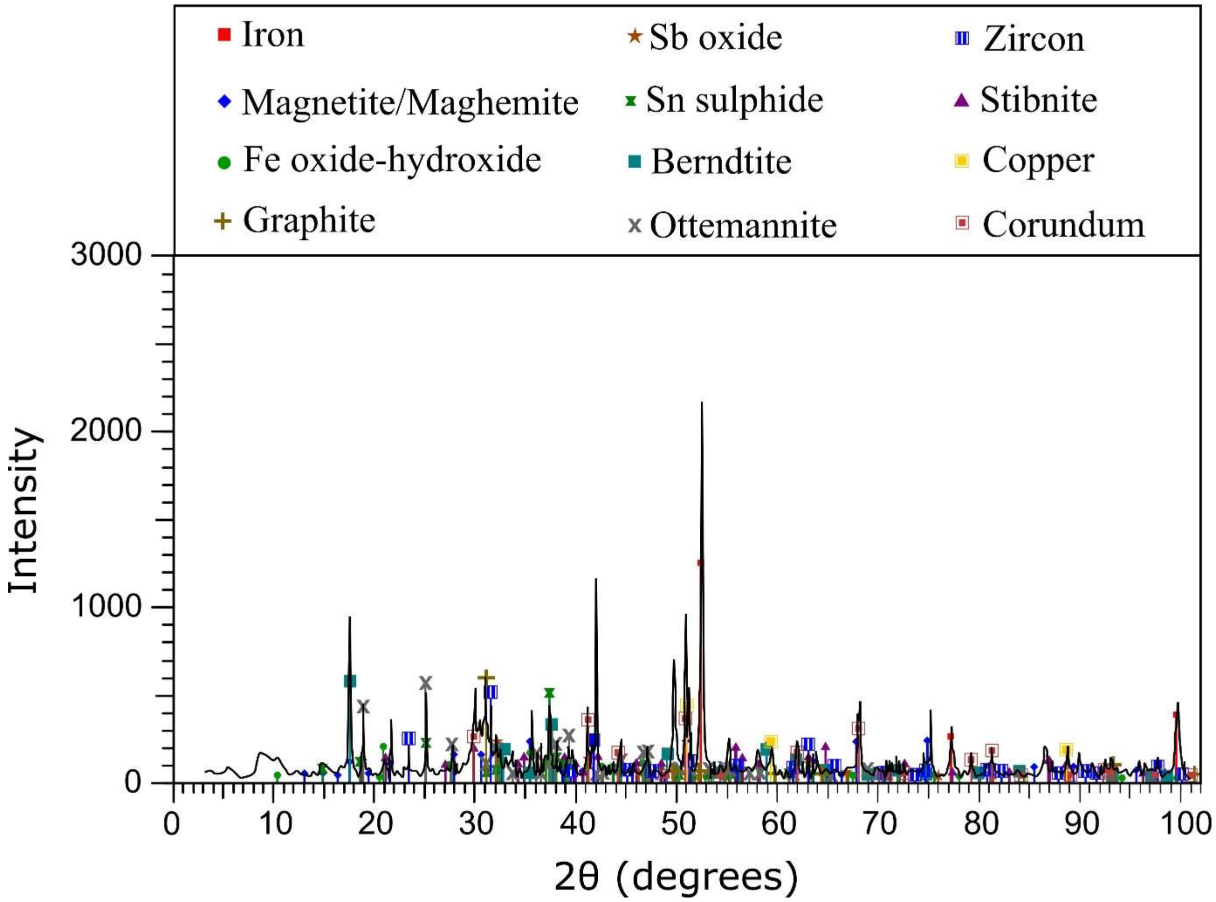

Figure A2. X-ray diffraction (XRD) spectrum for the brake pad used in this study, identifying 4 dominant phases, α-Fe, Fe oxides (magnetite/maghemite), Fe oxide-hydroxides and graphite. Note that non-crystalline phases are not included as XRD is unable to detect them.

A5: Analytical procedures and methodology used in Paper III. Magnetic measurements and estimation of mass concentrations of magnetite, haematite and metallic Fe.

Magnetic remanence measurements were conducted at the Centre for Environmental Magnetism and Palaeomagnetism, Lancaster University, UK. Isothermal remanent magnetisation (IRM) was imparted to all the samples at 1 T at room temperature, using a Newport Instruments electromagnet, and measured with a 2G RAPID cryogenic magnetometer (noise level of ~10^{-11} Am^2).

For the purpose of magnetic component analysis, detailed alternating field (AF) demagnetisation (in 69 steps, from 1 milliTesla, mT, up to 240 mT) of IRM was conducted, adapting the procedure proposed by Egli (2003, 2004a, 2004b, 2004c). Whereas this author used AF demagnetisation of anhysteretic remanent magnetisation (ARM), we used IRM due to a weak signal of ARM for the smaller size fractions, and to limit the potential influence of magnetic interactions between particles. For weaker samples, we repeated the measurements up to 6 times to increase the signal-to-noise ratio. In order to identify magnetic components of IRM, we used CODICA & GECA software (Egli, 2003), kindly provided by Dr. R. Egli. Each component is characterised by three main parameters: i) the median destructive field of IRM (MDF_{IRM}), i.e., the field required to destroy 50% of IRM; ii) a dispersion parameter, i.e. a parameter related to the standard deviation of the coercivity distribution; and iii) the magnetic contribution, the contribution of a specific component to the total IRM. The detailed AF demagnetisation of IRM enables estimation of coercivity distribution and identification of magnetic components (Figure A3; Table A1; see also Section 5.5. Discussion (Paper III) for the interpretation of the identified magnetic components).

Low-temperature magnetic measurements were carried out with an MPMS XL SQUID magnetometer (Quantum Design, USA) at the Centre for Science at Extreme Conditions, University of Edinburgh, U.K. To represent the range of particle sizes, 5 size-fractionated brake-wear samples were selected for low-temperature measurements: stage 1 (~0.016 µm), stage 3 (~0.054 µm), stage 7 (~0.380 µm), stage 11 (~2.5 µm) and stage 13 (~5.3 µm). IRM was imposed at 5 T (at both room temperature and 77 K) in order to saturate all magnetic phases. For stages 1 and 3, 10 DC scans were used in order to increase signal-to-noise ratio.

We estimated magnetite mass concentrations in the brake-wear samples based on IRM values for sized, pure, synthetic magnetite powders (Maher, 1988; Table A2). Mass concentrations of haematite (α-Fe_2O_3) in the brake-wear samples were estimated based on Maher *et al.* (2004), and metallic Fe (α-Fe) based on Maher & Thompson (1999) (Table A2).

In order to evaluate the grain size of haematite, we estimated MDF_{IRM} (median destructive field of IRM) for 3 synthetic haematite powder samples of different grain sizes (0.025×0.014 µm, ~0.100 µm and ~0.150 µm; from Maher *et al.* (2004)). Based on the MDF_{IRM} value for component C2 (81 mT; Table A1) and Figure A4, the haematite average grain size is estimated to be ~120 nm (Figure A4; Table A2). Figure A5 shows the average mass concentrations (in wt.%) of metallic Fe, haematite and magnetite in our sized brake-wear emissions (see Section 5.5. Discussion (Paper III) for the the interpretation).

Table A1. Average parameters of 3 magnetic components identified in brake-wear emissions (average value ± standard deviation).

Component	Median destructive field of IRM [mT]	Dispersion parameter [-]	Average magnetic contribution [%]
C1	12 ± 6	0.40 ± 0.09	37.6 ± 17.4
C2	81 ± 5	0.16 ± 0.02	5.6 ± 0.6
C3	28 ± 4	0.31 ± 0.04	56.8 ± 16.8

Table A2. Magnetic data from sized, synthetic magnetic mineral powders, used to estimate mass concentrations of haematite, metallic Fe and magnetite in brake-wear particle emissions.

Compound in brake emissions	Particle size of brake emissions [µm]	Synthetic data		Reference
		IRM_{1T} [Am^2/kg]	Grain size [µm]	
Haematite	~0.120*	0.18	~0.100	Maher *et al.* (2004)
Metallic Fe	-	80	-	Maher & Thompson (1999)
Magnetite	0.016 – 0.094 (stages 1 – 4)	7.5	<0.100	Maher (1988)
	0.150 – 0.380 (stages 5 – 7)	4.5	~0.190	
	0.600 – 1.6 (stages 8 – 10)	5.9	~1.0	
	2.5 – 10 (stages 11 – 14)	11.0	5 – 10	

*Estimated based on MDF_{IRM} data for synthetic haematites (Figure A4).

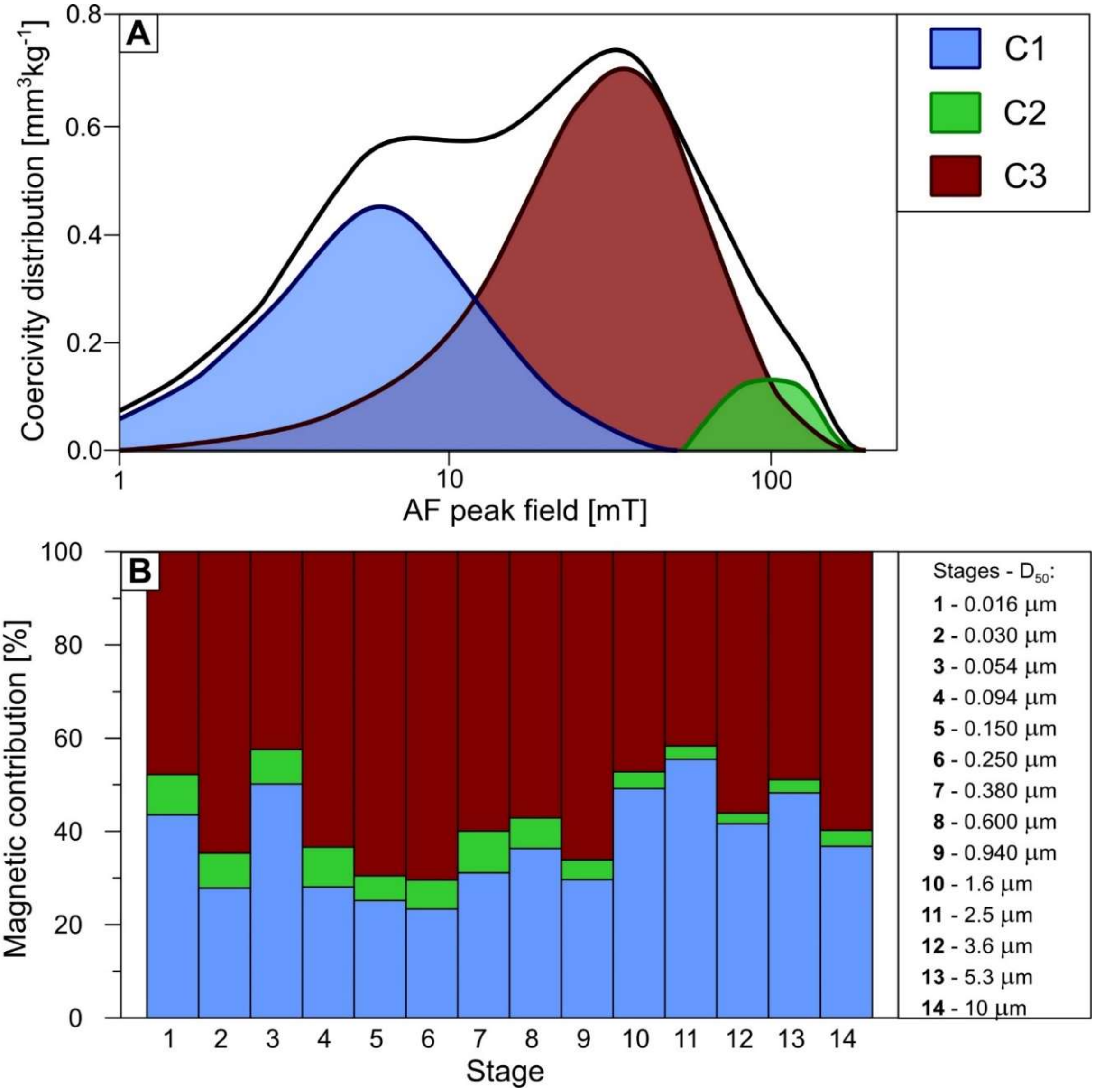

Figure A3. (A) Example of coercivity distribution for a size-fractionated brake-wear sample (stage 5; ∼0.150 μm) and (B) average magnetic contribution (contribution to total IRM) of 3 magnetic components for size-fractionated brake-wear samples, over 4 dynamometer sampling cycles.

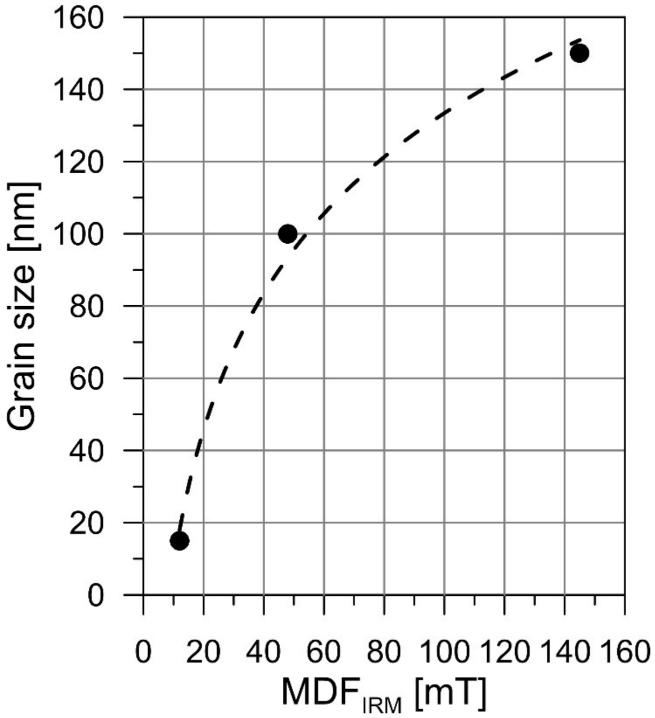

Figure A4. Median destructive field of IRM (MDF$_{IRM}$) for equidimensional synthetic haematites of different grain size (Maher *et al.,* 2004).

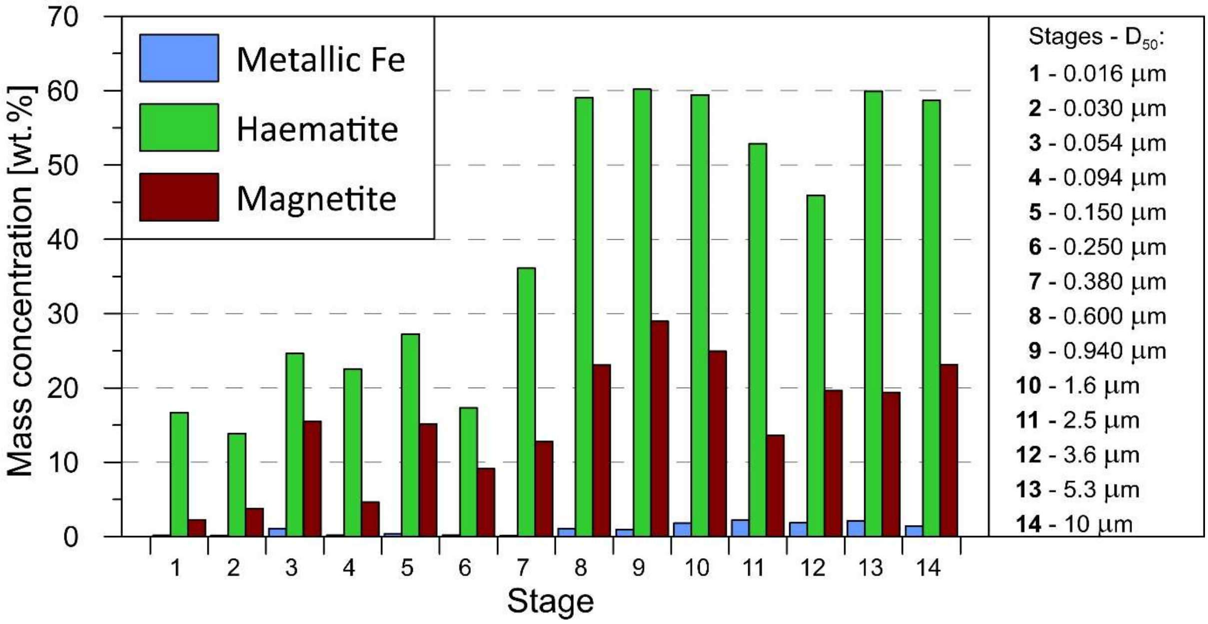

Figure A5. Mass concentration (wt.%) of metallic Fe, magnetite and haematite in dynamometer-derived, size-fractionated particulate brake emissions, estimated from magnetic component analysis.

A6: Analytical procedures and methodology used in Paper III. Scanning (SEM) and transmission (TEM) electron microscopy.

To obtain independent information on the composition, structure, morphology and particle size of the brake-wear particles, we used scanning and transmission electron microscopy to image and analyse the particles directly. For the SEM study, two units of the aluminium foil with the deposited particles (stage 10 with nominal particle size of ~1.6 µm and stage 11 with nominal particle size of ~2.5 µm) were cut and placed onto a double-sided sticky carbon tape on an aluminium stub. The samples were analysed using an Apreo LoVac, field-emission gun scanning electron microscope (Thermo Fisher Scientific). Secondary electron images and energy dispersive X-ray spectra (EDS) were obtained at 2 kV and 20 kV accelerating voltage, respectively. For the TEM study, pieces of the aluminium foil with their deposited particles were cut, placed in a 1.5 ml Eppendorf tube filled with 1 ml distilled water, and ultrasonicated for 10 minutes to remove the particles from the foil. Then a drop of the resultant suspension was placed onto a copper TEM grid coated with a lacey carbon film and left to dry. We used a Talos F200X transmission electron microscope (Thermo Fisher Scientific), operated at 200 kV accelerating voltage and equipped with a four-detector SuperX EDS system. Low-magnification bright-field and high-resolution (HRTEM) images, as well as selected-area electron diffraction (SAED) patterns, were obtained in conventional TEM mode. High-angle annular dark-field (HAADF) images and EDS elemental maps were obtained in scanning transmission (STEM) mode.

A7: Thermal changes in magnetic susceptibility of a non-airborne brake-wear sample (Paper III).

The evaluation of high-temperature (from room temperature up to 700°C) changes in magnetic susceptibility (κ(T)) allows the identification of magnetic minerals, as indicated by the Curie temperature (T_C, the temperature at which magnetically ordered ferromagnetic phase transforms into a disordered paramagnetic phase, represented by a sudden drop in magnetic susceptibility on the κ(T) curves). Figure A6 shows thermal changes in magnetic susceptibility of a non-airborne brake-wear sample. A Curie temperature of ~580°C can be noted on the heating curve, indicating the presence of magnetite. Subsequently, the magnetic susceptibility continues to decrease while heating up to 700°C. Upon cooling, magnetic susceptibility keeps decreasing from 700°C down to ~580°C. This characteristic 'tail' observed in the curve of κ(T) ~600 – 700°C is indicative of the presence of metallic Fe, as discussed in Górka-Kostrubiec & Szczepaniak-Wnuk (2017) and Górka-Kostrubiec *et al.* (2019).

The occurrence of metallic Fe is of high significance for the quantitative evaluation of magnetic mineralogy based on magnetic remanence (IRM). As its IRM_{1T} is much higher than these for magnetite (~7 – 18 times) and haematite (~400 times), the failure of identification of metallic Fe might lead to very high inaccuracies in estimations of mass concentrations of magnetic minerals (see also Section A8. Measurement uncertainties for mass concentrations estimated using magnetic component analysis (Paper III) and Section A9. Selected magnetic properties of materials). The occurrence of metallic Fe in air pollution samples might also be a confounding factor in assessment of magnetic grain size distribution. For example, metallic Fe causes an 'artificial' shift to the down-right corner in the Day plot, commonly used for the assessment of magnetic grain size distribution in environmental samples (Górka-Kostrubiec & Szczepaniak-Wnuk, 2017; Górka-Kostrubiec *et al.,* 2019).

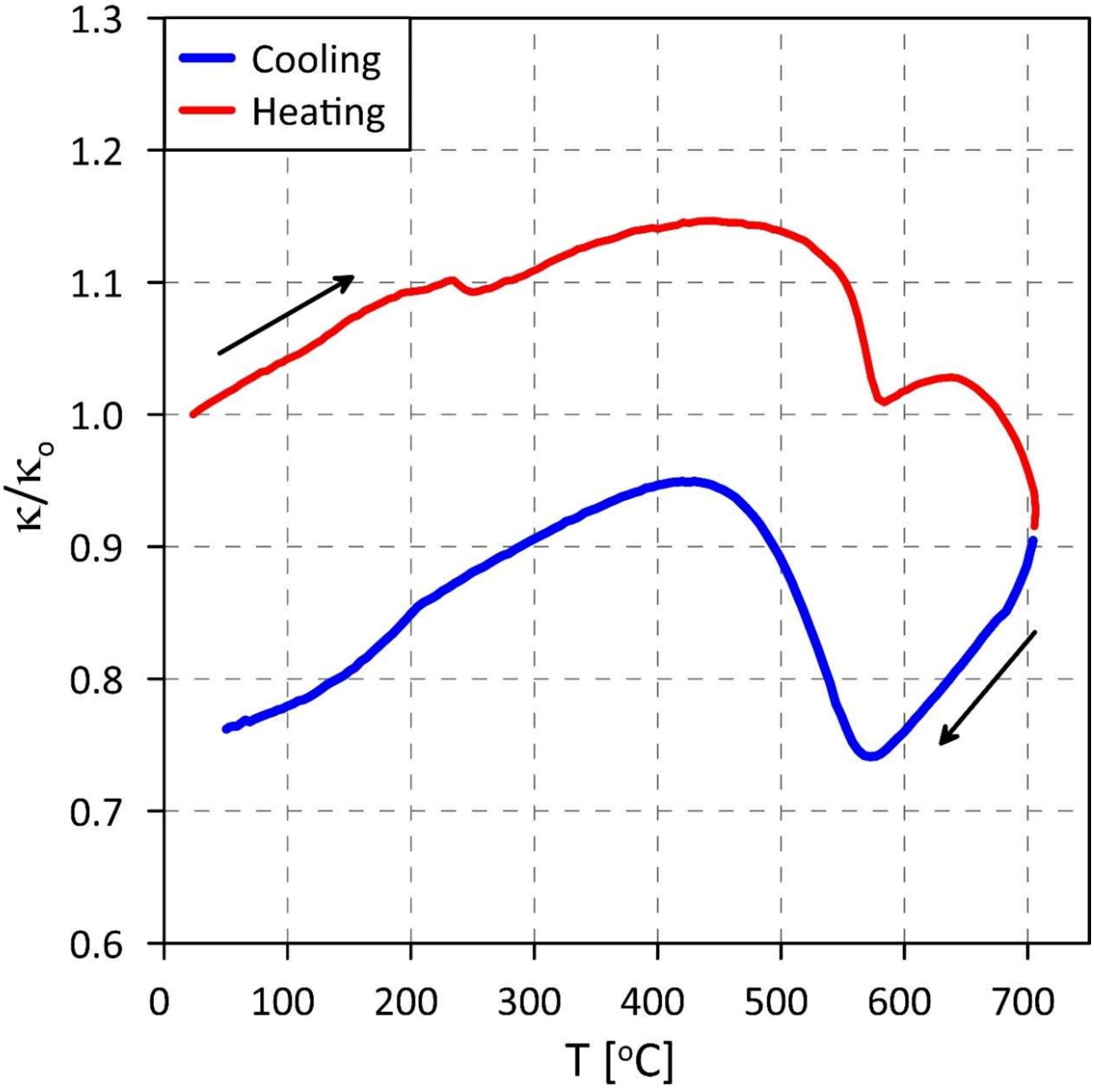

Figure A6. High-temperature thermal changes of magnetic susceptibility of non-airborne brake-wear sample.

A8: Measurement uncertainties for mass concentrations estimated using magnetic component analysis (Paper III).

Magnetic component analysis is based on stepwise AF demagnetisation of magnetic remanence (IRM). Although the noise level of the 2G RAPID magnetometer is low ($\sim 10^{-11}$ Am^2), realistic measurement uncertainty appears higher, due to imperfect alignment of the sample axis along magnetising/demagnetising coils, both in the Newport electromagnet (where samples are magnetised) and 2G magnetometer (where samples are demagnetised); imperfect intensity of magnetising field in the Newport electromagnet; and/or potential magnetic interactions between magnetised grains during demagnetisation. We estimate that this additional error is $\sim 1 - 2\%$ of the measured IRM + 10^{-11} Am^2 (inherent noise level of the 2G magnetometer).

This additional error has important consequences for the estimations of mass concentrations of magnetic phases, based on magnetic component analysis. The uncertainty for mass concentration of each magnetic phase present in the analysed brake-wear emissions can be estimated, depending on the values of IRM$_{1T}$ for synthetic minerals, used for the mass calculations (Table A2). Because haematite displays much lower IRM$_{1T}$ than magnetite and metallic Fe (25 – 450 times lower; cf. Table A2), the uncertainty in the estimation of mass concentrations of haematite is much higher, compared to metallic Fe and magnetite. We assumed the measurement error $\sim 1.5\%$ and estimated the uncertainties (Δ) according to the following equation:

$$\Delta = \frac{\left(\frac{1.5\% \cdot IRM_m}{IRM_s}\right)}{m} \tag{1}$$

where:

IRM_m – total IRM measured for particular stage (size fraction);

IRM_s – IRM for synthetic powders of metallic Fe, haematite or magnetite;

m – mass of the collected particles on particular stage (size fraction).

Table A3 shows the estimation uncertainties for each magnetic phase and size fraction, averaged over 4 dynamometer experiments analysed in this study (see Section 5.3.1. Brake-wear generation, braking cycle and particulate matter sampling (Paper III)). The uncertainties of both metallic Fe and magnetite mass concentrations are relatively low, ranging from 0.006 wt.% to 0.075 wt.% for metallic Fe, and from 0.07 wt.% to 0.78 wt.% for magnetite (Table A3), whereas the estimation uncertainties for haematite are much higher, reaching levels up to 32.8 wt.%.

Table A3. Uncertainties of estimation of mass concentrations of metallic Fe, haematite and magnetite, using magnetic component analysis.

Stage	Particle size [µm]	Measurement uncertainty		
		Metallic Fe	Haematite	Magnetite
1	0.016	± 0.006 wt.%	± 2.8 wt.%	± 0.07 wt.%
2	0.030	± 0.008 wt.%	± 3.6 wt.%	± 0.09 wt.%
3	0.054	± 0.040 wt.%	± 17.4 wt.%	± 0.42 wt.%
4	0.094	± 0.010 wt.%	± 4.4 wt.%	± 0.11 wt.%
5	0.150	± 0.020 wt.%	± 8.7 wt.%	± 0.35 wt.%
6	0.250	± 0.011 wt.%	± 4.9 wt.%	± 0.20 wt.%
7	0.380	± 0.014 wt.%	± 6.3 wt.%	± 0.26 wt.%
8	0.600	± 0.045 wt.%	± 19.5 wt.%	± 0.60 wt.%
9	0.940	± 0.049 wt.%	± 21.4 wt.%	± 0.66 wt.%
10	1.6	± 0.058 wt.%	± 25.2 wt.%	± 0.78 wt.%
11	2.5	± 0.064 wt.%	± 27.9 wt.%	± 0.46 wt.%
12	3.6	± 0.070 wt.%	± 30.9 wt.%	± 0.51 wt.%
13	5.3	± 0.075 wt.%	± 32.8 wt.%	± 0.54 wt.%
14	10	± 0.072 wt.%	± 31.7 wt.%	± 0.53 wt.%

A9: Selected magnetic properties of materials.

Isothermal remanent magnetisation is a commonly used parameter in environmental magnetism. It depends on the concentration, grain size distribution (Figure A7) and mineralogy (Table A4) of magnetically-ordered, remanence-capable magnetic grains. When measured for environmental samples (e.g. urban dusts, soils or rocks), this parameter is especially sensitive to the presence of strongly-magnetic Fe forms, especially metallic Fe, magnetite (and titanomagnetite), maghemite and greigite (Table A4).

Low-temperature magnetic measurements can be used to identify different magnetic minerals present in a sample. For example, if the sample contains haematite, the Morin transition is visible in the zero-field cooling curves. This first order transition results in a sudden decrease in IRM (Figure A8), at the transition temperature (T_M), which usually ranges between 210K and 260K (e.g. Muench *et al.,* 1985; Amin & Arajs, 1987; Maher *et al.,* 2004).

The presence of magnetite is indicated by the presence of another first order transition, the Verwey transition (Verwey, 1939; Özdemir *et al.,* 1993). Figure A9 shows an example of zero-field cooling curves for three samples, (1) a pure magnetite (~37 nm in size), (2) partially oxidised (maghemitised) magnetite (~37 nm in size), and (3) pure maghemite (~470 nm in size). Similar to the Morin transition, the Verwey transition results in a sudden decrease in IRM but at lower temperatures (usually between 80 K and 130 K) (Figure A9) (Verwey, 1939; Özdemir & Dunlop, 2010; Özdemir *et al.,* 1993). For pure magnetites, the Verwey transition is usually sharp, whereas partially oxidised (maghemitised) magnetites usually display broadened and indistinct Verwey transitions (Figure A9) (Özdemir & Dunlop, 2010). Zero-field cooling curves do not exhibit the Verwey transition of maghemite (Figure A9) (Özdemir & Dunlop, 2010). Zero-field cooling curves for partially oxidised magnetites exhibit so-called ‘hump’ behaviour which combines the monotonic increase in IRM of maghemite and the non-linear changes in IRM of magnetite (Figure A9) (Özdemir & Dunlop, 2010).

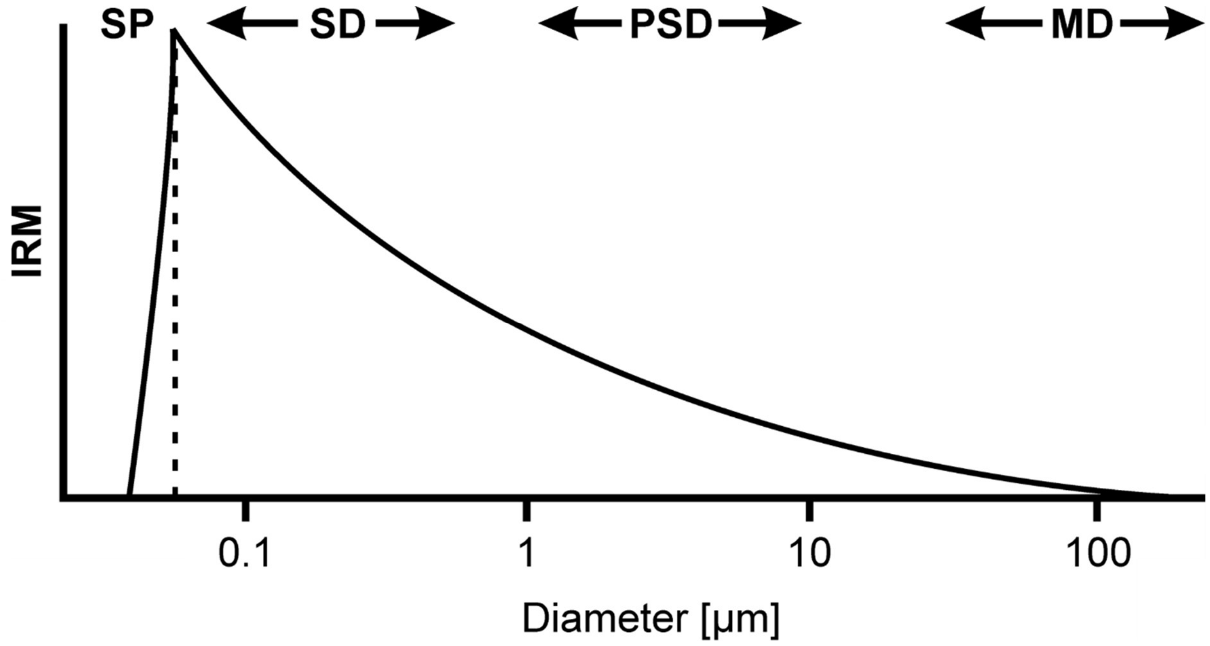

Figure A7. Diagram of the variation of saturation isothermal remanence magnetisation in magnetite (Thompson & Oldfield, 1986), which exerts strong influence on the magnetic configuration (domain state) and resultant magnetic properties of particles. The dashed line highlights the changes in trend of mineral magnetic properties at the superparamagnetic/single-domain boundary. SP – superparamagnetic; SD – single-domain, PSD – pseudo-single-domain, MD – multi-domain.

Table A4. Isothermal remanent magnetisation (IRM) and anhysteretic remanent magnetisation (ARM) of natural minerals (adapted from Maher & Thompson (1999)). ARM – anhysteretic remanence grown in a 100 mT peak AF biased with a 0.1 mT DC field; IRM – isothermal remanence magnetisation (acquired in a 1 T DC field).

Mineral	ARM [10^{-3} Am^{2}kg^{-1}]	IRM [Am^{2}kg^{-1}]
Magnetite	18 - 110	9 - 22
Titanomagnetite	80 - 480	7 - 12
Haematite	0.002	0.24
Greigite	110	11
Pyrrhotite	80	4.5
Goethite	0.005	0.05
Metallic iron	800	80
Paramagnets	0	0
Diamagnets	0	0

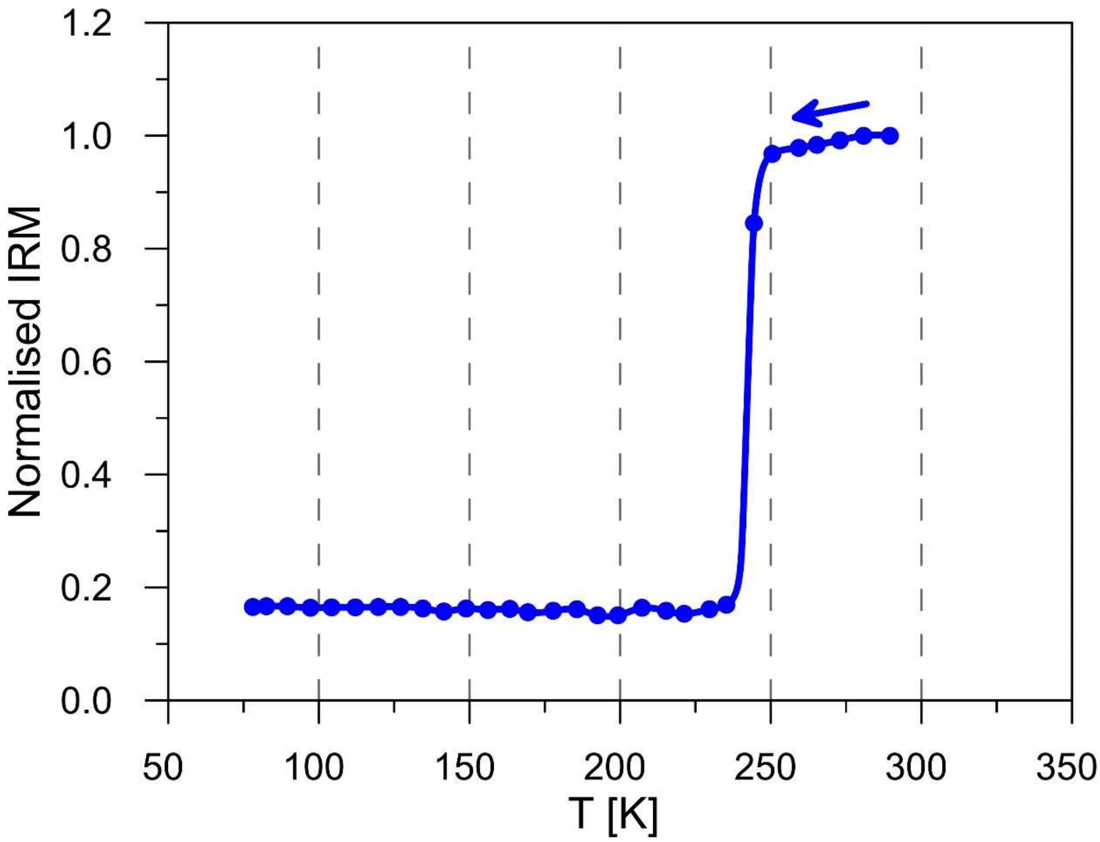

Figure A8. Zero-field changes in IRM during cooling of a synthetic haematite sample (~100 nm in size), after acquisition of IRM (at 7 T) at room temperature, with visible Morin transition at ~230 – 240K (adapted from Maher *et al.* (2004)).

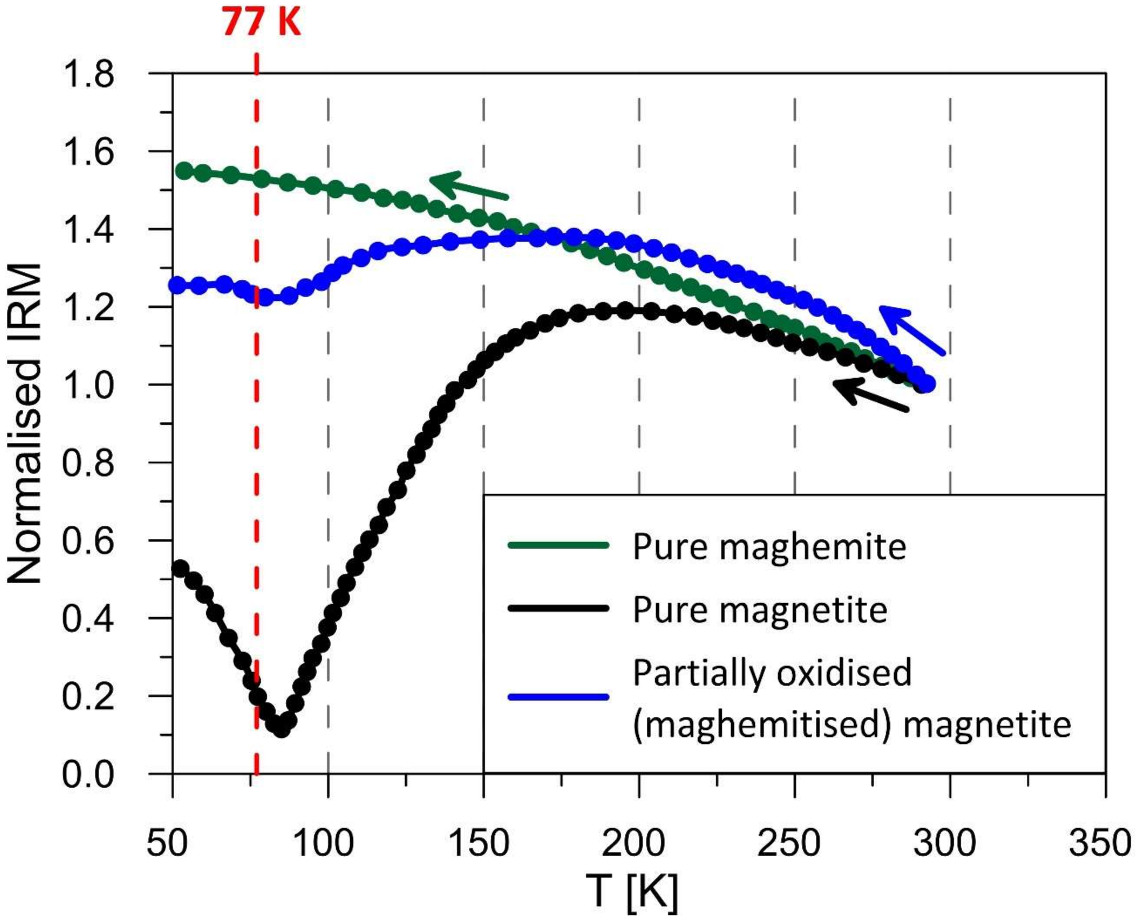

Figure A9. Zero-field changes in IRM during cooling of three synthetic samples, pure magnetite, pure maghemite and partially oxidised (maghemitised) magnetite, after acquisition of IRM (at 2.5 T) at room temperature, with visible Verwey transition at ~80 – 100 K (for pure magnetite) and ~70 – 90 K (for partially oxidised magnetite) (adapted from Özdemir & Dunlop (2010)). The red, dashed line marks the temperature to which samples were cooled down in this study (77 K).

A10: TEM images of UFP agglomerates (Paper III).

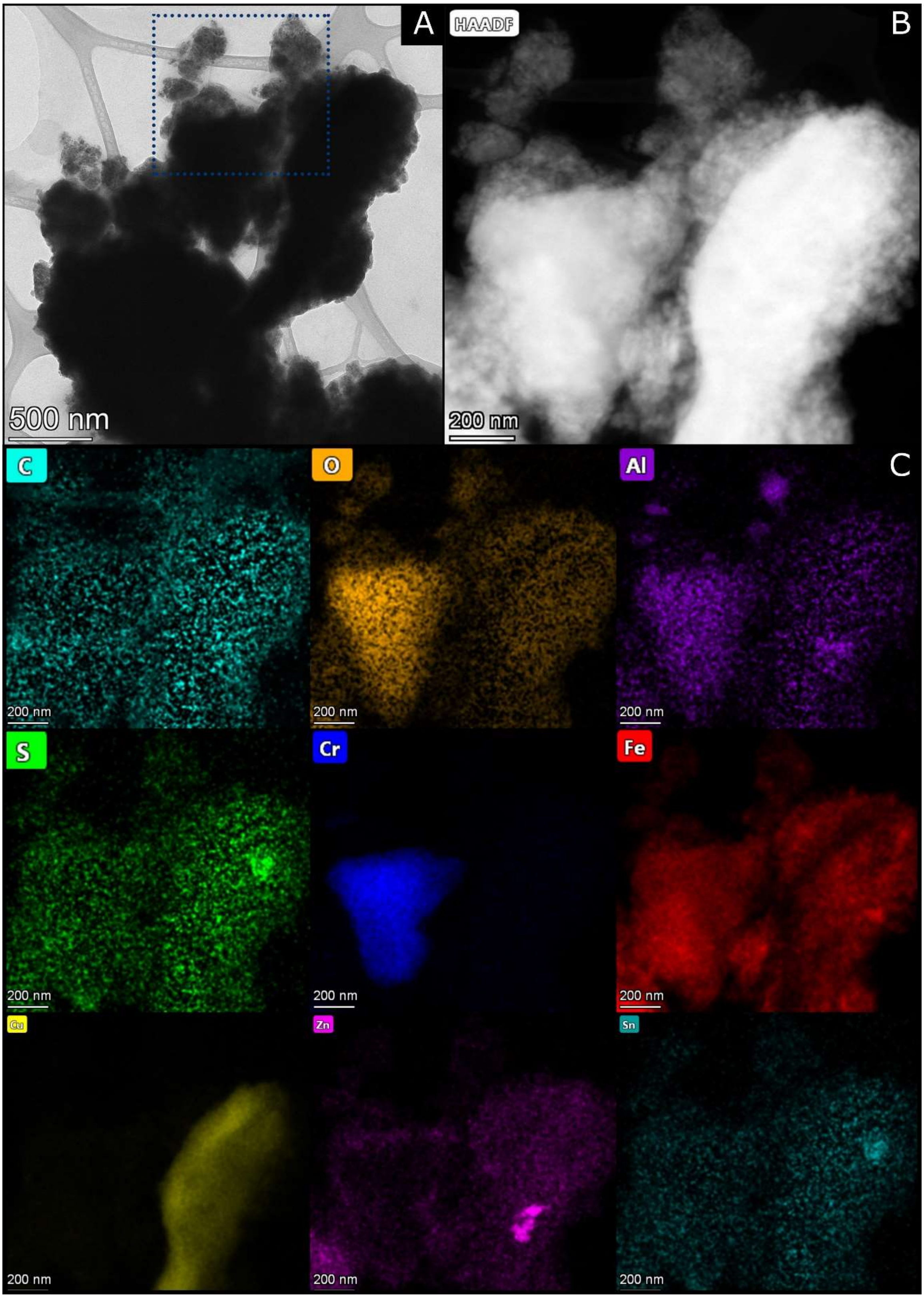

Figure A10. (A) TEM image of a Cu-rich UFP agglomerate; (B) HAADF image of the boxed area in (A); (C) STEM EDS elemental maps obtained from the same particle region shown in (B), with the elemental composition of the analysed region shown in the inserted table.

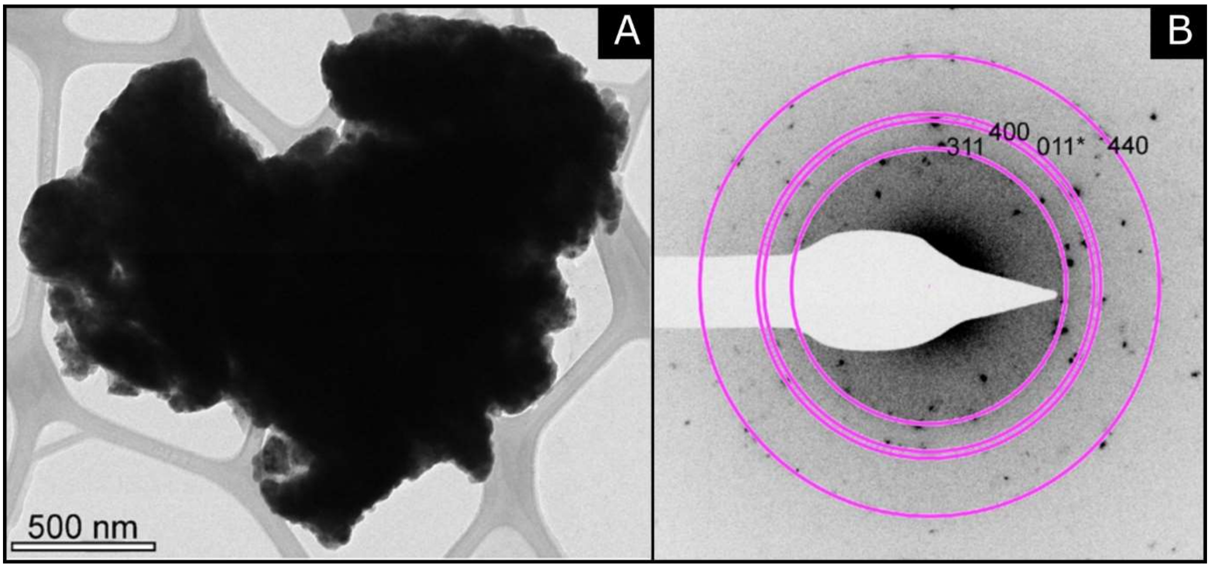

Figure A11. Brake-wear aggregate and its SAED pattern. The rings are redrawn for better visualisation. Three rings can be indexed based on the structure of magnetite and the starred one (011) is produced by metallic Fe (α-Fe).

Figure A12: Map with sampling sites in Paper II: heavily trafficked (Cable Street and Dalton Square) and urban background (Bailrigg House) sites in Lancaster, U.K.; and heavily trafficked (Bristol Road Observation Site) and urban background (Birmingham Air Quality Site) in Birmingham, U.K.

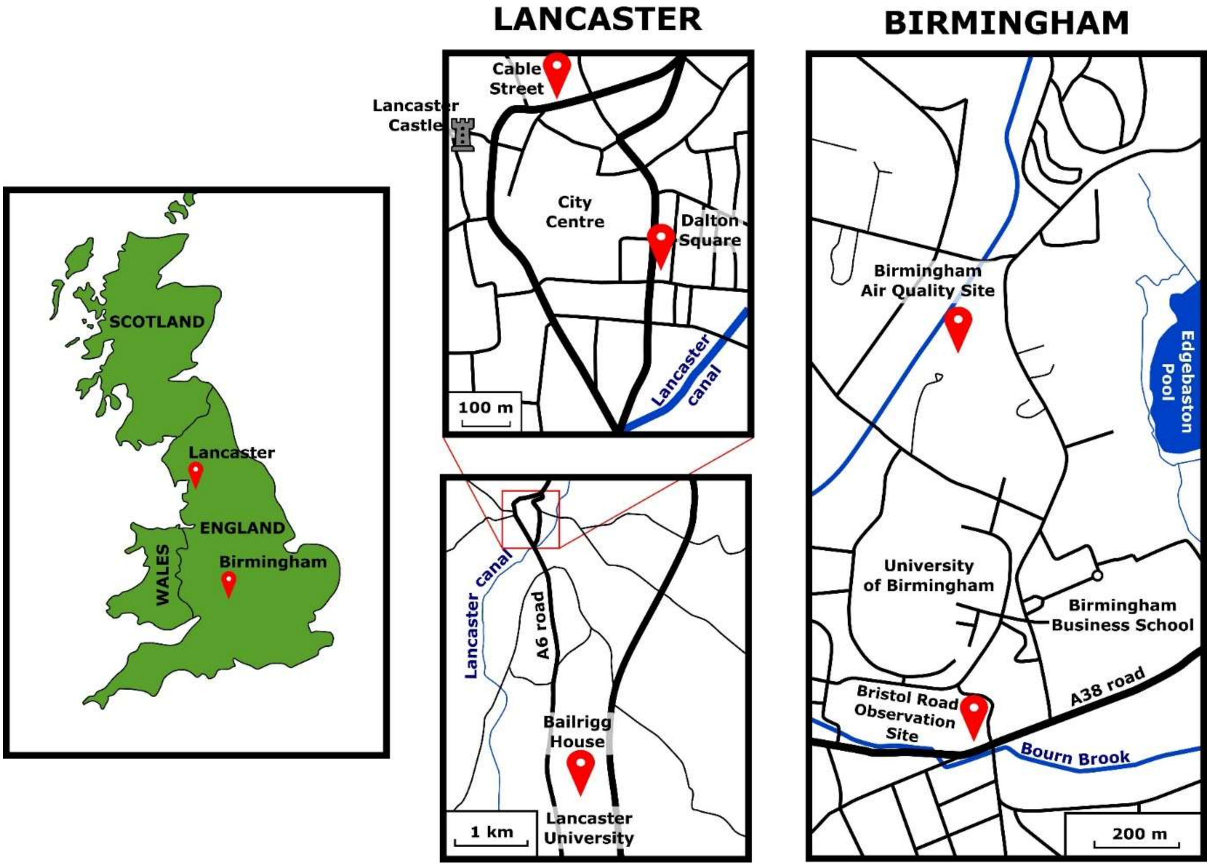

Table A5: Summary table of selected toxicological studies of vehicle-derived PM.

Reference	Title	Tested material	Cell type Animal species	Assay	Dose	Findings
Exhaust emissions						
Sugamata *et al.* (2006)	Maternal diesel exhaust exposure damages newborn murine brains	Airborne fraction of diesel emissions	Newborn mice (cerebral cortex and hippocampus) whose mothers were exposed do diesel emission during pregnancy	Microscopic observations; apoptosis detection (immunohistochemical staining for caspase 3)	0.3, 1.0 and 3.0 mg/m^3	Diesel emissions cause apoptosis in newborn mice, stenosis of some capillaries and degeneration of granular perithelial cytoplasmic granules
Cheung *et al.* (2010)	Emissions of particulate trace elements, metals and organic species from gasoline, diesel, and biodiesel passenger vehicles and their relation to oxidative potential	Airborne fraction of diesel, biodiesel, petro-diesel and gasoline emissions	Rat alveolar cell line NR8.383 (ATCC)	ROS generation (DTT and macrophage-ROS assays)	-	Biodiesel and petro-diesel emissions cause more ROS; soluble Fe is strongly (R=0.99) associated with ROS production

Brito *et al*. (2010)	Acute cardiovascular and inflammatory toxicity induced by inhalation of diesel and biodiesel exhaust particles	Airborne fraction of diesel and biodiesel emissions	Male Balb/c mice	Heart rate, heart rate variability (HRV), blood pressure; counts of red blood cells, platelets and white blood cells, fibrinogen, activated partial thromboplastin time, prothrombin time and thrombin time; bronchoalveolar lavage and lung histology; total count of bone marrow cells	550 µg/m^3 for 1h (corresponding to 22.9 µg/m^3 for 24h)	Biodiesel emissions are more toxic than diesel emissions, causing inflammation, bone marrow activation, increased platelets and increased HRV
Li *et al*. (2013)	Effects of exposure to nanoparticle-rich diesel exhaust on pregnancy in rats	Airborne fraction of diesel emissions (DE) and filtered diesel emissions (F-DE)	Pregnant Fischer rats (F344/DuCrlCrli)	Radioimmunoassay (RIA); RNA isolation, quantitative real-time polymerase chain reaction (PCR)	DE: 148.86 µg/m^3; F-DE: 3.10 µg/m^3; for 5 h/day, for 19 days	Diesel emissions, even in low doses (F-DE), disrupts steroid hormone production in the corpus luteum and adrenal cortex in pregnant rats, which may lead to abortion and impairment of the fetus development

Künzi *et al.* (2015)	Toxicity of aged gasoline exhaust particles to normal and diseased airway epithelia	Airborne fraction of gasoline emissions	Re-differentiated HBE and BEAS-2B cells	Cytotoxicity (lactate dehydrogenase release); inflammatory response (IL-6, IL-8, MCP-1, TNF-α)	-	Gasoline emissions, even after single, short-time exposure, increase necrotic cell death, and decrease cytokine release in cystic fibrosis epithelia

Brake-wear emissions						
Gasser *et al.* (2009)	Toxic effects of brake-wear particles on epithelial lung cells *in vitro*	Airborne fraction of emissions from low-metallic (LM) brake pad; bimodal PSD, with peaks ~60 nm and ~375 nm	Human lung epithelial cells (A549)	Cytotoxicity (lactate dehydrogenase release), fluorescence, release of IL-8	-	Brake-wear particles damage tight junctions, cause oxidative stress and increase pro-inflammatory responses
Kukutschová *et al*. (2009)	Wear mechanism in automotive brake materials, wear debris and its potential environmental impact	Ball-milled semi-metallic (SM) brake pad; non-airborne fraction of emissions from SM brake pad	Auxothropic *Salmonella typhimurium* His- strain (TA98); male rats	Ames test; SOS chromotest, pulmonary toxicity test	Ames test and SOS chromotest: 100 mg/ml; pulmonary toxicity test: 0.5, 1.0 and 3 mg/ml for 1, 3 and 7 days	Brake-wear particles damage DNA after metabolic activation. Exposure to ball-milled particles caused acute response of the lung tissue
Zhao *et al.* (2015)	Physico-chemical characterization and oxidative reactivity evaluation of aged brake-wear particles	Brake drums of different age	Human alveolar adenocarcinoma cells (A549)	Cellular (DCFH-DA) and acellular (DCFH) ROS generation	2, 5, 10 and 100 µg/ml	Brake-wear particles cause acellular ROS generation (dose dependent response)

Kazimirova *et al*. (2016)	Automotive airborne brake-wear debris nanoparticles and cytokinesis-block micronucleus assay in peripheral blood lypmhocytes: A pilot study	Airborne fraction of emissions from LM brake pad (brake pad designed by authors)	Peripheral blood lymphocytes	Cytokinesis-block micronucleus test (MNBNC & CBPI)	5.4, 27 and 135 µg/ml	Brake-wear particles induce chromosomal damage
Malachova *et al*. (2016)	Toxicity and mutagenicity of low-metallic automotive brake pad materials	Ball-milled LM brake pad and ‘non-airborne’ fraction of emissions from LM brake pad	Marine strain *Vibrio fischeri*; plate-incorporation version of the *Salmonella typhimurium*	Acute aquatic toxicity (bacterial bioluminescence assay); Ames test; SOS chromotest	50-450 µg/plate; 50-425 µg/ml	Brake-wear emissions are highly toxic; mutagenicity was not estimated due to high toxicity effects
Barosova *et al.* (2018)	Biological response of an in vitro human 3D lung cell model exposed to brake-wear debris varies based on brake pad formulation	Non-airborne emissions from LM and non-asbestos organic (NAO) brake pads; airborne fractions (0.25 – 1 µm, 1-2 µm and 2-4 µm) of emissions from LM brake pad	3D human alveolar lung model	Cell morphology, cell viability (propidium iodide assay), oxidative stress response (GSH), inflammatory response (ELISA; TNF-α, IL-1β, IL-8)	Non-airborne fractions: 0.5, 1.0 and 2.0 mg/ml; airborne fractions: 33 µg/ml	Brake-wear emissions from NAO cause morphology changes, decrease cell viability and invoke release of IL-8

Puisney *et al.* (2018)	Brake-wear (nano)particle characterization and toxicity on airway epithelial cells *in vitro*	Brake-wear emissions from LM brake pad; NP fraction: 50 – 150 nm (median: 66 nm) and non-airborne fraction	Bronchial epithelial cells (Calu-3)	Mitochondrial damage (WST-1); oxidative stress (fluorescence marker); pro-inflammatory response (ELISA; IL-6; IL-8; TNF-α)	3, 15, 30, 75, 150, 300 µg/ml	Brake-wear emissions cause mitochondrial damage (both fractions), increased ROS production (both fractions); 'non'airborne' fraction cause release of IL-6
Gerlofs-Nijland *et al.* (2019)	Inhalation toxicity profiles of particulate matter: a comparison between brake-wear with other sources of emission	Brake-wear emissions ($PM_{2.5}$) from LM, SM, NAO brake pads	Female BALB/cOlaHsd mice	Cytotoxicity (LDH release); pro-inflammatory response (Bio-PLex Pro Mouse Cytokine Group-I 8-plex and Group-II 2-plex assays; inflammatory response (IL-1β, IL-6, IL-12(p40 and p70), G-CSF, KC, MCP-1, TNF-α, IL-18 and MIP-2); oxidative stress (GSH)	9 mg/m^3 (0.009 µg/ml)	Brake-wear emissions are not cytotoxic and do not cause oxidative stress; brake-wear emissions induce inflammatory response (the strongest effect for NAO)

Rajhelová *et al.* (2019)	Determination of oxidative potential caused by brake-wear debris in non-cellular systems	Airborne and non-airborne fraction of brake-wear emissions from 10 different LM brake pads	Acellular system	Lipid peroxidation (LP); carbonylation of proteins (PC)	-	Both non-airborne and airborne fractions of brake-wear emissions induce oxidative stress in acellular systems

Tire wear emissions						
Gualtieri *et al.* (2005)	Impact of tire debris on *in vitro* and *in vivo* systems	Tire wear emissions (TWE); fraction <1 mm	Human lung epithelial cells (A549); human liver cells (HepG2); frog *Xenopus laevis* (XL) embryos	A549: Cell viability (Trypan Blue); DNA damage (Comet assay); HepG2: effects of $ZnSO_4 \cdot 7H_2O$; XL: FETAX test	A549: 10, 50, 60 and 75 µg/ml of TWE for 24, 48 and 72h; HepG2: 0.05 – 50 µg/ml of Zinc for 2, 4 and 24h; XL: 50, 80, 100 and 120 µg/ml of TWE for 120h	Tire emissions are toxic to human A549 cells, affecting cell morphology, cell proliferation and DNA, and producing severe malformations in developing XL embryos
Lindbom *et al.* (2006)	Exposure to wear particles generated from studded tires and pavement induces inflammatory cytokine release from human macrophages	Tire and road wear emissions; PM_{10} fraction	Human monocyte-derived macrophages; nasal epithelial cells (RPMI 2650); bronchial epithelial cells (BEAS-2B)	Inflammatory response (IL-6, IL-8, IL-10 and TNF-α); cell viability (Trypan Blue); endotoxin content (LPS; *Escherichia coli*)	10, 50, 100, 250 and 500 µg/ml; for LPS only 1 µg/ml	Tire/road wear emissions have an inflammatory effect on macrophages

Lindbom *et al.* (2007)	Wear particles generated from studded tires and pavement induces inflammatory reactions in mouse macrophage cells	Tire and road wear emissions; PM_{10} fraction	Murine macrophage like cell line (RAW 264.7)	Inflammatory response (IL-6, TNF-α); NO content; lipid peroxidation, formation of ROS (DTT); arachidonic acid (AA) release; cell viability (Trypan Blue); endotoxin content (EPS; *Escherichia coli*)	1, 10, 25, 50, 75 and 100 µg/ml for 18h	Tire/road wear emissions induce inflammatory cytokine release, NO, lipid peroxidation and ROS formation

Subway emissions						
Karlsson *et al.* (2005)	Subway particles are more genotoxic than street particles and induce oxidative stress in cultured human lung cells	PM_{10} from a subway station and nearby busy street	Human lung epithelial cells (A549)	DNA damage (Comet assay); oxidative stress (8-oxodG formation)	Comet assay: 50 µg/ml; 8-oxodG: 9-70 µg/ml;	Subway-derived emissions are approximately 8 times more genotoxic and 4 times more potent to cause oxidative stress than roadside PM_{10}
Karlsson *et al.* (2006)	Comparison of genotoxic and inflammatory effects of particles generated by wood combustion, a road simulator and collected from street and subway	PM from burning dry wood and wood pellets; PM_{10} of tire/road wear; PM_{10} from a subway station and busy street	Human lung epithelial cells (A549); human macrophages	A549: DNA damage (Comet assay); macrophages: inflammatory response (IL-6, IL-8 and TNF-α)	A549: 70 µg/ml for 4h; macrophages: 50 µg/ml	Subway-derived emissions are the most genotoxic, compared to other studied emissions; they cause DNA damage and inflammatory response

Karlsson *et al.* (2008)	Mechanisms related to the genotoxicity of particles in the subway and from other sources	PM_{10} from a subway station and busy street; PM_{10} of tire/road wear; PM from burning dry wood; diesel PM emissions; fraction <5 µm of Fe_3O_4, Fe_2O_3 and CuO; fraction <50 µm of Cu/Zn	Human lung epithelial cells (A549)	Mitochondrial depolarization (TMRE); intracellular ROS production (DCFH-DA); DNA damage (Comet assay)	TMRE: 70 µg/ml for 8h; DCFH-DA: 35 µg/ml for 2h; Comet assay: 50 µg/ml	Subway-derived emissions cause mitochondrial depolarization and intracellular ROS production
Loxham *et al.* (2013)	Physicochemical characterization of airborne particulate matter at a mainline underground railway station	$PM_{10-2.5}$, $PM_{2.5}$ and $PM_{0.18}$ of woodstove emissions, road wear simulator, from a subway station and busy street	Primary bronchial epithelial cells (PBEC)	DCF fluorescence (H_2DCF-DA dye)	25 and 50 µg/ml	Subway-derived emissions cause ROS generation; with $PM_{0.18}$ being the most potent
Janssen *et al.* (2014)	Oxidative potential of particulate matter collected at sites with different source characteristics	PM_{10} and $PM_{2.5}$ from a subway station, busy road and urban background site	Acellular system	Oxidative potential (acellular assays: dithiothreitol (DTT), electron spin resonance (ESR) and ascorbate depletion (AA))	-	Subway-derived emissions cause oxidative stress, and have higher oxidative potential than roadside PM

Loxham *et al.* (2015)	The effects on bronchial epithelial mucociliary cultures of coarse, fine, and ultrafine particulate matter from an underground railway station	$PM_{10-2.5}$, $PM_{2.5}$ and $PM_{0.18}$ from a subway station	Primary bronchial epithelial cells (PBEC)	Lipopolysaccharide (LPS) content; lactate dehydrogenase (LDH) release; inflammatory response (IL-8); FITC-dextran passage; expression of HO-1 and NQO1 (qPCR assay), and ubiquitin C and glyceraldehyde 3-phosphate dehydrogenase (PrimerDesign); ROS generation (DCF dye)	-	Subway-derived emissions cause inflammatory response and ROS production; $PM_{0.18}$ fraction cause more severe effects than $PM_{2.5}$ and $PM_{10-2.5}$; nano-sized PM has ability to penetrate the mucous layer
Moreno *et al.* (2017a)	Oxidative potential of subway $PM_{2.5}$	$PM_{2.5}$ from 6 different subway stations	Acellular system	Oxidative potential (ascorbic acid, urate and reduced glutathione content)	-	Oxidative potential of subway-derived emissions is probably associated with metallic trace elements like Cu and Sb

			Aircraft emissions			
He *et al*. (2018)	Pro-inflammatory responses to $PM_{0.25}$ from airport and urban traffic emissions	Ambient $PM_{0.25}$ collected at an airport; turbine and diesel emissions	Human bronchial epithelial cells (16HBE)	Redox activity (AA; ascorbic acid depletion assay); hydroxyl radical generation (electron spin resonance assay); cell viability (MTS assay); ROS activity (H2-DCFDA assay); inflammatory response (IL-6, IL-8 and TNF-α)	AA: 12.5 µg/ml for 2h; MTS: 5 – 160 µg/ml	Airport-related emissions affect cell viability, promote ROS generation and activate inflammatory responses

Shipping emissions						
Oeder *et al.* (2015)	Particulate matter from both heavy fuel oil and diesel fuel shipping emissions show strong biological effects on human lung cells at realistic and comparable *in vitro* exposure conditions	Airborne fraction of exhaust emissions from a ship engine running on heavy fuel oil (HFO) and cleaner-burning diesel fuel (DF)	Human lung epithelial cells (A549); human SV40-immortalised bronchial epithelial cells (BEAS-2B)	A549: SILAC-proteome, metabolome and metabolic flux measurement, cytotoxicity assay; BEAS-2B: transcriptome	-	Shipping-derived HFO emissions cause oxidative stress and inflammatory responses, whereas DF emissions induce broader biological response by affecting energy metabolism, protein synthesis and chromatin modification
Sapcariu *et al.* (2016)	Metabolic profiling as well as stable isotope assisted metabolic and proteomic analysis of RAW 264.7 macrophages exposed to ship engine aerosol emissions: Different effects of heavy fuel oil and refined diesel fuel	$PM_{2.5}$ of exhaust emissions from a ship engine running on heavy fuel oil (HFO) and diesel fuel (DF)	Mouse macrophage cell line (RAW 364.7)	Lactate dehydrogenase (LDH) content; metabolomics, proteomics	HFO: 760 µg/m^3; DF: 340 µg/m^3	Shipping-derived DF emissions are more cytotoxic than HFO; gas phase of HFO induce inflammatory response

Mousavi *et al*. (2019)	Impact of emissions from the ports of Los Angeles and Long Beach on the oxidative potential of ambient $PM_{0.25}$ measured across the Los Angeles County	Ambient $PM_{0.25}$ collected at 3 sites close to ports	Rat alveolar cells (NR8383)	Cell-based alveolar macrophage (AM) assay	-	Shipping-derived $PM_{0.25}$ is responsible for 16 ± 5% of $PM_{0.25}$ oxidative potential of total $PM_{0.25}$

Table A6: Total particle number and mass of brake dust emissions obtained with the ELPI®+ impactor (DEKATI, Finland) during a dynamometer test. Each sample stage corresponds to different mean aerodynamic diameters (D_i) (Verma *et al*., 2016).

Stage	Di [µm]	Total particle number [#/cm³]	Total particle mass [g/m³]
15	10	-	-
14	6.8	0.25 million	69.6
13	4.4	0.44 million	31.1
12	2.5	0.86 million	13.1
11	1.6	2.2 million	8.5
10	1.0	2.9 million	2.8
9	0.64	3.5 million	0.81
8	0.40	11.7 million	0.68
7	0.26	18.4 million	0.29
6	0.17	59.5 million	0.24
5	0.108	253.8 million	0.22
4	0.060	1.9 billion	0.36
3	0.030	7.9 billion	0.24
2	0.017	26.0 billion	0.13

Table A7: Selected magnetic parameters for exhaust and brake-wear emissions.

Magnetic parameter	**Brake emissions** Mean (st. dev.)	**Gasoline emissions** Mean (st. dev.)	**Diesel emissions** Mean (st. dev.)
χ* [10^{-8} m^{3}kg^{-1}]	15 819 (10 360)	1107 (763.3)	298.3 (307.5)
SIRM(300K)* [10^{-3} Am^{2}kg^{-1}]	884.6 (356.1)	134.9 (80.0)	26.2 (26.8)
ARM* [10^{-6} Am^{2}kg^{-1}]	13 783 (4 732)	1606 (736.3)	358.5 (297.4)
Bcr* [mT]	17.4 (14.0)	31.0 (5.4)	33.1 (8.6)
SIRM/κ* [10^3 Am^{-1}]	6.7 (2.5)	13.8 (6.3)	14.5 (12.1)
Bc(160K)**	6.2 (-)	9.8 (-)	-
Bc(10K)**	36.8 (-)	27.8 (-)	-
Bc(10K)/Bc(160K)**	5.9 (-)	2.8 (-)	-
SIRM(10K)/SIRM(160K)**	4.1 (-)	2.7 (-)	-

*Chaparro *et al.* (2010); **Sagnotti & Winkler (2012); χ – specific magnetic susceptibility, SIRM(10 K, 160 K, 300 K) – saturation isothermal remanent magnetization measured at 10 K, 160 K and 300 K, respectively, ARM – anhysteretic remanent magnetization, B_{cr} – coercivity of remanence, κ – volume magnetic susceptibility, B_c(10 K, 160 K) – coercivity measured at 10 K and 160 K, respectively.

Table A8: Inventory table of reported magnetic studies on pumped-air filters and tree leaves; κ – volume magnetic susceptibility; χ – specific magnetic susceptibility; IRM_{300} – isothermal remanent magnetization at 300 mT; SIRM – saturation isothermal remanent magnetization, NRM – natural remanent magnetization; M_S – saturation magnetization; χ_{ARM} – anhysteretic magnetic susceptibility.

Reference	Title	Location	Magnetic parameters	Values
PM collected on filters				
Morris *et al*. (1995)	Preliminary comparisons between mutagenicity and magnetic susceptibility of respirable airborne particulate	Hamilton, Ontario, USA	κ	$0\text{-}25\cdot 10^{-6}$ [CGS]
Shu *et al*. (2001)	Determining the sources of atmospheric particles in Shanghai, China, from magnetic and geochemical properties	Shanghai, China	χ SIRM	$213\text{-}2853\cdot 10^{-8}\ m^3kg^{-1}$ $21\text{-}549\cdot 10^{-3}\ Am^2kg^{-1}$
Muxworthy *et al*. (2001)	Comparison between magnetic parameters of urban atmospheric particulate matter with pollution and meteorological data	Munich, Germany	M_S	$(510\pm 70)\cdot 10^{-3}\ Am^2kg^{-1}$
Muxworthy *et al*. (2003)	Magnetic signature of daily sampled urban atmospheric particles	Munich, Germany	SIRM	$32\text{-}44\cdot 10^{-3}\ Am^2kg^{-1}$

Gómez-Paccard *et al.* (2004)	Low-temperature and high magnetic field measurements of atmospheric particulate matter	Madrid, Spain	χ SIRM	- -
Spassov *et al.* (2004)	Magnetic quantification of urban pollution sources in atmospheric particulate matter	Switzerland	χ_{ARM}	-
Sagnotti *et al.* (2006)	Magnetic properties of atmospheric particulate matter from automatic air sampler stations in Latium (Italy): Toward a definition of magnetic fingerprints for natural and anthropogenic PM$_{10}$ sources	Latium, Italy	χ	$11\text{-}4378 \cdot 10^{-8}$ m^{3}kg^{-1}
Halsall *et al.* (2008)	A novel approach to investigating indoor/outdoor pollution links: Combined magnetic and PAH measurements	Lancaster, UK	SIRM	$7\text{-}167 \cdot 10^{-3}$ Am^{2}kg^{-1}
Górka-Kostrubiec *et al.* (2012)	Dependence of air pollution on meteorological conditions based on magnetic susceptibility measurements: a case study from Warsaw	Warsaw, Poland	χ	$< 2500 \cdot 10^{-8}$ m^{3}kg^{-1}
Petrovský *et al.* (2013)	Magnetic particles in atmospheric particulate matter collected at sites with different level of air pollution	Bartovice, Prague and Košetice, Czech Republic	SIRM	$28\text{-}2400 \cdot 10^{-6}$ Am^{-1}

Revuelta *et al*. (2014)	Partitioning of magnetic particles in PM$_{10}$, PM$_{2.5}$ and PM$_{1}$ aerosols in the urban atmosphere of Barcelona (Spain)	Barcelona, Spain	χ SIRM	$30\text{-}200\cdot10^{-10}$ m $16\text{-}109\cdot10^{-6}$ A
Cao *et al*. (2015)	An economic passive sampling method to detect particulate pollutants using magnetic measurements	Linfen, China	χ SIRM	$297\text{-}15847\cdot10^{-8}$ m^{3}kg^{-1} -
Gargiulo *et al*. (2016)	Magnetic properties of air suspended particles in thirty eight cities from south India	Tamil Nadu, India	χ SIRM χ_{ARM}	$14\text{-}9533\cdot10^{-8}$ m^{3}kg^{-1} $3\text{-}700\cdot10^{-3}$ Am^{2}kg^{-1} $57\text{-}5246\cdot10^{-8}$ m^{3}kg^{-1}
Jeleńska *et al*. (2017)	Evaluation of indoor/outdoor urban air pollution by magnetic, chemical and microscopic studies	Warsaw, Poland	χ	$132\text{-}2715\cdot10^{-8}$ m^{3}kg^{-1}
		Tree leaves		
Flanders (1994)	Collection, measurement, and analysis of airborne magnetic particulates from pollution in the environment	-	NRM	-
Schaedlich *et al*. (1995)	Magnetic susceptibility in conifer needles as indicator of fly ash deposition	Liepzig, Germany	χ	-

Matzka & Maher (1999)	Magnetic biomonitoring of roadside tree leaves: identification of spatial and temporal variations in vehicle-derived particulates	Norwich, UK	IRM_{300}	$14\text{-}110\cdot10^{-6}$ A
Hanesch *et al*. (2003)	Mapping dust distribution around an industrial site by measuring magnetic parameters of tree leaves	Leoben, Austria	χ SIRM	$-2\text{-}325\cdot10^{-10}$ m $2\text{-}306\cdot10^{-6}$ A
Jordanova *et al*. (2003)	Magnetic response of soils and vegetation to heavy metal pollution – A case study	Sofia, Bulgaria	χ	$3\text{-}93\cdot10^{-8}$ m^3kg^{-1}
Moreno *et al*. (2003)	Biomonitoring of traffic air pollution in Rome using magnetic properties of tree leaves	Rome, Italy	χ SIRM	$0.2\text{-}49\cdot10^{-8}$ m^3kg^{-1} $0.3\text{-}1.3\cdot10^{-3}$ Am^2kg^{-1}
Urbat *et al*. (2004)	Biomonitoring of air quality in the Cologne conurbation using pine needles as a passive sampler – Part I: magnetic properties	Cologne, Germany	χ SIRM	$-0.1\text{-}16\cdot10^{-8}$ m^3kg^{-1} $11\text{-}107\cdot10^{-3}$ $Am^{-1}kg^{-1}$
Gautam *et al*. (2005)	Magnetic susceptibility of dust-loaded leaves as a proxy of traffic-related metal pollution in Kathmandu city, Nepal	Kathmandu, Nepal	χ	$0.01\text{-}54\cdot10^{-8}$ m^3kg^{-1}
Pandey *et al*. (2005)	Magnetic properties of vehicle-derived particulates and amelioration by *Ficus infectoria*: a keystone species	Singrauli, India	IRM_{300}	$16\text{-}85\cdot10^{-6}$ A

Davila *et al.* (2006)	Mapping the sources of urban dust in a coastal environment by measuring magnetic parameters of *Platanus hispanica* leaves	Vigo, Spain	SIRM	0.0004 – 0.0224·10^{-6} A
Lehndorff *et al.* (2006)	Accumulation histories of magnetic particles on pine needles as function of air quality	Cologne, Germany	χ SIRM	-0.5-8·10^{-8} m^{3}kg^{-1} 7-91 Am^{-1}kg^{-1}
Zhang *et al.* (2006)	Magnetic properties of high-road-side pine tree leaves in Beijing and their environmental significance	Beijing, China	χ SIRM	10-80·10^{-8} m^{3}kg^{-1} 2-12·10^{-3} Am^{2}kg^{-1}
Szönyi *et al.* (2007)	On leaf magnetic homogeneity in particulate matter biomonitoring studies	Rome, Italy	SIRM M_S	490-570·10^{-6} A 4600-6400·10^{-6} A
McIntosh *et al.* (2007)	The magnetic properties of particles deposited on *Platanus x hispanica* leaves in Madrid, Spain, and their temporal and spatial variations	Madrid, Spain	χ SIRM	-11-173·10^{-10} m 1-108·10^{-6} A
Hu *et al.* (2008)	Magnetic response to atmospheric heavy metal pollution recorded by dust-loaded leaves in Shougang industrial area, western Beijing, China	Beijing, China	χ SIRM	8-129·10^{-8} m^{3}kg^{-1} 1-28·10^{-3} Am^{2}kg^{-1}

Maher *et al.* (2008)	Spatial variation in vehicle-derived metal pollution identified by magnetic and elemental analysis of roadside tree leaves	Norwich, UK	SIRM	$27-96\cdot10^{-6}$ A
Szönyi *et al.* (2008)	A refined biomonitoring study of airborne particulate matter pollution in Rome, with magnetic measurements on *Quercus Ilex* tree leaves	Rome, Italy	χ	$1-70\cdot10^{-8}$ m^3kg^{-1}
Mitchell & Maher (2009)	Evaluation and application of biomagnetic monitoring of traffic-derived particulate pollution	Lancaster, UK	SIRM χ_{ARM}	$2-332\cdot10^{-6}$ A $7-704\cdot10^{-8}$ A
Sagnotti *et al.* (2009)	Compositional, morphological, and hysteresis characterization of magnetic airborne particulate matter in Rome, Italy	Rome, Italy	SIRM M_S	- -
Jordanova *et al.* (2010)	Magnetic signature of different vegetation species in polluted environment	Sofia and Plovdiv, Bulgaria	χ SIRM	$0.6-846\cdot10^{-8}$ m^3kg^{-1} $0.07-1.99\cdot10^{-3}$ Am^2kg^{-1}
Mitchell *et al.* (2010)	Rates of particulate pollution deposition onto leaf surfaces: temporal and inter-species magnetic analyses	Lancaster, UK	SIRM	$1-550\cdot10^{-6}$ A

Quayle *et al*. (2010)	Application and evaluation of biomagnetic and biochemical monitoring of the dispersion and deposition of volcanically-derived particles at Mt. Etna, Italy	Mt. Etna, Italy	χ SIRM	$0\text{-}75\cdot10^{-10}$ m $14\text{-}165\cdot10^{-6}$ A
Hansard *et al*. (2011)	Biomagnetic monitoring of industry-derived particulate pollution	An industrial site, South England	SIRM χ_{ARM}	$2\text{-}13\cdot10^{-6}$ A -
Kardel *et al*. (2011)	Leaf saturation isothermal remanent magnetization (SIRM) as a proxy for particulate matter monitoring: Inter-species differences and in-season variation	Ghent, Belgium	SIRM	$0.05\text{-}3.1\cdot10^{-3}$ Am^2kg^{-1}
Hansard *et al*. (2012)	Rapid magnetic biomonitoring and differentiation of atmospheric particulate pollutants at the roadside and around two major industrial sites in the U.K.	Port Talbot, UK	SIRM χ_{ARM}	$2\text{-}400\cdot10^{-6}$ A -
Kardel *et al*. (2012)	Intra-urban spatial variation of magnetic particles: Monitoring via leaf saturation isothermal remanent magnetisation (SIRM)	Ghent, Belgium	SIRM	$4\text{-}777\cdot10^{-6}$ A
Aguilar Reyes *et al*. (2012)	*Ficus benjamina* leaves as indicator of atmospheric pollution: a reconnaissance study	Morelia, Mexico	χ SIRM	$1\text{-}12\cdot10^{-8}$ m^3kg^{-1} $0.5\text{-}13\cdot10^{-3}$ Am^2kg^{-1}

Sadeghian (2012)	Biomonitoring of vehicles derived particulate matter using magnetic properties of *Ulmus carpinifolia* leaves	Isfahan, Iran	IRM$_{300}$	$10-90\cdot10^{-6}$ A
Sant'Ovaia *et al*. (2012)	Particle pollution – An environmental magnetism study using biocollectors located in northern Portugal	Braga, Porto, Valongo and Trancoso-Reboleiro, Portugal	χ SIRM	$-0.9-29\cdot10^{-8}$ m^3kg^{-1} $0.037-2.1\cdot10^{-3}$ Am^2kg^{-1}
Hofman *et al*. (2013)	Spatial distribution assessment of particulate matter in an urban street canyon using biomagnetic leaf monitoring of tree crown deposited particles	Ghent, Belgium	SIRM	$4-64\cdot10^{-6}$ A
Aguilar Reyes *et al*. (2013)	Reconnaissance environmental magnetic study of urban soils, dust and leaves from Bogotá, Colombia	Bogotá, Colombia	χ SIRM	- -
Van Wittenberghe *et al*. (2013)	Upward and downward solar-induced chlorophyll fluorescence yield indices of four tree species as indicators of traffic pollution in Valencia	Valencia, Spain	SIRM	$10-189\cdot10^{-6}$ A
Yin *et al*. (2013)	Magnetic properties of tree leaves and their significance in atmospheric particle pollution in Linfen City, China	Linfen, China	χ SIRM	$12-130\cdot10^{-8}$ m^3kg^{-1} $0.002-0.13\cdot10^{-3}$ Am^2kg^{-1}

Barima *et al.* (2014)	Assessing atmospheric particulate matter distribution based on saturation isothermal remanent magnetization of herbaceous and tree leaves in a tropical urban environment	Abidjan, Ivory Coast	SIRM	$< 45\cdot10^{-6}$ A
Hofman *et al.* (2014a)	Increasing the spatial resolution of air quality assessments in urban areas: A comparison of biomagnetic monitoring and urban scale modelling	Antwerp, Belgium	SIRM	$34\text{-}640\cdot10^{-6}$ A
Hofman *et al.* (2014b)	On the link between biomagnetic monitoring and leaf-deposited dust load of urban trees: Relationships and spatial variability of different particle size fractions	Antwerp, Belgium	SIRM	$43\text{-}234\cdot10^{-6}$ A
Hofman *et al.* (2014c)	On the temporal variation of leaf magnetic parameters: Seasonal accumulation of leaf-deposited and leaf-encapsulated particles of a roadside tree crown	Antwerp, Belgium	SIRM	$14\text{-}73\cdot10^{-6}$ A
Rai *et al.* (2014)	Monitoring of spatial variations of particulate matter (PM) pollution through bio-magnetic aspects of roadside plant leaves in an Indo-Burma hot spot region	Mizoram, India	χ SIRM	$110\text{-}280\cdot10^{-8}$ m^3kg^{-1} $1.5\text{-}2.7\cdot10^{-3}$ Am^2kg^{-1}

Rai & Chutia (2014)	Biomagnetic monitoring of atmospheric particulate matter pollution through roadside tree leaves in Aizawl city, Mizoran and their temporal and spatial varitions	Aizawl, India	χ SIRM	$111-244\cdot10^{-8}$ m^{3}kg^{-1} $1.2-2.8\cdot10^{-3}$ Am^{2}kg^{-1}
Rodríguez-Germade *et al.* (2014)	The influence of weather and climate on the reliability of magnetic properties of tree leaves as proxies for air pollution monitoring	Madrid, Spain	χ	$-0.9-32\cdot10^{-8}$ m^{3}kg^{-1}
Cao *et al.* (2015)	An economic passive sampling method to detect particulate pollutants using magnetic measurements	Linfen, China	χ SIRM	$2-504\cdot10^{-8}$ m^{3}kg^{-1} $0.4-65.0\cdot10^{-3}$ Am^{2}kg^{-1}
Chaparro *et al.* (2015)	An interval fuzzy model for magnetic biomonitoring using the specie *Tillandsia recurvata L*	Santiago de Querétaro, Mexico	χ SIRM	$2-172\cdot10^{-8}$ m^{3}kg^{-1} $0.8-28.8\cdot10^{-3}$ Am^{2}kg^{-1}
Castanheiro *et al.* (2016)	Magnetic- and particle-based techniques to investigate metal deposition on urban green	Antwerp, Belgium	SIRM	$20-444\cdot10^{-6}$ A

Norouzi *et al.* (2016)	Biomagnetic monitoring of heavy metals contamination in deposited atmospheric dust, a case study from Isfahan, Iran	Isfahan, Iran	χ	$1\text{-}12\cdot10^{-8}\ \mathrm{m^3kg^{-1}}$
Brackx *et al.* (2017)	Hyperspectral leaf reflectance of *Carpinus betulus L.* samplings for urban air quality estimation	Antwerp, Belgium	SIRM	$50\text{-}370\cdot10^{-6}\ \mathrm{A}$
Kardel *et al.* (2018)	Biomonitoring of atmospheric particulate pollution via chemical composition and magnetic properties of roadside tree leaves	Babolsar, Babol and Boumehen, Iran	SIRM	$<7.8\cdot10^{-3}\ \mathrm{Am^2kg^{-1}}$
Leng *et al.* (2018)	Leaf magnetic properties as a method for predicting heavy metal concentrations in $PM_{2.5}$ using support vector machine: A case study in Nanjing, China	Nanjing, China	χ SIRM χ_{ARM}	$0.3\text{-}8.0\cdot10^{-8}\ \mathrm{m^3kg^{-1}}$ $0.1\text{-}1.0\cdot10^{-3}\ \mathrm{Am^2kg^{-1}}$ $0.3\text{-}16.6\cdot10^{-8}\ \mathrm{m^3kg^{-1}}$

Table A9: Stages (size-fractions) of particles collected by Dekati ELPI+ impactor.

Stage	D_{50} [µm]
1	0.016
2	0.030
3	0.054
4	0.094
5	0.150
6	0.250
7	0.380
8	0.600
9	0.940
10	1.6
11	2.5
12	3.6
13	5.3
14	10

Appendix B (Paper IV): Prolific shedding of magnetite nanoparticles from banknote surfaces

Abstract

Here, we use magnetic methods first to quantify the content of strongly magnetic particles of banknotes (US dollars, USD, and British pounds sterling, GBP), and then examine the possibility of their release from handled banknote surfaces. The content of magnetic particles, from magnetic remanence measurements, for the USD and paper GBP banknotes is high; greater, for example, than that in vehicle engine-exhaust emissions, and similar to that for airborne roadside particulate matter (PM). Our magnetic analyses of USD and GBP banknotes, and of the ink pigment widely used in their printing, reveal not only that the banknotes are highly magnetic, but also that strongly magnetic, nano-sized particles are readily and prolifically shed from their surfaces (especially from the USD banknotes). A common practice, prior to increased automation, was for bank tellers to count banknotes by licking a finger to adhere to each successive counted note, and thus speed up the manual counting process. Given the rate of particle shedding reported here, this traditional manual counting procedure must have resulted in prolific transfer of iron-rich nanoparticles both to the fingers and thence to the tongue. We hypothesise that, pre-automation, magnetite and other metal-bearing nanoparticles were repetitively and frequently ingested by bank tellers, and subsequently entered the brain directly via the taste nerve pathway, and/or indirectly via the systemic circulation and the neuroenteric system. This hypothesis may plausibly account for the reported and currently unexplained association between elevated neurodegeneration-related mortality odds ratios and this specific occupation.

Published:

Maher, B. A.; Gonet, T. Prolific shedding of magnetite nanoparticles from banknote surfaces. *Science of the Total Environment* **2021**, 768, 144490.

LIST OF ABBREVIATIONS:

AD – Alzheimer’s disease
AF – alternating field
ARM – anhysteretic remanent magnetisation
CNS – central nervous system
DC – direct current
GBP – British pound sterling
$\mathrm{MDF}_{\mathrm{ARM}}$ – median destructive field of ARM
MND – motor neuron disease
MOR – mortality odds ratio
NDD – neurodegenerative disease
PAH – polycyclic aromatic hydrocarbon
PD – Parkinson’s disease
PM – particulate matter
PSD – pre-senile dementia
ROS – reactive oxygen species
SIRM – saturation isothermal remanent magnetisation or magnetic remanence
TEM – transmission electron microscopy
USD – United States dollar
χ_{ARM} – susceptibility of anhysteretic remanent magnetisation

Introduction

The global burden of neurodegenerative disease (NDD) continues to rise, with ~44 million individuals living with dementia (in 2016) and age-standardised incidence increasing from ~701 cases per 100,000 population in 1990 to 712 cases/100,000 population in 2016 (Nichols *et al*., 2019). Alzheimer's disease (AD) comprises the most prevalent NDD, accounting for 60 – 70% of NDD cases (WHO, 2019). Given the irreparable neuronal damage already incurred once dementia symptoms are manifest, prospects for post-onset therapeutic intervention and disease modification appear very limited. As dementia has severe, negative impacts on individuals, communities and health care systems, increased understanding of risk factors – and subsequent identification of potential pathways to prevention – thus become ever more important.

In comparison with studies of genetic and lifestyle factors, relatively little attention has so far been focused on potential NDD risk factors associated with an individual's occupation (Costa & Manzo, 1998). It is likely that occupational exposures to a range of potential neurotoxicants (Doty, 2008; Costa *et al.,* 2014; Pelclova *et al.,* 2016) might provide multiple routes to the common features of neuronal damage associated with NDD, including oxidative stress, protein misfolding and abnormal calcium signalling (Park *et al*., 2005).

Schulte *et al.* (1996) examined mortality data, from 1982 to 1991, in 27 USA states, and identified occupations with elevated mortality rates for AD, Parkinson's disease (PD), motor neuron disease (MND), and presenile dementia (PSD). In a follow-up, case-control study, Park *et al.* (2005) examined mortality and occupational data for deaths attributed or including reference to AD, PD, MND and PSD, for 22 participating USA states, for the period 1992–1998. In addition to testing the occupation/NDD associations identified in the original Schulte *et al*. (1996) study, Park *et al.* (2005) assessed hypothesized occupational exposure associations for solvents, magnetic fields, pesticides, and welding (Levy & Nassetta, 2003). For AD, the largest increases in mortality odds ratios (MORs) were associated with an apparently diverse range of occupations, including bank tellers, clergy, aircraft mechanics and hairdressers. For PSD, increased MORs were associated with dentists, clergy and graders/sorters (non-agricultural); for MND, veterinarians, hairdressers, and graders/sorters; for PD, teachers, biological scientists, and clergy. Farmers < 65 yrs in age displayed elevated MORs for PD, AD and PSD. Occupational exposure to 60 Hz magnetic fields displayed an exposure-response for AD, and for those <65 yrs, for PD and MND. Welding was associated with PD in those < 65 yrs in age at death.

Exposure to specific physical and chemical agents known to produce oxidative stress has been inferred to account form any of these observed associations between occupation and elevated MORs for NDD. For example, dentists have been exposed to mercury; farmers to organophosphate-rich pesticides; hairdressers to a range of solvents and often metal-bearing dyes; mechanics to engine emissions; welders to manganese. One occupational group reported by Park *et al.* (2005) to display significantly elevated MORs for AD (MOR = 1.40; 95% CI = 1.14 – 1.70; p = 0.001), yet arguably with no obvious route of neurotoxicant exposure, comprises U.S. bank tellers (who died in the interval 1992–1998).

With regard to development of AD and other NDDs, excess iron in some regions of the brain may represent a particular neurological threat. Iron overload can catalyse formation of damaging reactive oxygen species (ROS) via the Fenton reaction (Smith *et al*., 1997). Iron dyshomeostasis has been linked strongly to the pathogenesis of AD and other NDDs (e.g. Dobson, 2004; Zecca *et al*., 2004; Castellani *et al.,* 2007). Indeed, discrete nanoparticles of magnetite, a strongly magnetic mixed Fe^{2+}/Fe^{3+} iron oxide, have been found directly associated with AD plaques (Collingwood & Dobson, 2006; Quintana *et al*., 2006; Plascencia-Villa *et al.,* 2016).

It is possible, however, that endogenous sources and/or mishandling of iron by the brain may represent one part of a much wider problem. Exogenous particles of iron-rich, strongly magnetic magnetite and maghemite, co-associated with other 'exotic' (i.e. non-physiological) metal species (e.g. Cr, Pt, Ce, Mn) have recently been discovered in abundance in the frontal cortex (0.2 – 12 μg/g, corresponding to $2.7 \cdot 10^9 – 160 \cdot 10^9$ particles/g of freeze-dried tissue) and brainstem regions (0.01 – 2.63 μg/g, corresponding to $0.2 \cdot 10^9 – 33 \cdot 10^9$ particles/g of freeze-dried tissue) of the human brain (Maher *et al.*, 2016; Calderón-Garcidueñas *et al.,* 2020). Precisely-matching, iron-rich nanoparticles occur abundantly in airborne particulate pollution, including that emitted by traffic, arising from brake-wear, particularly, and from exhaust emissions (Maher *et al*., 2016; Gonet & Maher, 2019; Zhang *et al*., 2020). It appears that these iron-rich, airborne nanoparticles, prolific in urban airborne particulate matter (PM), can be transported readily into the brain, whether directly by inhalation via the olfactory bulb (Maher *et al.,* 2016), and/or through ingestion/swallowing and transfer via the gut wall and neuroenteric system

(Calderón-Garcidueñas *et al*., 2020), or indirectly by the systemic circulation (Lu *et al.,* 2020). Given the essential requirement for the brain to regulate tightly the location, transport and safe storage of iron (to avoid the risk of uncontrolled ROS formation), chronic intake of exogenous iron-rich nanoparticles into the brain may constitute a previously unrecognised environmental risk factor for disruption of key central nervous system (CNS) processes (Maher, 2019), including mitochondrial function, myelination and neurotransmitter signalling.

It is also possible that this new hypothesis, of a causal link between exposure to iron-rich pollution nanoparticles and development of NDD (Maher *et al.,* 2016; Maher, 2019), might account for several previously unresolved associations between occupation and NDD. Acute or chronic exposure would be predicted for occupations involving frequent and/or prolonged intervals of inhalation and/or ingestion of such iron- and co-associated metal-rich nanoparticles, produced in abundance by a notably diverse range of sources. In the outdoor environment, these sources include: traffic-related air pollution, arising from exhaust emissions and, especially, brake-wear (Gonet & Maher, 2019; Gonet *et al.,* 2021b); industrial emissions, especially from power generation plants (Szuszkiewicz *et al.,* 2015) and steelworks (Zajzon *et al.,* 2013); welding (Sowards *et al*., 2008) and biomass burning (McClean & Kean, 1993). At-risk occupations might therefore include professional drivers, engine mechanics, steelworkers, welders and farmers. In the indoor environment, iron-rich, and strongly magnetic nanoparticles are emitted from, for example, some printer inks (Gminski *et al.,* 2011), metal lathes (Chen *et al*., 2020), open fires (Maher *et al.,* 2021), and candles (Halsall *et al.,* 2008). At-risk occupations might thus also include, for example, office workers, and machinists.

Here, given the elevated MORs reported for NDD in US bank tellers (who died between 1992 and 1998; Park *et al.,* 2005), we examine magnetic properties of GBP and USD banknotes and the possibility of shedding of magnetite nanoparticles from the banknotes' surfaces. We use magnetic measurements to quantify the magnetic content of banknotes, and the release of strongly magnetic particles from their surfaces. We also assess the concentration and particle size of magnetic particles in Pigment Black 11 ink. Until very recently, the composition of banknotes has been cellulose-based, frequently coated with kaolinite (for opacity, and printability) and starch (for wet rub resistance). Universally, and over many decades, iron has been used in the black printing inks used in banknote production, in the form of the pigment known as 'Pigment Black 11', or 'Magnetic Black'. Not only do the banknotes display very high contents of ultrafine magnetite (especially the US dollars), they also shed magnetite particles prolifically from their surfaces. Given the elevated, currently unexplained

MORs for NDD reported for US bank tellers (who died between 1992 and 1998), we hypothesise that manual counting of banknotes (i.e., prior to automation from ~1980) resulted in exposure to these metal-rich particles through the taste nerve pathway, directly into the CNS, and/or via swallowing and transfer from the gut wall into the neuroenteric system, and/or dermal absorption. Such exposure through the working lifetime of these US bank tellers may constitute a plausible specific mechanism for excess CNS intake of iron-rich and co-associated toxic metals (specifically, lead), and subsequent neurodegeneration. Critically and prospectively, such a hypothesis would also indicate that, at the present day, occupations linked with excess exposure to iron-rich nanoparticles might also be causally linked with neurodegeneration. Further, newly developing technologies, such as metal 3D printing (Chen *et al.,* 2020), may be creating new versions of this specific occupational exposure and risk.

Materials and methods

To quantify the content and particle size of any magnetic particulates, and how easily such particles might be shed from the surfaces of banknotes, we made measurements of the magnetic remanence of a selection of banknotes. U.S. dollar (USD) and British pound sterling (GBP) banknotes were used. As paper banknotes were recently (2016 – 2020) replaced by polymer banknotes in the U.K., we measured both paper and polymer GBP notes; 3 banknotes of each type (paper and polymer) and value (£5, £10 and £20). For comparison, we measured circulated USD paper banknotes (3 USD banknotes of each value: \$1, \$5, \$10, \$20, \$50 and \$100).

Additionally, standard multipurpose wet wipes, which are magnetically 'clean', were used to assess whether strongly magnetic, iron-rich particles can be easily removed from the banknote surfaces. Each banknote was gently wiped for 45 s (each side). The wipes were magnetically measured before and after the wiping process; the difference was attributed to the magnetic particles removed from a banknote surface merely with wiping. We repeated the wiping experiment 3 times, using the same banknotes and new wet wipes each time.

All samples (the banknotes and pigment) were first dried for 24 h in a room with controlled temperature (20°C) and humidity (50%), and subsequently weighed, with a Mettler AT250 balance (accuracy of 0.00001 g). Each measurement was repeated 3 times. No metal tools were used during the laboratory work, to preclude any potential contamination of the samples.

In order to quantify the concentration of iron-rich particles in banknotes and wipes, magnetic remanence measurements were carried out. We used a Newport electromagnet to impart saturation isothermal remanent magnetisation (SIRM) to all samples at 1 Tesla (T) at room temperature. For the banknotes, an AGICO JR-6 spinner magnetometer (noise level ~$5 \cdot 10^{-11}$ Am^2) was used to measure the magnetic remanence (SIRM). Because of their weaker signal, we used a 2G RAPID cryogenic magnetometer (noise level ~10^{-11} Am^2) to measure the magnetic remanence (SIRM) of the wet wipes before and after they were used to simulate handling of the banknotes. Each measurement was repeated 3 times.

The susceptibility of anhysteretic remanent magnetisation (χ_{ARM}) was also measured both for the USD and GBP banknotes, and for the black ink pigment. This parameter is especially sensitive to the presence of magnetic grains ~30 – 50 nm in diameter (Özdemir & Banerjee, 1982; Maher, 1988). Anhysteretic remanent magnetisation (ARM) was imparted to all samples at 80 milliTesla (mT) in 4 different direct current (DC) biasing fields: 0.06 mT, 0.08 mT, 0.10 mT and 0.12 mT, and subsequently measured with a 2G RAPID cryogenic magnetometer. The susceptibility of ARM (χ_{ARM}) was calculated as the slope of the ARM(DC field) linear function.

The magnetite concentrations of the wet wipes, pre- and post-wiping of the banknotes, were estimated from experimental SIRM values for sized, synthetic magnetite powders (Maher, 1988). We used an SIRM value of 6.7 Am^2/kg (for grains < 200 nm; based on our observed particle size distribution of the ink pigment, see Results below) to estimate the mass of magnetite deposited on the wet wipes. We then estimated the number of magnetite particles on the wet wipes, assuming magnetite density of 5.15 g/cm^3 and grain size of ~60 nm (based on the median particle size of the banknote ink pigment, see Results below).

We made a similar suite of magnetic measurements on Pigment Black 11 (or 'Magnetic Black'; Cl 77499, Duranat), the ink long used internationally for printing banknotes. SIRM at 1 Tesla was imposed at room temperature using the Newport electromagnet and subsequently measured with a Molspin Minispin magnetometer (noise level ~10^{-9} Am^2). The SIRM measurements were conducted at room temperature, and, after cooling the sample with liquid nitrogen, at ~77 K. ARM was imparted using a Molspin demagnetiser with ARM attachment, and subsequently demagnetised in alternating fields (AF) of 5 mT, 10 mT, 15 mT, 20 mT, 50 mT and 100 mT. The ARM was measured using the Molspin Minispin magnetometer. The measurement of ARM after each step of AF demagnetisation enabled determination of MDF_{ARM} (median destructive field of ARM), i.e. the field required to demagnetise 50% of ARM. This parameter is helpful in determination of magnetite grain size (Maher, 1988).

All magnetic measurements were conducted at the Centre for Environmental Magnetism and Palaeomagnetism, Lancaster University, U.K.

The Pigment Black 11 was additionally analysed with transmission electron microscopy (TEM). Approximately 50 mg of ink pigment was first dispersed in 10 ml of ethanol. Then, 5 µl droplets of the suspension were placed on 2 TEM grids (holey carbon films on copper support grids), one selected at random and scanned using a FEI Titan3 Themis 300 STEM, operated at 300 kV. Imaging of the ink particles was used to obtain the particle size distribution, by measurement of 100 randomly-selected particles with well-defined crystal edges.

Results

Measurements of the USD and GBP paper banknotes revealed them to be strongly magnetic (unsurprisingly, since their magnetic signature is one common way of differentiating genuine from counterfeit banknotes). The highest SIRMs were observed for the USD banknotes, ranging from $35.6 \cdot 10^{-3}$ Am^2/kg (\$5 banknote) to $89.3 \cdot 10^{-3}$ Am^2/kg (\$100 banknote). The paper GBP banknotes had slightly lower values; $35.0 \cdot 10^{-3}$ Am^2/kg for £10, $28.9 \cdot 10^{-3}$ Am^2/kg for £20, and $24.6 \cdot 10^{-3}$ Am^2/kg for the £5 notes. The concentrations of ferromagnetic grains, as measured by SIRM, in the USD and paper GBP banknotes are notably higher than those in the new, polymer-composition GBP notes (Figure B1; Table B1). SIRMs for the polymer GBP banknotes (circulated) are ~50–130 times lower than those for the paper GBP banknotes, reaching values of $0.47 \cdot 10^{-3}$ Am^2/kg, $0.42 \cdot 10^{-3}$ Am^2/kg and $0.26 \cdot 10^{-3}$ Am^2/kg for the £5, £10 and £20 banknotes, respectively (Figure B1; Table B1). No notable difference was noted between unused and circulated polymer GBP banknotes (~$0.38 \cdot 10^{-3}$ Am^2/kg, ~$0.49 \cdot 10^{-3}$ Am^2/kg and ~$0.26 \cdot 10^{-3}$ Am^2/kg for the unused £5, £10 and £20 banknotes).

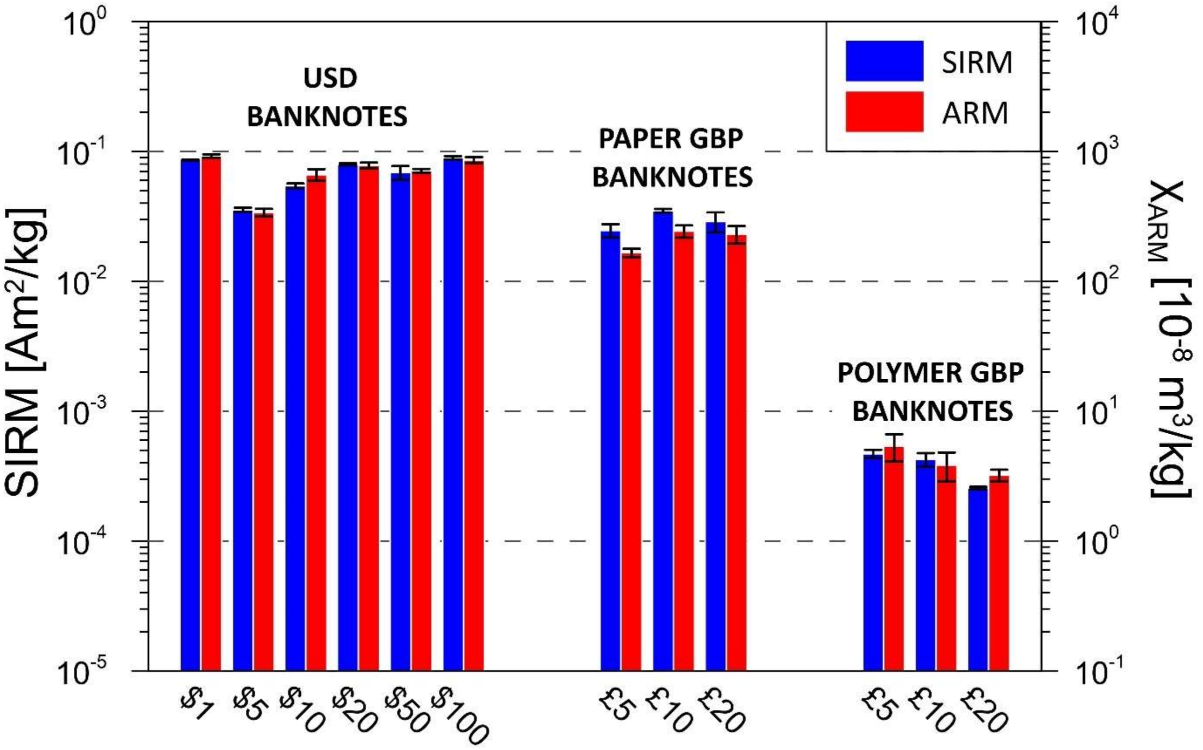

Figure B1. Saturation isothermal remanent magnetisation (SIRM) and susceptibility of anhysteretic remanent magnetisation (χ_{ARM}) for USD banknotes, and paper and polymer GBP banknotes. Note that the y axis is on a log scale.

To put these magnetic values into environmental context, Figure B2 shows SIRM values for the USD, paper GBP and polymer GBP banknotes compared with those for a range of indoor and outdoor airborne particulate emissions: specifically, from burning fossil fuels (i.e. peat, wood and coal) in residential open fires; vehicle exhaust emissions (both diesel and petrol); roadside dust; and brake-wear emissions. The measured SIRM values for the USD ($35.6\cdot10^{-3} - 89.3\cdot10^{-3}$ Am^2/kg) and paper GBP banknotes ($24.6\cdot10^{-3} - 35.0\cdot10^{-3}$ Am^2/kg) are greater than those for diesel- ($\sim8.6\cdot10^{-3}$ Am^2/kg) and petrol-engine ($\sim5.1\cdot10^{-3}$ Am^2/kg) exhaust emissions (Gonet *et al.,* 2021b), and PM emitted from open fires ($\sim8.3\cdot10^{-3}$ Am^2/kg) (Maher *et al.,* 2021); and fall within the range of SIRM values for airborne roadside PM (collected on filters) in Lancaster, U.K. ($7\cdot10^{-3} - 167\cdot10^{-3}$ Am^2/kg) (Halsall *et al.,* 2008; Figure B2).

Table B1. Mass, saturation isothermal remanence magnetisation (SIRM) and susceptibility of anhysteretic remanent magnetisation (χ_{ARM}) for the USD banknotes, and paper and polymer GBP banknotes (3 banknotes of each type and value; average value ± standard deviation).

Banknote	Mass [g]	SIRM [10^{-3} Am^2/kg]	χ_{ARM} [10^{-8} m^3/kg]
United States dollar (USD) banknotes			
\$1	1.035 ± 0.003	85.8 ± 0.6	922 ± 28
\$5	0.974 ± 0.009	35.6 ± 1.3	338 ± 23
\$10	0.976 ± 0.002	54.4 ± 2.3	662 ± 68
\$20	1.016 ± 0.018	79.6 ± 1.5	779 ± 42
\$50	0.993 ± 0.010	68.8 ± 8.5	708 ± 25
\$100	0.978 ± 0.005	89.3 ± 2.3	857 ± 46
British pound sterling (GBP) banknotes			
Paper £5	0.926 ± 0.026	24.6 ± 2.9	165 ± 12
Paper £10	0.943 ± 0.003	35.0 ± 1.1	243 ± 26
Paper £20	1.091 ± 0.025	28.9 ± 5.1	230 ± 36
Polymer £5	0.754 ± 0.003	0.47 ± 0.03	5.4 ± 1.3
Polymer £10	0.824 ± 0.010	0.42 ± 0.05	3.8 ± 1.0
Polymer £20	0.926 ± 0.003	0.26 ± 0.01	3.2 ± 0.3

We also measured another magnetic parameter, χ_{ARM}, which is sensitive to the presence of single-domain magnetic grains, i.e., of ~30 – 50 nm in diameter (Maher, 1988). The χ_{ARM} values were very high, with the highest obtained for the USD banknotes ($338 \cdot 10^{-8}$ – $922 \cdot 10^{-8}$ m^3/kg), ~1.4 – 5.6 times higher than those for the paper GBP banknotes ($165 \cdot 10^{-8}$ – $243 \cdot 10^{-8}$ m^3/kg). As with the SIRM values, the χ_{ARM} values for the USD and paper GBP banknotes are notably higher than the polymer-based GBP notes ($3.2 \cdot 10^{-8}$ – $5.4 \cdot 10^{-8}$ m^3/kg) (Figure B1; Table B1).

Again, to put these magnetic values for the paper banknotes into environmental context, in comparison with our χ_{ARM} values for the GBP paper banknotes, similar values have been reported for total roadside dust (~$150 \cdot 10^{-8}$ – $190 \cdot 10^{-8}$ m^3/kg) in Warsaw, Poland (Dytłow *et al.,* 2019), and for moderately-polluted soil (~$60 \cdot 10^{-8}$ – $470 \cdot 10^{-8}$ m^3/kg) in Shanghai (Hu *et al.,* 2007). In highly polluted areas, χ_{ARM} values can sometimes reach even higher levels, up to ~$5{,}200 \cdot 10^{-8}$ m^3/kg for roadside dust (in south India) (Gargiulo *et al.,* 2016) and ~$3{,}000 \cdot 10^{-8}$ m^3/kg for highly-polluted soil (in Shanghai) (Hu *et al.,* 2007).

In order to assess whether magnetic, iron-rich particles can be easily removed from the banknote surfaces (e.g. by handling for counting purposes), we gently wiped the banknote surfaces with a magnetically-‘clean’ wet wipe. First, we measured the SIRMs of clean wipes, then we wiped each banknote and measured the wipes again (Table B2). The difference (Δ_{SIRM}) was attributed to the SIRM of the particles removed from each banknote with gentle wiping. In all 36 cases, we found that a portion of magnetic, iron-rich particles was readily removed from the banknotes. Δ_{SIRM} is especially high for the USD banknotes, reaching levels up to $12{,}718 \cdot 10^{-10}$ Am^2 in the first round of wiping (Table B2). In the case of the GBP banknotes, Δ_{SIRM} is lower, ranging between $146 \cdot 10^{-10}$ Am^2 and $244 \cdot 10^{-10}$ Am^2 for the paper GBP banknotes, and between $9 \cdot 10^{-10}$ Am^2 and $187 \cdot 10^{-10}$ Am^2 for the polymer GBP notes (Table B2). We repeated the surface wiping test three times, in order to check if the removed magnetic particles merely represented surface dirt, from handling of notes during circulation, and/or any excess, or residual, printing ink post-production. In the second round of wiping, Δ_{SIRM} ranges from $493 \cdot 10^{-10}$ Am^2 to $4{,}927 \cdot 10^{-10}$ Am^2 for USD banknotes, from $50 \cdot 10^{-10}$ Am^2 to $518 \cdot 10^{-10}$ Am^2 for the paper GBP banknotes, and from $27 \cdot 10^{-10}$ Am^2 to $96 \cdot 10^{-10}$ Am^2 for the polymer GBP banknotes (Table B2). In the third round of wiping, Δ_{SIRM} varies between $3054 \cdot 10^{-10}$ Am^2 and $27{,}155 \cdot 10^{-10}$ Am^2 for the USD banknotes, between $16 \cdot 10^{-10}$ Am^2 and $200 \cdot 10^{-10}$ Am^2 for the paper GBP banknotes, and between $35 \cdot 10^{-10}$ Am^2 and $79 \cdot 10^{-10}$ Am^2 for the polymer GBP banknotes (Table B2).

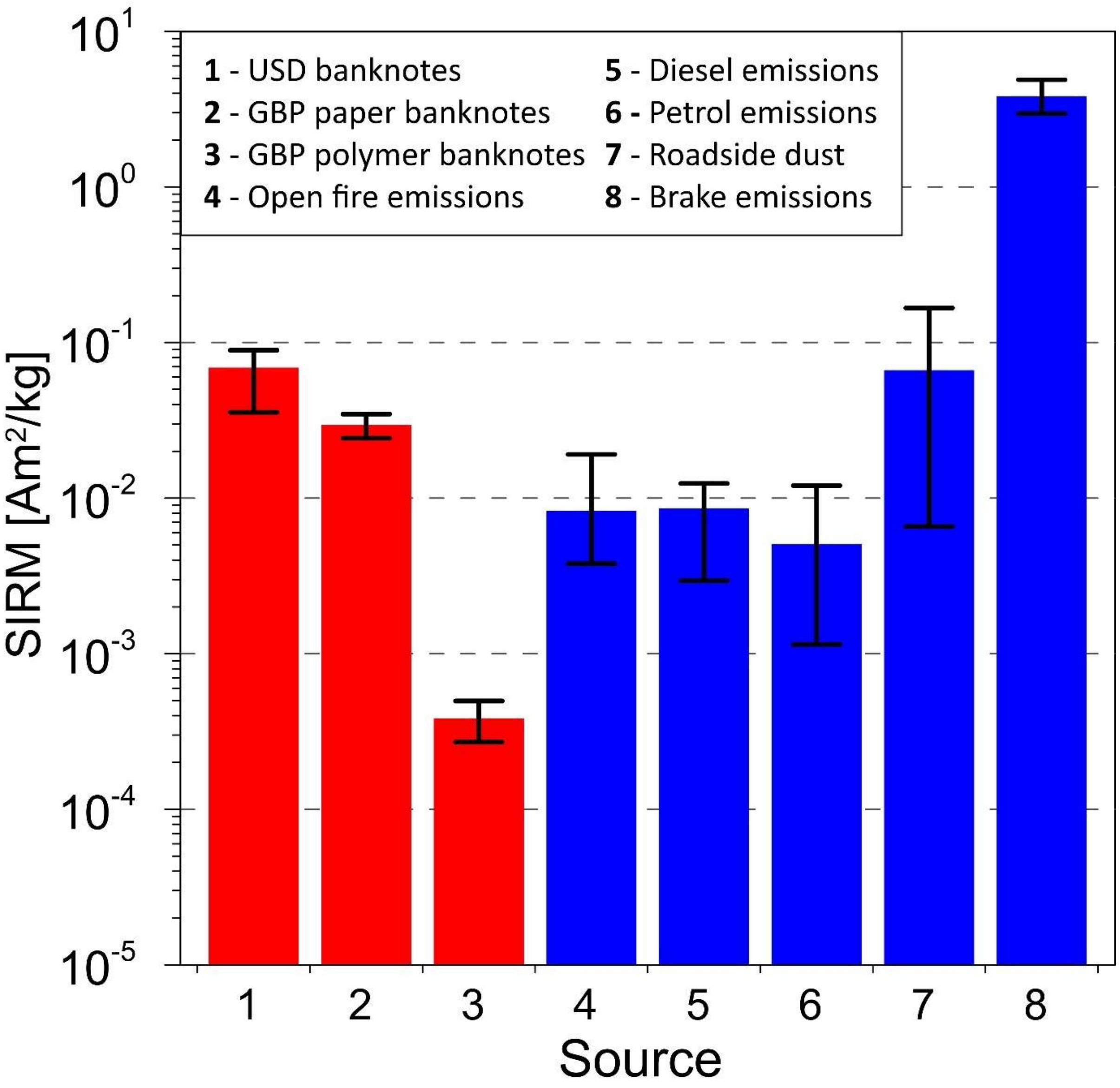

Figure B2. Saturation isothermal remanent magnetisation (SIRM) for: (1) USD banknotes, (2) paper and (3) polymer GBP banknotes, (4) emissions from open fires (Maher *et al*., 2021), (5) vehicle diesel exhaust emissions (Gonet *et al*., 2021b), (6) vehicle petrol exhaust emissions (Gonet *et al*., 2021b), (7) roadside airborne PM (Halsall *et al*., 2008) and (8) brake-wear PM (Gonet & Maher, 2019). Note the y axis is shown in a log scale.

Based on SIRMs for sized, pure magnetite powders (Maher, 1988), we can estimate the amount of magnetite removed from the banknotes by each round of gentle wiping. These range from ~45 µg to 190 µg of magnetite being removed, with a single wiping, from the USD banknotes in the first round of wiping (Table B2). Again, in the case of the GBP banknotes, the amount of magnetite easily removable from the banknotes by wiping is much lower,

~2.18 μg to 3.64 μg and ~0.13 μg to 2.79 μg from paper and polymer GBP banknotes, respectively (Table B2). In the second round of wiping, ~7 μg to 74 μg of magnetite is removed from the surface of the USD banknotes, ~0.74 μg to 7.74 μg from the paper GBP banknotes, and ~0.40 μg to1.44 μg from the polymer GBP banknotes. In the third round of wiping, the mass of the removed magnetite ranges from ~46 μg to 405 μg, ~0.24 μg to 2.99 μg and ~0.52 μg to 1.17 μg for the USD banknotes, paper and polymer GBP banknotes, respectively. The amount of magnetite removed from the banknote surfaces is thus variable but similar for all 3 rounds of wiping, indicating that magnetic (nano)particles shedding from the banknote surfaces originate from the ink pigment, rather than a surface environmental contamination or production-related ink excess.

In order to assess the particle size distribution of the magnetite particles shedding readily from the banknote surfaces, we measured several magnetic parameters for a sample of Pigment Black 11 (Table B3), the pigment traditionally used in printing paper banknotes. We observed extremely high values of room-temperature SIRM (12.6 Am^2/kg) and χ_{ARM} ($212.5 \cdot 10^{-5}$ m^3/kg) (Table B3); indeed, comparable with values for pure magnetite powders (Maher, 1988). Pure magnetite particles which are larger than 200 nm in diameter usually have χ_{ARM} values < $100 \cdot 10^{-5}$ m^3/kg (Maher, 1988). The χ_{ARM} value obtained for Pigment Black 11 is notably higher ($212.5 \cdot 10^{-5}$ m^3/kg), indicating that it is dominated by magnetite particles < 200 nm. Demagnetisation of the pigment's χ_{ARM} removes half of its initial value by a low demagnetising field, 13 mT, also characteristic of magnetically-'soft', nano-sized magnetite particles (Maher, 1988). We can further narrow down the dominant size of the pigment's magnetite particles by measuring its SIRM at low temperature (77 K). The $SIRM_{77K}$ increases by 28% (15.4 Am^2/kg compared to the $SIRM_{RT}$ value of 12.6 Am^2/kg; Table B3), indicating the presence of 'superparamagnetic' grains (~20 – 30 nm in size), which are thermally-agitated at room temperature (and thus contribute no magnetic remanence) but which 'block in' at low temperature, contributing the observed $SIRM_{77K}$ increase.

To obtain independent confirmation of the ink particle size, we analysed the ink pigment particles using high-resolution TEM. Its mineralogy confirmed by electron diffraction, the particle size of the magnetite ink ranges between ~15 nm and 400 nm (Figure B3), with the majority (~80%) being smaller than 100 nm (Figure B3D).

Table B2. Saturation isothermal remanent magnetisation (SIRM) for wipes before and after wiping banknote surfaces (3 banknotes of each type and value; average value ± standard deviation).

Banknote that was wiped		SIRM for wipes $[10^{-10}\ \mathrm{Am}^2]$			Magnetite removed from the banknote [µg]
		Before wiping	After wiping	Difference (Δ_{SIRM})	
1st wiping					
USD banknotes	$1	73 ± 1	10,989 ± 2,145	10,916 ± 2,146	163 ± 32
	$5	72 ± 4	3,109 ± 1,188	3,037 ± 1,183	45 ± 18
	$10	73 ± 2	4,142 ± 763	4,070 ± 761	61 ± 11
	$20	65 ± 7	12,783 ± 3,620	12,718 ± 3,627	190 ± 54
	$50	61 ± 1	5,837 ± 1,422	5,776 ± 1,423	86 ± 21
	$100	65 ± 4	5,723 ± 1,237	5,659 ± 1,234	84 ± 18
GBP banknotes	Paper £5	69 ± 6	313 ± 125	244 ± 120	3.64 ± 1.79
	Paper £10	109 ± 23	254 ± 63	146 ± 53	2.18 ± 0.79
	Paper £20	73 ± 34	285 ± 127	212 ± 154	3.16 ± 2.30
	Polymer £5	67 ± 3	254 ± 77	187 ± 75	2.79 ± 1.12
	Polymer £10	37 ± 3	166 ± 60	129 ± 57	1.93 ± 0.85
	Polymer £20	55 ± 9	63 ± 3	9 ± 7	0.13 ± 0.10
2nd wiping					
USD banknotes	$1	58 ± 3	2,231 ± 206	2,173 ± 203	32 ± 3
	$5	57 ± 1	550 ± 38	493 ± 39	7 ± 1
	$10	58 ± 1	1,958 ± 441	1,900 ± 441	28 ± 7
	$20	61 ± 2	4,988 ± 400	4,927 ± 398	74 ± 6
	$50	59 ± 1	2,022 ± 669	1,963 ± 669	29 ± 10
	$100	61 ± 6	3,006 ± 305	2,946 ± 299	44 ± 4
GBP banknotes	Paper £5	63 ± 15	210 ± 21	147 ± 19	2.19 ± 0.29
	Paper £10	68 ± 7	118 ± 21	50 ± 26	0.74 ± 0.39
	Paper £20	71 ± 4	589 ± 359	518 ± 361	7.74 ± 5.39
	Polymer £5	60 ± 4	156 ± 15	96 ± 17	1.44 ± 0.26
	Polymer £10	55 ± 4	94 ± 5	40 ± 8	0.59 ± 0.12
	Polymer £20	55 ± 1	81 ± 23	27 ± 22	0.40 ± 0.33
3rd wiping					
USD banknotes	$1	64 ± 4	27,219 ± 785	27,155 ± 781	405 ± 12
	$5	64 ± 1	3,118 ± 578	3,054 ± 578	46 ± 9
	$10	65 ± 3	5,439 ± 861	5,374 ± 864	80 ± 13
	$20	67 ± 5	6,021 ± 1,704	5,954 ± 1,710	89 ± 26
	$50	63 ± 2	8,872 ± 626	8,809 ± 628	131 ± 9
	$100	69 ± 4	9,886 ± 1,262	9,817 ± 1,262	147 ± 19
GBP banknotes	Paper £5	53 ± 1	99 ± 27	46 ± 27	0.69 ± 0.41
	Paper £10	61 ± 15	77 ± 5	16 ± 12	0.24 ± 0.17
	Paper £20	62 ± 17	262 ± 147	200 ± 154	2.99 ± 2.30
	Polymer £5	54 ± 1	133 ± 30	79 ± 31	1.17 ± 0.46
	Polymer £10	53 ± 2	91 ± 14	38 ± 14	0.57 ± 0.20
	Polymer £20	54 ± 1	89 ± 4	35 ± 4	0.52 ± 0.06

Discussion

It is critical to understand the processes and exposure pathways through which certain occupational groups appear to have become unusually susceptible to development of neurodegenerative disease. Although it has been established that some occupational groups experience(d) exposures to known neurotoxicants, other groups also display significant elevation in neurodegeneration-linked MORs yet have no known or obvious disease aetiology (Schulte *et al.,* 1996; Park *et al.,* 2005). From a study of death certificate information for 22 contributing U.S. states for the interval 1992–1998, bank tellers were reported to display elevated – and unexplained – MORs for both pre-senile dementia and Alzheimer's disease (Park *et al.,* 2005). Given that iron overload and cell damage through excess oxidative stress have been implicated increasingly in neurodegenerative disease (e.g. Quintana *et al.,* 2006; Castellani *et al.,* 2007; Smith *et al*., 2010; Tabner *et al.,* 2010), it seems timely and important to assess possible routes of metal-rich neurotoxicant exposure in this particular, currently enigmatic occupational group.

Table B3. Magnetic parameters for Pigment Black 11 (Cl 77499).

Magnetic parameter	Value
SIRM [Am^2/kg]	12.6
$SIRM_{77K}$ [Am^2/kg]*	15.4
χ_{ARM} [10^{-5} m^3/kg]	212.5
MDF_{ARM} [mT]	13

*$SIRM_{77K}$ = SIRM measured at 77 K.

Our approach builds upon the growing body of work which demonstrates that exposure to urban airborne PM is associated not only with respiratory and cardiovascular problems, but also neurodegeneration and cognitive impairments (Calderón-Garcidueñas *et al.,* 2002; Pope & Dockery, 2006; Hoek *et al.,* 2013; Beelen *et al.,* 2014; Costa *et al.,* 2014; Weichenthal *et al.,* 2017a; Liu *et al.,* 2018; Malik *et al.,* 2019; Maher *et al.,* 2020). Both indoor and outdoor PM often comprises a complex mixture of components, some of which might be toxic (e.g. Karlsson *et al.,* 2006; Jordanova *et al.,* 2012; Yang *et al.,* 2016; Maher, 2019).

Iron-rich and often strongly magnetic nanoparticles are particularly abundant in the solid (non-volatile) fraction of ultrafine (< 100 nm in diameter) air pollution. Because iron can catalyse the formation of reactive oxygen species (ROS), inducing oxidative stress, such iron-rich nanoparticles (whether or not dissolved in the brain subsequently) might constitute a specific neurotoxicant, potentially contributing to the oxidative stress and Alzheimer-like pathology in the human brain (Maher, 2019). Importantly, not only can iron-rich nanoparticles be toxic on their own; they are also often co-associated with other toxic metals, including Al, Ce, Cr, Co, Cu, Mn, Ni, Pb, Pt, Ti and Zn (Spassov *et al.,* 2004; Chen *et al.,* 2006; Kim *et al.,* 2007; Maher *et al.,* 2016; Yang *et al.,* 2016; Hofman *et al.,* 2020) and surface-adsorbed organic species, including polycyclic aromatic hydrocarbons (PAHs) (Lehndorff & Schwark, 2004; Halsall *et al.,* 2008).

Iron-rich nanoparticles, with characteristic high-temperature (> 100 °C) surface features and shapes, co-associated with other exogenous metal species, have been found in cortical and brainstem samples in the brains even of young people (< 35 yrs old) exposed lifelong to high concentrations of airborne PM (Maher *et al.,* 2016; Calderón-Garcidueñas *et al.,* 2020). Compared to low-pollution controls, who demonstrate little neuropathology and up to 10 times lower brain nanoparticle numbers, these highly-exposed young people already display multiple aberrant proteinopathies (Calderón-Garcidueñas *et al.,* 2020). Such associations between exposure to airborne, metal-rich pollution particles (dominated by iron-bearing compounds), the abundant presence of precisely-matching nanoparticles inside both autonomous and cortical brain regions, and substantial neuropathologies even in young people, strongly indicates a causal neurodegenerative role for inhaled and ingested metal-rich air pollution nanoparticles (Maher *et al.,* 2016; Calderón-Garcidueñas *et al.,* 2020).

Hence, chronic exposures to environmental iron-rich nanoparticles may be an important route into neurodegenerative disease. Here, our magnetic analyses of USD and GBP banknotes, and of the ink pigment widely used in their printing, have revealed not only that the banknotes (especially the USD and paper GBP notes) are highly magnetic, but also that strongly magnetic nano-sized particles are shed readily and repeatedly from their surfaces. Just gentle wiping of the banknote surface by a moist wipe resulted in transfer of very high numbers of magnetite particles ($12 \cdot 10^9 – 695 \cdot 10^9$ for the USD banknotes; $0.4 \cdot 10^9 – 13 \cdot 10^9$ for paper and $0.2 \cdot 10^9 – 4.8 \cdot 10^9$ for polymer GBP banknotes) from the banknote to the wipe. Magnetite particles continued to be shed from all banknote surfaces over three successive wipings.

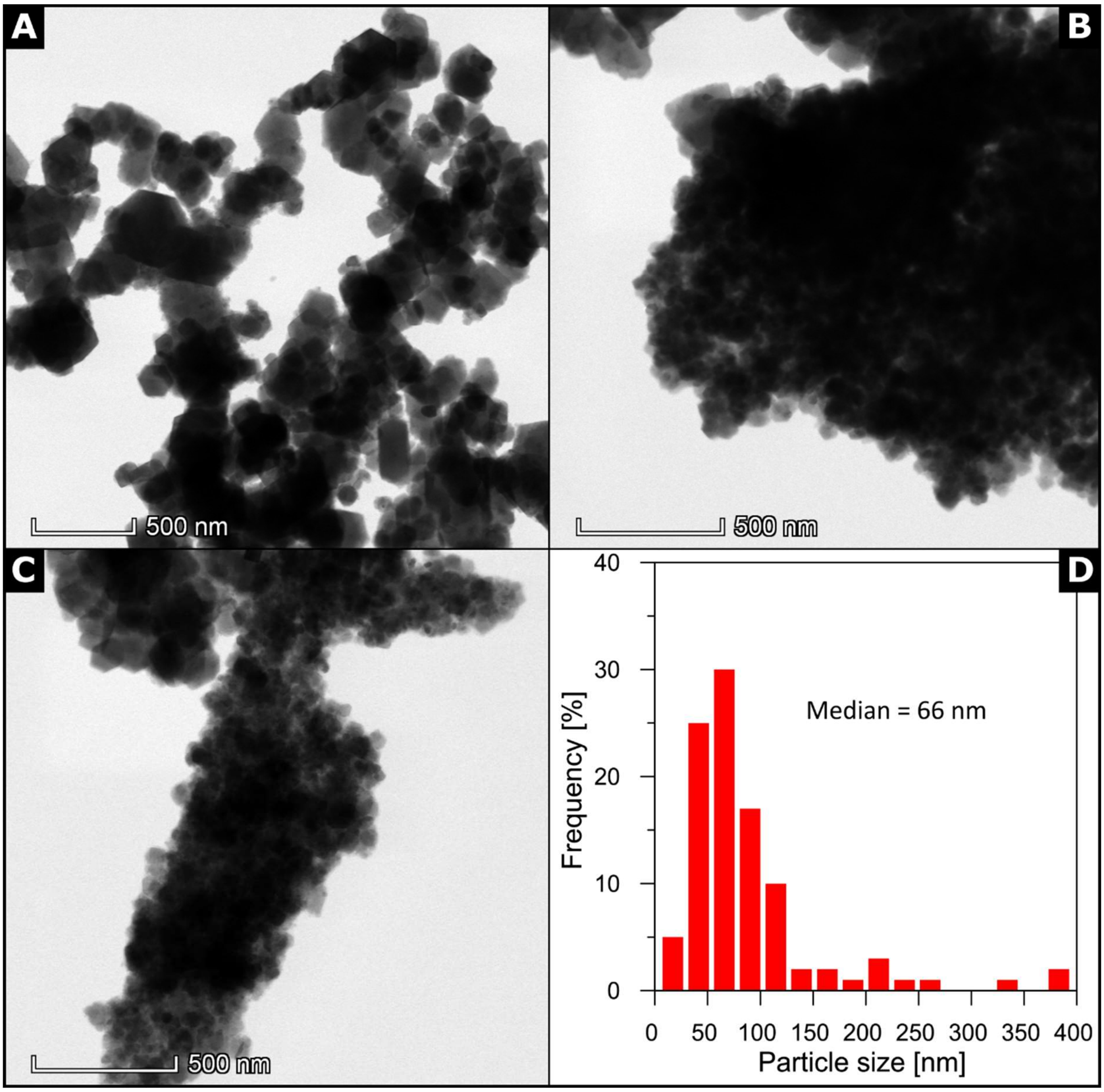

Figure B3. TEM images of Pigment Black 11 particles (A, B and C) and their particle size distribution (D).

We hypothesise that such shedding of iron-rich, magnetic nanoparticles may provide a possible insight into the elevated MORs observed for U.S.-based bank tellers who died during the period 1992 – 1998. A common practice, prior to increased automation, was for bank tellers to count banknotes by licking a finger to adhere to each successive counted note, and thus speed up the manual counting process. Given the rate of particle shedding reported here, this traditional manual counting procedure must have resulted in prolific transfer of iron-rich nanoparticles first to the fingers (with the possibility of some dermal absorption) and thence to the tongue. Critically, the tongue is an effective and direct pathway to the brain via the taste nerve translocation pathway (VII and IX cranial nerves); readily demonstrated in animal models by elicitation of CNS neurotoxicity through glossal instillation of metal-bearing (Zn, Ti) nanoparticles (Chen *et al.,* 2017c; Liang *et al.,* 2018).

This postulated route to an occupational exposure to a potential neurotoxicant specific to bank tellers (in pre-automation times) is somewhat reminiscent of that of the so-called 'radium girls', in the early 20th century. Female factory workers at three United States Radium factories contracted radiation poisoning from painting watch dials with radioluminescent paint. Having been told that the paint was harmless, they were advised to 'point' their brushes with their tongue or lips, to produce a fine paintbrush tip. As a result of ingestion of this radioactive substance, unknown numbers of the women died, typically having developed anaemia, bone fractures and necrosis of the jaw ('radium jaw') (e.g. Gunderman & Gonda, 2015; Cohen & Kim, 2017).

For the U.S.-based bank tellers who died in the interval 1992 – 1998, and started their working lives from ~1930 onwards (assuming the U.S. average lifespan in the 1990s of 79 yrs for women and 72 yrs for men), glossal exposure not only to magnetite-rich particles but also to other cytotoxic metal-bearing particles is additionally likely. Lead, for example, was used in 'Brunswick Green' ink ($PbSO_4 \cdot xPbCrO_4 \cdot yFe_4[Fe(CN)_6]$) at intervals (1928 – 1963, 1969, 1977 – 1988) before being phased out for health reasons; chromium oxide (Cr_2O_3) replacing lead in 'Pigment Green' (Hall & Chambliss, 2004). Titanium dioxide (TiO_2) has been used in production of U.S. banknotes since 1934, as a paper whitener (presaging the vast international expansion in synthesis and use of TiO_2 for diverse applications, from food additives, to cosmetics, paints, plastics and electronics (e.g. Chen & Mao, 2007)).

Given the human, societal and economic costs of the pandemic of neurodegenerative disease, growing year on year as average lifespans increase around the world, it is increasingly urgent and important to identify the diverse pathways of exposure to metal-rich nanoparticles as plausible and pervasive neurotoxicants. Our analysis and discussion here are focused on the potential exposure experienced, pre-automation, by bank tellers (who died between 1992 and 1998). Prospectively, however, these results also indicate that current and newly-developing occupational routes might be inducing harmful exposures. For instance, operators of 3D metal printers (Chen *et al.,* 2020), might be exposed to harmful levels of iron-rich neurotoxicants.

Indeed, the prevalence of iron-rich nanoparticles in the environment may even be growing. Iron-rich and strongly magnetic nanoparticle powders, easily and cheaply produced, are increasingly widely used as pigments, catalysts, fillers and even brake friction materials (i.e. designed to be abraded and consequently efficiently released into roadside air). The abundant and pervasive presence of magnetite nanoparticles in both indoor (Maher *et al.,* 2021) and outdoor (Sanderson *et al.,* 2016; Gonet & Maher, 2019) environments indicates growing levels of human exposure to these potentially neurotoxic particles, especially if individuals are exposed not only during daily commuting, but also at home (e.g. when using open fires for heating) and, as hypothesized here, at their place of work.

Conclusions

1. Because of the magnetic pigments used in their production, banknotes (especially paper banknotes) are strongly magnetic; equivalent in their magnetite concentrations to, for example, the air pollution particles emitted at heavily-trafficked roadsides.

2. Even gentle wiping of paper banknotes (here, with a moist wipe) results in the ready, abundant and repeated shedding of strongly magnetic particles, even up to $\sim 7 \cdot 10^{11}$ particles per wiping. Such shedding of magnetic particles was observed both for U.S. and British banknotes, but was greatest for the USD.

3. The black pigment, ‘Black 11/Magnetic Black’, used for many decades in the printing of banknotes, consists of almost pure magnetite, characterised by nanoscale particulate dimensions, with the majority smaller than 100 nm. Such particles are sufficiently small to access all major organs of the human body, whether by inhalation, ingestion or the taste nerve pathway, and to enter critical sub-cellular organelles, including mitochondria.

4. Excess iron loading in the brain can catalyse excess formation of reactive oxygen species, inducing oxidative stress and cell damage or death. Given the high content and prolific shedding of magnetite nanoparticles we observe from banknote surfaces, we hypothesise that magnetite and other metal-bearing nanoparticles were repetitively and frequently ingested by bank tellers (pre-automation), and subsequently entered the brain directly via the taste nerve pathway and/or indirectly via the systemic circulation and the neuroenteric system. Such an exposure route may plausibly account for the reported and currently unexplained association

between elevated neurodegeneration-related MORs and this specific occupation (in a cohort who died between 1992 and 1998).

5. Notwithstanding that neurodegenerative diseases encompass neuropathological and genetic variants, and potentially differing aetiologies, given the scale and costs of such disease on the international scale, investigation of current and newly-developing occupational groups with high exposure to iron-rich nanoparticles, in terms of incidence of neurodegenerative disease, seems both warranted and timely, in combination with well-controlled prospective studies.

Contributions of authors

Barbara A. Maher: Conceptualization, Supervision, Writing – original draft, Writing - review & editing. **Tomasz Gonet**: Conceptualization, Data curation, Writing – original draft, Writing - review & editing.